Optimization and Performance of Grinding Circuits: The Case of Buzwagi Gold Mine (BGM)

To the Faculty of Mechanical, Process and Energy Engineering

of the Technische Universität Bergakademie Freiberg

approved

THESIS

to attain the academic degree of

Doctor of Engineering

(Dr.-Ing.)

submitted

by **MSc. Alphonce Wendelin Wikedzi**

born on the 17th of July 1975 in Njombe, Tanzania

Reviewers**: Prof. Dr. -Ing. Urs Peuker, Freiberg, Germany**

Prof. Dr.-Ing. Holger Lieberwirth, Freiberg, Germany

Date of the award: **3rd April, 2018**

Declaration

I hereby declare that I completed this work without any improper help from a third party and without using any aids other than those cited. All ideas derived directly or indirectly from other sources are identified as such. In the selection and use of materials and in the writing of the manuscript I received support from the following persons:

- Prof. Dr.-Ing. Urs Peuker
- Dr.-Ing. Thomas Mütze
- Dr.-Ing. Thomas Leißner

Persons other than those above did not contribute to the writing of this thesis. I did not seek the help of a professional doctorate-consultant. Only those persons identified as having done so received no any financial payment from me for any work done for me.

This thesis has not previously been published in the same or a similar form in Germany or abroad.

Date: 3rd April, 2018 MSc. Alphonce Wendelin Wikedzi

Abstract

Buzwagi Gold Mine (BGM) is operated by Acacia Mining and located in the Lake Victoria Goldfields of central Tanzania. The mine commenced its operation since April 2009 and treats a sulphide copper-gold ore to produce gold in form of doré bars and a concentrate containing gold, copper and silver. The BGM comminution circuit includes a primary crushing stage with a gyratory crusher and a two grinding circuits using a Semi-Autogenous Grinding (SAG) mill and a ball mill. The SAG mill circuit also includes a single-deck screen and a cone crusher while the ball mill circuit utilizes hydrocyclones.

Currently, the grinding circuits are inefficient in achieving the aspired product fineness of $x_{P,80}$ = 125 µm even at low to normal throughputs (450-600 t/h). An evaluation and optimization study of the circuit performance was conducted to improve the product fineness through circuit surveys, experimental lab work and simulations. In three full scale sampling campaigns, size distributions and solids contents of the samples were determined at selected points in the circuit. Further, several types of breakage tests were conducted; standard Bond tests to determine ore grindability and work indices, batch grinding tests to determine parameters for breakage and selection functions , and standard ball mill tests for mineral liberation characterization by an automated mineral liberation analyzer (MLA).The tests were conducted in a size range from 0.063 to 2 mm.

Then, mass balance of the circuit was calculated and the models for mills, screens and hydrocyclones were employed in MODSIM (version 3.6.24). Firstly, simulations were conducted to optimize the existing plant. Several options were evaluated such as reduction of SAG screen aperture, adjustment of cyclone feed solids content and reduction of vortex finder and apex diameters. Moreover, simulations were also evaluated for a possible modification of the existing circuit and include; partial splitting of the cyclone underflow back to SAG mill, introduction of a second classification stage as well as introduction of a second ball mill.

The evaluation of breakage tests and survey data revealed the following; the Bond work index obtained for the current ore ranges between 17.20 - 18.70 kWh/t compared to 14.50 - 16.50 kWh/t which was estimated during plant design.This indicates a change in hardness of the ore during the last 7 years. Harder ore means more energy requirement for an efficient operation, the consequence of which is increased costs.

Thus, a periodic review of the ore hardness for ongoing mining operation is recommended. This will help in establishing better blends as well as prediction of appropriate tonnages for the existing ore types, so as to be efficiently treated by the available plant design. The work indices of the ore blends treated during survey were correlated with their quartz content and showed a strong linear relationship (R^2= 0.95). Therefore, the work index for the BGM ore could be predicted based on known quartz content of the material. Further, the model could be used as a control tool for monitoring hardness variation of the SAG mill feed. The mineral liberation studies indicated that the valuable phase (pyrite-pyrrhotite) could be liberated at relatively coarser particle sizes (200-400 µm). This implies that, there could be no problem with the efficiency of the gravity circuit for the BGM operation, where the gold contained in pyrite-pyrrhotite could be easily concentrated. However, the efficiency of flotation and cyanidation processes will still require finer feed. In overall, the liberation characteristics of the ore blends treated during survey showed minor differences.

The Bond efficiency factors of 48-61 % were obtained for the BGM grinding circuit, indicating an inefficient operation. This suggests that the operation could achieve targets by lowering the throughput. Further, the SAG mill circuit was characterized by fluctuating feed size of between $x_{F,80}$ =102 to 185 mm. A need for control of the feed size as well as blending ratios was recommended for an efficient operation in terms of throughput and final product size. This could be achieved through closer monitoring of the primary crusher performance and proper control of the ratios for the SAG mill feeders drawing the ore from the stockpile.

The ball mill grinding efficiency was poor and could be indicated by the fraction < 125 µm of only 5-9 % or $x_{P,80}$: >400 µm in the mill discharge. This was deemed due to poor hydrocyclone performance which was characterized by higher feed solids content, coarser overflow $x_{P,80}$: >200 µm as well as cut sizes, x_T : > 200 µm.

An improvement of product fineness up to 327 µm could be achieved during the simulation and optimization of the existing design. This could be achieved by modification of the operating conditions such as reduction of SAG screen aperture from 12 mm to 10 mm, reduction of vortex finder from 280 mm to 270.3 mm, reduction of apex diameter from 150 mm to 145.6 mm as well as adjustment of the cyclone feed solids content from 66.7 to 67.1 %. Based on this result, it was concluded that the current equipment could not achieve the target product quality (i.e. $x_{P,80}$ = 125 µm).

Further simulations based on flowsheet modification options showed that a second ball mill (series configuration) can help to achieve the desired product fineness as well as an increase of throughput from 618 t/h to 780 t/h. Although the circulating load increases to approximately 500 % in this configuration, it is outweighed by the benefits. Importantly, this option is cost intensive and hence may be considered as a long term solution and especially after cost-benefit analysis.

Finally, the results based on optimization of the existing design is recommended as short term solution for improvement of the BGM operation. Although the fineness achieved is still low (i.e. $x_{P,80}$ = 327 µm) compared to the target (i.e. $x_{P,80}$ = 125 µm), this gives additional advantage in the sense that, also better hydrocyclone performance is achieved in terms of overflow product ($x_{P,80}$ = 105 µm vs. > 240 µm) , cut size (x_T =133.1 µm vs. > 220 µm) and circulating load (CL =350 %). The improved overflow fineness will contribute to improved efficiency for the downstream processes.

Acknowledgments

First of All, I would like to thank God-the Almighty for giving me strength to undertake this task all the way through. It was not possible without his mercy.

Secondly, I would to thank Prof. Dr.-Ing. Urs Peuker for giving me an opportunity to pursue doctoral studies at TU Bergakademie Freiberg and also as my supervisor, for his support during the whole period of my research work.

In an exceptional way, I would like to thank my second supervisor Dr.-Ing. Thomas Mütze for his tireless guidance and support. I miss a word to express my gratitude for his cooperation, advice and tolerance. It was a wonderful experience working with him.

The comments and suggestions by Prof. Dr.-Ing. Holger Lieberwirth and Dr.-Ing. Thomas Leißner on my thesis work are also highly appreciated**.**

Moreover, special thanks go to all colleagues at the Institute of Mechanical Process Engineering and Mineral Processing, TU Bergakademie Freiberg, for their assistance and support.

At BGM, my heartfelt thanks go to Philbert Rweyemamu (General Manager), Karel Schultz (Process Plant Manager) and Festo Shayo (Head-Metallurgy) for giving me an opportunity to conduct this research at the process plant between April and June 2015. The metallurgical team and all employees of the process plant are also appreciated.

I am also highly indebted to the German Academic Exchange Service (DAAD) and the Tanzanian government through ministry of Education (MoEVT) for the financial support during the whole period of my research work. The University of Dar es Salaam is also appreciated for the support and permission to attend to this doctoral programme.

More special thanks goes to my mother Dzilaga Mwenda for her encouragement. I'm also thankful to all my relatives and close friends for their support in different ways.

My extended appreciation goes to my students and assistants namely; Muhammad Alfi Arinanda, Sondos Saquran and Ruth Rieger.

Lastly, but not for the importance, I am grateful to my wife Rosemary Giteta and our wonderful children Athalia Wikedzi and Amos Wikedzi for their patience and understanding in times when I was not with them because of this work. Their company and emotional support has made this possible.

Table of Contents

Abstract iii

Acknowledgments vi

Table of Contents vii

List of Figures xii

List of Tables xvii

List of Symbols xix

1 Background 1

2 The Grinding Circuit at Buzwagi Gold Mine 3

2.1 Research Problem 4

2.2 Research Objectives 5

3 Literature Survey 6

3.1 Comminution 6

3.1.1 Particle Breakage Mechanisms 7

3.1.2 Comminution Laws 10

Bond's Law 11

3.1.3 Mineral Liberation 13

3.2 Tumbling Mills 18

3.2.1 Operation of Tumbling Mills 19

3.2.1.1 SAG Mill Operation 22

3.2.1.2 Ball Mill Operation 25

3.2.2 Power Prediction in Tumbling Mills 29

3.3 Grinding Circuits 35

3.3.1 Grinding Circuits Configuration 35

3.3.1.1 Open Circuit Grinding 36

3.3.1.2 Closed Circuit Grinding 37
3.3.2 Advances in Grinding Circuits 39
3.3.3 Operation and Control of Grinding Circuits 42
3.3.4 Grinding Circuits Efficiency 44
3.4 Modelling and Simulation in Comminution 45
3.4.1 Modelling Fundamentals 45
3.4.2 Breakage and Selection Functions 47
3.4.2.1 Estimation of Breakage Function 47
3.4.2.2 Estimation of Selection Function 50
3.4.3 Scale-up of Batch Grinding Data 53
3.4.4 Models for Grinding Processes 55
3.4.4.1 The Population Balance Model 57
3.4.4.2 The Perfect Mixing Ball Mill Model 59
3.4.5 Models for Classification Processes 63
3.4.5.1 Dahlstrom Model 65
3.4.5.2 Plitt Model 66
3.4.5.3 Lynch and Rao Model 66
3.4.5.4 Schubert Model 66
3.4.5.5 Nageswararao Model 67
3.4.5.6 Lippek and Espig Model 69
3.4.6 Simulation and Optimization of Grinding Circuits 70
3.4.7 Comminution Software Packages 75
3.5 Summary of Literature Survey 75
4 Material and Methods 79
4.1 Material and Initial Preparation 79
4.2 Grinding Circuit Survey at BGM 80
4.2.1 SAG Mill Feed 81

4.2.2 Pebble Crusher Feed and Product 82
4.2.3 Sampling Slurry Streams 82
4.2.4 Other Data Collected 83
4.2.5 Processing of Samples 84
4.2.5.1 Determination of Moisture 84
4.2.5.2 Determination of Percent Solids 85
4.2.5.3 Particle Size Analysis 85
4.2.5.4 Mineral Distribution in the Circuit 86
4.3 Grinding Tests 87
4.3.1 Batch Kinetic Grinding Tests 87
4.3.2 The Standard Bond Test 89
4.4 Characterization 91
4.4.1 Mineral Liberation Analysis 91
4.4.2 X-ray Diffractometry (XRD) 92
4.5 Modelling and Simulation with MODSIM (3.6.24) 92
4.5.1 SAG Mill Modelling 93
4.5.2 Ball Mill Modelling 94
4.5.3 Hydrocyclone Modelling 96
4.5.4 Data definition in MODSIM 97
5 Results and Discussions 99
5.1 BGM Grinding Circuit Assessment Based on Survey 99
5.1.1 Grindability Studies 99
5.1.2 Mass Balance 99
5.1.3 SAG Mill Circuit 101
5.1.3.1 Pebble Crusher Performance 101
5.1.3.2 SAG Mill Performance 102
5.1.3.3 SAG Discharge Screen Performance 103

5.1.4 Ball Mill Circuit 104
5.1.4.1 Ball Mill Performance 104
5.1.4.2 Hydrocyclone Performance 105
5.1.5 BGM Grinding Circuit Efficiency 111
5.1.6 Mineral distribution within the circuit 112
5.1.7 First Conclusion and Recommendation on Circuit Survey 114
5.1.7.1 Observation and conclusions 114
5.1.7.2 Recommendations 116
5.2 Liberation Characteristics of BGM Ore 117
5.2.1 Modal Mineralogy 117
5.2.2 Particle and Mineral Grain Size Distributions 118
5.2.3 Mineral Liberation 119
5.2.4 Mineral Locking 124
5.2.5 Correlations 125
5.2.6 Conclusions and Recommendations 127
5.3 Simulation Studies 128
5.3.1 Mass Balance and Modelling 128
5.3.2 Optimization studies 132
5.3.2.1 Optimization of the Existing SAG mill Circuit 132
5.3.2.2 Optimization of the Existing Ball Mil Circuit 134
5.3.2.3 Modification of Existing Flowsheet 143
5.3.3 Conclusions and Recommendations 153
5.3.3.1 SAG Mill Circuit 153
5.3.3.2 Ball Mill Circuit 153
5.3.3.3 Modification of the Flowsheet 154
5.3.3.4 Recommendations 154
6 Overall Conclusions and Recommendations 156

6.1 Findings 156
6.2 Future Work 158
References 160
Appendices 171
Appendix A: BGM Grinding Circuit Survey Data 171
Appendix B: Mineral Liberation Data for BGM Ore Blends 174
Appendix C: MODSIM Input Data Definition 175
Appendix D: Simulation and Optimization Data 178
Appendix E: Miscellaneous information 184

List of Figures

Figure 2-1: Simplified BGM grinding circuit showing major equipment. 3
Figure 2-2: BGM grinding circuit efficiency trends from 2009 to 2015. 5
Figure 3-1: Particles Breakage Mechanisms (adopted from (Rao 2011). 9
Figure 3-2: Relationship between Energy Input and Size Reduction in Comminution (after Hukki 1961). 11
Figure 3-3: Variation in Mineral Association for Progeny Particles from Breakage of Multiphase Composite (Napier-Munn, Morrel et al. 1996). 15
Figure 3-4: Degree of Liberation as a Function of Particle to Grain Ratio (adopted from Gaudin Model (1939). 16
Figure 3-5: Tumbling mill (Wills and Finch 2016). 18
Figure 3-6: Mill shell liners (Wills and Finch 2016). 19
Figure 3-7: Radial motion states in a tumbling mill, (a) unrolling (cascade movement), b) - falling (cataract movement), c) centrifugation (Schubert 2003). 20
Figure 3-8: Media motion in the tumbling mill (King 2001) 21
Figure 3-9: Relation between volumetric loading and SAG mill power for low ball charge and soft ore (Gupta and Yan 2006). 23
Figure 3-10: Maximum height drop as function of mill speed (Napier-Munn, Morrel et al. 1996). 24
Figure 3-11: Schematic of various sections of an AG mill (Wills and Napier-Munn 2006). 25
Figure 3-12: Types of ball mills based on discharge mechanism: (a) grate discharge, b) overflow discharge (Wills and Napier-Munn 2006)). 26
Figure 3-13: Energy input versus charge volume. 27
Figure 3-14: Illustration of forces of friction and gravity of turning moment about the centre of a ball mill (King 2001). 29
Figure 3-15 : Effects of mill filling on power draw for ball mills (King 2001). 31
Figure 3-16: Calculated ball mill power draw for the BGM ore system based on Bond and Rose and Sullivan models (D=6.10 m, L=9.05 m, and ψ_c=75 %). 34
Figure 3-17: Open Circuit Grinding. 37
Figure 3-18: Closed Circuit Grinding. 38
Figure 3-19: SAG Mill with scats recycle. Figure 3-20: SAG mill in closed circuit. 40

Figure 3-21: Semi-autogenous/Ball Mill Circuit Closed with a Cyclone (adopted from (Wills and Finch 2016)). 41
Figure 3-22: SAG Mill, HPGR and Ball Mill in an ABC Closed Circuit. 42
Figure 3-23: The breakage distribution function, illustrating its resolution into two components (Kelly and Spottiswood 1990). 49
Figure 3-24: Plot for the breakage function that is defined in terms of the parameter t_{10}. 50
Figure 3-25: First order plot for breakage rate determination (Gupta and Yan 2006) 51
Figure 3-26: An example of a plot for the specific rate of breakage as a function of particle size (King 2001). 52
Figure 3-27 : Mass balance for a single size fraction inside a mill (Napier-Munn, Morrel et al. 1996). 58
Figure 3-28: Grinding rates variation with particle size (Napier-Munn, Morrel et al. 1996). 60
Figure 3-29: Schematic diagram of AG/SAG mill process mechanisms (Napier-Munn, Morrel et al. 1996). 62
Figure 3-30 : Typical partition curve for hydrocyclones. 64
Figure 3-31: Hdrocyclone schematic diagram. D_c: cyclone diameter, D_o: vortex finder diameter, D_i: inlet diameter, l: vortex finder length inside the cyclone, Lc: cylindrical section length, h: hydrocyclone length, θ: cone angle, D_a: apex diameter. 65
Figure 3-32: Steps Involved in Modeling and Simulation of Industrial Comminution Circuits 73
Figure 3-33: Model Parameter Estimation ('Calibration') Using Plant Survey Data (Napier-Munn, Morrel et al. 1996). 74
Figure 4-1: Overall preliminary sample preparation steps for the major tests. 80
Figure 4-2: BGM grinding circuit flowsheet with sampling points. 81
Figure 4-3: Procedure used for preparation of samples for moisture determination. 85
Figure 4-4: Procedure used for preparation of samples for solids content determination. 85
Figure 4-5: Lab-scale selection function fitted with Austin model for the three BGM ore blends. 94

Figure 4-6: MODSIM form showing properties of the ore and streams with input data (bulk sample S-1). 97
Figure 4-7: Particle size distribution and feed rate of the feed (bulk sample S-1)..... 98
Figure 5-1: Pebble crusher streams particle size distribution. 101
Figure 5-2: SAG mill feed and product particle size distribution for survey 1, 2 and 3. 102
Figure 5-3: SAG Discharge Screen efficiency curves. 103
Figure 5-4: Ball mill feed and product particle size distribution for survey 1, 2 and 3. 105
Figure 5-5 : Hydrocyclone product streams particle size distribution for survey 1. . 106
Figure 5-6 : Hydrocyclone product streams particle size distribution for survey 2. . 106
Figure 5-7 : Hydrocyclone product streams particle size distribution for survey 3. . 107
Figure 5-8: Hydrocyclone uncorrected and corrected efficiency curves for survey 1, 2 and 3. 108
Figure 5-9: Correlation between model calculated and measured (survey) cut size, X_T. 110
Figure 5-10: Influence of apex, D_a and vortex finder, D_o diameters on cut size, x_T(μm)..... 110
Figure 5-11: Distribution of gold in grinding mill discharge streams. The symbols stands for; SAGD: SAG mill discharge, BMD: Ball mill discharge. 112
Figure 5-12: Distribution of gold in the hydrocyclone product streams. The symbols stands for; UF: Underflow and OF: Overflow. 113
Figure 5-13: Distribution of copper in grinding mill discharge streams. The symbols stands for; SAGD: SAG mill discharge, BMD: Ball mill discharge. 113
Figure 5-14: Distribution of copper in the hydrocyclone product streams. The symbols stands for; UF: Underflow and OF: Overflow. 114
Figure 5-15: Particle and mineral grain size distributions for the blend of survey 1. 119
Figure 5-16: Liberation of pyrite-pyrrhotite based on the sieved fractions (average of three sample). 120
Figure 5-17 : Cumulative pyrite-pyrrhotite liberation vs. class mean particle size... 121
Figure 5-18: Pyrite-pyrrhotite enrichment with particle size. 122
Figure 5-19 : Pyrite-pyrrhotite cumulative liberation as a function of geometric mean grain size; (a), and also as a function of the size reduction ratio; (b), for the three samples. 123

Figure 5-20: Pyrite-pyrrhotite locking as a function particle size, S- 1. 124
Figure 5-21: Pyrite-pyrrhotite locking as a function particle size, S-2. 125
Figure 5-22: Pyrite-pyrrhotite locking as a function of particle size, S-3 125
Figure 5-23: Dependence of Work index on Quartz content in the ore material 126
Figure 5-24: Measured and MODSIM predicted size distributions around BGM grinding circuit (survey 1). Points and solid lines represent survey and predicted values, respectively. 130
Figure 5-25: Comparison between MODSIM predicted and experimental particle size distributions. 131
Figure 5-26: Simulated particle size distributions for the SAG mill circuit under base case (Bc) and optimum (Op) SAG screen aperture. Base case refers to survey simulation. 134
Figure 5-27: Effect of cyclone feed solids content on circulating load and ball mill discharge fineness..... 135
Figure 5-28: Effect of cyclone feed solids content on the cut size and overflow fineness. 136
Figure 5-29: Simulated particle size distributions for the ball mill circuit under base case (Bc) and optimum (Op) cyclone feed solids. Base case refers to simulation under optimum SAG screen aperture. 137
Figure 5-30: Effect of vortex finder diameter on circulating load and ball mill product fineness. 138
Figure 5-31: Simulated particle size distributions for the ball mill circuit under base case (Bc) and optimum (Op) vortex finder diameter. Base case refers to simulation at optimum cyclone feed solids. 139
Figure 5-32: Effect of vortex finder diameter on cyclone cut size and overflow fineness. 140
Figure 5-33: Effect of apex diameter on circulating load and ball mill discharge fineness. 141
Figure 5-34: Simulated particle size distributions for the ball mill circuit under base case (Bc) and optimum apex diameter (Op). Base case refers to simulation under optimum vortex finder diameter. 141
Figure 5-35: Effect of apex diameter on cyclone cut size and overflow product fineness. 142

Figure 5-36: Simulated particle size distributions for the ball mill circuit under base case as well as optimized split of the underflow material back to the SAG mill circuit. Base case refers to simulation under optimum apex diameter. 144
Figure 5-37: Two stage classification BGM grinding circuit flowsheet as modeled by MODSIM. 146
Figure 5-38: Simulated particle size distribution of the key streams for the proposed ball mill circuit with two classification stages under base case (Bc) and optimum conditions. Base case refers to survey simulation. 147
Figure 5-39: BGM grinding circuit flowsheet with ball mills in series configuration as modelled by MODSIM. 150
Figure 5-40: BGM grinding circuit flowsheet with parallel configuration of ball mills as modelled by MODSIM. 151
Figure 5-41: Simulated size distributions under survey (Bc) and optimum conditions (Op) for the proposed circuit with two ball mills in series configuration..... 152
Figure 5-42: Simulated size distributions under survey (Bc) and optimum conditions (Op) for the proposed circuit with two ball mills in parallel configuration..... 152

List of Tables

Table 3-1: Power prediction models for tumbling mills. 31
Table 3-2: Normal Size Range and Approximate Energy Efficiencies for Various Devices..... 36
Table 4-1: Mass and assay of bulk samples as collected on site. 79
Table 4-2: Belt cut samples for the SAG mill feed for the three surveys..... 82
Table 4-3: Total mass of samples collected for pebble crusher streams. 82
Table 4-4: Slurry streams composite sample weights collected. 83
Table 4-5: Recommended representative sample mass for grinding circuit's survey. 84
Table 4-6: Particle size analysis procedure for the survey samples. 86
Table 4-7: Parameters used for dry kinetic batch grinding tests. 88
Table 4-8: Parameters used for wet kinetic batch grinding tests. 89
Table 4-9: The standard Bond mill operating parameters used for the tests. 90
Table 4-10: Number of particles analysed by MLA for the three bulk samples. 91
Table 4-11: The number of grain counts analysed by MLA for the three samples. ... 92
Table 4-12: Work index, abrasion and impact breakage mechanisms parameters for the BGM ore. 94
Table 4-13: Estimated lab-scale model parameters for the selection function. 95
Table 4-14: Scaled-up model parameters for the selection function. 95
Table 4-15: Estimated model parameters for the breakage function. 95
Table 4-16: Comparison of the cut size from different hydrocyclone models and with survey. 96
Table 4-17: NAGE'S model calibration coefficients for BGM hydrocyclone (S-1). 97
Table 5-1: Comparison of the design and the current work indices for the BGM ore. 99
Table 5-2: Operational and mass balanced streams around BGM milling circuit (tonnage rates in dry basis). 100
Table 5-3: Pebble crusher performance indicators. 102
Table 5-4: SAG mill performance indicators. 103
Table 5-5: SAG discharge screen efficiency indicators. 104
Table 5-6: Ball mill performance indicators. 105
Table 5-7: Hydrocyclone performance indicators. 107
Table 5-8: Hydrocyclone efficiency indicators..... 108

Table 5-9: Hydrocyclone efficiency category based on imperfection, *I* (Murthy and Basavaraj 2012). 109
Table 5-10: Factors for conversion of % passing in the overflow to X_T (Metso 2010). 109
Table 5-11: Energy consumption and operating work index for the current BGM operation. 111
Table 5-12: Input energy and throughput required for the current operation to achieve $x_{P,80}$ of 125 µm 111
Table 5-13: Modal mineralogy of the BGM ore material (wt. %). 117
Table 5-14 : Pyrite-pyrrhotite particle counts for the fractions measured. 120
Table 5-15: Pyrite-pyrrhotite particle counts based on liberation classes for S-2 . . 121
Table 5-16: Comparison of measured and mass balanced values around BGM milling circuit. 129
Table 5-17: Survey and MODSIM predicted stream values around BGM grinding circuit. 131
Table 5-18: Influence of SAG discharge screen on SAG mill performance. 133
Table 5-19: Influence of optimized SAG discharge screen on ball mill circuit performance. 133
Table 5-20: Influence of cyclone feed solids content on Ball mill performance. 137
Table 5-21: Summary of key parameters after simulation of the influence of vortex finder. 139
Table 5-22: Overall circuit simulation after optimization of the apex diameter. 143
Table 5-23: Effect of partially splitting cyclone underflow back to SAG mill. 144
Table 5-24: Performance figures after addition of second classification stage. 147
Table 5-25: Overall circuit performance after addition of a second ball mill. 149

List of Symbols

Symbol	Description	Units
a	First-order breakage rate constant	min^{-1}
$B_{i,j}$	Cumulative breakage function of particles from top size interval x_j breaking to size interval x_i	-
$b_{i,j}$	Breakage function: mass fraction arriving in size interval i from breakage of size interval j	%
$A.b$	Impact breakage parameter	
B_{ef}	Bond efficiency factor	%
C_1 to C_5	Multipliers describing the variations of selection function with mill design and operating variables	-
D	Internal mill diameter	m
d	Grinding media diameter (balls)	mm
D_a	Hydrocyclone underflow (apex) diameter	cm
D_c	Hydrocyclone diameter	cm
D_i	Hydrocyclone inlet diameter	cm
D_o	Hydrocyclone overflow diameter	cm
E	Input energy (kJ)	kJ
E_{oa}	Corrected efficiency curve based on whiten function	
E_R	Enrichment ratio	-
F_B	Ball size factor	kW/t_{-balls}
$F1$	Material constant defined in Eqn. (71)	-
H	distance from the bottom of the vortex finder to the top of the underflow orifice	cm
H_s	Hindered settling factor	-

I	An index for classifier imperfection	-
K	Material characteristic parameter defined in Eqn. (75)	-
k	A mill factor defined in Eqn. (16)	-
KD_o	Solids characteristic parameter defined in Eqn. (78)	
KQ_o	Calibration factor for the total slurry flow rate, Eqn. (78)	
KW_1	Calibration factor for water recovery to underflow	
L	Mill length	m
L_m	Fractional liberation	-
m	Sample mass	gm/kg
$\dot{m}$	Mill throughput	t/h
N	Mill speed	rpm
N_o *to* N_2	correction factors for change in mill diameter and ball size from batch to full-scale milling	-
P_i *(t)*	Weight fraction of material less than size x_i at time t	%
P	Power	kW
p_{in}	Inlet pressure	bar
Q (x_i)	Correction factor of selection function in the abnormal breakage region	-
R	Recovery	-/ %
R_f	Recovery of water to underflow	%
r_i	Rate of breakage	min^{-1}
R_v	Volumetric recovery of slurry to underflow	%
S_i	Specific rate of breakage or selection function of material of size interval i	min^{-1}
t_a	Abrasion breakage parameter	%
T_o	Splitting factor	-
t_{10}	Fineness index	-

V	Volume	cm^3
$\dot{V}$	flow rate	m^3/h
W	Total work	kWh/t
W_i	Bond ball mill work index	kWh/t
x	Particle size	mm/μm
x_T	Cut size for a classifier	μm
γ	Breakage parameter characteristic of the material used	-
β	Breakage parameter characteristic of the material used	-
β^*	Fish-hook parameter defined in Eqn. (81)	-
β^{**}	Dummy parameter defined in Eqn. (81)	-
ϕ_j	Breakage parameter characteristic of the material used, represents the fraction of fines that are produced in a single fracture event	-
σ	Breakage parameter characterizing the degree of normalization of the breakage function	-
α	Selection function parameter characteristic of the material	-
α_1	Separation efficiency parameter defined on Eqn. (81)	-
λ	Positive number representing an index of how rapidly the rate of breakage falls as size increases in the abnormal breakage region	-
ψ_c	Mill rotational speed	%
φ	Fraction of the mill volume occupied	-
τ	Residence time	min
ε	Bed porosity of the mill charge	%
ρ	Specific gravity	kg/m^3
η	viscosity	mPa

∇	A factor for mill rotational speed	-
κ	Separation efficiency	-

Indices

b	balls
v	void
c	Charge
s	Solids
l	Liquid
p	Pulp
GM	grinding media
MG	grindig powder
opt	Optimum
max	Maximum
cs	comminution specific
ce	Conical end
M	Mill
F	Feed
P	Product
G	Grinding
circ	circulating
o	ore
S	Shaft

Abbreviations

BGM	Buzwagi Gold Mine
EGL	Effective Grinding Length

SAG	Semi-Autogenous Grinding
FAG	Fully-Autogenous Grinding
AG	Autogenous Grinding
HPGR	High Pressure Grinding Rolls
HG/MG	High grade/Medium grade
XRD	X-ray Diffraction
SEM	Scanning Electron Microscope
MLA	Mineral Liberation Analyzer
BSE	Back-Scattered Electrons
XBSE	Extended BSE Liberation Analysis
AAS	Atomic Absorption Spectrometry

1 Background

Comminution is one of the most important unit operations in mineral processing and chemical industry (Fuerstenau, Phatak et al. 2011, Vedat 2011). In mineral processing, liberation of valuables from the gangue mineral is a necessary stage for all the downstream separation and/or extraction processes. This is achieved by rock fragmentation, that is, comminution of the ore and is usually carried out in various stages starting with primary crushing and ending with fine size reduction using tumbling mills (Fuerstenau, Phatak et al. 2011). It is important to liberate valuable minerals from gangue constituents so as to easily facilitate separation, and for producing products with the desired particle size, the desired particle property function respectively. However, comminution processes are both; energy-intensive and expensive, with tremendous room for improvement (Pokrajcic and Lewis-Gray 2010, Denız 2011). It is estimated that comminution accounts for up to 50 % of the energy used in mining operations (Ballantyne, Powell et al. 2012, Curry, Ismay et al. 2014, Jeswiet and Szekeres 2016, Boucaut 2017) and that only 1 % to 2 % of the supplied energy is effectively translated in the creation of new surface areas (Tromans 2008, Rosario 2010, Wills and Finch 2016). The majority of this energy is lost as heat or mechanical energy due to the operating nature of mills, where energy transfer between grinding media and particles is unconstrained and completely random (Pokrajcic and Lewis-Gray 2010).

This expensive and inefficient comminution process also represents a significant fraction of the global electric power consumption. In the United States, it is estimated that 30% of the total energy costs consumed in mining industry goes for comminution processes (DOE indices for 2005) (NRC 1981, Tromans 2008). Thus, comminution energy makes around 0.39% of total national energy consumption. In Canada, in turn, the respective index comes to nearly 2%, similarly in the Republic of South Africa. In Australia comminution consumes roughly 1.5% of total national energy (Tromans 2008). It has to be noted that, USA, Canada, South Africa, and Australia are the leaders in the application of modern mining technology and in recent years the values of energy consumption indices have generally decreased as a result of the application of modern processing technologies and equipment, especially in ore preparation circuits. As a result of the above, it is estimated that industrial comminution processes can absorb from 3 to 5 % of global electric energy consumption (Saramak, Tumidajski et al. 2010,

Jeswiet and Szekeres 2016). These and many other statistics reveal the importance and impact of size reduction processes and the reason for the extensive amount of effort made on this subject over the last 50 years (Acar 2013). More importantly, it is worth noting that, the basis for the quoted values of the fraction of energy attributable to comminution from a mining operation is still contradicting.

In recent years, there have been significant developments in comminution efficiency, both due to the expansion of machines with the capability to boost energy utilization, and also due to optimal design of grinding circuits and operating variables that enable more efficient application of existing machines (Denız 2011). However, as a consequence of depleting high grade ores; the mining industry future trends indicate that the need will continue to mine and treat low grade, finely disseminated ores at much higher tonnages and finer product size. The effective liberation of valuables from such ores remains one of the major challenges for the mining industry (Danha 2013).

Design and optimization of full-scale comminution circuits by direct experimentation is difficult and expensive because of the cost of modifying and operating the circuits to conduct these experiments. Mathematical simulation of the process is therefore necessary in order to make a preliminary determination of the most promising routes for optimizing the processes. Simulation has continued to be a decision support tool in all stages of mineral processing projects; from the conceptual design, through the development, implementation, commissioning and operational stages. By modeling the system, the process engineer reduces the surprises that can happen in designing complex systems and can use simulation as a cost-savings and cost avoidance tool during design phases of a project. It allows the designers to „test drive" and optimize a system before a design is finalized and implemented.

The combination of energy intensive and poor performance of comminution process implies that there is a great opportunity for significant energy and economic savings by the improvement of this process (Rosario 2010) . Even small improvements to the power utilization efficiency can have a significant influence on the economic performance of a plant. Hence, continued research and development that will contribute to continued efforts in improving these processes is necessary for the long term viability of the mining industry and is the main motivation for the present investigation.

2 The Grinding Circuit at Buzwagi Gold Mine

Buzwagi Gold Mine (BGM) is owned by Pangea Minerals Limited and operated by Acacia Mining. It is located in the Lake Victoria Goldfields of central Tanzania. The mine treats a sulphide gold ore to produce gold in form of doré bars and a concentrate containing gold, copper and silver. The average ore feed grade is approximately 1.8 g/t Au, 1.6 g/t Ag and 0.12 % Cu.

According to the flowsheet of the process plant, the grinding circuit consists of one SAG mill with 8.53 m diameter and 4.35 m EGL (Effective Grinding Length) and one ball mill with 6.10 m diameter and 9.05 m EGL, each with an installed power of 6 MW. Figure 2-1 presents a simplified section of BGM grinding circuit. The overall flowsheet of the process plant is shown in Appendix A.

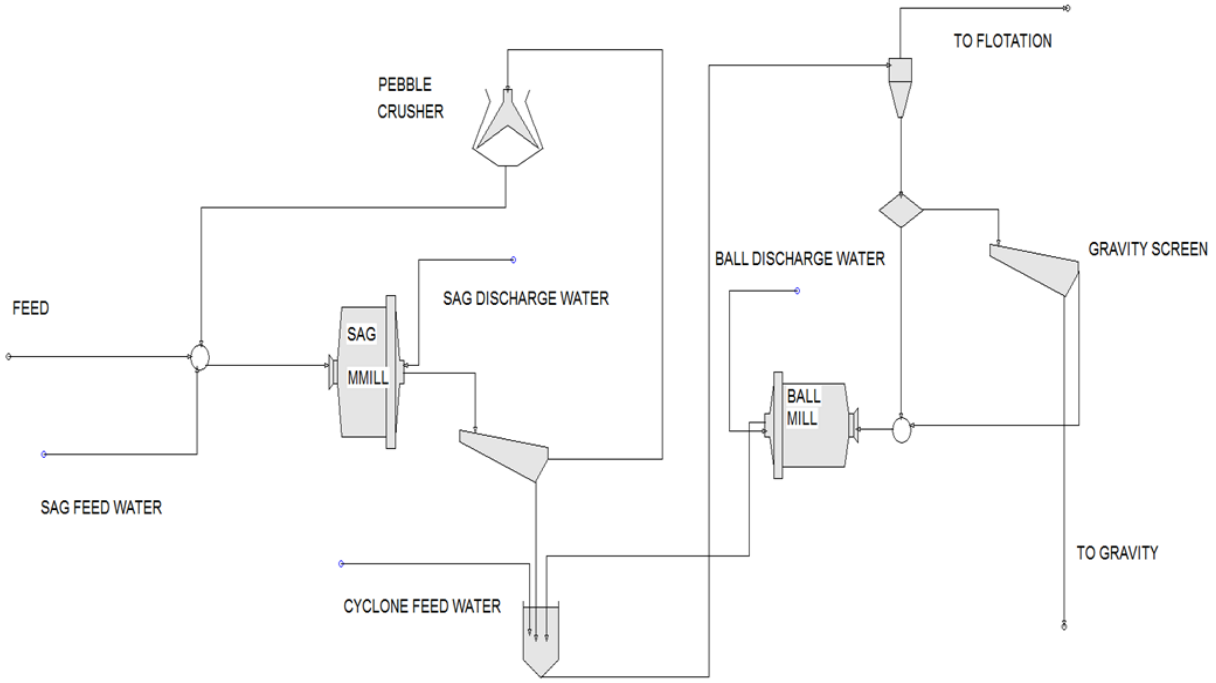

Figure 2-1: Simplified BGM grinding circuit showing major equipment.

The discharge from the SAG mill is controlled by steel discharge grates and the SAG mill product is discharged onto a 3.05 m x 6.10 m vibrating single deck heavy duty pebble dewatering screen. The oversized pebbles (+10 mm) are washed free of residual slurry and transferred to the pebble crusher via pebble discharge and transfer conveyors. A Metso HP500 cone crusher crushes the pebbles from a nominal top size of 70 mm to a product size $x_{P,80}$ of approximately 12 mm. Crushed pebbles are transferred back to the SAG mill feed conveyor via pebble crusher discharge conveyor.

The discharge from the SAG mill, ball mill, and gravity circuit are combined into a common discharge hopper and diluted with process water prior to being pumped to the cyclones. 10 x 660 mm diameters Krebs gMax hydrocyclones are installed (for details see Appendix A). Cyclone overflow flows through two 3.05 m x 6.10 m vibrating single deck heavy duty trash screens for grit and woodchip removal. Trash screen oversize reports to the trash bay and underflow to the flotation. Underflow from 6 cyclones (5 operating, 1 standby) flows to the ball mill feed distribution box. Underflow from 4 cyclones (2 operating, 2 standby) flows to the gravity scalping screens.

2.1 Research Problem

Buzwagi Gold Mine commenced its operation in April 2009 and since then the grinding circuit has been inefficient in achieving the optimum product fineness as can be reflected in Figure 2-2. The circuit was designed to produce final product size of 125 µm, which is not achieved under both, low to normal (i.e. 450-600 t/h) and high (i.e. > 650 t/h) throughputs. It is also reported that the performance behavior of the circuit has not been reviewed since its commissioning. The problem is anticipated to have not only lowered the flotation performance, but also given blindness on the state of the art performance of the overall process plant.

Therefore, any effort aimed at improving the performance of the operation became necessary. This could be achieved through several full scale plant surveys in order to analyze the state of the art performance of the circuit as well as to investigate and improve ore breakage and grindability properties through feed ore characterization.

Furthermore, based on analysis of the survey data and feed ore characterization tests, circuit optimization opportunities could be implemented by using a suitable modelling and simulation technique.

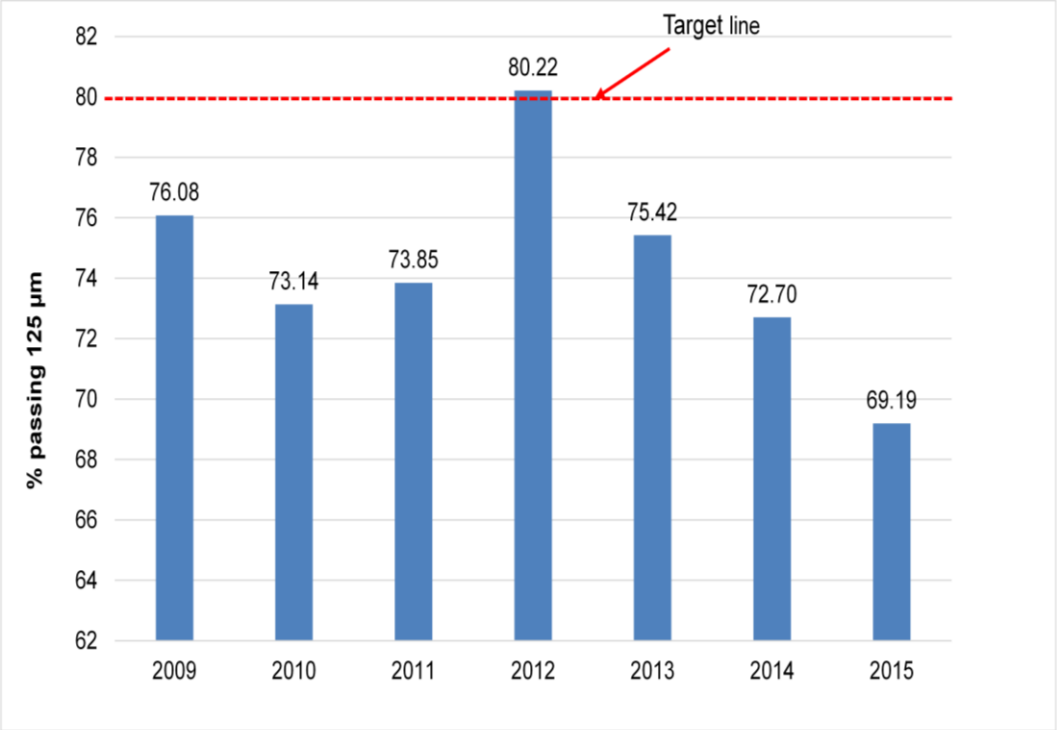

Figure 2-2: BGM grinding circuit efficiency trends from 2009 to 2015.

2.2 Research Objectives

The main objective of this work is to improve the product fineness for the BGM grinding circuit from $x_{P,80} > 125$ µm to $x_{P,80} \leq 125$ µm. This will be achieved through the following specific objectives:

- Assessing the performance of the grinding circuit using plant survey data
- Developing concepts to improve the performance of the grinding circuit by computer simulation
- Investigating the influence of ore composition on specific energy consumption and mineral liberation

3 Literature Survey

3.1 Comminution

In mineral processing, comminution is a process whereby the ore is reduced by blasting, crushing, and grinding to the particle size required for downstream processing. Because most minerals are finely disseminated and intimately associated with gangue, they must be initially liberated before separation can be undertaken (Wills and Napier-Munn 2006). Comminution liberates valuable minerals from the ore matrix, thereby increasing the surface area for higher reactivity (in hydrometallurgy) and facilitating the particle transport between unit operations (Masuda, Higashitani et al. 2007).

Crushing reduces the particle size of run-of-mine ore to such a level that grinding can be carried out until the mineral and gangue are substantially produced as separate particles (Fuerstenau and Han 2003, Wills and Napier-Munn 2006, Masuda, Higashitani et al. 2007). Crushing devices are usually fed by up to 2 m lump ore, which is reduced to 10–200 mm size. The crusher product is then fed to grinding processes and is reduced to between 2 mm to 74 µm (Mular, Haibe et al. 2002, Rao 2011). Various types of crushing and grinding equipment have been used industrially as mechanical way of producing particulate solids. The working phenomena in these types of equipment are complex, and different principles are adopted.

The mechanism of size reduction by crushers is based on the slow compression of large particles against rigid surfaces (Sba'rbaro and Villar 2010) or by particle impact against surfaces in a rigidly constrained motion path. Crushing is usually a dry process and performed in several stages with small reduction ratios, ranging from 3 to 6 in each stage (Wills and Napier-Munn 2006).

Grinding is most frequently performed in rotating cylindrical steel vessels known as tumbling mills. These mills usually contain a charge of loose crushing bodies (grinding medium) which is free to move inside the drum, breaking the ore with the combination of impact, attrition and abrasion forces, producing the specified product size. The grinding media normally employed in tumbling mills are steel rods or balls, ceramic pebbles, hard rock, or in some instances, the ore itself. Grinding is usually performed wet", although, dry grinding has limited applications (Schlanz 1987, Mular, Haibe et al. 2002, Wills and Napier-Munn 2006).

Grinding processes can also be performed in stages utilizing different equipment combinations. The primary grinding stage can be carried out by rod mills, in which the grinding media consists of iron rods, by autogenous mills, which use large ore particles, and by semi-autogenous mills, which use a small load of balls and big lumps of the ore. The final stages of grinding in mineral processing (secondary and rarely tertiary) are normally accomplished by ball mills, where the grinding media is made of steel balls or slugs. In a very few cases, ball mills are also used in the primary grinding stage. The discharge product of the ball mills requires size classification via hydrocyclones or mechanical classifiers such as rake or spiral, to produce a fine stream (cyclone overflow) which is fed to the separation circuits, and a coarse stream (cyclone underflow) which is returned back to the ball mill for further grinding (Sba'rbaro and Villar 2010).

Mills continue to be the power house of most new comminution circuits. The current trend has seen repeated installation of a large, low capital cost, generic circuits featuring two or three stages of crushing, a large SAG mill(s), or to a lesser extent AG mill (s), followed by one or two large ball mills with a single stage of classification. These types of comminution circuits (more details in chap. 3.3.2) are favoured over the traditional multistage crushing and rod mill/ball mill circuits, primarily due to the lower operating costs, fast ramp up time and large throughput capacity (Pokrajcic and Lewis-Gray 2010).

3.1.1 Particle Breakage Mechanisms

By knowing the fracture mechanism of a specific ore, proper design and selection of comminution machines with higher efficiency can be achieved. Fracture of particles occurs as a result of the application of an external force. When an external force is applied, stress develops within the particle. When this stress exceeds the ultimate stress, the particle will break (Rao 2011). The manner in which the particle fractures depends on the nature of the particle material and inner structure and on the manner in which the force on the particle is applied (Rumpf 1965, Schönert 1996, Gupta 2003).

The size reduction devices which are in use today break particles by applying various types of forces (e.g. compressive, shear, impact or abrasion) to the assemblages of particles. The strength of a particle is defined as the applied stress at the first breaking point. In this case breaking strength is the force per unit area of a particle cross section at the point of first fracture, whereas breaking energy is the work that must be applied

to get it to fracture (Fuerstenau and Han 2003). The breaking energy is the integral of the applied force over the resulting deformation. It is important to realize that the actual strengths of materials are much lower than their theoretical strengths (Fuerstenau and Han 2003), which is due to material defects in the inner structure.

The underlying assumption of the theoretical strength is that the material is homogeneous. However, flaws are always present in normal bulk materials as lattice faults, grain boundaries, and microcracks. Stress concentrations at these flaws are much larger than in other portions of the body. Owing to the higher stress levels, fracture will initiate at these points. Thus, the actual strength is lower than the theoretical strength because of the presence of these flaws. Fracture of materials occurs with the initiation and propagation of cracks. The energy consumed in the fracture or breakage of materials goes to the extension of these cracks. Some of the energy consumed by cracks is caused by the creation of new surfaces, (specific surface free energy), and to the plastic deformation of material near the crack tip (Fuerstenau and Han 2003).

Basically, materials can be classified as either ductile or brittle. A ductile material, when stressed to failure, will normally break into two pieces. Stressing of a brittle material will result in shattering, or breakage into many pieces of different sizes of which the fracture paths cannot be controlled. Because ores behave as a brittle material, the pattern of breakage presents problems in grinding by attempting to create fracture within specified limits without having any control over the fracture process.

Griffith (1921) showed that materials fail by crack propagation when this is energetically feasible, i.e. when the energy released by relaxing the strain energy is larger than the energy of the new surface produced. Brittle materials relieve the strain energy mainly by crack propagation, whereas "tough" materials can relax strain energy without crack propagation but instead by the mechanism of plastic flow. Here the atoms or molecules slide over each other and energy is consumed in distorting the shape of the material. Crack propagation can also be inhibited by encounters with other cracks or by meeting crystal boundaries (Wills and Napier-Munn 2006).

Real particles are irregularly shaped, and loading by external forces is not uniform but is achieved through points, or small areas, of contact. Therefore, the mechanism into which particles fracture depends on the external forces model of loading (i.e. direction

or point of application of the force) (Schlanz 1987). Hence, particles can fracture through (Figure 3-1):

- Impact or compression, where forces are applied normally
- Chipping, where forces are applied obliquely and
- Abrasion or attrition, where forces are applied parallel

Regardless of the mechanism involved, in any fracture process the particle must be submitted to a state of strain which will initiate the propagation of fracture cracks. In order to create this state of strain, energy larger than or equal to the stored strain energy of the particle must be supplied. The following factors are determinants for the amount of energy required to initiate the propagation of fracture cracks (Schlanz 1987):

- Presence of pre-existing cracks or flaws
- Degree of plastic flow in the solid vs. complete brittleness
- Geometry and rate of stress application

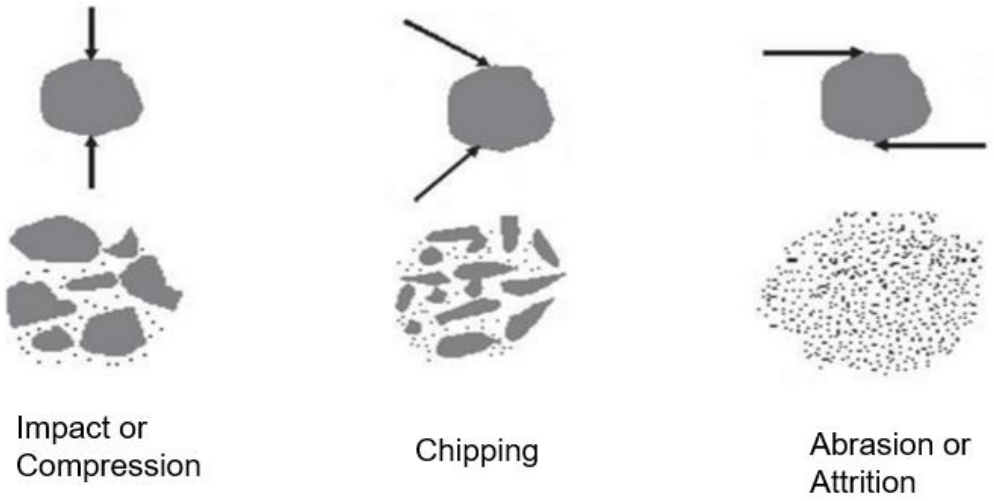

Figure 3-1: Particles Breakage Mechanisms (adopted from (Rao 2011).

When an irregular particle is broken by compression, as in crushing, the products fall into two distinct size ranges; coarse particles resulting from the induced tensile failure, and fines from compressive failure near the points of loading or by shear at projections. The amount of fines produced can be reduced by minimising the area of loading which is often done in compressive crushing machines by using corrugated crushing surfaces (Wills and Napier-Munn 2006).

In impact breaking, due to the rapid loading, a particle experiences a higher average stress while undergoing strain than is necessary to achieve simple fracture, and tends

to break apart rapidly, mainly by tensile failure. Many areas in the particle are overloaded and the result is a comparatively large number of particles with a wide size distribution. Impact causes immediate fracture with no residual stresses.

Abrasion fracture occurs when a force (i.e. shear force) acts parallel to the surface of the particle. Due to insufficient energy applied on the particle, localized stress occurs and a small area is fractured to generate very fine particles. Abrasion occurs due to particle-particle interaction, which may occur if a crusher is fed too fast, contacting particles thus increasing the degree of compressive stress and hence shear failure (Wills and Napier-Munn 2006, Rao 2011).

In practice, these events do not occur in isolation. For example, when particles are crushed by compression in a jaw crusher, coarse particles will be produced resulting from the induced tensile stress, while, fine particles will be produced from compressive stress near points of loading and by attrition due to particles interaction (Rao 2011).

3.1.2 Comminution Laws

In design, operation, and control of comminution processes, it is necessary to correctly evaluate the comminution energy (i.e. size reduction energy). The main challenge in quantifying the comminution energy lies in the fact that most of the energy input to a crushing or grinding machine is absorbed by the machine itself or lost due to friction, and only a small fraction of the total energy is available for breaking the material (Napier-Munn, Morrel et al. 1996, Wills and Napier-Munn 2006). It is to be expected that there is a relationship between the energy required to break the material and the new surface produced in the process, but this relationship can only be made evident if the energy consumed in creating new surfaces can be separately measured (Wills and Napier-Munn 2006). Over the history, semi-empirical energy-size reduction relationships were proposed by Rittinger, Kick, and Bond, known as comminution laws (Francioli 2015). Nevertheless, none of these three laws is applicable over a wide range of sizes (Rao 2011).

Various attempts have been made to show that the relationships of Rittinger, Kick, and Bond are interpretations of single general equations and were unsuccessful for a large range of particle sizes. Hukki (1975) as cited in Wills and co-workers (Wills and Napier-Munn 2006) suggests that the relationship between energy and particle size is a composite form of the three laws and pointed out different applicability regions for each comminution law as shown in Figure 3-2. The probability of breakage in comminution

is high for large particles, and rapidly diminishes for fine sizes. He shows that Kick's law is reasonably accurate in the crushing range above about 1 cm in diameter; Bond's theory applies reasonably in the range of conventional rod-mill and ball-mill grinding, and Rittinger's law applies fairly well in the fine grinding range of 10-1000 microns (Francioli 2015).

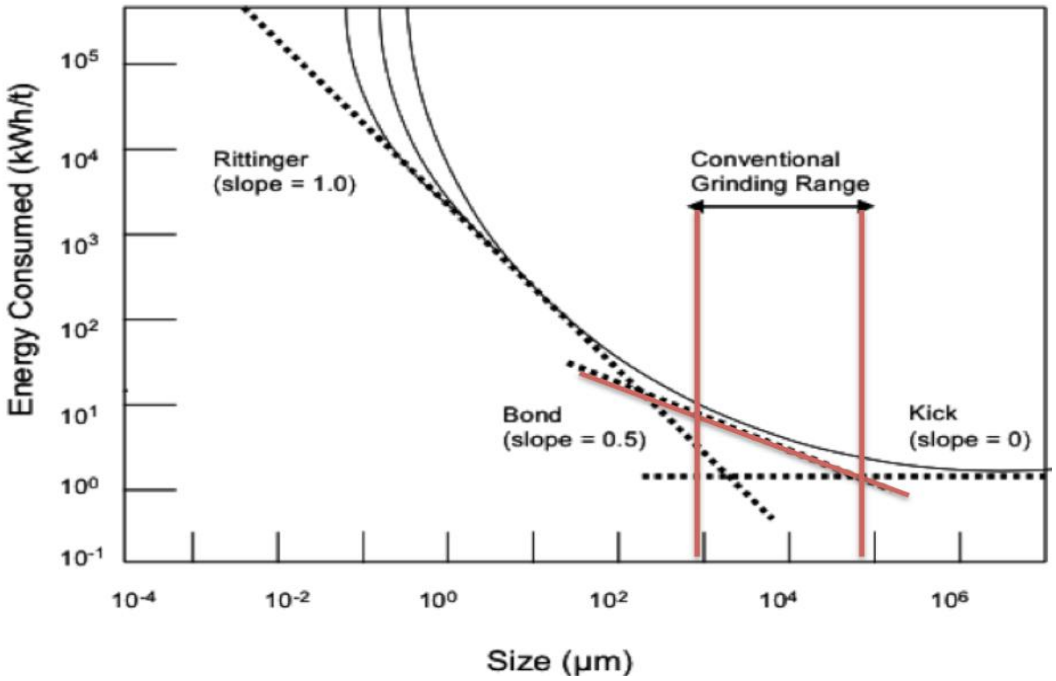

Figure 3-2: Relationship between Energy Input and Size Reduction in Comminution (after Hukki 1961).

Although Bond was successful at theoretically proving his assumption, it is known nowadays that Bond's law is an empirical relation that provides acceptable fit to results from grinding experiments. Moreover, Bond's theory is still commonly used as a tool for sizing crushing and grinding equipment in the industry. It is also recognized that this methodology may present discrepancies around 20% in respect to the actual energy consumption for ball mills and even higher in for crushers (Francioli 2015).
Several aspects of the current investigation rely on Bond's third law and this section will mainly concentrate on the same.

Bond's Law

The third law of comminution was proposed by Bond in 1952. He suggested that any comminution process can be considered as an intermediate stage in the breakdown of a particle of infinite size to an infinite number of particles of zero size. Bond states that the total work applied to a homogeneous broken material is inversely proportional to the square root of the average size of the product particles, direct proportional to the

length of crack tips formed and direct proportional to the square root of the new surface created (Bond 1952).

This law assumes that the work input,*W* is proportional to the new crack tip length produced in particle breakage, and equals the work represented by the product minus that represented by the feed (Bond 1952). For particles of similar shape, the surface area of unit volume of material is inversely proportional to the diameter. The crack length in unit volume is considered to be proportional to one side of that area and therefore inversely proportional to the square root of the diameter (Bond 1952). Mathematically, Bond's law is expressed as:

$$W = K\left(\frac{1}{\sqrt{x_2}} - \frac{1}{\sqrt{x_1}}\right) \tag{1}$$

Where *K* is Bond's constant (i.e. work index, W_i) and can be determined experimentally in the laboratory. The work index is an important factor in designing comminution processes and has been widely used (Masuda, Higashitani et al. 2007). W_i is defined as the energy required, in kWh/t, to reduce 1 ton of the material from an infinite size to a point where 80 % of the material passes the 100 microns sieve. This size is commonly referred as $x_{P,80}$ and the third law of comminution can then be re-written based on this definition as follows:

$$\text{If} \quad x_{F,80} = \propto \text{ and } x_{P,80} = 100 \text{ μm} \tag{2}$$

Then,

$$W = W_i \Rightarrow K = 10 * W_i \tag{3}$$

Thus, Bond's equation becomes;

$$W = W_i\left(\frac{10}{\sqrt{x_{P,80}}} - \frac{10}{\sqrt{x_{F,80}}}\right) \tag{4}$$

Bond's comminution law can be applied for crushers, rod and ball mills. Thus, W_i is different depending on the equipment and must be measured separately. The standard Bond's laboratory test to determine W_i was designed to produce an index that would correctly predict the power required by a test with specified parameters. In order to apply Bond's equation to industrial mills, which differ from the standard, a series of efficiency factors should be taken into consideration (King 2001, Francioli 2015).

In Bond's Eqn. (1) the grinding energy, W_G, required for size reduction of rocks in industrial tumbling mills was based on mills shaft power, P_S, and on mill capacity ($\dot{m}$). The relationship between these parameters is:

$$W_G = \frac{P_S}{\dot{m}} \tag{5}$$

On the basis of Hukki's evaluation, Morrel (Morrell 2004) has proposed a modification to Bond's equation and explains that a more appropriate energy-size relationship relies on the particle size exponent that is a function of size as follows Eqn. (6):

$$W = \frac{KM_i}{x_{P,80}^{f(x_{P,80})}} - \frac{KM_i}{x_{F,80}^{f(x_{F,80})}} \tag{6}$$

Where M_i is the material index related to the breakage property of the ore and K is a constant chosen to balance the units of the equation.

By working with industrial data for 27 AG/SAG and ball mills sets, the form of the exponent function (i.e. f($x_{P,80}$ or $x_{F,80}$) was obtained (Morrell 2004) as:

$$f(x) = \left(a^* + x^{b^*}\right) \tag{7}$$

Where a^* and b^* are constants, x=80 % passing size

The application of the new energy-size relation has been shown to be valid across the size range covered by most modern grinding circuits, i.e. with work indices from the standard Bond tests 0.1-100 mm (Wills and Napier-Munn 2006).

3.1.3 Mineral Liberation

According to Wills (Wills and Finch 2016), mineral liberation, also termed as ''the degree of mineral liberation'' refers to the percentage of the mineral occurring as free particles in the broken ore in relation to the total mineral content in locked and free particles. The main purpose of a mineral beneficiation plant is to separate the valuable components of the ore from the worthless parts, and to concentrate them to make a saleable product. The concentration steps are usually preceded by a comminution stage whose purpose is to break the ore to a size small enough to free or liberate the valuable components from the gangue (Napier-Munn, Morrel et al. 1996, Wills and Finch 2016). It is well known that comminution constitutes a large part of the cost of mineral processing: it is therefore important to avoid overgrinding while sufficiently liberating the valuable minerals (Bérubé and Marchand 1984).The current practice is

to try to obtain a product with a steep particle size distribution at the grinding stage in order to improve separability of the material. Unfortunately, the textural properties of the valuable mineral phases may vary naturally in the orebody and such a strategy may involve either too low or too high a liberation. The degree of liberation must then be verified periodically, or at least each time the characteristics of the mineralization are suspected to have changed (Bérubé and Marchand 1984).

An objective of comminution is to achieve liberation at the coarsest possible particle size. If such an aim is achieved, then not only is energy saved but also by reducing the amount of fines produced any subsequent separation stage becomes easier and cheaper to operate, also the throughput will be increased (Wills and Finch 2016). However**,** effective liberation of material of value remains one of the major challenges in treating modern ores which, due to the increasing complexity and smaller grain sizes, requires finer grinding to achieve the necessary degree of liberation (Veasey and Wills 1991, Danha 2013).

One of the most critical design criteria for mineral processing plants is the choice of size to which the comminution step has to reduce the host rock (optimum grind size or mesh of grind) to ensure an economic level of liberation. Size reduction and liberation are inextricably linked. If the size to which the rock is reduced is insufficient, then a relatively large proportion of the valuable constituents will not be extracted, leading to loss of potential revenue. If the size chosen is too small, an oversized and over costly plant with unnecessarily high energy costs will result. To ensure an efficient process, therefore, mineral liberation and its association with size reduction should be well characterized (Napier-Munn, Morrel et al. 1996)**.**

A particle is liberated when its composition is such that the downstream process can selectively recover it into a concentrate (or conversely, if it is gangue material, reject it). An extreme example is a particle of a single phase (value or gangue) whose composition is then no longer a limiting factor in its recovery (Figure 3-3). The figure shows an imaginary multiphase section of rock before and after breakage, illustrating the different forms of particle which are the products of comminution. It is clear that the size of each phase and its relationship to every other phase, both before and after breakage, is critical to understanding and describing the liberation process. These relations are collectively embodied in a property called the *texture* of the rock**.**

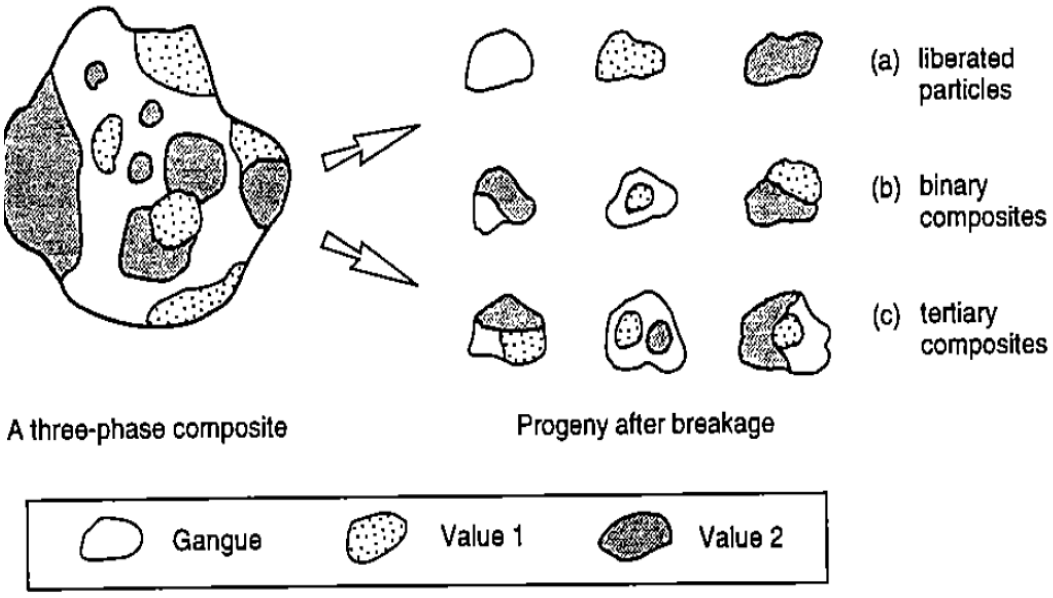

Figure 3-3: Variation in Mineral Association for Progeny Particles from Breakage of Multiphase Composite (Napier-Munn, Morrel et al. 1996).

It should be noted that a high degree of liberation is not always necessary and may be undesirable in some cases. For instance, it is possible to achieve a high recovery of values by gravity and magnetic separation even though the valuable minerals are completely enclosed by gangue, and hence the degree of liberation of the values is zero. As long as a pronounced density or magnetic susceptibility difference is apparent between the locked particles and the free gangue particles, the separation is possible. However, the quality of such concentrates is low as the valuable mineral phases are partly still locked with gangue. On the other hand, leaching and flotation require at least a surface of the valuable mineral to be exposed (Wang, Shi et al. 2012, Wills and Finch 2016). In practice, ores are ground to an optimum grind size, determined by laboratory and pilot scale testwork, to produce an economic degree of liberation. The concentration process is then designed to produce a concentrate consisting predominantly of valuable mineral, with an accepted degree of locking with the gangue minerals, and a middlings fraction, which may require further grinding to promote optimum release of the minerals. The tailings should be mainly composed of gangue minerals (Wills and Finch 2016).

Apart from being relatively energy consuming, tumbling mills are also inefficient with regard to mineral liberation because of the random (non-selective) nature of the grinding forces. Approaches to increase the degree of liberation involve directing the breaking stresses at the mineral grain boundaries, so that the rock can be broken without breaking the mineral grains (Wills and Atkinson 1993). For example,

microwaves can be used, which cause differential heating among the constituent minerals and thus create stress fractures at grain boundaries (Kingman, Jackson et al. 2004). However, the industrial applicability of this technology remains an unresolved challenge (Somani, Nandi et al. 2017). Liberation can be high if there are weak boundaries between mineral and gangue particles, which is often the case with ores composed mainly of rock-forming minerals, particularly sedimentary minerals. This is sometimes referred to as “liberation by detachment”. Usually, however, the adhesion between mineral and gangue is for most ores as strong as a the durability of the individual components and thus during comminution the various constituents are split across the grain boundaries; that is, breakage is random (Wills and Finch 2016).

Many researchers have tried to quantify (model) the degree of liberation (King 2012). These models, however, suffer from many unrealistic assumptions (i.e. pure random breakage and isometric particle shape) that must be made with respect to the grain structure of the minerals in the ore. For this reason liberation models have not found much practical application. However, some fresh approaches by Gay (Gay 2004) have demonstrated that there may yet be a useful role for such models**.** Figure 3-4 shows predictions using the simple liberation model based on random breakage derived by Gaudin (1939) as cited in Hsih and co-worker (Hsih and Wen 1994).The model (Eqns. (8) and (9)) is sufficient to introduce an important practical point.

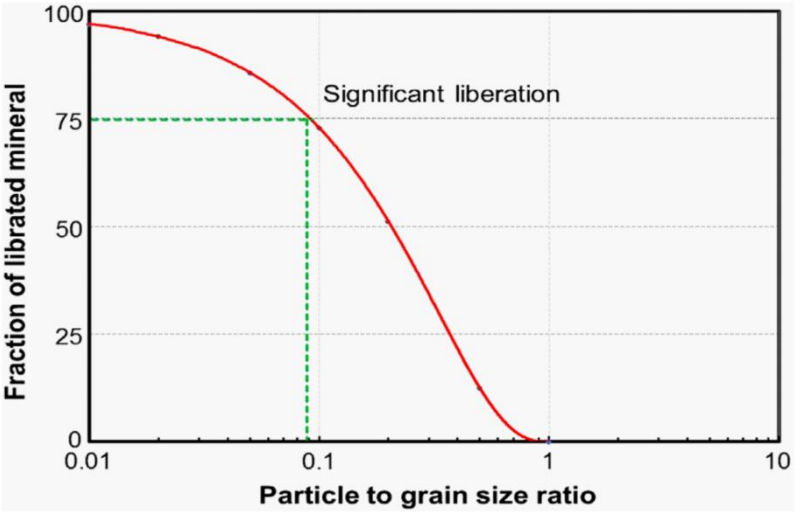

Figure 3-4: Degree of Liberation as a Function of Particle to Grain Ratio (adopted from Gaudin Model (1939).

$$L_m(x) = \frac{(K-1)^3}{K^3} \qquad K > 1 \tag{8}$$

And

$$L_m(x) = 0 \qquad K \leq 1 \tag{9}$$

Where $L_m(x)$ =fractional degree of liberation of the less abundant mineral (less than 50 % by volume fraction), $K=G/x$, G= grain size of mineral m in the uncrushed ore, and x= particle size of the crushed ore.

In Figure 3-4, the degree (fraction) of liberation is given as a function of the particle size to grain size ratio and illustrates that to achieve high liberation, say 75 %, the particle size has to be much smaller than the grain size, in this case ca. 1/10th the size. So, for example, if the grain size is 1 mm then size reduction must produce a particle size at least 0.1 mm (100 µm) or less, and if the grain size is 0.1 mm the particle size should be 10 µm or less. This result helps in understanding the fine size required from the comminution process (Wills and Finch 2016).

Considering the today's challenge for increasing ore body complexity, improving the plant throughput and process efficiency will not only depend on large equipment, but rather, governed by the ore feed mineralogy, texture and better control of the variance thereof (Petruck 2000, Baum 2014, Cropp and Goodall 2017). Hence, substantial mineralogical characterization is required in order to avoid poor processing performance (Baum, Lotter et al. 2004, Hoal, Stammer et al. 2009, Evans, Wightman et al. 2011, Lotter 2011, Smythe, Lombard et al. 2013, Baum 2014).

A conventional optical microscopes can be used for examination of thin and polished sections of mineral samples. However, it is today increasingly common to employ quantitative automated mineral analysis using scanning electron microscopy combined with energy dispersive X-ray analysis, such as the Mineral Liberation Analyser (MLA) (Gu 2003, Fandrich, Gu et al. 2007), the QEMSCAN (Gottlieb, Wilkie et al. 2000), and the Tescan Integrated Mineral Analyser (TIMA), which scan polished sections using an electron beam to generate 2D mineralogical information, and X-ray microcomputed tomography (micro CT) that allows for 3D visualization of particulates (Wills and Finch 2016).

3.2 Tumbling Mills

A tumbling mill consists of a horizontal rotating steel shell supported by end bearings (e.g. Figure 3-5) on which hollow trunnions revolve (Wills and Napier-Munn 2006, Rao 2011, Wills and Finch 2016). Usually the material is fed at one end of the mill and discharged at the other end. Loose grinding bodies, known as grinding medium (i.e. steel balls, rods or pebbles), are placed inside the shell. They are free to move inside the rotating shell making the particles break by repetitive blows and by rolling and sliding one over the other.

Attrition, or shearing, forces which result from the application of forces by rolling and sliding bodies (see also chap. 3.1.1) tend to produce more fine particles than impact forces applied on particles by repetitive blows (Rao 2011).

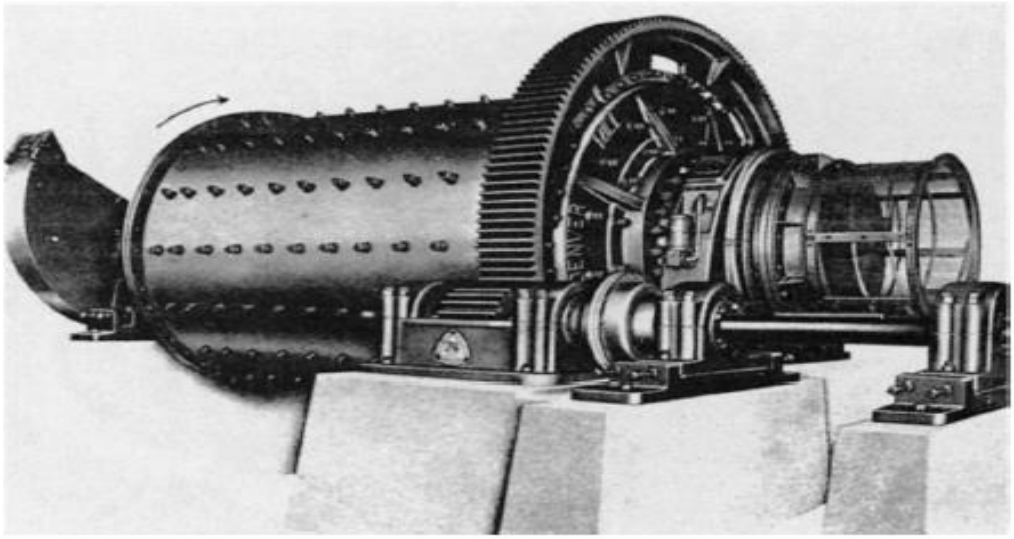

Figure 3-5: Tumbling mill (Wills and Finch 2016).

The interior of tumbling mill is lined by replaceable liners usually made of alloy steel but sometimes of rubber (Wills and Napier-Munn 2006, Rao 2011, Wills and Finch 2016). Some types of liners are smooth, shiplap, wave, wedge bar, rib, stepped, osborn, lorain, etc (Figure 3-6). Smooth liners favour abrasion resulting in fine grinding but high metal wear. Liners other than smooth are designed to help in lifting the ball load as the mill is revolved and sometimes to minimize the slip between the layers of balls. Also liners protect the mill body from wear and damage (Rao 2011).

Tumbling mills are grouped based on the grinding medium used as follows (Schlanz 1987, Wills and Napier-Munn 2006, Rao 2011, Wills and Finch 2016):

- Rod mills; charged with steel rods.

- Ball mills; charged with steel balls.
- Autogenous/Semi-autogenous (AG/SAG) mills; charged with large lumps of ore (AG), charged with large lumps of ore and some steel balls (SAG).

The mill diameter determines the level of impacts exerted by the grinding media on the ore particles. Larger mill diameter is therefore required for larger feed size material. Further, the mill length determines its volume and hence the capacity (Wills and Napier-Munn 2006, Wills and Finch 2016).

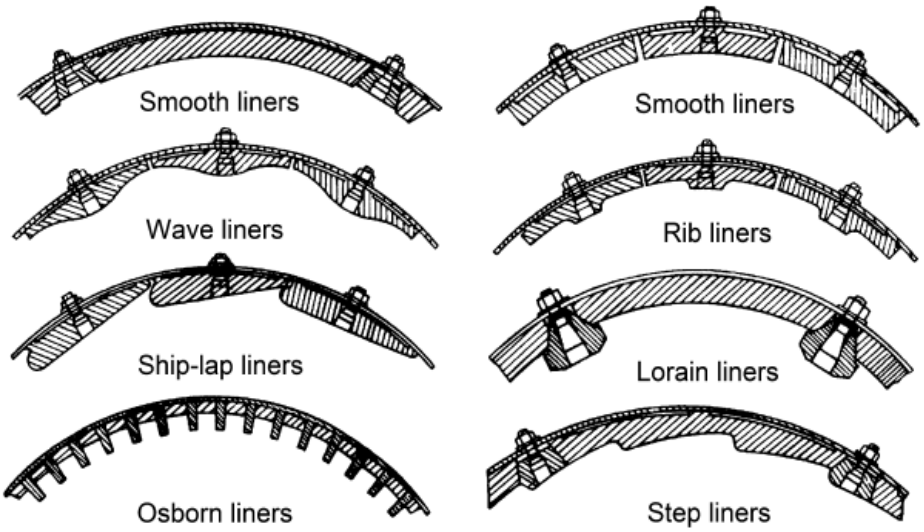

Figure 3-6: Mill shell liners (Wills and Finch 2016).

Tumbling mills can be operated wet or dry, batch-wise or continuously. They are robust and the loose grinding medium can usually be added without stopping the mill. Nevertheless, tumbling mills are relatively high in power consumption and require expensive foundations (Rao 2011).

Currently, Semi-autogenous (SAG) and ball mills are the dominant, especially in the precious metals industry .The same type of devices are also installed at Buzwagi Gold Mine, which is the case study for the present investigation. Hence, an overview of the operational aspects of these mills will be the main focus in this section.

3.2.1 Operation of Tumbling Mills

Irrespective of the grinding media utilized all tumbling mills effect the breakage by the same basic principles. When the mill rotates the grinding charge is raised from a level surface position with liners preventing slippage of the charge so that the media moves with the shell until they fall and tumble down over the mass of the charge. The pattern in which the charge tumbles (Figure 3-7) is related to the speed of rotation of the mill.

Cascading describes the portion of the media that tends to roll down to the toe of the mill which results in abrasive-type comminution, leading to finer grinding and increased liner wear. Cataracting is experienced by the portion of the charge that is raised high enough in the mill to actually fall back down to the toe. This action leads to impact comminution, which produces coarser product. In actual operation most mills utilize a combination of cascade and cataract movement. This is due to the concept that most of the grinding action in the mill takes place at the toe of the charge, where not only is there direct impact of the cataracting medium on to the charge, but also the ore packed between the cascading medium receives the shock transmitted (Wills and Napier-Munn 2006) .

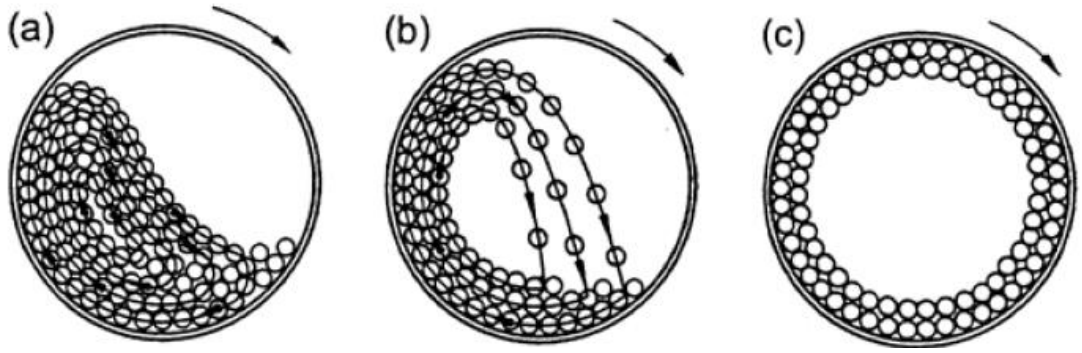

Figure 3-7: Radial motion states in a tumbling mill, (a) unrolling (cascade movement), b) - falling (cataract movement), c) centrifugation (Schubert 2003).

For each mill there is a critical speed that creates centrifuging (Figure 3-7-c) of the charge and no tumbling action occurs. The media is theoretically carried around in a fixed position against the shell. Hence, tumbling mills have to be operated at a percentage of this critical speed to achieve correct tumbling patterns.

With the help of Figure 3-8, the concepts used in derivation of tumbling mill's critical speed are summarized .The critical speed of the mill N_c, is defined as the speed at which a single ball will just remain against the wall for a full cycle. At this point, the centrifugal (F_{cf}) and gravitational forces (F_g) (Eqn. (10)) are in balance (King 2001, Wills and Napier-Munn 2006).

$$F_{cf} = m_{pr}\omega^2 \frac{D}{2} = F_g = m_{pr}g \tag{10}$$

And

$$N_c = \frac{\omega}{2\pi} \tag{11}$$

ω is the angular velocity, m_{pr} is the mass of any particle (media or charge) in the mill, D is the diameter of the mill inside liners and g is the acceleration due to gravity.

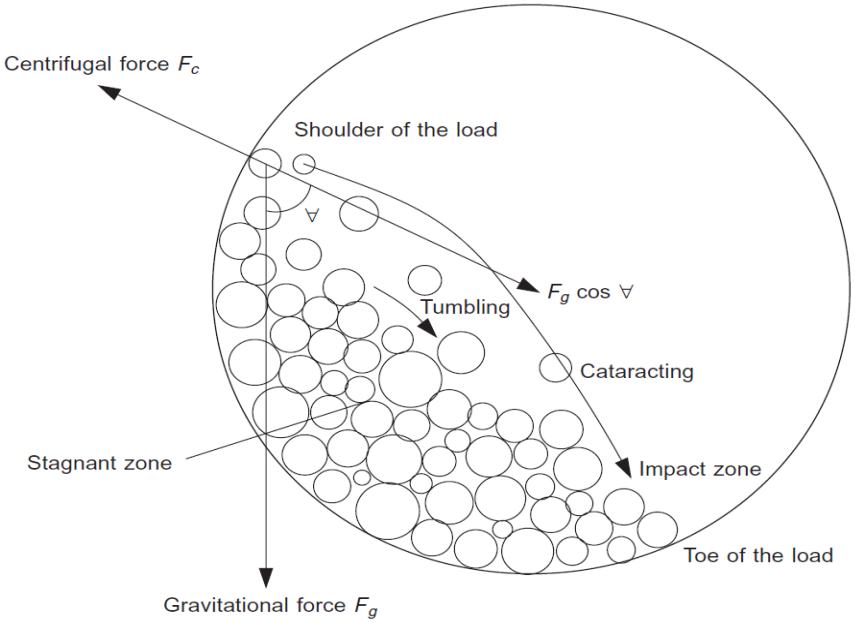

Figure 3-8: Media motion in the tumbling mill (King 2001) .

Under the assumption that the ball diameter is very small compared to the inner diameter of the mill (i.e. $d<<D$), the final relationship between mill critical speed, N_c and relative rotational speed ψ_c, both expressed in revolutions per minute is given as (King 2001, Wills and Napier-Munn 2006):

$$N_c = \sqrt{\frac{g}{2\pi^2 D}} \tag{12}$$

And

$$\psi_c = \frac{N}{N_c} = N \cdot \sqrt{\frac{2\pi^2 D}{g}} \tag{13}$$

In practice, most mills are driven at speeds of 50-90 % of the critical speed, where the choice being dictated by the economic gains (Wills and Napier-Munn 2006).

3.2.1.1 SAG Mill Operation

Semi-Autogenous (SAG) mills utilize steel balls in addition to coarse pieces of the ore itself as grinding media. They can handle feed ore as large as 200 mm and achieve a product of 0.1 mm in one piece of equipment (Wills and Napier-Munn 2006). Since the breakage of ore in SAG mills is mostly due to impact on particles and media from a height, these mills generally have a large diameter to length (*D*/*L*) ratio. They fall into three groups: high aspect ratio mills where the diameter is 1.5-3 times the length, "square mills", where the diameter is approximately equal to the length, and low aspect ratio mills where the length is 1.5-3 times the diameter (Schlanz 1987, Gupta and Yan 2006, Wills and Napier-Munn 2006). A number of variables influence their performance and will be highlighted in following paragraphs.

a) Feed size and ore hardness:

For SAG mills it is usually found that softer ores give a higher throughput. This is due to the fact that coarser rocks, particularly the critical size, are more easily broken by the steel balls. The product size, however, usually becomes coarser. This is because the coarser rocks spend less time being slowly worn away by abrasion and chipping which typically produces very fine products (Napier-Munn, Morrel et al. 1996). The influence of feed size on SAG mill performance is significant due to the fact that a significant amount of the ore acts as grinding media. Any change in the feed size distribution will therefore result in a change in the grinding media size distribution. This will in turn affect the breakage characteristics of the mill. Also any change in the feed ore hardness will affect the breakage of the ore (Wills and Napier-Munn 2006). The mill charge level will also be changed, which affects the mill power draw. In response to the variation in feed size and hardness, the mill feed rate has to be changed significantly (Napier-Munn, Morrel et al. 1996, Wills and Napier-Munn 2006).

b) Mill charge:

A SAG mill is usually charged to 30-35 % of its interior volume. The grinding balls occupy 5-15 % of the volume (Gupta and Yan 2006). The charge volume can be estimated by measuring the distance between the top level of the charge and the central axis of the mill. It can also be computed from known bulk volumes of ore (slurry densities for wet milling) and bulk density of balls. The charge volume may also be measured indirectly during operation by the use of predetermined relationships between mill load and power (Figure 3-9).

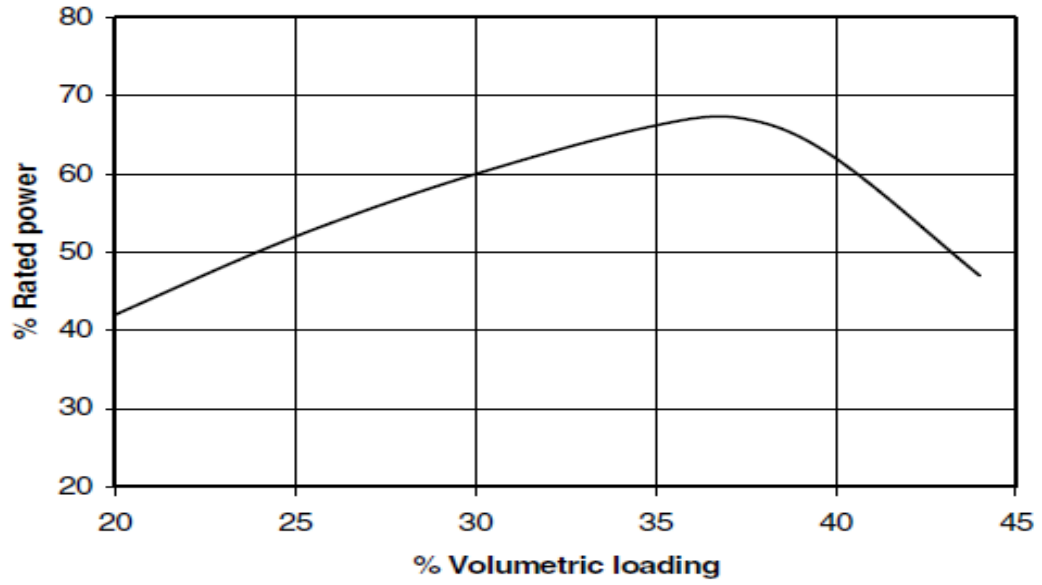

Figure 3-9: Relation between volumetric loading and SAG mill power for low ball charge and soft ore (Gupta and Yan 2006).

c) Ball charge volume and ball size:

The introduction of steel balls in SAG mill is very important especially for the impact breakage where they can generate very high kinetic energies. These sterns from the relatively high specific gravity of steel (7.8-8.0) compared to most ores (2.5-4.5) as well as higher strength. As larger rocks have more mass than smaller ones, more energy is needed to break them. Hence larger steel balls are required if larger rocks are to be broken. However, the choice of ball size will be dictated by the hardness of the ore and its feed size distribution. Softer and/or finer ore will require smaller balls whilst a harder /coarser ore will require larger balls.

d) Mill speed:

Increasing mill speed promotes impact breakage. This usually results in an increase in coarser rock breakage which leads to higher throughputs (Gupta and Yan 2006). The reduction in cascading motion, coupled to the inevitable destruction of ore grinding media, results in less favorable conditions for finer grinding, resulting in a coarser product. The relative operating speed of Autogenous (AG) mills are much higher than conventional tumbling mills (i.e. 80-85 %). SAG mills of comparable size which contain 10 % ball charge, normally operate between 70 to 75% of the critical speed (Gupta and Yan 2006).

As the mill speed is increased the amount of lift imported to the charge increases to a maximum. After this it reduces until, at the point where the mill centrifuges (i.e. lift is

effectively zero). The relationship between lift, as measured by the difference in height between the toe and shoulder (refer Figure 3-8), and mill speed is shown in Figure 3-10. The lift is expressed relative to the mill diameter. The speed at which maximum lift occurs is seen to be a function of mill filling though it is also affected by lifter type/height.

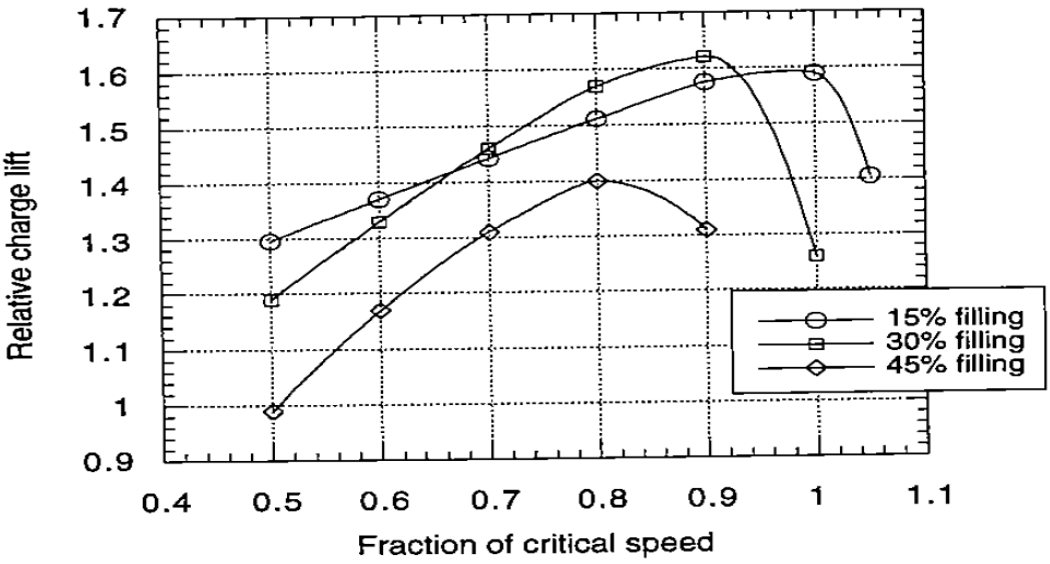

Figure 3-10: Maximum height drop as function of mill speed (Napier-Munn, Morrel et al. 1996).

e) Effect of a classifier on SAG mill circuit:

If a mill is run in closed circuit with a classifier, the flow of material into the mill increases due to the coarser classifier stream feeding back to the mill feed. The mill will therefore fill up with more slurry until sufficient head is developed to allow an equal flow at the grates (see Figure 3-11). Provided the flow of recycle slurry is not too high, it will tend to accumulate in the grinding media interstices. Attrition grinding will then increase and abrasion breakage will increase slightly as well. Also the charge density and hence power will increase. As attrition breakage favors breakage of fine particles, this mechanism is consistent with the requirement of closing the mill circuit with a fine classifier, i.e. finer grinding will result. If the flow of recycle material is increased further, a point will be reached where all the interstices are filled with slurry and therefore attrition grinding will reach its maximum. Any further increase in the recycle flow will lead to slurry build-up in a pool at the toe of the charge which prevents further attrition grinding. This presence of a slurry pool will cause a drop in the power draw. This is caused by a reduction of impact breakage at the toe since the grinding media will no longer directly impact on the toe but has to penetrate the slurry pool, thus reducing the kinetic energy available for breakage. Therefore, when closing a SAG mill circuit, the

classifier must be chosen to give an efficient separation at a cut-point that ensures little or no excess slurry pool at the charge toe (Napier-Munn, Morrel et al. 1996)

f) Effect of the recycle crusher on SAG mill circuit:

A natural phenomenon in SAG mills is that a build-up of pebbles usually occurs in the 25-50 mm size fraction. These can occupy a large volume within the mill and hence be a large contributor to mill power draw. Their occupation of the mill volume prevents more new feed and therefore limits throughput. The material is famously called “critical fraction”. By installing large holes in the grate /pebble ports (e.g. Figure 3-11) up to 100 mm in diameter, pebbles can be removed from the mill and crushed to a size below the critical fraction. The result is that the charge in the mill reduces in volume and mass as does power draw. The throughput of the SAG mill can therefore be increased by the pebble crusher (Napier-Munn, Morrel et al. 1996).

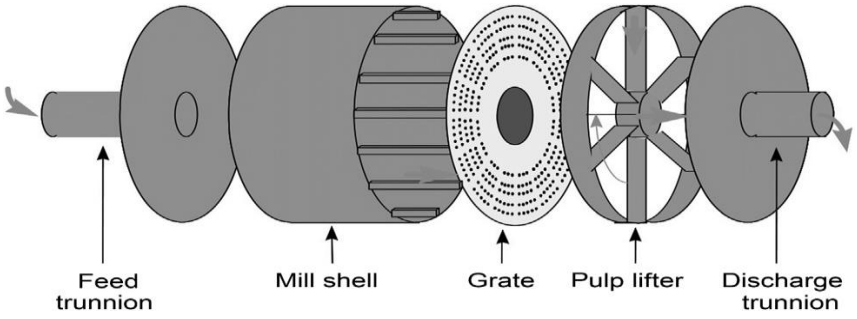

Figure 3-11: Schematic of various sections of an AG mill (Wills and Napier-Munn 2006).

3.2.1.2 Ball Mill Operation

Ball mills utilize steel balls as the only grinding medium. They work effectively over a wide range of length to diameter aspect ratios of 1.5 to 1.0 and even less (Schlanz 1987, Napier-Munn, Morrel et al. 1996, Wills and Napier-Munn 2006). Based on discharge mechanism, two main forms of ball mills exist. The overflow mill (Figure 3-12-b) has an exit hole at the discharge trunnion which is larger than the inlet, generating a hydraulic gradient which drives the slurry through the mill. A scalping screen is normally required to collect smaller or worn-out grinding medium which may overflow with the pulp. Power consumption may be up to 15 % less than the other type although in terms of milling efficiency are nearly equal.

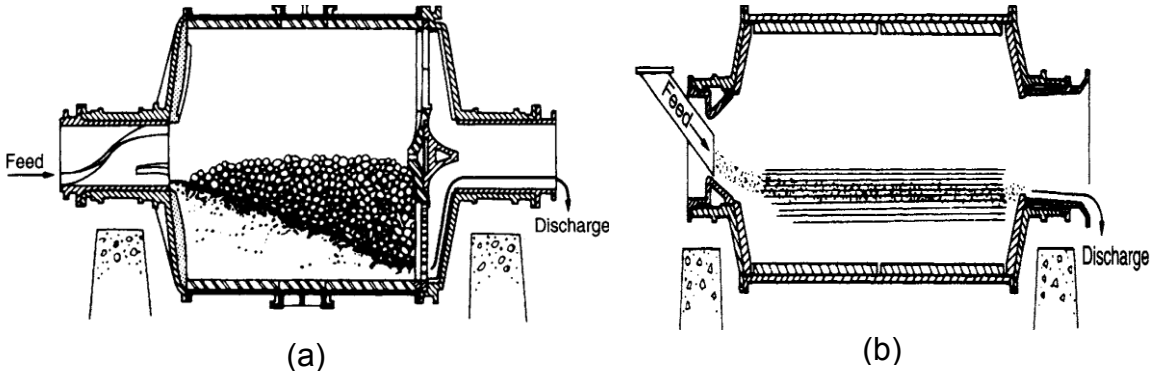

Figure 3-12: **Types of ball mills based on discharge mechanism: (a) grate discharge, b) overflow discharge (Wills and Napier-Munn 2006)).**

The grate discharge mill (Figure 3-12-a) is fitted with discharge grates between the cylindrical mill shell and the discharge trunnion. This type requires a lower pulp density which reduces retention times, resulting to little overgrinding but also discharges a large fraction of coarse particles, necessitating closed circuit configuration (Gupta and Yan 2006, Wills and Napier-Munn 2006). There are several factors influencing ball mills efficiency which will be highlighted in following sections.

a) Charge volume:

It is important that the mill is not overfilled or under filled with the charge. Overloading causes accumulation of fines at the toe of the mill, which leads to a cushioning effect thus absorbing the impact, which causes breakage. When the rock load is low, excessive ball-to-ball contact reduces the rate of breakage. The operator therefore has to compute the optimum quantity of each parameter to obtain the required product size and to maintain the predetermined output rate while maximizing energy efficiency. The percent of mill volume occupied by the charge is a function of the bulk volume of the rock and balls. The ball filling degree (φ_{GM}) in Eqn. (14) is defined as the fraction of the internal volume of the mill occupied by grinding balls at rest including the interstices between the balls. It is estimated as follows (Gupta and Yan 2006, Austin, Julianelli et al. 2007, Mulenga 2017)**:**

$$\varphi_{GM} = \frac{V_b}{V_M} = \frac{M_b}{\frac{\rho_b\left(\pi D^2 L\right)(1-\varepsilon)}{4}} \tag{14}$$

Where M_b and ρ_b are the total mass and specific density of grinding balls loaded in the batch mill; D and L are the internal diameter and length of the mill used; and ε represents the porosity of the grinding balls at rest.

The volumetric fraction of voids between grinding balls at rest that is filled with the dry material to be milled is defined as powder filling ratio (φ_{MG}) and based on Gupta and others (Gupta and Yan 2006, Austin, Julianelli et al. 2007, Mulenga 2017) is given as:

$$\varphi_{MG} = \frac{V_O}{V_V} = \frac{m_O}{\rho_s \left(\frac{\pi D_T^{\,2} L}{4} \right) \varepsilon \varphi_{GM} \left(1 - \varepsilon\right)} \tag{15}$$

m_o and ρ_s are the mass and specific density of the dry ore, respectively.

The maximum possible bed porosity is approximately 40 % and the charge is about 40-50 % of the internal mill volume (Gupta and Yan 2006, Wills and Napier-Munn 2006). The energy input to a mill increases with the ball charge, and reaches a maximum at a charge volume of approximately 50 % (Figure 3-13). In overflow mills the charge volume is usually 40 %, but there is a larger choice for the grate discharge mills. The optimum mill speed increases with charge volume, as the increased weight of charge reduces the amount of cataracting taking place.

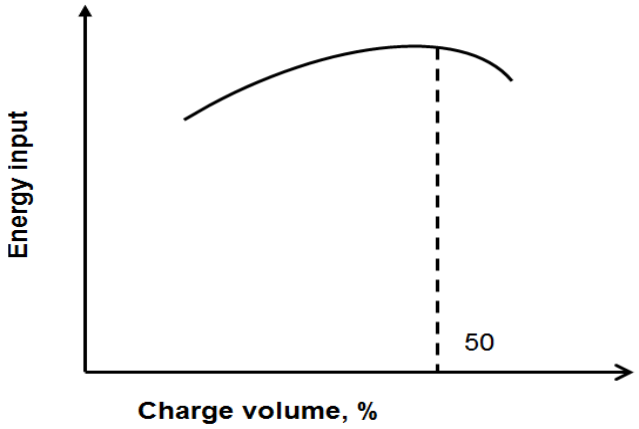

Figure 3-13: Energy input versus charge volume.

b) Ball size and ball charge:

Ball sizes commercially available for charging in grinding mills range from 10 - 150 mm. The ball charge should contain as small balls as possible to offer the largest grinding area. Harder ores and coarser feeds require high impact energy and large ball sizes. Very fine grind sizes require substantial media surface area and small grinding balls (Gupta and Yan 2006). The largest balls should be just heavy enough to break the coarsest particle (Schlanz 1987, Napier-Munn, Morrel et al. 1996, Wills and Napier-Munn 2006). The number, size and mass of each ball size used depend on the mill load and whether the balls are being charged for the first time to commence an

operation or as replacements for worn out. In determining the size of balls to be charged to commence a milling process, Bond (Bond 1958) indicated that the initial ball size was related to the maximum size of the feed. Thus if *d* is the ball diameter (mm), *W*i; the work index of the material (kWh/t), $x_{F,80}$ the feed size and ψ_c , the relative rotational speed, then the largest size of the ball, *d* is estimated by:

$$d = 25.4\left[\left(\frac{x_{F,80}}{k}\right)^{0.5}\left(\frac{\rho_S W_i}{100\psi_c(3.281D)^{0.5}}\right)^{0.33}\right] \text{ in mm} \qquad (16)$$

D= the inside diameter of the mill (m) and

k= a constant designated as the mill factor. For steel or cast iron balls the value of the constant k is dependent on the mill type and the grinding circuit.

c) Mill speed:

Initially when the mill speed is increased the grinding action increases as well as the throughput. But when the speed is higher than a certain value, the charge together with the grinding media tend to cling to the inner wall where neither cataracting nor cascading takes place and the charge centrifuges (Figure 3-7-c). In such cases the grinding action is considerably reduced and the power required to turn the mill drops drastically. The speed at which maximum mill power can be drawn is therefore critical. For a ball mill with effective lifters, industrial mill rotational speeds in use are found to be between 70 % and 80 % of the critical speed (Shoji, Austin et al. 1982) because there is an optimum in energy utilization. This allows more of the cataracting action of the charge, which results in more impact on the particles (Schlanz 1987, Gupta and Yan 2006, Wills and Napier-Munn 2006).

d) Pulp density:

The pulp density in ball mills is maintained as high as possible, usually in the range of 65 to 85 % solids by weight, depending on the ore. This allows the balls to be coated with a layer of ore. If the pulp becomes too dilute metal to metal contact increases, resulting in increased steel consumption and inefficient grinding (Schlanz 1987, Napier-Munn, Morrel et al. 1996, Wills and Napier-Munn 2006). The viscosity of the pulp increases with the fineness of the particles, therefore fine-grinding circuits may need lower pulp densities (Wills and Napier-Munn 2006).

e) Circulating load:

A lower circulating load will allow for a longer mill residence time and a finer ball mill discharge. Hence, the optimum circulating load will provide a good compromise between overgrinding and minimization of coarse particles at the mill discharge. In practice, this means matching the classifier cut-size to the mill product size with maximum water split to overflow (Napier-Munn, Morrel et al. 1996).

3.2.2 Power Prediction in Tumbling Mills

Power draw during grinding is one of the most important items in the operation of mills. The supplied power is used primarily to lift the load (i.e. medium and charge) and to keep the mill rotating (King 2001)**.** The objective in efficient operation is to make sure the mill is operating at low specific grinding energy (contingent upon high capacity and low wear) (Austin, Klimpel et al. 1984).

Attempts to derive equations for power requirement in tumbling mills have been either by measuring the energy required to lift the charge till it cascades, or by determining the forces required by the charge to overcome the frictional forces between the charge and the inner surface of the mill and equating it with the forces required to turn the charge round the centre of the mill (King 2001).

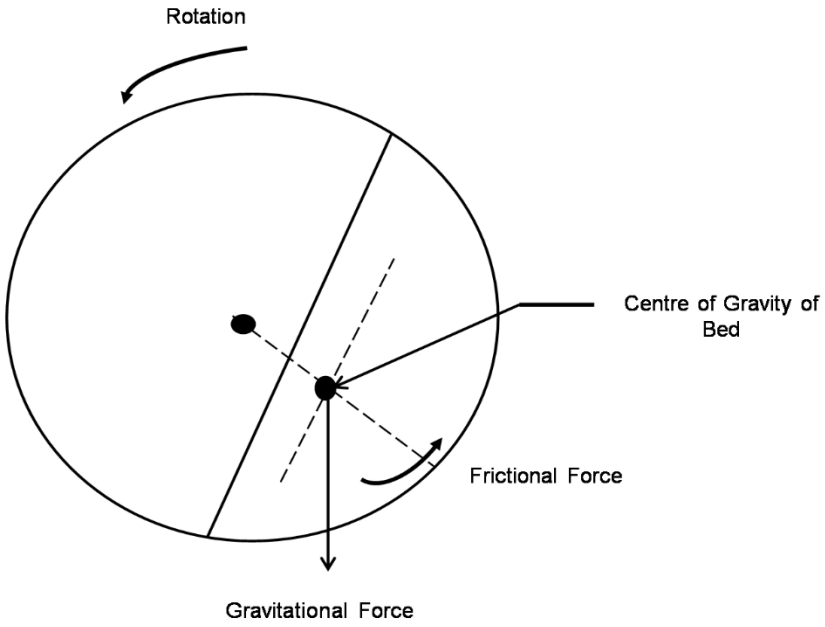

Figure 3-14: Illustration of forces of friction and gravity of turning moment about the centre of a ball mill (King 2001).

The frictional force presumably arises from friction between the shell and the bed of grinding balls and material to be ground plus friction of ball-on-ball as balls move up

through the bed. In both cases, the energy used to turn a well-balanced empty mill is small since it consists only of the bearing friction. From Figure 3-14, an approximate description is that a ball enters into the bed surface below the halfway mark on the surface and moves round in a circular path without slip with respect to other balls (a locked condition) until it reaches the surface (Austin, Klimpel et al. 1984). As it emerges it rolls down the surface, so that there is a stream of rolling balls forming a free-flowing surface, referred to as cascading. However, there are some balls plus some quantity of powder, which cataract by ejection from the bed. More cataracting occurs as the rotational speed is increased, while cascading occurs more at lower speeds, but both are always present at the speeds of interest in milling. In principle, a correct analysis of the forces holding the bed in the inclined position against the turning moment due to gravity must lead to the answer as an analysis of the energy of raising the balls, assuming no slip of ball-over-ball on the bed (locked bed) (Austin, Klimpel et al. 1984). More accurate estimations have been attempted from data observed in the laboratories and also in commercial operations (Gupta and Yan 2006). In this section, the generally accepted models for computing mill power, which are mostly derived from the mechanical approach are described (Table 3-1).

According to Austin and co-workers (Austin, Klimpel et al. 1984), if it is assumed that the mean height through which the balls are lifted and fall are the same , then for a mill of length L and diameter D loaded with balls of density ρ_b, then the mill power (kW) could be computed from Eqn. (17) (Austin, Klimpel et al. 1984, King 2001, Gupta and Yan 2006).

Where K_L is the loading factor and can be obtained from Figure 3-15 for the popular mill types.

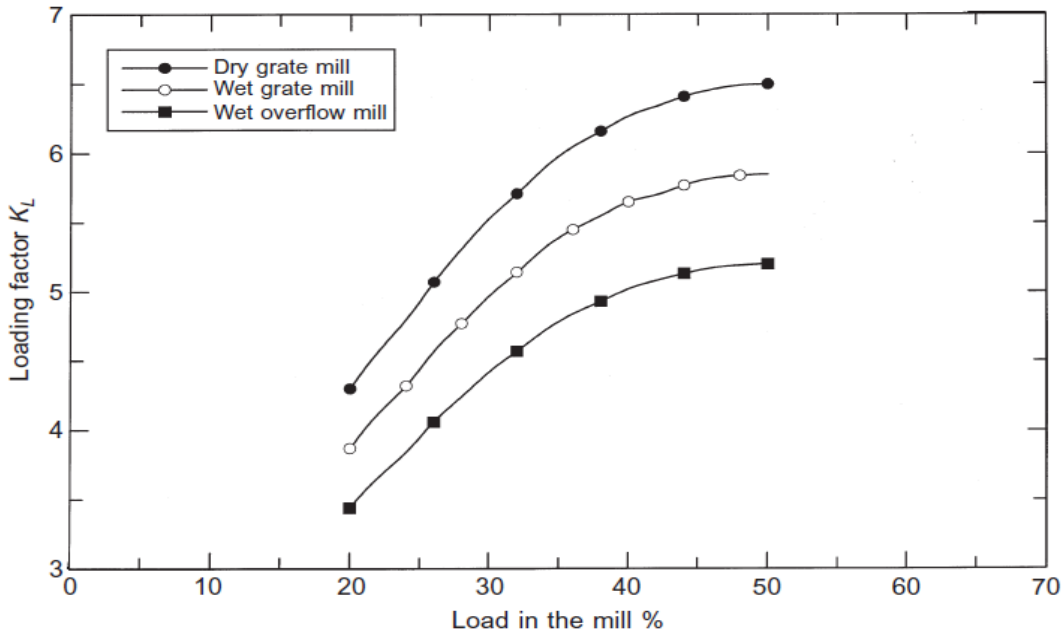

Figure 3-15 : Effects of mill filling on power draw for ball mills (King 2001).

Later workers such as Morrell (Morrell 1996) have shown that K_L is constant only at lower loadings. The value of K_L will vary with the ball load in the mills. At very low loads, it is reasonable to expect that the power draw will increase in proportion to the load. On the other hand, at high loads where the volume of balls almost completely fills the mill, the load will tend to centrifuge round in a mass without tumbling, which would require only low power. Thus it is expected that the power will pass through a maximum as ball load is increased (Austin, Klimpel et al. 1984).

Table 3-1: Power prediction models for tumbling mills.

Model		Reference
$P_M = K_L \rho_b L D^{2.5}$	(17)	(Austin, Klimpel et al. 1984)
$P_M = 1.12 * 10^{-3} \left(D^{2.5} L \rho_b\right) \left(1 + \frac{0.4 \rho_s \varphi_{MG}}{\rho_b}\right) * \psi_c f(\varphi_{GM})$	(19)	(Austin, Klimpel et al. 1984, Gupta and Yan 2006)
$P_S = 7.33 \psi_c \varphi_{GM} \left(1 - 0.937 \varphi_{GM}\right) \left(1 - \frac{0.1}{2^{9-10\psi_c}}\right) \rho_b L D^{2.3}$	(21)	(Austin, Klimpel et al. 1984, Gupta and Yan 2006)
$Net\ power = K D^{2.5} L \rho_c \Delta\delta$	(22)	(Austin 1990, Morrell 1996)
$No\text{-}load\ power = 1.68 D^{2.5} \left(\psi_c \left(0.667 L_{ce} + L\right)\right)^{0.82}$	(23)	(Morrell 1996)

Rose and Sullivan (Austin, Klimpel et al. 1984, Gupta and Yan 2006) theoretically derived an expression for the power (kW) required by mills by assuming that the power drawn was proportional to the fraction of the critical speed, ψ_c, and that the rock particles travel in the same manner as the balls. In deriving their expression they also assumed that the porosity of the charge (balls plus crushed rock) equals to 0.4. The final mill power for dry grinding, in kW was estimated from Eqn. (19) . Where ρ_s is the density of the solid material, φ_{MG} is fraction of mill volume occupied by ore and $f(\varphi_{GM})$ is a function of ball load, φ_{GM}.

Eqn. (19) is valid when the mill speed is less than 80 % of the critical speed. The function $f(\varphi_{GM})$ was determined experimentally by Austin who found that the power increased until 50 % of mill load and with further load decreased. For the range 0-50 %, the ball load-power relation could be expressed by a polynomial as:

$$f(\varphi_{GM}) = 3.045\varphi_{GM} + 4.55\varphi_{GM}^{\ 2} - 20.4\varphi_{GM}^{\ 3} + 12.9\varphi_{GM}^{\ 4}, \ for \ \varphi_{GM} < 0 \qquad (24)$$

For comparison purposes, Austin and co-workers (Austin, Klimpel et al. 1984) proposed that it is more convenient to express Eqn. (19) in terms of the mass of grinding media, where the media is usually steel balls. The mass of the media (i.e. based on bed porosity of 35-45 %) in the mill is:

$$M_b = 0.47\varphi_{GM} L D^2 \rho_b \qquad (25)$$

And

$$\frac{P_M}{M_b} = 2.38 D^{0.5} \psi_c \left(1 + 0.4\sigma\varphi_{MG}\right)\left(\frac{f(\varphi_{GM})}{\varphi_{GM}}\right) \text{, kW/t, } \psi_c \le 0.8 \qquad (26)$$

Where M_b is in metric tons and D in m.

Using a large number of laboratory and industrial mills, Bond (1960) proposed an empirical equation for computing the shaft power, P_S (Eqn. (21)) for wet mills (Austin, Klimpel et al. 1984, Gupta and Yan 2006). Further, he also empirically determined an expression for power in terms of unit mass of the grinding media (M_b) as:

$$\frac{P_M}{M_b} = 15.6 D^{0.3} \psi_c \left(1 - 0.937\phi_{GM}\right)\left(1 - \frac{0.1}{2^{9-10\psi_c}}\right), \ \text{kW/t} \qquad (27)$$

For D in meters, M_b in metric tons (i.e. diameters are inside mill linings)

He states that the results should be multiplied by 1.08 for dry grinding in grate discharge mills and 1.16 for wet low level grate discharge mills. In practice the shaft power for wet overflow mills calculated using Eqn.(27) appeared to yield higher results than the computed value when:

- Maximum ball diameter, d_{max} < 45.7 mm and
- Mill internal diameter > 2.400 mm.

In order to correct this, Bond introduced a factor described as the slurry factor:

$$F_S = 1.102\left(\frac{45.72 - d_{\max}}{50.80}\right), \text{kW/t} \tag{28}$$

Where F_S is to be subtracted from values obtained from Eqn. (27) for wet overflow mills, d_{max} is the maximum ball diameter in mm.

Rowland (1974) found that Eqn.(28), had to be modified to suit mills for D > 3.3 m. The modified ball size factor is added to Eqn. (27) and is given as:

$$F_B = 1.102\left(\frac{d_{\max} - 42.5D}{50.8}\right), \text{kW/t} \tag{29}$$

Where D is in m and d_{max} in mm

When the mill power is computed according to Rose and Sullivan method, Eqn. (19) , and the results compared with that from Bond's equation, Eqn. (21), it is observed that the fractional filling at which a ball mill draws the maximum differs (see Figure 3-16). Rowland and Kjos have applied Bond's Eqn. Eqn. (21) and suggested a slightly modified form when applied to compute the power required for wet over-flow ball mills:

$$\frac{P_M}{M_b} = 4.879D^{0.3}\left(3.2 - 3\phi_{GM}\right)\psi_c\left(1 - \frac{0.1}{2^{9-10\psi_c}}\right) + F_B, \quad \text{kw/t-balls} \tag{30}$$

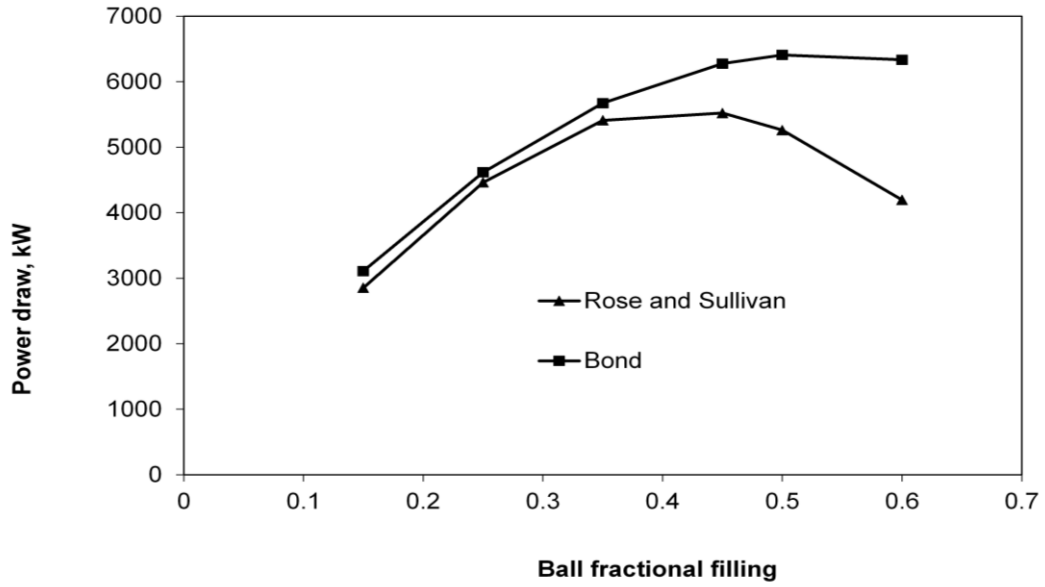

Figure 3-16: Calculated ball mill power draw for the BGM ore system based on Bond and Rose and Sullivan models (*D*=6.10 m, *L*=9.05 m, and ψ_c=75 %).

Eqn. (30) is applicable for mill power estimations of wet grinding mills with D> 3.3 m.

More reliable models for the prediction of power drawn by ball, semi-autogenous and fully autogenous mills have been developed by Austin and co-workers (Austin 1990, Morrell 1996), (Eqn.(22) and Eqn. (23)). The relationship between gross power and net power is given by:

$$\text{Gross power} = \text{No load power} + \text{Net power drawn by the charge} \qquad (31)$$

The net power is calculated from Eqn. (22), where, *D* is the diameter inside the mill liners and *L* is the effective length of the mill including the conical ends. ρ_c is the specific gravity of the charge and Δ and δ are factors that account for the fractional filling and the speed of rotation respectively. *K* is a calibration constant that varies with the type of discharge. For overflow mills *K* = 7.98 and for grate mills *K* = 9.10. This difference is ascribed to the presence of a pool of slurry that is present on the bottom of overflow-discharge mills but which is not present to the same extent in grate-discharge mills.

This pool is situated more or less symmetrically with respect to the axis of the mill and therefore does not draw significant power. Austin recommended *K* = 10.6 for overflow semi-autogenous mills, however a value of *K* = 9.32 gives a better fit between Austin's formula and Morrell's data and this value is recommended (King 2001).

The No-load power accounts for all frictional mechanical losses in the drive system of the mill and can be calculated from Eqn. (23) (Morrell 1996). L_{ce} is the mean length of

the conical ends and is calculated as half the difference between the centre-line length of the mill and the length of the cylindrical section (King 2001).

3.3 Grinding Circuits

In minerals industry, after blasting and crushing the ore, the final size reduction is carried out in grinding circuits. Typical grinding circuits comprise of tumbling mills, screens and classifiers. They are processes responsible for breaking of the ore such that the mineral and gangue is substantially produced as separate particles. Grinding circuits have an impact on all phases of the mining operation, including efficient mill operation and successful production, with its main purpose being to exercise close control on product size. In other words, the grinding mill must produce an optimum mesh of grind, which is important for several reasons, with the most basic being achievement of liberation of the mineral species contained in the ore. If the mill is not grinding fine enough or under grinding the ore, it produces a product which is coarse and may have a low degree of liberation and therefore cannot be processed. This inefficient liberation will result in poor recoveries, poor concentration ratios and uneconomical operation (Schlanz 1987).

3.3.1 Grinding Circuits Configuration

There is no such thing as a ‘’best” configuration of equipment for grinding. The circuit which works well on one ore may be totally unsatisfactory for another ore (Schlanz 1987). The appropriate selection and combination of equipment are driven by feed size, ore type, tonnage, and final product size. The general trend in industry today is flowsheet simplification, using larger parallel circuits instead of multiple-line circuits with smaller mills. This change has been brought about by the savings of both capital and operating costs that are associated with larger equipment. Table 3-2 lists the size ranges within which various comminution methods operate most efficiently and the fact that the inherent efficiency of some devices is higher than others. This list causes circuit designers to select equipment that produces a favorable overall efficiency (Fuerstenau and Han 2003).

Table 3-2: Normal Size Range and Approximate Energy Efficiencies for Various Devices.

Device	Normal Size Range, mm	Approximate Efficiency, %
Gyratory crusher	1000-200	80
Cone crusher	200-20	60
Autogenous/Semi autogenous	200-2	3
Rod mill	20-5	7
Ball mill	5-0.2	5
Stirred mill	0.2-0.001	1.5
High-pressure grinding rolls	20-1	20-30

In any grinding installation a choice must be made between wet or dry grinding. The advantages of wet grinding over dry grinding include (Schlanz 1987):

- lower power consumption per ton of product
- higher capacity per unit of mill volume
- possible use of wet screening or classification for close product control
- elimination of dust problems
- allows the use of simple handling and transport methods (i.e. pumps, pipes, launders, etc.) and
- mixing ore with water for further processing (flotation)

Wet milling also has some disadvantages:

- higher wear rate of balls and liners
- scaling of piping and other equipment

Nevertheless, wet milling is preferred over dry grinding since the advantages outweigh. The type of mill for a particular grind, and the circuit in which it is to be used, must be considered simultaneously. Grinding circuits are divided into two broad categories, open and closed (Wills and Finch 2016).

3.3.1.1 Open Circuit Grinding

Open circuit grinding consists of one or more grinding mills, either parallel or in series (Figure 3-17), that discharges a final ground product without classification equipment and no returns of coarse discharge back to the mill (Schlanz 1987). There is no control of product size distribution for this type of grinding operation (Rao 2011) . Some

examples of open circuit grinding equipment are: rod mill, ball mill, and rod mill, ball mill combination (Schlanz 1987, Gupta and Yan 2006, Wills and Napier-Munn 2006, Rao 2011).

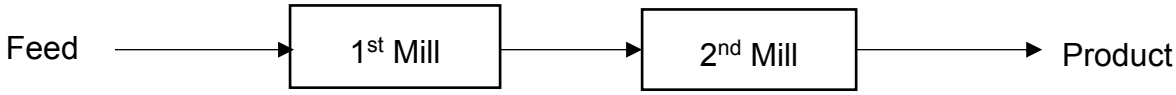

Figure 3-17: Open Circuit Grinding.

Not all ores can be ground in an open grinding circuit type. Some conditions which do favor the application of an open circuit grinding are:

- small reduction ratios
- reduction of particles to a coarse (natural grain size)
- recirculation of cleaner flotation middlings for regrinding and
- a non-critical size distribution of the final ground product

Some advantages for open circuit mode vs closed circuit are (Schlanz 1987):

- minimum equipment requirements
- high pulp density discharge, and
- simplicity of operation

The disadvantage of single-stage milling is that if a high reduction ratio is required, then relatively large balls are required for coarse feed, which may not efficiently grind the finer particles (Wills and Finch 2016).

3.3.1.2 Closed Circuit Grinding

Closed circuit grinding consists of one or more mills discharging ground product to classifiers which in turn return the coarse product from the size separation back to the mill for further grinding (Figure 3-18) (Masuda, Higashitani et al. 2007, Rao 2011, Wills and Finch 2016). The grinding efficiency is very dependent upon the size separation applied, so care should be exercised in selecting the type and size of classifier used to close the system. The closed circuit is the most common type of grinding circuits in mineral processing facilities, mainly because a lot of ores and product requirements are not suitable for open circuit grinding (Schlanz 1987).

In closed-circuit grinding, no effort is made to effect all the size reduction in a single pass. Instead, every effort is made to remove material from the circuit as soon as it reaches the required size. This has the effect of creating a narrower size distribution

in the circuit product (classifier fine product) compared to open circuit, as finished product (fine material) is removed quickly and avoids “over-grinding” while the coarse material is preferentially recycled and ground (Schlanz 1987, Rao 2011, Wills and Finch 2016). Although closed circuit grinding offers many choices for arrangement of the equipment as well as combinations of equipment, some of the most circuit’s equipment combinations are:

- Rod mill/classifier,
- SAG mill/ball mill/classifier
- Ball mill/classifier,
- Rod mill/ball mill/classifier and
- Rod mill/classifier /Ball mill/classifier.

Some of the possible classifier options for the circuit’s combination are hydrocyclone, spiral, rake and sedimentation cones (Barkhuysen 2009, Barkhuysen 2010).

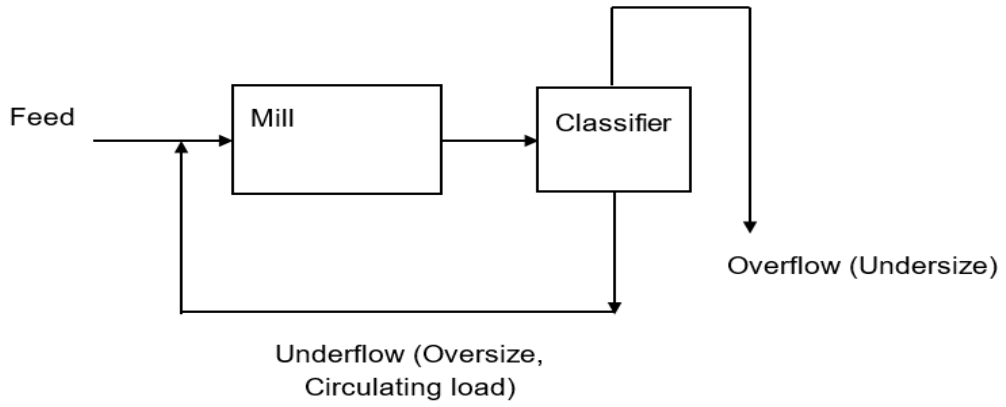

Figure 3-18: Closed Circuit Grinding.

The amount of solids fed back to the grinding mill is called *circulating load* and is expressed as a percentage of the weight of new feed:

$$CL = \frac{\dot{m}_{\text{circ}}}{\dot{m}_{\text{F}}} * 100 \tag{32}$$

where $\dot{m}_{\text{circ}}$ is mass flow oversize , $\dot{m}_{F}$ is mass flow feed .

Most grinding circuits closed by classifiers (e.g. hydrocyclones) operate with high circulating loads that range between 100-350 % (Barkhuysen 2009, Barkhuysen 2010, Wills and Finch 2016). Under relatively low classifier efficiency, the circulating load can be as high as 600 % (Rao 2011, Wills and Finch 2016).The higher the circulating load the shorter the residence time in the mill and thus the higher is the content of coarse material in the mill product.

Various types of classifying devices can be used to close the grinding circuit. Mechanical classifiers (e.g. rake or spiral classifiers) are still found in some older mills, but suffer from classifying by gravitational force, which restricts their capacity when dealing with fine material (Wills and Finch 2016). Hydrocyclones (or simply “cyclones”) classify by centrifugal force, which intensifies the classification of fine particles, giving sharper separations at fine cut sizes and allowing higher circulating loads (Wills and Finch 2016). They occupy much less floor space than mechanical classifiers of the same capacity and have lower capital and installation costs. Due to their fast response, the grinding circuits can rapidly be brought into balance if changes are made and the reduced dwell time of particles in the circuit gives less time for oxidation to occur, which may be important with sulfide minerals that are to be subsequently floated (Wills and Finch 2016). Cyclones have, therefore, come to dominate grinding circuits preceding flotation operations (Barkhuysen 2009, Barkhuysen 2010, Wills and Finch 2016). Hence, hydrocyclones or cyclones are the main classification devices that will be referred in this work.

The action of all classifiers in grinding circuits is dependent on the differential settling rates of particles in a fluid, which means that particles are classified not only by size but also by specific gravity and particle form. Consequently, a small dense particle may classify in a similar way to a large, low-density particle. Thus, when an ore containing a heavy valuable mineral is fed to a closed grinding circuit, this mineral is preferentially recycled compared to the low density mineral (usually gangue) and is ground finer. Other strategies aim to take advantage of the concentration of heavy minerals in the circulating load. A flotation unit (“flash flotation”) or gravity separation stage can be incorporated in the grinding circuit, e.g., on the cyclone underflow, cyclone feed or ball mill discharge. Incorporation of gravity separation is almost universal in gold circuits with a high degree of “gravity recoverable gold”, and in some instances can be extended to the recovery of platinum group minerals.

3.3.2 Advances in Grinding Circuits

The grinding mills in which comminution takes place without grinding aids are known as Autogenous Grinding (AG) mills. These mills use large lumps of rock as the grinding media. Mills that use intermediate size rock or pebbles as a grinding medium are also autogenous mills but are known as pebble mills. Mills that grind hard ores with fracture characteristics that do not lend themselves to fully autogenous milling are charged with

a small amount of steel balls to assist in the size reduction. These are known as Semi-autogenous Grinding (SAG) mills (Gupta and Yan 2006).

The operation of AG/SAG mills involves the use of cheap grinding media as a replacement for expensive steel balls and rods which greatly affect the wear on liners. They are therefore less expensive to operate. It is necessary that the ore should provide a sufficient amount of lumps that would last for a reasonable time to act as grinding medium. Such ores have been described as competent ores in contrast to non-competent ores which break up easily. In recent times AG/SAG mills have successfully replaced the conventional rod mill-ball mill configurations (Gupta and Yan 2006).

Most AG/SAG operate in open circuit (Figure 3-19) when the product size is usually coarse. Even in open circuits, provisions exist however, for installing a classifier such as a trommel screen or a vibrating screen to remove critical sized pebbles (scats). The oversize material is recycled either externally or internally. In internal recycling, the coarse material is conveyed by a reverse spiral or water jet back down the center of the drum into the mill. External recycling can be continuous, achieved by conveyor belt, or is batch where the material is stockpiled and periodically fed back into the mill by front-end loader (Gupta and Yan 2006, Wills and Finch 2016). For finer and more uniform product, closed circuit grinding with classifiers, like a hydrocyclone, is usually employed (Figure 3-20) (Gupta and Yan 2006, Wills and Finch 2016).

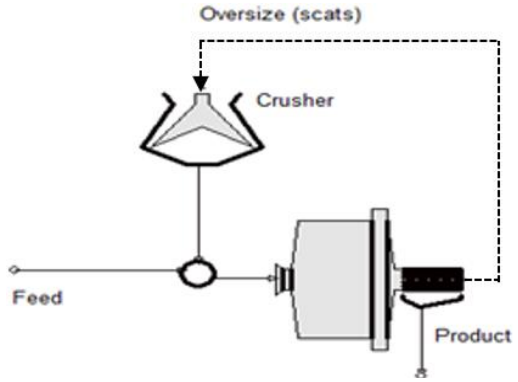

Figure 3-19: SAG Mill with scats recycle.

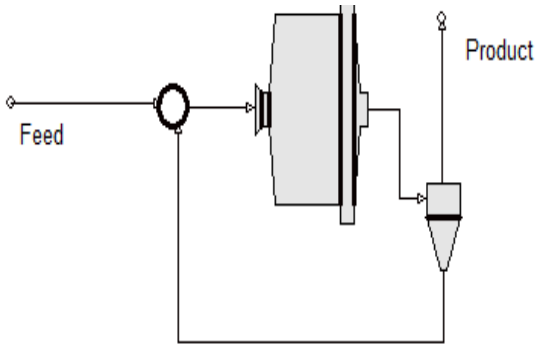

Figure 3-20: SAG mill in closed circuit.

Figure 3-21 shows a SAG/Ball mill circuit where both mills are in a closed circuit, the SAG mill is closed with a crusher (recycle or pebble crusher) to control the amount of “critical size” (i.e. 25-50 mm) material in the circuit. If the critical size is accumulated, the mill energy efficiency will deteriorate, and the mill feed rate decreases. As a solution, additional large holes, or pebble ports (e.g., 40-100 mm), are cut into the mill

grate, allowing coarse material to exit the mill. This circuit configuration is common as it usually produces a significant increase in throughput and energy efficiency due to the removal of the critical size material (Wills and Finch 2016).

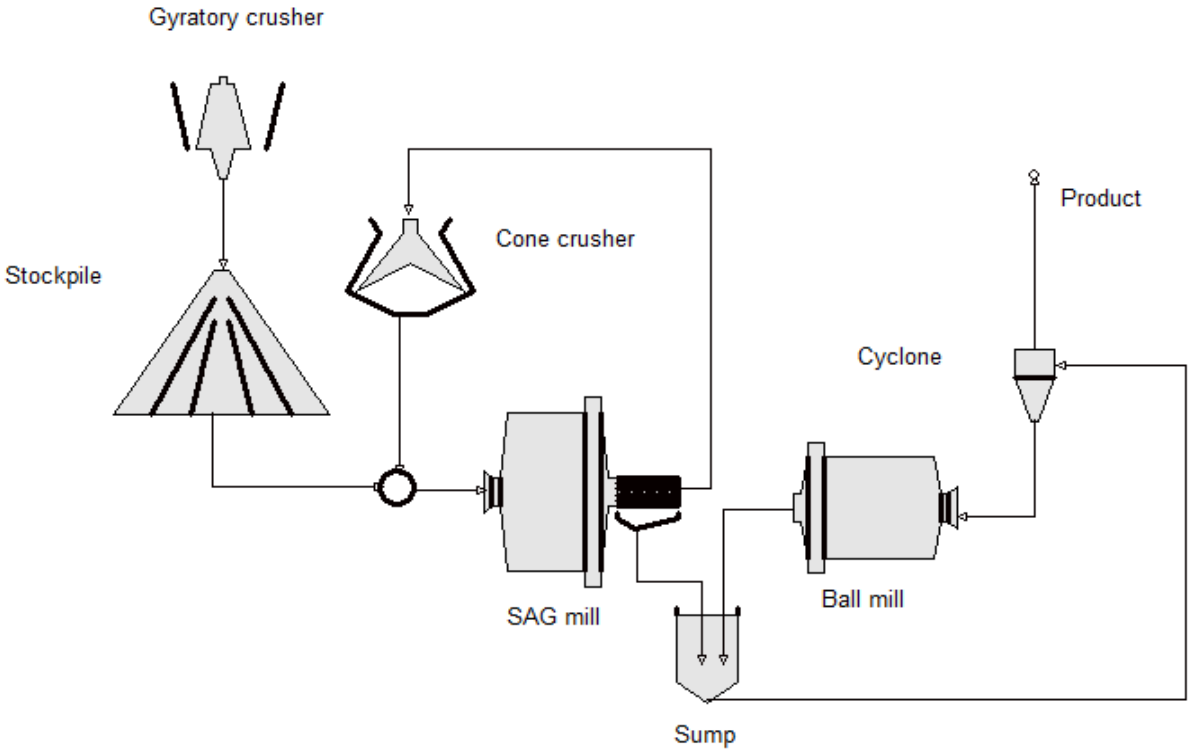

Figure 3-21: Semi-autogenous/Ball Mill Circuit Closed with a Cyclone (adopted from (Wills and Finch 2016)).

High unit capacity SAG mill/Ball mill circuit is dominant today and has contributed toward substantial savings in capital and operating costs, which has in turn made many low-grade, high-tonnage operations such as copper and gold ores feasible. Future circuits may see increasing use of high pressure grinding rolls**.** It has been suggested that High Pressure Grinding Roll (HPGR) mills be included in AG/SAG grinding circuits in order to take care of the presence of critical size pebbles in the SAG product streams and to produce a finer and more uniform product. It has been claimed that the final product is more amenable to flotation and leaching circuits that follow in some operations. This is due to the better liberation achieved through grain boundary breakage caused by the high pressure grinding rolls (Celik, Oner et al. 2007, Ozcan and Benzer 2013, Michaelis 2017). A typical SAG-HPGR-Ball mill circuit is presented in Figure 3-22 (Gupta and Yan 2006).

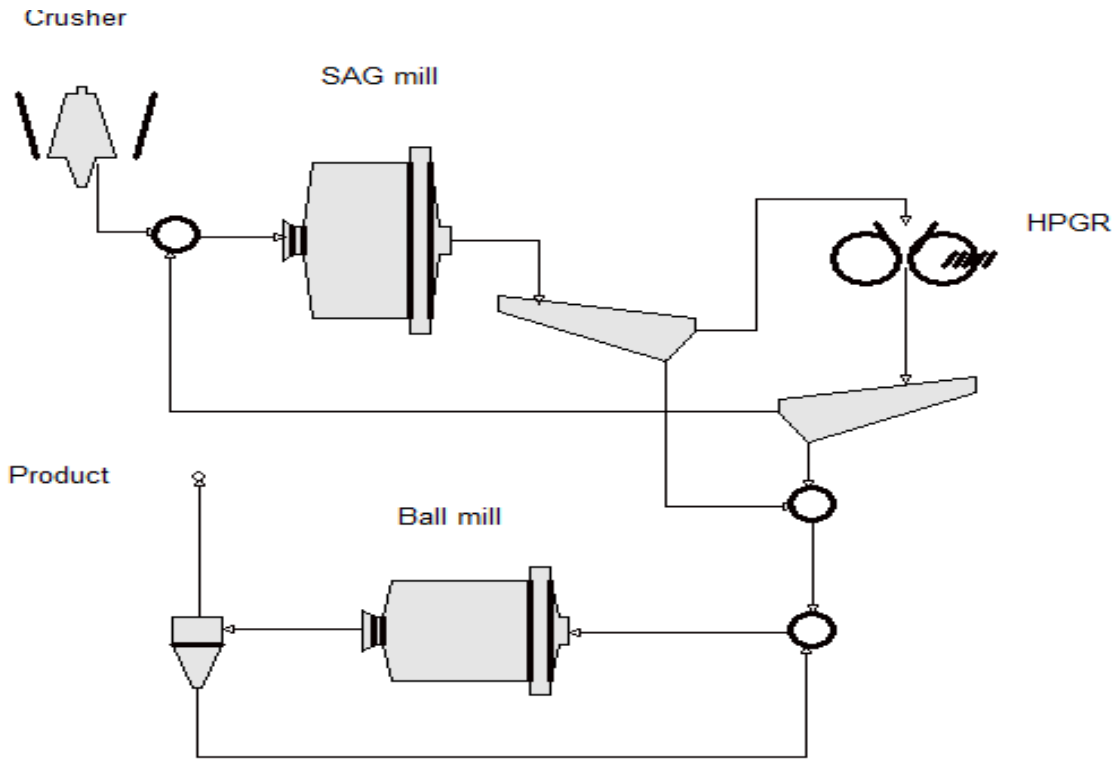

Figure 3-22: SAG Mill, HPGR and Ball Mill in an ABC Closed Circuit.

3.3.3 Operation and Control of Grinding Circuits

Probably the most critical reason for good operation and control over the grinding circuits is due to the tremendous amount of energy consumed in these units (Schlanz 1987). Thus, it is essential that the milling circuit does not only treat a certain tonnage of ore per day, but should also produce the target product size distribution (Wills and Finch 2016). Automatic control of milling circuits is one of the most advanced and successful areas of the application of process control in the minerals industry (Herbst, Alba et al. 1988, Wills and Finch 2016).

Grinding circuits are fed at a controlled rate from the stockpile or bins holding the crusher plant product. There may be a number of grinding circuits in parallel, each taking a definite fraction of the feed. Parallel mill circuits increase circuit flexibility, since individual units can be shut down or the feed rate can be changed, with a manageable effect on production. Fewer mills are, however, easier to control and capital and installation costs are lower, so the number of mills must be decided at the design stage (Wills and Finch 2016).

There are many factors which can contribute to the fluctuations in the performance of a mill within a grinding circuit, but some of the most common in industrial practice are (Schlanz 1987, Wills and Finch 2016):

- changes in the feed rate and circulating load
- changes in the size distribution and hardness of the ore and
- changes in the rate of water addition to the milling circuit

Other variables affecting control of grinding mills may include:

- interruptions in operation (i.e. stoppage for replacement of grinding medium, clearing of chocked classifiers, etc.)
- changes in crusher settings (also: wear of crusher)
- screen damage in the crusher circuit.

Of these variables, feed size distribution and ore hardness are the two most significant because they can affect the actual breaking mechanics (Schlanz 1987).

The only two variables that can be independently controlled by the operator are feed rate and water addition. All other variables depend on and respond to changes in these two items, thus these are used to control the grind. Too dilute a pulp, which can arise from a decrease in feed rate or an increase in water addition, will decrease retention time in the mill, resulting in a coarser product and increased wear. Under opposite circumstances, pulp densities can become too high which leads to an increase in retention time resulting in a finer product. The viscosity of the slurry will increase with increase in solids concentration due to increased frictional interactions per unit volume with increase in solids concentration (Wills and Napier-Munn 2006).

Fluctuation in feed size and hardness are probably the most significant factors disturbing the balance of a grinding circuit. Such fluctuations may arise from differences in composition, mineralization, particle size of the feed, texture of the ore from different parts of the mine, changes in mining methods (e.g., blast pattern), changes in the crusher settings, often due to wear, and from damage to screens in the crushing circuit. Minor fluctuations in ore characteristics can be smoothed out by ore blending prior to feeding to the crusher. Ore storage increases smoothing out of variations, provided that ore segregation does not take place in the coarse-ore stockpile.

Increase in feed size or hardness produces a coarser mill product unless the feed rate is proportionally reduced. Conversely, a decrease in feed size or hardness may allow an increase in mill throughput. A coarser mill product results in higher circulating load from the classifier, thus increasing the volumetric flow rate. Since the product size from

a hydrocyclone is affected by flow rate, the size distribution of the product will change. The control of the circulating load is therefore crucial for the control of the product particle size. A high circulating load at a fixed product size means lower energy consumption (specific energy), but excessive circulating loads may result in the mill, classifier, conveyor, or pump overloading, hence there is an optimum to the mill feed rate (Wills and Finch 2016).

Virtually all plants built today have a sophisticated digital control system that enables all basic control functions, providing the human–machine interface, and acting as the gateway to plant management information systems, which couple process and business controls. In addition, most new plants adopt advanced process control applications to deal with the multivariable nature of process optimization in real time. Industry has increasingly accepted process control as one of the most capital-effective investments available in the pursuit of lower costs and increased revenues.

The need for process control is made evident in early stages of comminution circuit design. Although the comminution process may well be stable to these fluctuations without intervention, control systems are normally required to ensure stability and to enhance the overall economic performance of the process. The complexity of the control strategy depends in part on the complexity of the process (the so-called “resiliency factor,” articulated by Morari (Morari 1983)) and in part on the nature of the disturbances. Estimates of the nature of disturbances are increasingly available at the design stage, opening new avenues for the a priori design of control strategies. Operationally, efforts to mitigate disturbances upstream (at the mine or crusher) will simplify the control requirements, although the spatial variability of ore characteristics often precludes effective blending. The combination of the magnitude and frequency of disturbances will also have an impact on control requirements (Fuerstenau and Han 2003).

3.3.4 Grinding Circuits Efficiency

The most applicable technique in determining the efficiency of comminution circuits is the use of Bond efficiency factor (B_{ef}), which is the relative efficiency of the grinding circuit compared to the prescribed Bond standard energy for a ‘conventional’ grinding circuit (C. A. Rowland and Mclavor 2008). The Bond efficiency factor is calculated as:

$$B_{ef} = \frac{W_i}{W_{i,op}} \tag{33}$$

Where B_{ef}, W_i, and $W_{i,op}$ are Bond efficiency factor (%), laboratory Bond index (kWh/t) and operating Bond work index (kWh/t), respectively. Efficiency factor values larger than 100 % imply that the mill consumes less energy than the laboratory Bond tests estimate and thus the throughput can be increased. On contrary, efficiency values less than 100 % imply that the milling operation is inefficient and energy is wasted by the grinding operation (C. A. Rowland and Mclavor 2008, Alamouti, Rezai et al. 2011). The operating Bond index, $W_{i,op,}$ was determined from survey data by :

$$W_{i,op} = \frac{P}{\dot{m}\left(\frac{10}{\sqrt{x_{P,80}}} - \frac{10}{\sqrt{x_{F,80}}}\right)} \tag{34}$$

Where, P is the circuit power in kW, $\dot{m}$ is circuit throughput (t/h) and $x_{P,80}$ and $x_{F,80}$ are the circuit product and feed size, respectively.

The laboratory work index is obtained using the standard Bond test procedure (see also chap. 4.3.2) and using Bond Eqn. (4), it is used for estimation of specific power requirements for industrial mills (Rowland 2006). The operating work index is the specific power consumption under real plant conditions based on known mill throughput, power draw and size distributions of feed and product. It is regularly used for monitoring energy efficiency of existing grinding circuits (Napier-Munn, Morrel et al. 1996, Gupta and Yan 2006, Rowland 2006).

3.4 Modelling and Simulation in Comminution

3.4.1 Modelling Fundamentals

Comminution processes have been studied over the years and statistical correlations of variables have been used to develop mathematical models describing unit involved and integrated operations. With a better understanding of the processes and application of basic laws of physics, mathematical models have been developed to describe comminution operations more in detail. The developed models help to simulate the processes (Gupta and Yan 2006). Simulation is a powerful and cost-effective tool for design, analysis, and optimization not only of comminution processes, but also mineral processing operations in general (Brochot, Wiegel et al. 2006, Wills

and Napier-Munn 2006, Rosario 2010, Sba'rbaro and Villar 2010). It offers clear advantages in terms of accurate predictions of performances of alternative circuits, is used to optimize circuit design, and flow rates of process streams, and is used for sizing pumps and pipelines. Therefore simulation eliminates largely the need for laborious and expensive plant trials with the aid of computers (Gupta and Yan 2006, Wills and Napier-Munn 2006). In gold industry for example, modelling and simulation for decision support is becoming a project requirement as independently verified simulation models increase investor confidence in the proposed process or optimization (Smith 2005).

Generally the mathematical models used are either dynamic (involving time) or steady state. The latter predominate at present, although it is expected that dynamic models will become more prevalent in the future (Powell and Morrison 2007). Almost all of the applicable models are strongly nonlinear and are not usually amenable to straightforward mathematical solution, nor are they always very convenient for easy computation using calculators or spreadsheets. Models in mineral processing are difficult to develop because of the complexity of the unit operations used in virtually all mineral recovery systems. The major problem (among these difficulties) is the fact that the feed material is variably a particulate solid.

Many conventional mathematical modelling techniques commonly used for processing equipment have limited their application to particulate systems and the models for most unit operations in mineral processing have unique features. Real time dynamic computer simulation has been a powerful tool not only in traditional high-tech aerospace and military industries, but also in other areas such as automotive, steel making and chemical processing industries. However, until very recently, there has been limited practical application of the dynamic simulation in most of the mineral processing sectors, instead of relying on pilot plant studies and steady-state flowsheet simulation for plant design, equipment dimensioning and pre-control optimization (Rosario 2010).

In modelling comminution systems, the basic idea is to obtain a mathematical relation between the feed and the product size. It is necessary to take into account all the variables involved in the operation including the machine characteristics. The process of comminution is considered to be represented by two processes:

— a particle is selected for breakage,

— a broken particle produces a given distribution of fragment sizes.

The distribution of sizes produced from a single breakage event is described by the *breakage function* (see also Chap. 3.4.2.1). This function denotes the relative distribution of each size fraction after breakage and is often found to be independent of the initial particle size. In the matrix form the breakage function is written as a lower triangular matrix. The probability of breakage of certain particle sizes will be higher than others as they pass through the breakage process. This selective behavior leads to a proportion of particles broken from an initial size interval which is described by the *selection function* (see also Chap. 3.4.2.2). Using these concepts, mathematical relations between feed and product size have been developed (Gupta and Yan 2006). A good review of modelling and simulation methods is provided by King and co-workers (King 2001, Gupta and Yan 2006) . Also comminution and classification models are well developed and in routine use for design and optimization of comminution operations (Napier-Munn, Morrel et al. 1996, Rosario 2010).

3.4.2 Breakage and Selection Functions

All comminution processes impart forces to break and reduce ore size and in order to identify the products in different size fractions; two conventions have been adopted. Firstly, the mass fraction of particles retained in size j after breakage of particles of size j into the i^{th} size fraction is designated as $b_{i,j}$. Here the coarsest size fraction would be size class 1, followed by 2 until the finest size class N.

The second convention advocated by Austin and co-workers (Austin, Klimpel et al. 1984) is to record the cumulative amount passing a certain size instead of that retained on the screen (i.e. first convention). This is represented as $B_{i,j}$ where i and j have the same convention.

3.4.2.1 Estimation of Breakage Function

The breakage function describes the average size distribution resulting from the fracture of a single particle (Kelly and Spottiswood 1990). Therefore the relative distribution of each size fraction after breakage is interpreted as a full description of the product. The primary breakage distribution function of a particle of size *j* to size *i* is defined as:

$$b_{i,j} = \frac{mass\ of\ particles\ from\ class\ j\ broken\ to\ size\ i}{mass\ of\ particles\ of\ class\ j\ broken} \tag{35}$$

A more convenient way of describing the breakage distribution function is to use the cumulative breakage function defined as follows (Austin, Klimpel et al. 1984):

$$B_{i,j} = \sum_{k=n}^{i} b_{k,j} \tag{36}$$

k = the finest size fraction into which particles breaking from top size j can reach.

The cumulative breakage function, $B_{i,j}$, is the weight fraction of the material leaving the top size interval *j* going to all size fractions finer than size i. The values of $B_{i,j}$ can be estimated from the size analysis of a grinding product after a short grinding interval and with an initial mill charge. Here, the material is predominantly in size class *j* (Austin, Klimpel et al. 1984) (i.e. mono-size fraction, BII method) and no re-breakage of primary progeny fragments has occurred. Therefore the product of the breakage rate function and the breakage distribution function is approximately constant.

According to BII method (mono-size fraction approach), the breakage distribution function is obtained (Austin, Klimpel et al. 1984, Gupta and Yan 2006) as:

$$B_{i,1} = \frac{\log[(1-P_i(0))/(1-P_i(t))]}{\log[(1-P_2(0))/(1-P_2(t))]},\ i > 1 \tag{37}$$

Where $P_i(0)$ = cumulative mass fraction less than size i at time 0

$P_i(t)$ = cumulative mass fraction less than size i at time t, and

$B_{i,1}$ = cumulative mass fraction of particles passing the top size of interval i from breakage of particles of size 1.

The breakage function can be fitted to an empirical function relating particle size x_i (Austin and Luckie 1972) as follows:

$$B_{i,j} = \phi_j \left(\frac{x_{i-1}}{x_j}\right)^{\gamma} + (1-\phi_j)\left(\frac{x_{i-1}}{x_j}\right)^{\beta},\ i > j \tag{38}$$

$$\phi_j = \phi_1 \left(\frac{x_j}{x_1}\right)^{-\sigma} \tag{39}$$

β is a parameter characteristic of the material used whose values range from 2.5 to 5.

γ is also a material-dependent characteristic whose values typically are found to be between 0.5 to 1.5. ϕ represents the fraction of fines that are produced in a single fracture event and is also dependent on the material used.

Eqn. (38) represents an empirical model relating the cumulative breakage function to the particle size (relative size) and is illustrated in Figure 3-23. Further, it is postulated that the first term in Eqn. (38) describes the size distribution of the fine fraction in the progeny particles, resulting from localised fracture of large particles (cleavage breakage), while the second term describes the size distribution of the coarse fraction in the progeny particles, resulting from the main fracture of particles (shatter breakage) (Kelly and Spottiswood 1990, King 2001).

A simple but effective assumption is to consider the breakage function as independent of the initial particle size and therefore normalizable. In this case, ϕ is not a function of the parent size *j*. Although this is still arguable , the assumption has proven to be reasonable for many materials (King 2001, Mütze 2012, Klichowicz, Reichert et al. 2014). If $B_{i,j}$ values are independent of the initial size (i.e. dimensionally normalizable), then $\sigma = 0$. This parameter characterizes the degree of non-normalization.

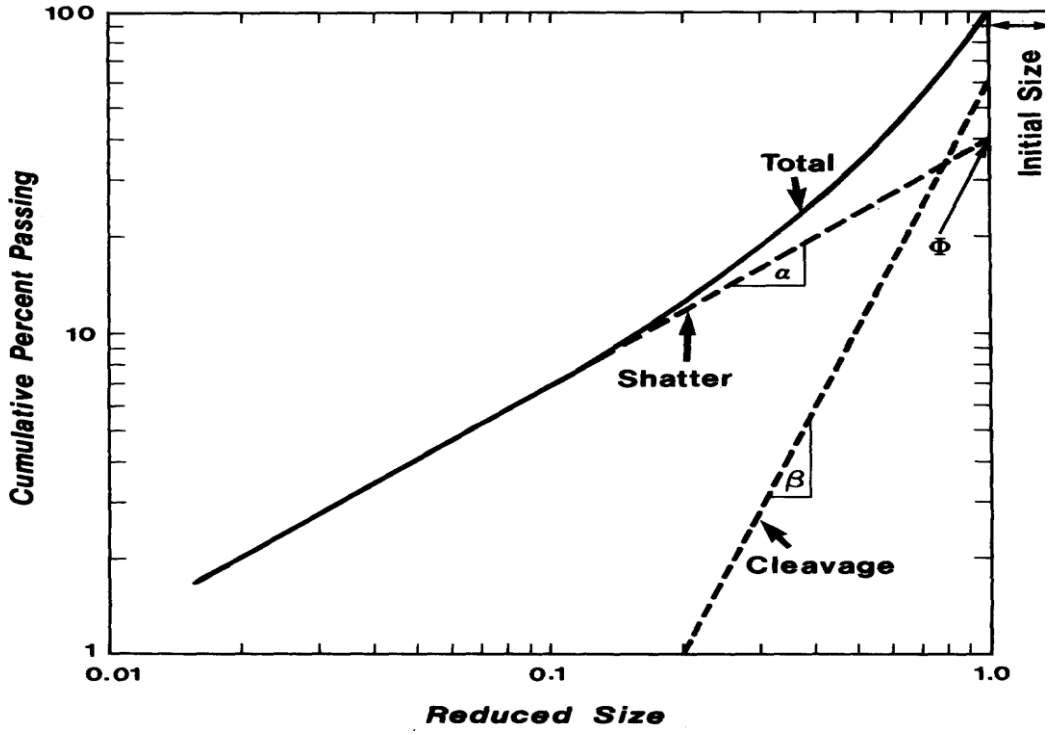

Figure 3-23: The breakage distribution function, illustrating its resolution into two components (Kelly and Spottiswood 1990).

An alternate method of determining the breakage function has been advocated by Napier-Munn (Napier-Munn, Morrel et al. 1996). In this method the relative size

distribution after breakage (x_{i-1}/x_j) is plotted against the cumulative percent passing and the t_{10} index is determined. A plot of the breakage index t_{10} (fraction or %) against t_n (fraction or % passing 1/n of the parent size) gives the material breakage function. Figure 3-24 presents an example of plots for breakage functions which are defined in terms of the parameter t_{10}. This relationship is expressed (King 2001, Gupta and Yan 2006) as:

$$t_n = 1 - \left(1 - t_{10}\right)\left(\frac{10-1}{n-1}\right)^{\alpha} \tag{40}$$

where *a* = α specific parameter.

n =parent size/progeny size

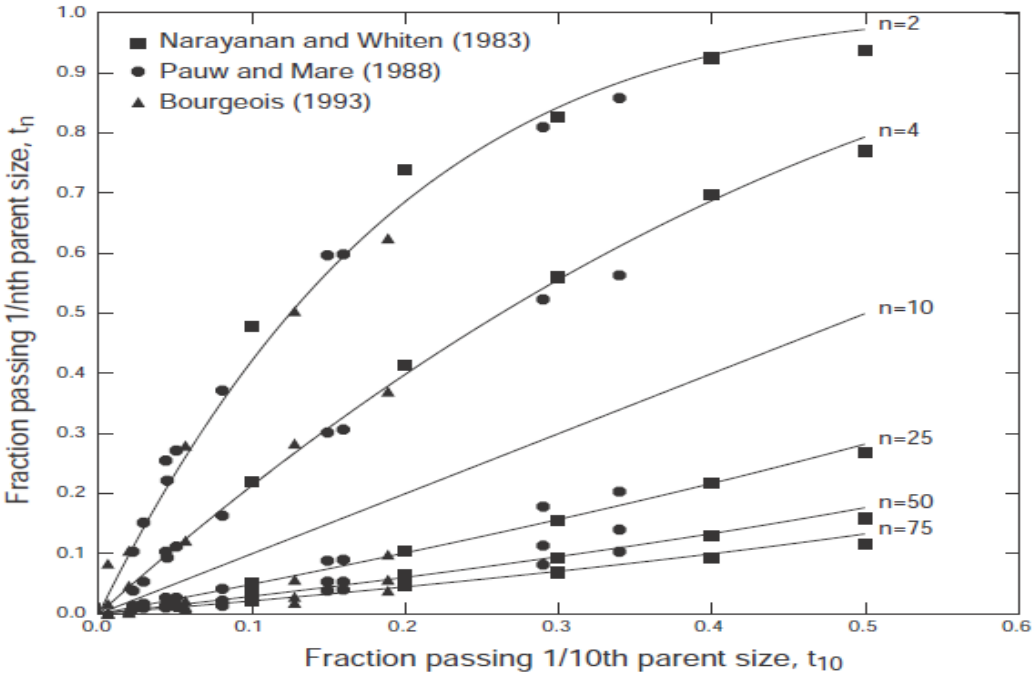

Figure 3-24: Plot for the breakage function that is defined in terms of the parameter t_{10}.

3.4.2.2 Estimation of Selection Function

The disappearance of particles per unit time and unit mass due to breakage is assumed to be proportional to the instantaneous mass fraction of particles of that size fraction present inside the mill. This statement is known as *first-order breakage law* and is written as follows (Austin 1972, Gupta and Yan 2006):

$$-\frac{d\left[m_i(t)M\right]}{dt} = -S_i m_i(t) M \tag{41}$$

Where M =total mass load in the mill

S_i = the mass proportionality constant (selection function)

$m_i(t)$ = the mass fraction of size i after a grind time, t

Since the total mass is constant in the batch mill and if S_i is independent of time, then Eqn. (41) can be integrated to:

$$m_i(t) = m_i(0)\exp(-S_i t) \quad or \quad \log\left[m_i(t)\right] = \log\left[m_i(0)\right] - \frac{S_i t}{2.303} \tag{42}$$

A plot of $m_i(t)/m_i(0)$ versus grind time, t, should give a straight line of slope $(-\frac{S_i}{2.303})$ on a log-linear scale as shown in Figure 3-25 (Gupta and Yan 2006).

It is not yet established in theory why particles follow this law. But until that is achieved, the model is reasonably good for many materials over a wide range of operation (Austin, Klimpel et al. 1984, Napier-Munn, Morrel et al. 1996).

However, substantial deviations from the first-order law are noted for coarse materials (Austin 1972). In this case breakage is said to occur in the abnormal region.

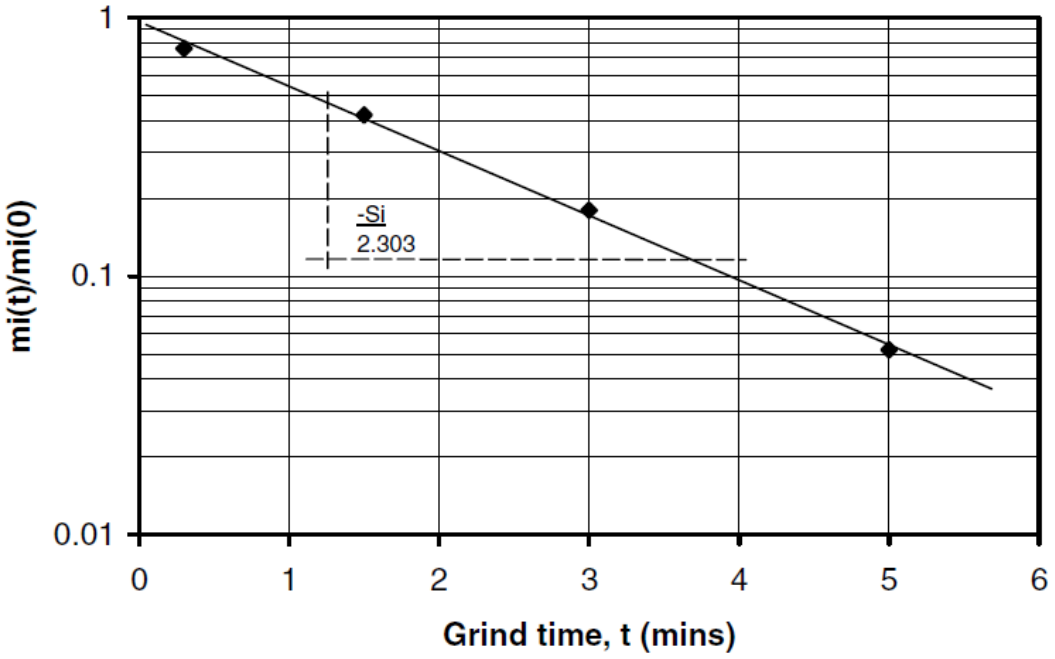

Figure 3-25: First order plot for breakage rate determination (Gupta and Yan 2006) .

Perhaps the most important point is how the rate of breakage changes with respect to particle size. According to Griffith theory of breakage (Austin, Klimpel et al. 1984) for the same size of balls in a mill, very fine particles are hard to break. This suggests that

as the particle size increases the breakage rate should continuously increase. The general observed trend line (Figure 3-26) agrees consistently with this statement. But then comes a turning point after which particles become too large to be nipped by balls. The rate of breakage steadily drops and tends to zero.

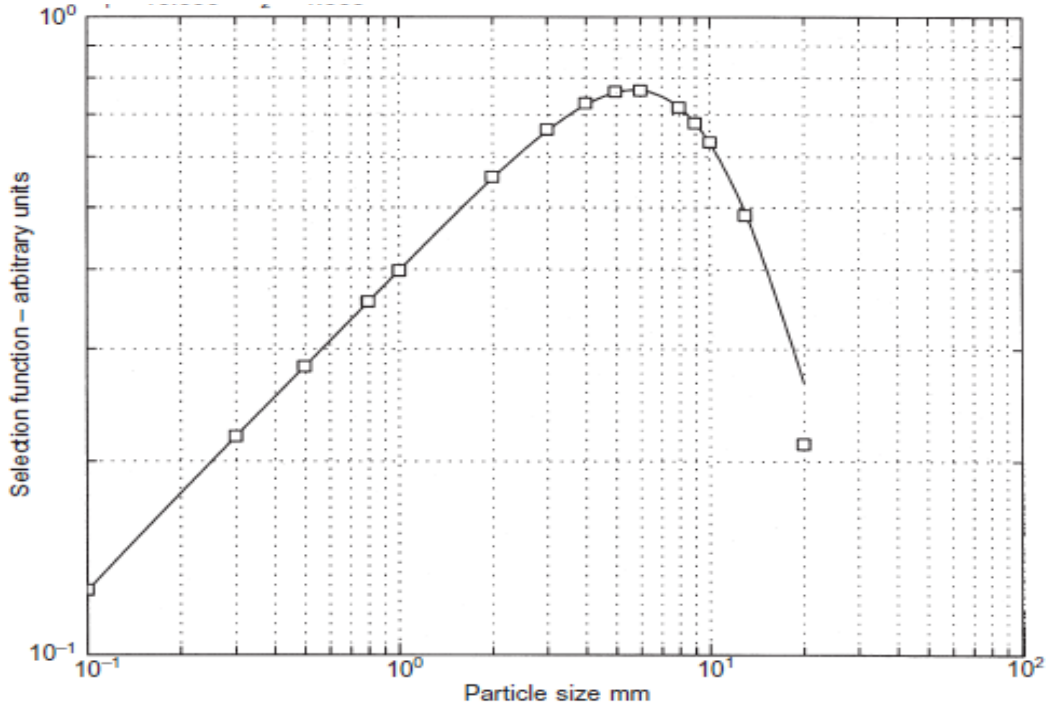

Figure 3-26: An example of a plot for the specific rate of breakage as a function of particle size (King 2001).

Now, based on results of several laboratory tests, Austin and co-workers (Austin, Klimpel et al. 1984) were able to show that the rate of disappearance of particles as a function of size is given by:

$$S_i = a \cdot x_i^{\alpha} \cdot Q(x_i) = a \cdot x_i^{\alpha} \frac{1}{1+\left(\frac{x_i}{\mu}\right)^{\lambda}} \tag{43}$$

where x_i is the particle size of class i in mm

α and *a* are parameters strongly dependent on the material used

μ is the median size varying with mill conditions

λ is a material characteristic allowing the selection function to decrease with increasing particle size.

For finer materials, it is readily seen that $Q(x_i)$ reduces to approximately 1, and therefore Eqn. (43) becomes:

$$S_i = a \cdot x_i^{\alpha} \tag{44}$$

The parameter α is a positive number normally in the range 0.5 to 1.5. It is characteristic of the material and does not vary with rotational speed, ball load, ball size or mill hold-up over the normal recommended test ranges for dry milling, but the value of *a* will vary with mill conditions (Austin and Brame 1983). λ is a positive number which is an index of how rapidly the rates of breakage decreases as size increases: the higher the value of λ the more rapidly the values decrease (Katubilwa and Moys 2009, Francioli 2015).

3.4.3 Scale-up of Batch Grinding Data

Modelling and simulation of industrial scale mills relies on data from laboratory scale batch grinding tests. The data are scaled-up prior application to industrial mills. In the scale-up process, material specific parameters are distinguished with those that are mill specific (King 2001). The breakage function parameters do not need any scale-up if the material is considered normalisable (see also chap. 3.4.2.1) (Chimwani, Mulenga et al. 2014).

A procedure for scaling-up of the selection function from batch grinding tests is proposed by Austin and others (Austin, Klimpel et al. 1984, Austin and Klimpel 1985, Austin, Menacho et al. 1987). The empirical equations predict how the selection function change with ball and mill diameters (*d* and *D*), ball filling (φ_{GM}), powder filling (φ_{MG}) and rotational speed (ψ_c):

$$S_i(d) = a_T (x_i)^{\alpha} \left(\frac{1}{1 + \left(\frac{x_i}{C_1 \mu_T} \right)^{\lambda}} \right) C_2 C_3 C_4 C_5 \tag{45}$$

$$C_1 = \left(\frac{D}{D_T} \right)^{N_2} \left(\frac{d}{d_T} \right)^2 \tag{46}$$

$$C_2 = \left(\frac{d_T}{d} \right)^{N_0} \tag{47}$$

$$C_3 = \begin{cases} \left(\dfrac{D}{D_T}\right)^{N_1}, & D \le 3.81\ \text{m} \\ \left(\dfrac{3.81}{D_T}\right)^{N_1}\left(\dfrac{D}{3.81}\right)^{N_1-N_3}, & D > 3.18\ \text{m} \end{cases} \tag{48}$$

$$C_4 = \left(\frac{1+6.6\,\varphi_{\mathrm{GMT}}{}^{2.3}}{1+6.6\,\varphi_{\mathrm{GM}}{}^{2.3}}\right)\exp\left[c\left(\varphi_{\mathrm{MG}}-\varphi_{\mathrm{MGT}}\right)\right] \tag{49}$$

$$C_5 = \left(\frac{\psi_c - 0.1}{\psi_{cT} - 0.1}\right)\left(\frac{1+\exp\left[15.7\left(\psi_{cT}-0.94\right)\right]}{1+\exp\left[15.7\left(\psi_c-0.94\right)\right]}\right) \tag{50}$$

The subscript T refers to the laboratory test. C_1-C_5 are multipliers that describe the variations of selection function with design and operating variables (Austin, Menacho et al. 1987, Austin, Julianelli et al. 2007). The parameters N_o, N_1, and N_2 are correction factors accounting for the change in mill diameter and ball size from batch to full-scale milling (i.e. N_o = 1, N_1 = 0.5, N_2 = 0.2). Parameter N_3 accounts for the adjustment needed for larger mills; its default value is 0.2. The value of c is dictated by milling environment of the full-scale mill, where c values of 1.2 and 1.32 are recommended for dry and wet milling, respectively. The ball filling (φ_{GM}), and the powder filling (φ_{MG}) (fractions in Eqn.(49) are determined using Eqn. (14) and Eqn. (15), respectively.

The residence time of the material in a mill can vary. Some particles of the material may leave immediately, while some may hold up for longer time. Therefore, a residence time distribution exists which can be measured by tracer tests. The mean residence time of the material can be calculated by:

$$\tau = \frac{V_{\mathrm{mill}}}{\dot{V}} \tag{51}$$

In order to determine the hold-up in the mill, an empirical equation describing the variation of powder filling degree (φ_{GM}), with solid flow rate, $\dot{m}$, in a wet overflow mill have been proposed (Sönmez and Demirel 1996) as:

$$\varphi_{MG} = 0.63\sqrt{\left(\frac{\dot{m}}{\psi_c D^{3.5}}\right)} \tag{52}$$

3.4.4 Models for Grinding Processes

Useful comminution models have to find a way to represent the application of energy by a machine to an ore. The models therefore have to describe two elements (Napier-Munn, Morrel et al. 1996):

- the breakage properties of the rock, essentially the breakage which occurs as a result of the application of a given amount of specific energy
- the features of the comminution machine:
    - the amount and nature of energy applied
    - the transport of the rock through the machine

The modelling of comminution has historically been dependent on the computational power available to perform the necessary calculations. Before computers, all models related energy input to the degree of size reduction.

The early modelers, such as Austin, Lynch and Whiten, were severely limited by the available computational power. This challenge did result in some elegant and simple models which were very useful. However, as computational power per unit cost has doubled about every 18 months since perhaps 1960, computational cost has largely ceased to be an issue, except for discrete element models (DEM) and computational fluid dynamics (CFD) (Cleary 2001, Powell and Morrison 2007, Weerasekara, Powell et al. 2013, Brosh, Kalman et al. 2014, Tavares 2017). An unfortunate side effect is a tendency to increase model complexity. This complexity reduces model utility as tools for understanding comminution processes (Napier-Munn, Morrel et al. 1996). Although still in the development, DEM research is ready for application in the design, monitoring, and control of tumbling mill circuits (Mishra 2003).

Comminution models can be divided into two main classes:

- those where a comminution device is considered as a transform between the feed and product size distributions
- those where each element within the process is considered

The first category are now in common use. The latter require huge computational resources but will become practical as computer power continues to rise. For simplicity of terminology these classes are referred to as *Black box* and *Fundamental* respectively.

A Black box model aims to predict the product size distribution from an ore feed size distribution, breakage characterization and experience with similar devices, i.e. a data base, encapsulated in an appropriate algorithm. It is phenomenological in the sense that it seeks to represent the phenomenon of breakage, rather than the underlying physical properties. The population balance model is the widely used example of this class. It is commonly used to simulate comminution processes and is more realistic representation of the process (Smith 2005).

A fundamental model considers directly the interactions of ore particles and elements within the machine, largely on the basis of Newtonian mechanics, they are also referred to as mechanistic. Adequate computer power for fundamental modelling has only become affordable on the desktop since about 1990, and such models are much less developed than the black box variety (Napier-Munn, Morrel et al. 1996, Powell and Morrison 2007).

The objective of a fundamental model is to generate a relationship of detailed physical condition within a machine and its process outcome. In practice, this means considering a substantial number of elements within grinding mill or flows within a classifier (Powell and Morrison 2007, Weerasekara, Powell et al. 2013). To make the computational manageable, earlier workers selected zones of each problem. Mmishra and Rajamani at Utah (Napier-Munn, Morrel et al. 1996) considered a ball mill as a two dimensional slice of circles. However, the 'circles' were provided with the mass of equivalent spheres. Radziszewski and co-workers (Radziszewski et. al 1989) reduced computational demand by dividing the mill into zones of impact, abrasion /attrition and little action, and then characterizing each. For either approach, the simple application of Newton's laws of motion very quickly becomes quite complex (Napier-Munn, Morrel et al. 1996). As *Black box* models are currently the most applicable from lab scale to scale-up of industrial operations, they are the main focus in this section.

For ball mill modelling, two variations of black box models dominate the application of simulation techniques. These are the population balance model, and a related model, the Whiten perfect mixing ball mill model. A variation on the perfect mixing model is the Whiten crusher model (Napier-Munn, Morrel et al. 1996, King 2001, Gupta and Yan 2006)**.** For long period there was vigorous academic rivalry between these two models. However, Whiten (1972) demonstrated that they were more similar than different. Both models remain in common use and have been used to model many types of

comminution devices. They differ essentially in the assumptions made about mixing and residence time.

3.4.4.1 The Population Balance Model

This model was introduced by Epstein (1947) with further development by many including Kelsall et al. (1969), Whiten (1974), Herbst and Fuerstenau (1968, 1972), and Austin and co-workers (Austin et al. 1983). The model concepts are widely used in modern process simulation.

This model is sometimes called *"first order rate model"* because it effectively assumes that the production of ground material per unit time within the mill depends only on the mass of that size fraction which is present in the mill contents, i.e. there is a rate constant S_i for each size fraction, which characterizes its rate of disappearance. This rate describes the breakage probability of a certain specimen under defined load and is also known as breakage rate.

$$Breakage\ \ rate = S_i m_i \tag{53}$$

Where S_i =specific rate of breakage or selection function (min^{-1})

m_i =mass of $_{ith}$ size fraction in the mill

While this assumption has the advantage of simplicity, it is clearly not justifiable over a wide range of operation. What does remain approximately constant is the number of available impacts in each energy range. If there are too few particles to match the available number of impacts, this key assumption is clearly invalid. However, in an industrial context with only relatively small changes in operating conditions, this model proved to be very useful and has certainly increased grinding efficiency worldwide. Because of the inherently short ranges on prediction the model must be used as part of an iterative optimisation process.

To derive the actual model, we can consider a simple mass balance for a particular size fraction i, within a mill (or a section of a mill) with transport into a breakage zone, breakage in and transport out of the zone (Napier-Munn, Morrel et al. 1996, King 2001) as shown in Figure 3-27.

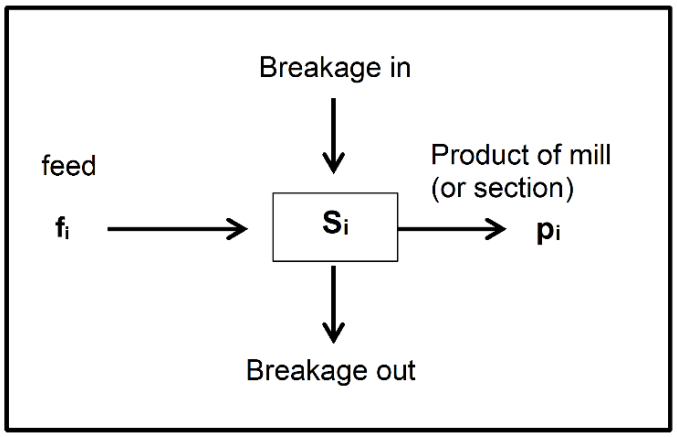

Figure 3-27 : Mass balance for a single size fraction inside a mill (Napier-Munn, Morrel et al. 1996).

It follows that:

$$\text{Feed in} + \text{Breakage in} = \text{Product out} + \text{Breakage out} \tag{54}$$

In addition to S_i, the rate of breakage, *a* breakage function, b_{ij} describes the fraction of size range *j* which reports to size range i after breakage.

Now the balance equation can be written as:

$$f_i + \sum_{j=1}^{i-1} b_{i,j}\, S_j\, m_j = p_i + S_i m_i \tag{55}$$

f_i = feed rate of particles of size i

p_i = product rate of particles of size i

S_i = breakage rate of particles of size i

m_i = mill contents (hold-up) of particles of size i

$b_{i,j}$ = breakage function (*j* denotes starting size for the breakage event)

S_j = breakage rate of particles of size *j*

m_j = mass of size j material in the mill

To estimate the product, this equation is re-arranged to:

$$p_i = f_i - S_i m_i + \sum_{j=1}^{i-1} b_{i,j}\, S_j m_i \tag{56}$$

Given measurements of p_i, f_i and m_i and a suitable function (or matrix) for $b_{i,j}$, a set of S_i values can be calculated starting from the coarsest size fraction.

3.4.4.2 The Perfect Mixing Ball Mill Model

Although derived independently, the perfect mixing model is quite similar to the general population balance model, and can be considered a special case. Most of complexities in the general population balance model arise from the consideration of mixing. The assumption of perfectly mixed mill removes these complications (Napier-Munn and Lynch 1992). Start with the same material balance; i.e. Eqn. (54) :

$$\text{Feed in} + \text{Breakage in} = \text{Product out} + \text{Breakage out}$$

However, the Whiten terminology uses r_i for the rate of breakage and a_{ij} for a breakage function in which some of the original particle may remain in that size fraction after breakage. As the mill is perfectly mixed, mill contents are related to the mill product with a discharge rate d_i for each size fraction.

$$p_i = d_i m_i \quad or \; m_i = \frac{p_i}{d_i} \tag{57}$$

The balance equation around each size fraction is

$$f_i + \sum_{j=1}^{i} a_{ij} r_j m_j = p_i + r_i m_i \tag{58}$$

Now substituting Eqn. (57) into Eqn. (58) yields

$$f_i + \sum_{j=1}^{i} \left[\frac{a_{ij} r_j p_j}{d_j} \right] = p_i + \frac{r_i p_i}{d_i} \tag{59}$$

r_i = breakage rate of particles of size i

r_j = breakage rate of particles of size j

d_i = discharge rate of particles of size i

a_{ij} = appearance or breakage distribution function

Other parameters are as previously defined in Eqn. (55).

This means that the ratio $\frac{r_i}{d_i}$ can be calculated for each size fraction from a set of actual feed and product measurements, subject to a reasonable form of breakage distribution function.

To provide a simple correction for variations in residence time, d_i is scaled up in terms of the mill volume and volumetric feed rate, $\dot{V}$ to the term d_i^* (Napier-Munn, Morrel et al. 1996, Gupta and Yan 2006).

$$d_i^* = \left(\frac{D^2 L}{4\dot{V}} \right) d_i \tag{60}$$

Where *D* and *L* are the diameter and length of the mill.

Calculating $\frac{r}{d_i^*}$ starting at the coarsest size is very simple and is very easy to program for a spreadsheet or almost any computer language. A full set of $\frac{r}{d_i^*}$ values provides an exact transform between feed and product. However, these rates are poorly determined as individual values. Each value is a result of a set of difference equations. Hence individual values are less well determined than measured inputs. To overcome this, the $\frac{r}{d_i^*}$ function is represented by cubic spline function as shown in Figure 3-28.

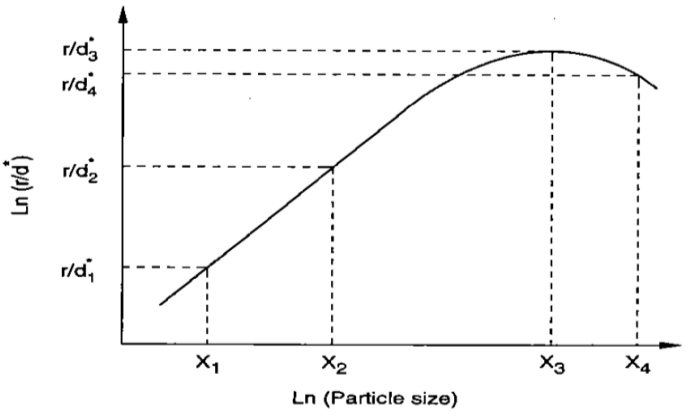

Figure 3-28: Grinding rates variation with particle size (Napier-Munn, Morrel et al. 1996).

The spline function (Whiten 1972) provides a smooth curve which is defined by 3 or 4 values at user-selected size knots (x_1-x_4). Three or four values are appropriate for ball mills with five used for AG/SAG mill modelling.

To use this model f_i, p_i and mill conditions are measured. A breakage function a_{ij} is then measured or assumed from previous results on similar ores. Suitable values of r_1-r_4 are selected and the best values are sought using a suitable search technique such as nonlinear least squares. This technique chooses values of r_1-r_4 which minimize the sum of squares of the differences between observed and model predicted product size distribution. This model has proved to be very robust and adaptable in practice. It is implemented for example in the JksimMet simulator.

Where a suitable breakage function can be defined, the perfect mixing mill model can be used to describe almost any grinding device. If the breakage characterization method can relate breakage energy to breakage function, then the model can be used to estimate effective comminution energy.

Modelling of AG/SAG Mill Processes

The perfect mixing mill model is also applied in modelling of AG/SAG milling processes (Napier-Munn, Morrel et al. 1996, King 2001, Gupta and Yan 2006). Schematically, the processes which occur in AG/SAG mills can be presented in a highly simplified form as shown in Figure 3-29. The feed enters the mill and is subjected to breakage from collision with other particle and or the mill shell. The products either exit via the grate or remain in the milling chamber to undergo further collisions. The process has essentially three components:

- collision frequency (selection function);
- ore size distribution after collision (breakage function); and
- particle transport out of the mill (discharge rate).

At steady state all components are combined in the perfect mixing model mass balance Eqn. (57) and Eqn. (58) as demonstrated earlier (chap. 3.4.4.2).

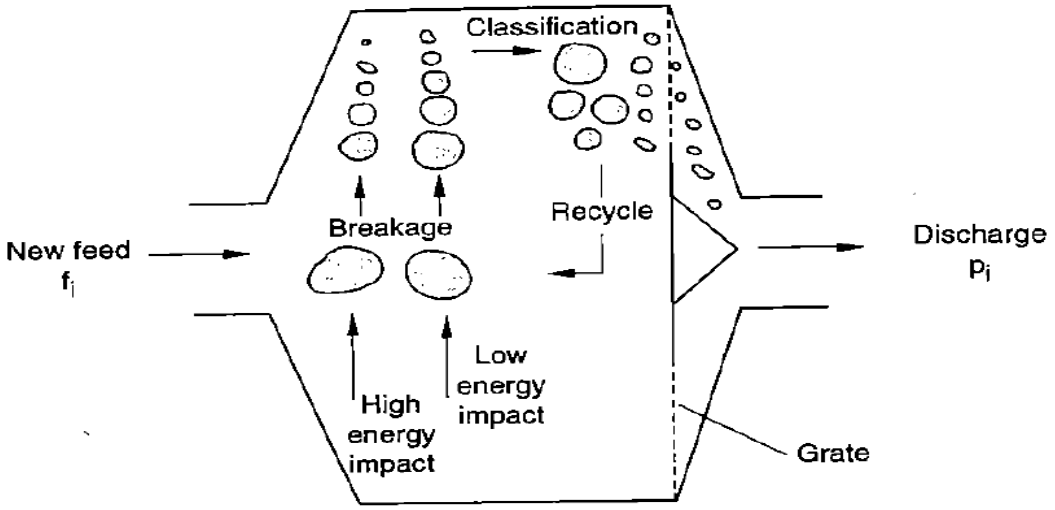

Figure 3-29: Schematic diagram of AG/SAG mill process mechanisms (Napier-Munn, Morrel et al. 1996).

In AG/SAG mills, there are two breakage mechanisms; namely impact (high energy) and abrasion (low energy). The concept of percentage of broken product passing 1/10 the original size, t_{10} (refer to Eqn.(40)), developed by JKMRC, is used for determination of ore breakage or appearance function. Eqn. (61) relates t_{10} to E_{CS} which is the specific energy of comminution (Napier-Munn, Morrel et al. 1996):

$$t_{10} = A\left(1 - e^{-bE_{cs}}\right) \tag{61}$$

The t_{10} can be interpreted as a ”fineness index” with larger values indicating a finer product size distribution. The impact breakage parameters, A and b, are determined using a high energy impact breakage device called JK Drop Weight Tester.

A is the maximum t_{10} value that can be achieved and is significant for higher energy breakage. The parameter b is related to the overall slope of t_{10} versus E_{CS} curve at the lower energies. A and b are interdependent, since the value of one will directly affect the other. Both are usually reported by $A \cdot b$ as a single value to indicate the ore hardness in terms of impact breakage. The $A \cdot b$ parameter is the slope of the t_{10} vs. E_{CS} curve at its origin and therefore is a measure of breakage of the ore at lower energy levels.

To characterize abrasion breakage mechanism, the parameter t_a is defined as one tenth of t_{10} as follows (Napier-Munn, Morrel et al. 1996):

$$t_a = \frac{t_{10}}{10} \tag{62}$$

The abrasion breakage parameter, t_a, is determined by performing a tumbling test. A lower value of t_{10} (hence a lower t_a value) indicates that there is a lower percentage of material passing 1/10th the original particle size, or higher resistance to abrasion breakage. Napier-Munn and co-workers (Napier-Munn, Morrel et al. 1996) indicate a possible correlation between the impact ($A \cdot b$) and abrasion (t_a) parameters with the Bond ball mill work index given by the equations:

$$A \times b = -3.5\ W_i + 117 \tag{63}$$

$$t_a = 19.7\ W_i^{-1.34} \tag{64}$$

Where t_a and A are in %, b is in % t/kWh and W_i in kWh/t

3.4.5 Models for Classification Processes

Ideally there is no technical classifier which can achieve 100 % separation of the feed into a stream of fines only and another stream of coarse particles only at a defined cut size. Due to stochastic factors of particle collisions and turbulence and flow pattern within the separating medium some of the fine particles will report to the stream of coarse particles and also some of the coarse particles will report to the stream of fine particles (Schubert 1985, Schubert and Mühle 1991, Khumalo 2007).

The efficiency of classification devices like screens and hydrocyclones is typically presented by the partition curve $T(x)$ (Figure 3-30) also known as performance curve (Schubert 2003, Gupta and Yan 2006, Wills and Napier-Munn 2006). The partition curve relates the weight fraction of each individual particle size which reports to the apex (also underflow or coarse product), to the weight fraction of the same particle size in the feed. From the curve, the cut size x_T is defined as the size for which 50 % of the particles in the feed report to the coarse product stream. Particles of this size have an equal chance of going either with the overflow or underflow.

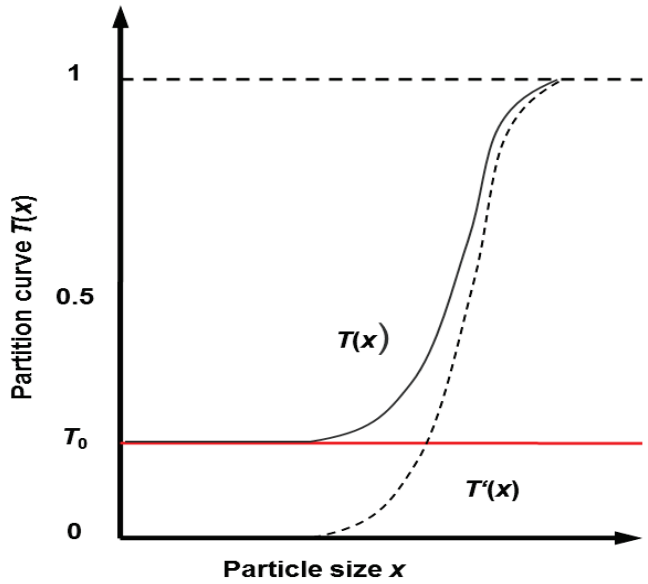

Figure 3-30 : Typical partition curve for hydrocyclones.

It has to be noted that $T(x)$ does not pass through the origin due to the fact that, a fraction of particles bypasses the classifier and is not being classified (Gupta and Yan 2006), which is especially relevant for all (hydro-) dynamic classifiers. Thus the cut size calculated from $T(x)$ has to be corrected in order to account for the bypass effect. The usual symbol for the corrected cut size is x'_T. The following equations are involved in the assessment of a given classifier:

$$T(x) = (1 - R_{m,f}) \frac{m_C(x)}{m_F(x)} \tag{65}$$

Where: $R_{m,f}$ = Fraction of particles recovered in the fine product stream

$m_C(x)$= weight fraction of particle size x in the coarser product stream

$m_F(x)$ = weight fraction of particle size x in the feed stream

$$T'(x) = \frac{T(x) - T_o}{1 - T_o} \tag{66}$$

And $$x'_T = T(x'_T) = 0.5 \tag{67}$$

T_o = the splitting factor.

The sharpness of the cut is represented by the slope of the central section of the partition curve; the closer to vertical is the slope, the higher is the efficiency. The imperfection (I) as well as efficiency of separation (κ) are given by eqns. (68) and(34):

$$I = \frac{x_{75} - x_{25}}{2x_{50}} \tag{68}$$

$$\kappa = \frac{x_{25}}{x_{75}} \tag{69}$$

x_{25} and x_{75} are sizes at which 25 % and 75 % of the feed particles report to the coarse stream.

For the case of hydrocyclones, several empirical relationships are available for their design and performance predictions. They are established from experimental investigations of hydrocyclone performances on:

- Influence of operational variables such as feed pressure, feed pulp density, flow rate etc.
- Influence of design parameters such as D_c, D_i, D_o, D_a, etc. (refer Figure 3-31)

The main performance indicators estimated from such hydrocyclone models are cut size, separation efficiency and pressure drop. This section gives an overview on such models which are widely applicable in mineral processing operations.

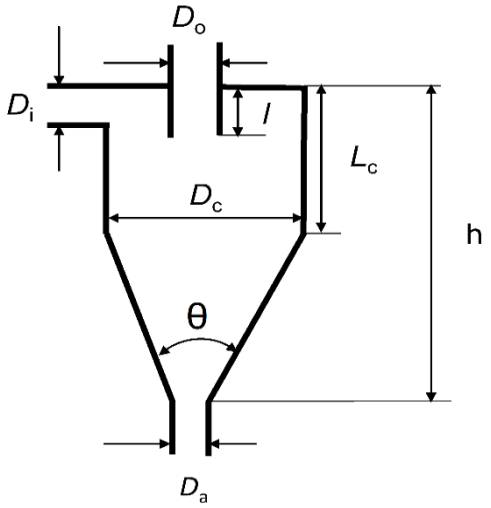

Figure 3-31: Hdrocyclone schematic diagram. D_c: cyclone diameter, D_o: vortex finder diameter, D_i: inlet diameter, l: vortex finder length inside the cyclone, Lc: cylindrical section length, h: hydrocyclone length, θ: cone angle, D_a: apex diameter.

3.4.5.1 Dahlstrom Model

Dahlstrom (1954) established an empirical relationship for determination of cut size for dilute slurries in small diameter cyclones as follows:

$$x_T = \frac{13.7\left(D_o\, D_i\right)^{0.68}}{\left(\dot{V}\right)^{0.53}\left(\rho_S - \rho_F\right)^{0.5}} \tag{70}$$

Where x_T is the cut size (in µm), D_o and D_i in cm and are as defined in Figure 3-31 above, $\dot{V}$ is the feed flow rate of the slurry (m^3h^{-1}), ρ_s is the specific gravity of solids and ρ_F is the specific gravity of the liquid (gcm^{-3}).

3.4.5.2 Plitt Model

Plitt (Napier-Munn, Morrel et al. 1996, Nageswararao, Wiseman et al. 2004, Wills and Napier-Munn 2006) developed a model Eqn. (71) that is applicable on cyclones with large diameters operating at high solids content over a wide range of operating conditions. This mathematical model can be used to calculate the efficiency of a cyclone accurately without experimental data.

$$x_T = \frac{(F1)39.7 D_c^{0.46} D_i^{0.6} D_o^{1.21} \eta_F^{0.5} \exp(0.063\varphi_{v,s})}{D_a^{0.71} h^{0.38} \left(\dot{V}\right)^{0.45} \left(\frac{\rho_S - \rho_F}{16}\right)^k} \tag{71}$$

Where D_c, D_a and h are in cm and also as defined in Figure 3-31, $\varphi_{V,s}$ is solids content by volume, η_F is fluid viscosity (Pa.s), k is hydrodynamic exponent (i.e. k = 0.5 for laminar flow), and $F1$ is material specific constant.

3.4.5.3 Lynch and Rao Model

An empirical model by Lynch and Rao (Napier-Munn, Morrel et al. 1996, Gupta and Yan 2006), Eqn. (72), is among the well-established models for cyclone design and performance prediction.

$$\log x_T = 4.18 D_o - 5.43 D_a + 3.04 D_i + 0.0319 C_{w(F)} - 3.6 \dot{V} - \\ - 4.2 * 10^{-3} Z_1 + 4 * 10^{-4} Z_2 \tag{72}$$

Where $C_{W(F)}$: % solids by mass in the feed

Z_1: + 420 µm material in the feed (%)

Z_2: -53 µm material in the feed (%)

x_T, D_o and D_i are in cm.

3.4.5.4 Schubert Model

Another interesting model has been set up by Schubert and co-workers (Schubert 1985, Schubert and Mühle 1991, Schubert 2010), Eqn. (73). This is a theoretical model based on flow characteristics (i.e. turbulent two-phase flow theory). Hence it accounts

for two flow regimes; dilute flow (<25 % solids vol. fraction) and dense flow (>25 % vol. solids fraction).

$$x_T = K\sqrt{\frac{\eta_F D_c}{\left(1-\varphi_{V,s}\right)^{4.65}\left(\rho_S-\rho_F\right)\sqrt{\frac{p_A}{\rho_P}}}\ln\left(\frac{D_a}{D_o}\right)}^{z} \tag{73}$$

$$z=\begin{cases}5D_c & \text{for } D_c < 0.1\,\text{m}\\ 0.5 & \text{for } D_c \geq 0.1\,\text{m}\end{cases} \tag{74}$$

Where ρ_P: Pulp density (kg/m^3)

p_A: Inlet pressure (bar)

z: exponent

K is the correction factor

3.4.5.5 Nageswararao Model

Hydrocyclone classifiers may also be modeled using an empirical relationship developed by Nageswararao (Napier-Munn, Morrel et al. 1996), Eqn. (75).The model was developed at JKMRC and is an extension of the original model for the performance of the hydrocyclone that was developed by Lynch and Rao. It was developed by multilinear regression of experimental data that was obtained from tests on several Krebs cyclones. The set of model equations are (Napier-Munn, Morrel et al. 1996):

$$\frac{x_T}{D_c} = KD_1\left(\frac{D_o}{D_c}\right)^{0.52}\left(\frac{D_a}{D_c}\right)^{-0.47} H_S{}^{0.93}\left(\frac{P_A}{\rho_P g D_c}\right)^{-0.22}\left(\frac{D_i}{D_c}\right)^{-0.5}\left(\frac{L_c}{D_c}\right)^{0.2}\theta^{0.15} \quad \text{and} \tag{75}$$

$$KD_1 = KD_o D_c{}^{-0.65} \tag{76}$$

Where KD_O depends on feed solids characteristics only.

$$\dot{V} = KQ_1 D_c{}^2\left(\frac{P}{\rho_P}\right)^{0.5}\left(\frac{D_o}{D_c}\right)^{0.68}\left(\frac{D_i}{D_c}\right)^{0.45}\theta^{-0.1}\left(\frac{L_c}{D_c}\right)^{0.2} \tag{77}$$

For cyclones of Krebs geometry treating identical feeds:

$$KQ_1 = KQ_o D_c^{-0.1} \tag{78}$$

Where KQ_o depends on feed solids characteristics only

$$R_f = K_{W1}\left(\frac{D_o}{D_c}\right)^{-1.19}\left(\frac{D_a}{D_c}\right)^{2.40}\left(\frac{P_A}{\rho_P g D_c}\right)^{-0.53} H_S{}^{2.7}\left(\frac{\mathrm{D_i}}{\mathrm{D_C}}\right)^{-0.5}\theta^{-0.24}\left(\frac{L_c}{D_c}\right)^{0.22} \tag{79}$$

$$R_v = K_{V1}\left(\frac{D_o}{D_c}\right)^{-0.94}\left(\frac{D_u}{D_c}\right)^{1.83}\left(\frac{P_A}{\rho_P g D_c}\right)^{-0.31}\left(\frac{D_i}{D_c}\right)^{-0.25}\theta^{-0.24}\left(\frac{L_c}{D_c}\right)^{0.22} \tag{80}$$

Where:

θ = Cone full angle

L_C = Length of cylindrical section

$\mathrm{H_S}$ = Hindered settling correction term

R_f = Recovery of water to underflow (%)

R_v = Volumetric recovery of feed slurry to underflow (%)

K = Constant to be estimated from data

KD_o = Calibration factor for x_T

KQ_O = Calibration factor for total slurry flow rate

K_{W1} = Calibration factor for water recovery to underflow

The x_T predicted in Eqn. (75) is inserted in the Whiten function (Eqn. (81)) to determine the corrected efficiency curve for the cyclone (Napier-Munn and Lynch 1992, Luis-Bahena 2001, Ergün, Giilsoy et al. 2005, Dundar, Benzer et al. 2011):

$$E_{oa} = C\left[\frac{\left(1+\beta^{*}.\beta^{**}.Y\right)\left(\exp\left(\alpha_1\right)-1\right)}{\exp\left(\alpha.\beta^{**}.Y\right)+\exp\left(\alpha_1\right)-2}\right] \tag{81}$$

Where $Y = \dfrac{x}{x_T}$ (82)

E_{oa} = The actual efficiency expressed as the particles reporting to overflow

$C =$ Recovery of water to overflow $(1 - R_f)$

$\alpha_1 =$ An efficiency parameter

$\beta^* =$ A fish-hook factor

$\beta^{**} =$ A dummy parameter introduced to preserve the definition of x_T (i.e. $x = x_T$) when $E_{oa} = (1/2)(C)$

The calibration of hydrocyclone model involves the calculation of the best fit values for α_1, β^*, x_T and *C to* the plant data. If the fish-hook behavior does not exist, then β^{**} is taken as equal to zero. The fishhook effect denotes the shape of the separation efficiency curves showing a minimum in the range of about 10 μm or below and rising again towards the finest end (Schubert 2003, Neesse, Dueck et al. 2004, Schubert 2010, Zhu, Liow et al. 2012, Minkov, Dueck et al. 2014) (refer also to Appendix F). This phenomena originates from the hydrodynamic interaction of particles of different sizes, where fine particles are entrained by large ones for poly-dispersed suspensions. The fishhook effect interferes with the separation efficiency of fine particles resulting in poor separation.

Many empirical correlations have been presented by other authors in effort to improve design and performance of cyclones (Flintoff et al., 1987; Bradley, 1965; Lynch et al., 1975). However, here detailed coverage is concentrated mainly on models reported to have wide range of industrial application and also incorporated into MODSIM simulation package.

3.4.5.6 Lippek and Espig Model

An air classifier mathematical model by Lippek and co-workers (Lippek, Espig et al. 1988) is also presented. The model is also recommended for the simulation of grinding circuits. It was obtained based on theoretical derivations and with experimental results. The separation function is described based on classifier throughput, feed fineness and speed of the disturbing plate. Although it is reported to have a wide application in the cement industry, especially in modelling and simulation of sifter classifiers, it is recommended to perform better even for other type of classifiers. The separation function is a four parameter equation described as follows:

$$T(x)=\left(1-\exp\left[-0.693\left(\frac{|x-x_o|}{x_T-x_o}\right)^{\delta}\right]\right)(1-T_o)+T_o \tag{83}$$

For separation functions where x>> x_T that and T=1 does not apply, T is replaced by an infinity value and the modified separation function is:

$$T(x)=\left(1-\exp\left[-0.693\left(\frac{|x-x_o|}{x_T-x_o}\right)^{\delta}\right]\right)(T_\infty-T_o)+T_o \tag{84}$$

δ is a separation sharpness characteristic parameter. Other parameters remain as defined previously.

3.4.6 Simulation and Optimization of Grinding Circuits

Simulation of comminution, particularly grinding and classification processes, has received great attention for many years, due to the fact that this is by far the most important unit operation both in terms of energy consumption as well as overall plant performance (Wills and Napier-Munn 2006). It has become a popular field of research and a great deal of good work has been done to make simulation into a viable and practical tool (King 2001).

A simulation of any physical process is the examination of that process using its models (i.e. mathematical models) without running the process itself. The models will respond to the given inputs much as the real operation would be expected to behave(Maria 1997, King 2001). Using it the engineer can test various ideas and options to get an understanding of how the actual operation would behave in certain circumstances. In general, simulation can aid the process engineer to accomplish the following tasks (Maria 1997, King 2001, Smith 2005, Drozdiak 2011):

- size new plant and equipment,
- try new equipment or control strategies and see how the system performs at different loads or ore blends.
- remove uncertainty from engineering decisions
- ‘test drive’ and optimize systems before design is finalized and implemented (i.e. cost-savings and cost-avoidance tool)

Simulation implies the prediction of the steady state performance of a circuit, in terms of stream properties such as mass flow, solids concentration and size distribution, as a function of material properties, machine specifications and operating conditions (Napier-Munn, Morrel et al. 1996). Generally, a simulation is only an approximation to the real behavior; especially for a process as complicated as milling. The mathematical models can be more or less complex depending on how closely one wishes to simulate the real situation (King 2001).

Digital computers are the effective tools to make simulation a practical tool for design, analysis and optimization for most of unit operations in mineral processing. The digital computer is programmed to mimic the behaviour of the actual plant and can provide a description of what the plant will do and how it will perform under a variety of circumstances. This is advantageous in the sense that the computer can expose many aspects of the plant performance without the inconvenience of operating the plant itself under experimental conditions (King 2001).

The computer is an essential component of simulation for two reasons: In most systems of interest to the mineral processing engineer, the individual unit operations are so complex that they can only be usefully described in mathematical terms if these can be translated into computer code. In addition the systems of interest reveal complex interactions and interconnections among the individual units. In many cases these complex interactions cannot be described adequately by purely mathematical methods and the ability of the computer to transfer information from one sub-model to another is exploited effectively to simulate the transfer of actual material, information or energy in a real system (King 2001).

Simulation of a complex engineering system is only possible once a detailed understanding of each component of the system has been achieved. The simulator predictions can only be as good as the basic understanding of the component parts. Purely mathematical formulations of complex systems are really effective only when the systems are linear in the mathematical sense. Then the full power of linear and matrix algebra can be brought to bear on the problem. Regrettably most systems of real interest are strongly non-linear and it is necessary to use the heuristic capabilities of the computer to take the place of purely mathematical descriptions. A computer simulation is an abstract representation of reality constructed in computer code. To be useful it must represent the appropriate aspects of the real situation in such a way that

useful information can be gained. Models for the unit operations are synthesized from mathematical models of the component parts (King 2001).

One of the principal application areas of process simulation is in the design and optimization of comminution circuits (Drozdiak 2011). However, before diving into a simulation, the engineer must first determine the key objective of the simulation and second have a very good idea of the amount and reliability of data available for the simulation. These two points are of utmost importance to any modelling project, but are often overlooked (Smith 2005). Optimization is a critical process for maximizing the profitability of all metallurgical facilities within the constraints of the mining project.

The impact of comminution on project economics is also increasing with the observed dramatic shift in the minerals industry to low grade disseminated ore reserves. Optimization typically involves three principal criteria;

- knowledge of the process
- methodology to apply this knowledge to the objective of optimization
- a baseline to judge the outcome of optimization studies

Further, there are some benefits for grinding operation optimization using simulation including decreased unit operation costs, increased capacity and production of more valuable metals and improved performance of downstream processes due to improved feed size distribution.

On the other hand, optimization using simulation consists of several stages (Napier-Munn, Morrel et al. 1996, Gupta and Yan 2006):

- characterizing the feed material in laboratory tests
- estimating machine parameters using plant survey for model calibration
- performing simulations by changing circuit flowsheet, process equipment or operating conditions to explore possible optimization solutions, and
- evaluation of solutions found through simulation studies by running plant tests under proposed flowsheet modification or operating conditions

Figure 3-32 illustrates the stages in more detail (Allen, Orrock et al. 1988):

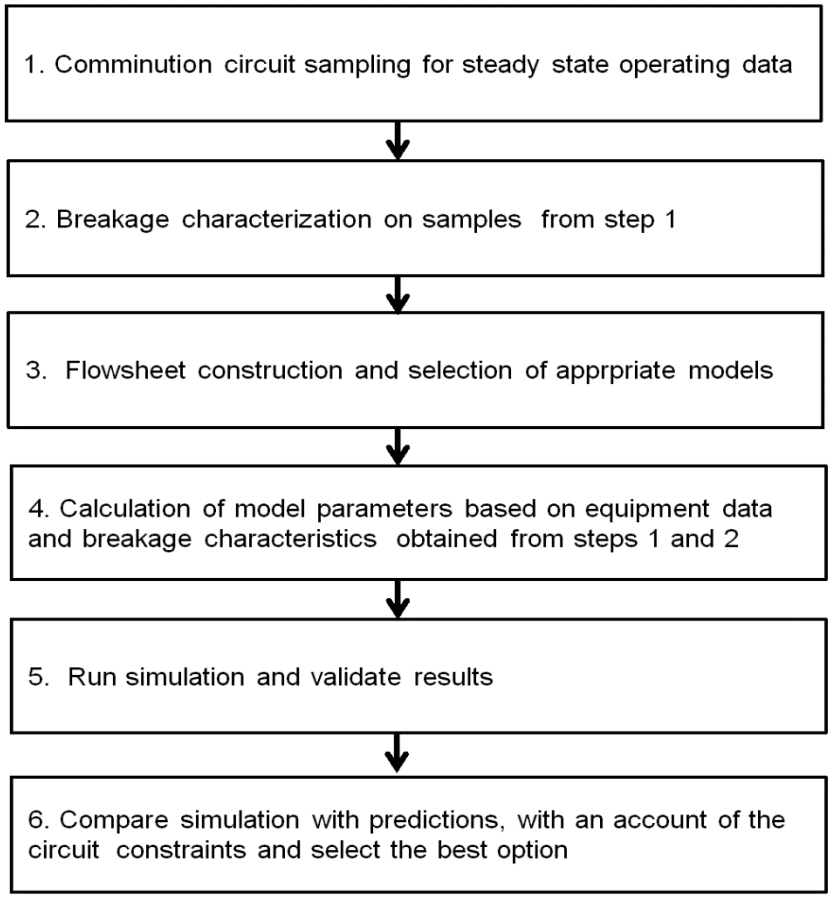

Figure 3-32: Steps Involved in Modeling and Simulation of Industrial Comminution Circuits

Regardless of whether or not computer simulation is to be used in the optimization program, it is imperative that an accurate picture is first obtained of the way the plant is currently operating. This should involve detailed surveys of the circuits concerned. Such surveys will not only provide essential data on quantities such as flowrates, size distributions etc. but also provide initial indications of where spare capacity and poor operations exist. For simulation studies, the data are used to calibrate the unit models, which are then linked together in a flowsheet drawn in the simulator which represents the current plant operation. This representation is commonly referred to as the “base case” and is subsequently used as the reference point against which the results of proposed changes are compared (Napier-Munn, Morrel et al. 1996).

The availability of reliable data from plant surveys and good models from simulation packages do not guarantee successful simulation experimentation. The proper selection and calibration of models to be used is also an important aspect which has to be considered in advance. This is due to the fact that good and well calibrated models will give predictions which are very closely with real operations. Figure 3-33 summarize steps involved for calibration of models to be used for simulation purposes.

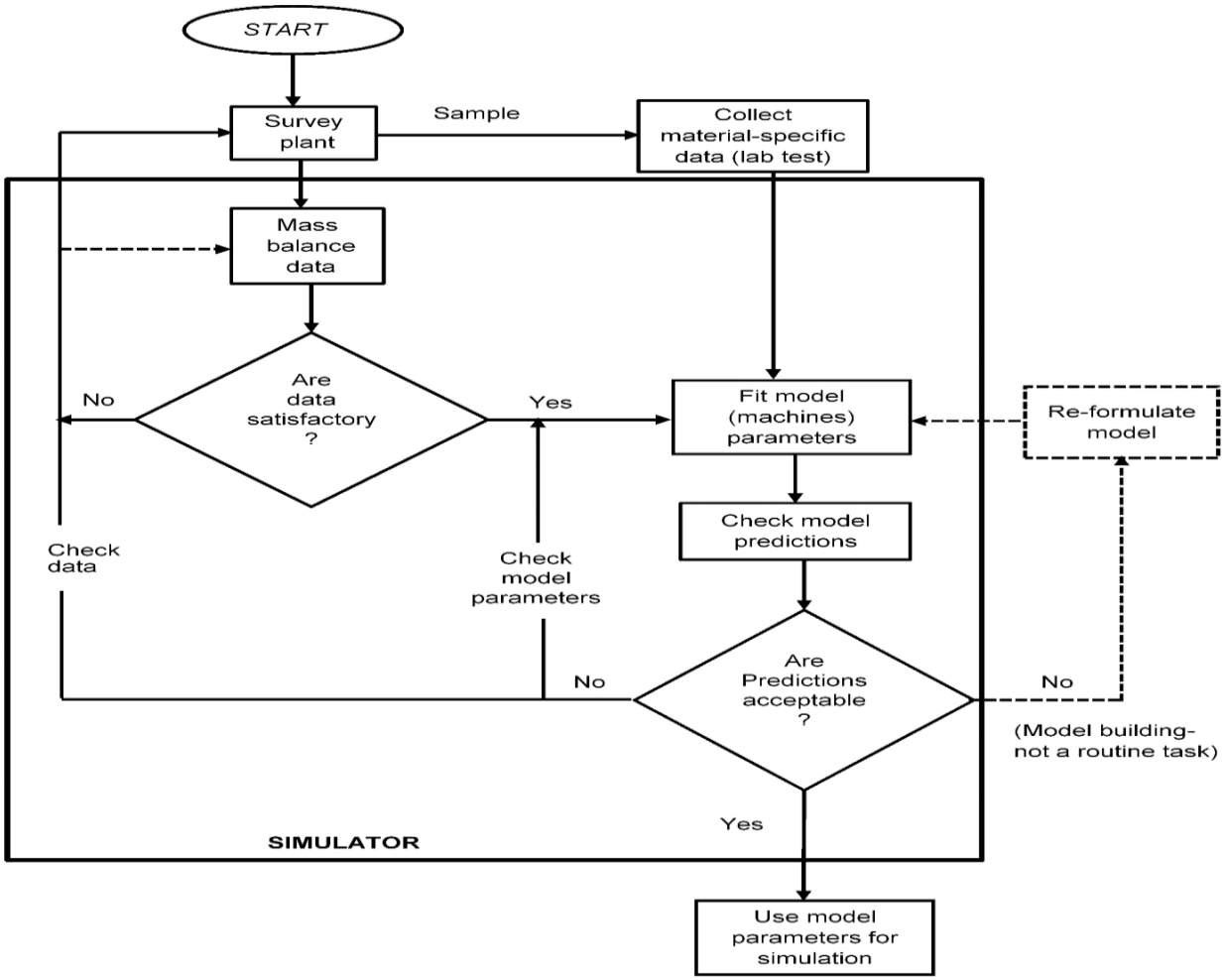

Figure 3-33: Model Parameter Estimation ('Calibration') Using Plant Survey Data (Napier-Munn, Morrel et al. 1996).

The power of simulation as an optimization and design tool is its ability to explore many different scenarios quickly and efficiently. This enables the engineer to prescribe with confidence the condition for optimum performance without the need for expensive, difficult and often inconclusive plant-scale testwork. At very least, simulation permits confirmatory plant work to be efficiently designed, leading to reduced costs (e.g. minimizing lost production) and better confidence in the final result (Napier-Munn, Morrel et al. 1996, Wills and Napier-Munn 2006).

However, the dangers of computer simulation come from its large computational power and relative ease of use. It is always necessary to bear in mind the realistic operating range over which the models are used as well as the realistic limits which must be placed on equipment operation, such as pumping capacity. Also it is worth remembering that good simulation models combined with poor data or poor model parameter estimates can produce highly plausible looking nonsense. Simulation studies are a powerful and useful tool, complementary to sound metallurgical

judgement and familiarity with the circuit being simulated and its metallurgical objectives (Wills and Napier-Munn 2006).

3.4.7 Comminution Software Packages

Different computer packages have been developed purposely for simulating mineral processing plants, and are commercialized with a varying degree of success. These simulators are used in different levels of operations; for example in understanding the system chemistry (HSC, STABCAL), design and optimization of mineral processing circuits (USIM PAC, JKsimMet, MODSIM), and in heat and mass balances (METSIM, IDEAS) using dynamic simulation (Nikkhah and Anderson 2001).

This section gives an overview of MODSIM simulation package, which is chosen for the simulation and optimization studies in the current work. The choice is motivated by the fact that MODSIM is based on a modular structure which allows for new models to be added, giving more options for simulation of various unit operations (King 2001).

MODSIM is a simulator for mineral processing plants. The software is able to give detailed mass balancing of circuits in any ore dressing plant including the assay of materials being processed. The mass balance will include total flowrates of water and solids, the particle size distribution of the solid phase, the distribution of particle composition and the average assay of the solid phase. MODSIM is unique among currently available simulation packages as it also includes liberation models for possible simulation of mineral liberation properties during comminution .This aspect of mineral processing plant operation is becoming increasingly relevant as plant managers seek higher operating and plant efficiency (Mineral Technologies International 2009).Comminution unit models integrated in MODSIM include that for;

- crushing (jaw, gyratory and cone crusher)
- grinding (HPGR, SAG/AG, ball and rod mill) and
- classification (screen-single/double and hydrocyclone)

3.5 Summary of Literature Survey

Comminution remains as the most energy-intensive and expensive unit operation in the minerals industry, hence necessitating continued research for improvement.The main purpose of this work is to assess and improve the performance of an existing grinding circuit. Therefore, understanding of the state of the art in the subject area

through literature survey is necessary. The aspect of operation and control in grinding circuits was reviewed in order to understand its state of the art in terms of operating practices as well as quality control measures. It has been revealed that grinding efficiency is dictated by several factors which require a control mechanism in place:

- Changes in feed rate and circulating load
- Changes in size distribution and hardness of the ore
- Changes in rate of water addition in the circuit

The feed size distribution and hardness of the ore are considered as the most significant factors as they influence the actual grinding mechanics. The feed rate and water addition are the only variables independently controlled by the operator. Therefore all other variables depend on changes in these two, thus are used to control the grind. Fluctuations in feed size and hardness is hinted as the most significant factor disturbing the balance of grinding circuits. This problem is caused by differences in composition, mineralization, particle size, texture of the ore from different parts of the mine, changes in mining method (e.g. blast pattern), changes in crusher settings, etc. Ore blending prior to primary crushing is recommended as a solution for fixing of minor fluctuations. Also if no segregations exist in the coarse-ore stockpile, ore storage is recommended for minimization of variations. Advantageously, the current control practices have been boosted by the advancement in automation, where plants have sophisticated digital control systems enabling all basic control functions and also dealing with multivariable nature of process optimization in real time.

The current state of the art in grinding machines development indicate that Autogenous (AG) and Semi-autogenous (SAG) mills have replaced the conventional rod mill-ball mill configurations. The main reason for the shift is explained by the fact that AG and SAG mills use cheap grinding media (ore) as replacement of the expensive steel balls and rods which contribute highly to the wear of liners. It is further revealed that a high capacity SAG-ball mill circuit is the dominant today. In such circuits, the SAG mill is closed with a pebble crusher to control the amount of “critical size” (25-40 mm) material. This size represents material too large to be broken by the steel grinding media, but also has a low self-breakage rate. If this size is left to accumulate in the mill, the mill energy efficiency deteriorates and the feed rate decreases. The critical size is normally rejected from the mill through pebble ports (i.e. 40-100 mm openings), normally cut into the mill grate. The pebble crusher is in turn used to reduce the size

of the critical size material and return it to the mill. The ball mill is closed with a hydrocyclone to provide finer and more uniform product for proceeding operations.

In terms of grinding circuit's configuration, the literature reveals that appropriate selection of equipment for a suitable configuration is dictated by ore feed size, ore type and final product size. Today, the mining industry is directed towards flowsheet simplification where larger mills in parallel circuits are more applied instead of multiple-line circuits with smaller mills. This is considered as a low cost due to savings of both capital and operating costs associated with use of less equipment.

The closed grinding circuits are the most common type of circuit configurations in mineral processing due to the fact that most ores and product requirements are not suitable for open circuit grinding. The efficiency of a closed grinding circuit relies much on the efficiency of a classifier and hence sizing and selection of this unit is of crucial consideration. In terms of classifiers, hydrocyclones have continued to dominate in grinding operations today. Their centrifugal classification mechanism intensifies classification of fine particles, giving sharper separation and fine cut sizes. They occupy much less floor space than other mechanical classifiers of the same capacity and have lower capital and installation costs.

Simulation is still valued as one of the cheapest techniques for optimization not only of grinding circuits, but also other sub-processes in mineral processing operations. The power of simulation as an optimization and decision tool is its ability to explore many different scenarios quickly and efficiently. The most effective simulation method is through the use of digital computers. This is because a digital computer can be programmed to mimic the behaviour of the actual plant and can provide a description of what the plant will do and how it will perform under a variety of circumstances. Nevertheless, there are dangers of computer simulation due to its great computational power and relative ease of use. Hence, it is always necessary for the users to bear in mind on the realistic operating range over which the models are used as well as the realistic limits which must be placed on equipment operation.

Before implementation of any simulation studies, it is necessary that an accurate picture is first established on the state of the art performance of the current operation. This has to be achieved through detailed survey campaign of the circuits concerned. Such surveys are very essential as will not only provide operating data, but also provide initial indications of where spare capacity and poor performances exist. Further, the

availability of reliable data from circuit surveys and good models from simulation software packages do not guarantee successful simulation experimentation. Hence, proper selection and calibration of models is vital and requires prior consideration.

USIM PAC, JKsimMet and MODSIM are the widely applicable computer software packages for simulation and optimization of comminution processes. The population balance model and the Whiten perfect mixing ball mill model are still widely applicable for simulation of grinding processes. The partition curve remains as the useful tool for performance assessment and improvement of classification devices, where acceptable separation functions are deduced from. The breakage and selection function parameters are site specific and thus have to be established case-wise before implementation to a modelling and simulation study.

The state of the art models for prediction of power draw in tumbling mills are those developed by Morrel (Morrell 1996) and Austin (Austin 1990). Bond's third law of comminution (Bond 1952) is still the most acceptable approach for estimation of work input in comminution devices. Furthermore, the literature review has provided an overview of the subject area. Its output is a benchmark for selection and establishment of suitable methods for solving for existing comminution problem at BGM.

4 Material and Methods

4.1 Material and Initial Preparation

The materials used in this work are three samples (S-1, S-2, and S-3) of low grade sulphide gold ore with particle size below 200 mm. The average specific gravity of the material is 2.8 g/cm^3.The samples were obtained by belt cut from the feed conveyor of the SAG mill at Buzwagi Gold Mine in Tanzania. Based on mineralogical reports of the deposit, gold and silver occurs as inclusions in pyrite, inclusions in unaltered chalcopyrite, free grains, inclusions in quartz, and inclusions in bornite. Copper occurs primarily in the chalcocite-chalcopyrite replacement grains. The mass and assay of the bulk samples as obtained from the mine site are presented in Table 4-1.

Table 4-1: Mass and assay of bulk samples as collected on site.

Item	S-1	S-2	S-3
Mass in kg	377.50	341.14	314.94
Au in g/t	1.94	1.75	1.33
Ag in g/t	2.36	3.0	1.90
Cu in wt.%	0.07	0.10	0.08

For the main investigations (i.e. mineral liberation, Bond test, and kinetic batch grinding tests), representative sub-samples were prepared by stage crushing (laboratory jaw and cone crushers), followed by splitting (riffle splitter). This general procedure is shown in Figure 4-1 , but details are given in respective test section below.

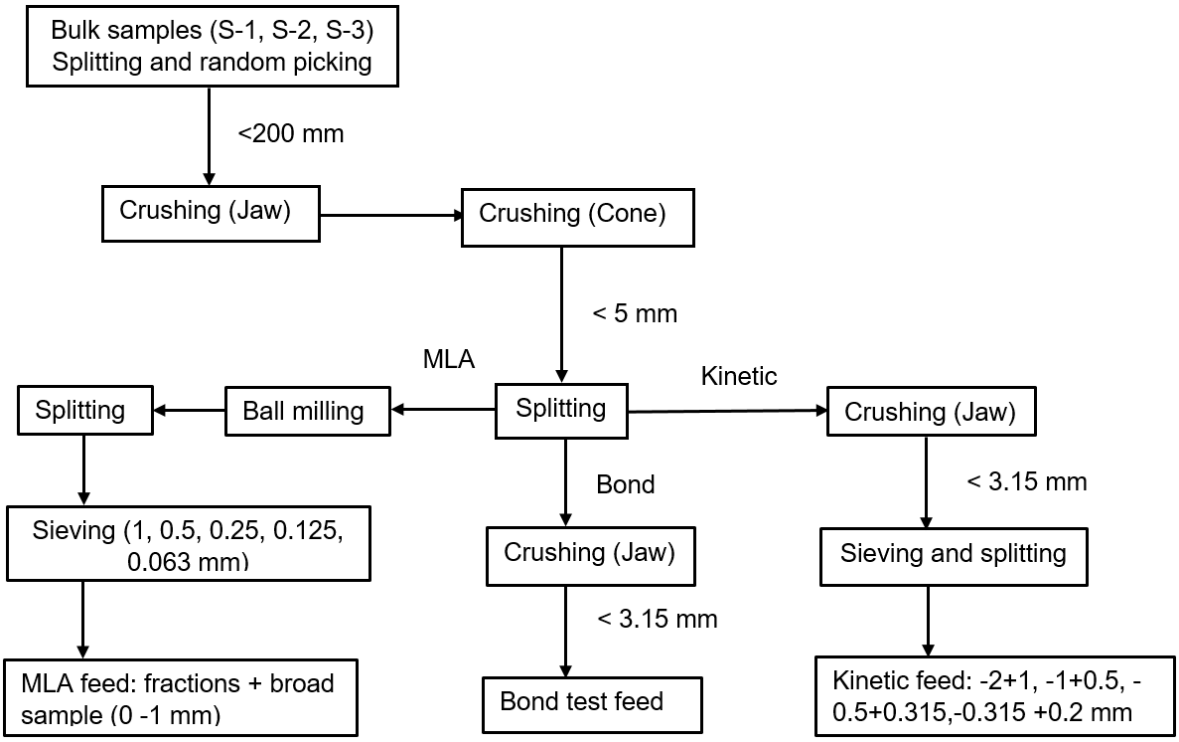

Figure 4-1: Overall preliminary sample preparation steps for the major tests.

4.2 Grinding Circuit Survey at BGM

Grinding circuit survey is an essential tool for gaining understanding on the performance of the circuit over a particular time period. It involves collection of representative samples and operating data from the circuit over a particular operating period. However, a good survey has to be conducted based on standard survey procedures and protocol as proposed by Napier-Munn and others (Napier-Munn, Morrel et al. 1996, Mular, Haibe et al. 2002), which were also implemented in the current study.

In this investigation, three (3) full scale sampling campaigns, each lasting for maximum periods of two hours were implemented. Prior to sampling, circuit operating conditions were monitored to ensure that the plant is under steady state conditions. This was verified by examining the real time circuit trends for the key parameters (i.e. circuit feed rate and cyclone feed pressure) from the control system for at least 2 hours.

The sampling and steady state monitoring points are shown in Figure 4-2 and the respective samples are listed as follows:

1) SAG mill feed

2) SAG discharge screen undersize
3) Pebble crusher feed
4) Pebble crusher product
5) Cyclone feed
6) Cyclone underflow
7) Cyclone overflow
8) Ball mill discharge

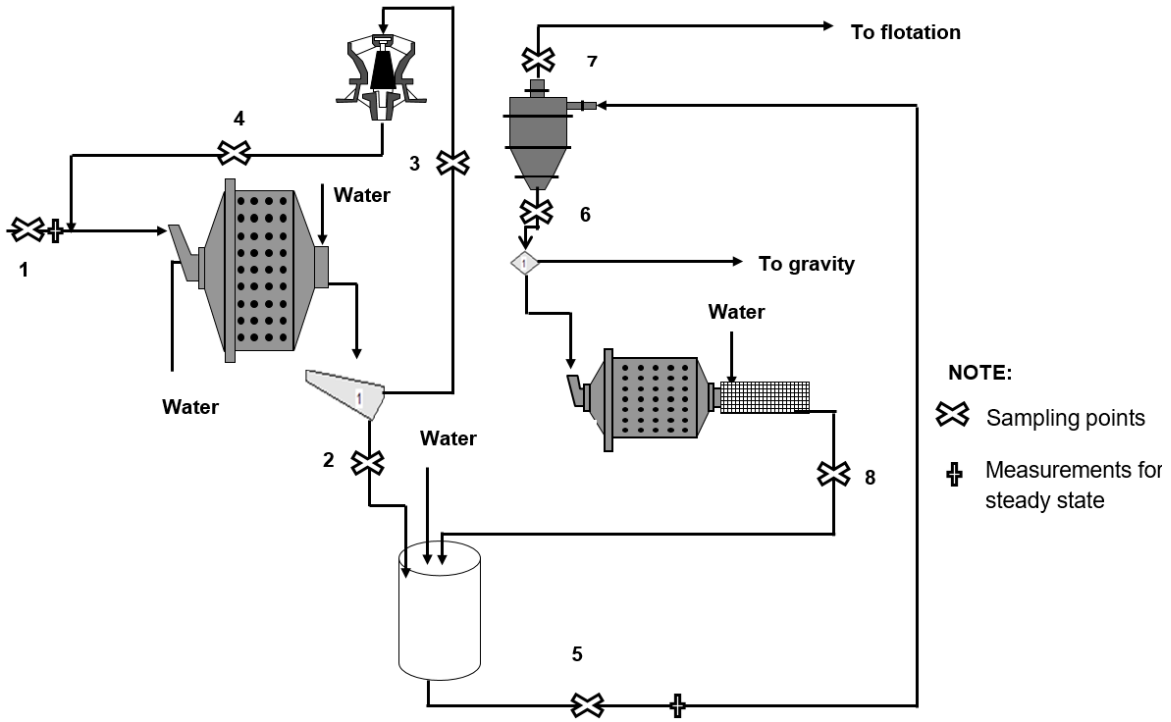

Figure 4-2: BGM grinding circuit flowsheet with sampling points.

Based on the design of the circuit, it was not possible to sample for SAG mill discharge. The flow rate for this stream was later determined from the mass balance of the other streams sampled. It has also to be realized that sample 1, 3 and 4 are mainly solids, while the rest are slurry. A brief procedure of how the two categories of samples were obtained is provided below. Additional details of the sampling plan implemented and tools used in the survey campaign can be referred in Appendix A.

4.2.1 SAG Mill Feed

The SAG mill feed sample was obtained by stopping the circuit feed conveyor and then stripping the ore. The stripped conveyor length was 3-4 m. The quantities of the SAG feed samples, approximate lengths of the conveyor belt cut applied as well as ore blends milled during the specific surveys are shown in Table 4-2. HG stands for high

grade and MG stands for medium grade. The spray grade is found at the boundary between HG and MG and possess the properties of the two. No other details could be obtained on the respective values of grades of these ores (i.e. confidential information).

Table 4-2: Belt cut samples for the SAG mill feed for the three surveys.

Survey	Belt cut length in m	Mass in kg	Grades for the blend	Blending ratio
1	4	377.50	1.79 g/t Au, 0.136 % Cu	1HG1 : 2MG1 : 1HG Splay : 2MG1
2	3	341.14	1.43 g/t Au, 0.131 % Cu	1HG1: 1MG1 : 2MG Splay: 1HG Splay : 1MG1 : 2 MG Splay
3	4	315.0	1.21 g/t Au, 0.109 % Cu	1HG1 : 6MG1 : 6MG Splay

4.2.2 Pebble Crusher Feed and Product

In each survey, the pebble crusher feed sample was grabbed from the pebble crusher feed diverter chute after every 20 minutes interval by the aid of a shovel. Pebble crusher product samples were obtained from the pebble crusher product discharge chute using the same time interval, procedure, and device as for the feed. Table 4-3 shows the collected sample mass for each stream.

Table 4-3: Total mass of samples collected for pebble crusher streams.

Stream Name	Survey		
	1	2	3
Pebble crusher feed in kg	27.74	33.45	40.42
Pebble crusher product in kg	16.70	26.00	24.00

4.2.3 Sampling Slurry Streams

Slurry sampling was done for the undersize material of the SAG discharge screen, the cyclone feed, overflow, and underflow as well as the ball mill discharge. During the whole campaign, each slurry stream was sampled every 15 minutes for a period of two hours. A total of 8 subsamples were collected to make the composite weight (i.e. Table 4-4) for the final sample. This was done in order to reduce possible sampling error due to operation or process fluctuations (i.e. plant dynamics). However, the other possible

source of errors (Napier-Munn, Morrel et al. 1996) could be due to sample cutter design, sub-sampling (e.g. splitting) of primary sample, analytical errors (e.g. weighing, inadequate sieving time, etc.) as well as propagation errors due to calculation of quantities (e.g. solids concentration).

Table 4-4: Slurry streams composite sample weights collected.

Stream/sample name	Survey		
	1	2	3
SAG discharge screen undersize in kg	18.12	20.04	20.30
Ball mill product in kg	7.15	20.30	20.80
Cyclone feed in kg	14.22	17.66	20.83
Cyclone underflow in kg	15.60	10.40	12.50
Cyclone overflow in kg	6.60	7.80	9.90

4.2.4 Other Data Collected

In order to successfully assess any grinding circuit, apart from sampling exercise, also design and current operating parameters are required. Design parameters were obtained from the design documents and include equipment specification, equipment type and operating conditions. Current operating parameters were recorded from the control system and comprise of feed rate, mill power draw, mill weight, water addition rate, mill speed, cyclone pressure, etc.

The mill ball load was determined by measuring the free height between balls and the mill shell (Napier-Munn, Morrel et al. 1996, Gupta and Yan 2006) during plant breakdown which occurred a day before survey. Details for the design and current operating conditions can be referred in Appendix A.

Napier-Munn and co-workers (Napier-Munn, Morrel et al. 1996) recommends the range of sample mass required (Table 4-5) for a representativeness of the survey campaign. All samples collected at BGM are within this recommendation. In all of the proceeding sections, the notation S-1, S-2 and S-3 will be used to refer to survey 1, survey 2 and survey 3 samples, respectively.

Table 4-5: Recommended representative sample mass for grinding circuit's survey.

S/N.	Sample Name	Sample mass (i.e. overall) in kg
1	SAG mill feed	500-800
2	Pebble crusher feed	25-50
3	Pebble crusher product	
4	Hydrocyclone overflow	3-5
5	Hydrocyclone underflow	10-15

4.2.5 Processing of Samples

All samples collected around the grinding circuit were dried and sieved to determine the amount of solids and particle size distributions. Slurry samples and pebble crusher samples were treated onsite. The SAG mill feed samples were transported and processed at the Institute of Mechanical Process Engineering and Mineral Processing, TU Bergakademie Freiberg. Apart from particle size analysis, SAG mill feed samples were further used for mineral liberation studies from batch ball mill tests, ore selection and breakage parameters determination from kinetic batch grinding tests, and grindability and work indices determination from standard bond tests.

4.2.5.1 Determination of Moisture

The moisture was determined for the SAG mill feed and pebble crusher samples. A simple block diagram (Figure 4-3) presents the procedure involved. The percentage moisture was then determined from the relation:

$$\text{Moisture content } (\%) = \left(1 - \frac{m_{dry}}{m_{wet}}\right) \cdot 100\% \tag{85}$$

Where m_{wet} and m_{dry} are wet and dry sample weights, respectively.

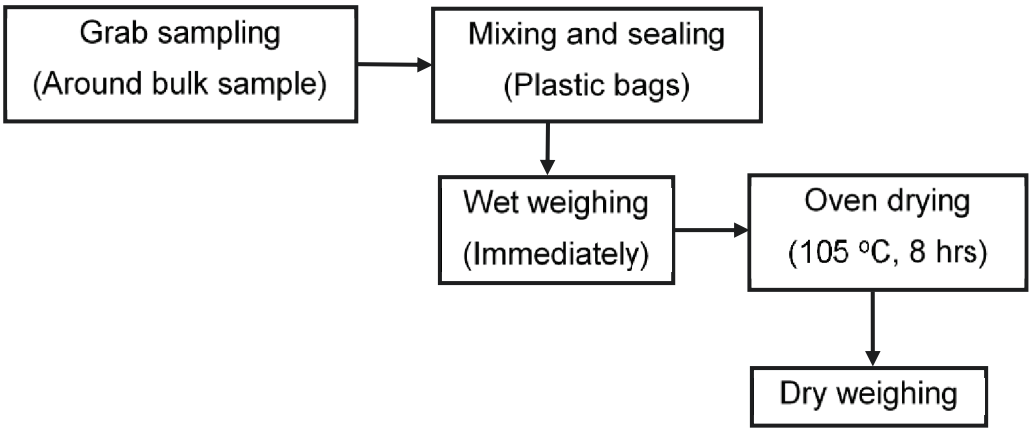

Figure 4-3: Procedure used for preparation of samples for moisture determination.

4.2.5.2 Determination of Percent Solids

The solids content was determined for all slurry samples and Figure 4-4 shows in brief what was involved.

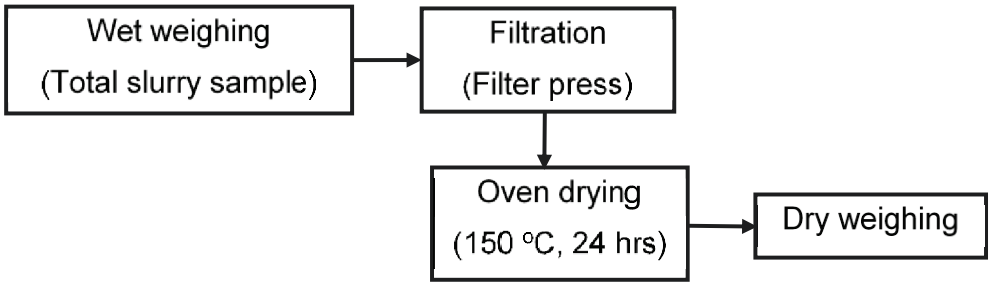

Figure 4-4: Procedure used for preparation of samples for solids content determination.

The percentage solid was later calculated from the relation:

$$\text{Solids}\ (\%) = \left(\frac{m_{dry}}{m_{wet}}\right) \cdot 100\% \tag{86}$$

Where the symbols hold the same as in Eqn. (85).

4.2.5.3 Particle Size Analysis

The dried slurry samples used for percent solids determination were also used for particle size analysis. The sieving process involved for all samples is summarized in Table 4-6.

Table 4-6: Particle size analysis procedure for the survey samples.

Sample	Procedure	Device/Equipment used
SAG mill feed	- whole bulk sample used - >45 mm: Manual sieving - <45 mm: analytical sieving machine	- 450 mm sieves - Sieve series in mm: 200, 150, 125, 90, 63, 45, 31.5, 25, 20, 16, 12.5, 10
Pebble crusher feed	whole weight of dried sample was used	- 450 mm sieves - Sieve series in mm: 50, 37.5, 26.5, 19, 13.2, 9.5
Pebble crusher product		- 450 mm sieves - Sieve series in mm: 26.5, 19, 13.2, 9.5, 6.7, 4.75, 3.35, 2.36
Hydrocyclone feed	- Splitting dried samples to obtain representative subsample	- Riffle splitter - 200 mm sieves - Sieve series in mm: 4.75, 3.35, 2.36, 1.7, 1.18, 0.85, 0.6, 0.425, 0.3, 0.212, 0.15, 0.106
Hydrocyclone underflow		
Ball mill discharge		
Hydrocyclone overflow		- Riffle splitter - 200 mm sieves - Sieve series in mm: 0.425, 0.3, 0.212, 0.15, 0.106, 0.075, 0.063

4.2.5.4 Mineral Distribution in the Circuit

The classification of particles in a hydrocyclone is influenced by their size and specific gravity. Due to its high specific gravity, gold is preferentially recycled in closed grinding circuits. This is indicated by high grade of this metal in the hydrocyclone underflow stream. This property can be used in monitoring of the circulating load in these circuits (Wills and Napier-Munn 2006). Within the same scope, and in order to investigate this phenomenon at BGM, using Atomic Absorption Spectrometry (AAS) method, gold and

copper minerals were analyzed between 0.85 mm to 0.053 mm fractions for the following streams:

- SAG discharge screen undersize
- Ball mill discharge
- Hydrocyclone feed
- Hydrocyclone underflow and
- Hydrocyclone overflow

The other important information that could be obtained from the assay of these samples are the indications for the fractions where the valuable minerals are concentrated and hence highlighting the mesh of grind or liberation size for the material.

4.3 Grinding Tests

4.3.1 Batch Kinetic Grinding Tests

The main purpose of these tests is to determine the grinding kinetics of the material, which is applied in establishing breakage function and selection function parameters. After scale-up, these parameters are finally applied as inputs to the modelling and simulation of the grinding circuit (i.e. BGM in this case). Therefore, samples have been prepared to study the grinding kinetics following the protocol as proposed by previous investigators (Austin et al., 1984). For each sample, four mono-size fractions (-2 +1 mm, -1 +0.5 mm, -0.5 +0.315 mm, and -0.315 +0.2 mm) were prepared and used as feed to the grinding tests. The fractions were prepared by sieving of the cone crusher product (refer Figure 4-1).

Two categories of tests were conducted; dry and wet grinding tests. A 30.5 by 30.5 cm, standard Bond mill was used for the dry tests. The mill design and operating variables for dry tests are presented in Table 4-7. For the wet tests, a mill with 21.8 cm length and 15.5 cm diameter was utilized. The mill design and operating variables for wet tests are presented in Table 4-8.

Table 4-7: Parameters used for dry kinetic batch grinding tests.

Mill	Inner diameter	mm	305
	Length	mm	305
	Volume	cm^3	22273
Mill speed	Critical	rpm	79.94
	Operational (75% critical)	rpm	59.95
Balls	Material	alloyed steel	
	Specific gravity	g/cm^3	7.81
	Diameter	mm	25
	Total media mass	kg	9.85
	Fractional ball filling		0.10
Material	Specific gravity	g/cm^3	2.8
	Total material mass	g	1407
	Fractional filling		0.04
	Void filling	%	100

For both categories of tests, the procedure involved is such that, the sample and steel balls were loaded to the mill and grinding tests were run for different time intervals (1, 2, 4 and 8 minutes). After each grinding interval, the entire mill charge was discharged, and a representative sample (i.e. 75-100 g) taken for sieve analysis. Later, the materials retained on the sieves were combined with the rest of the mill discharge as feed for the next grinding interval.

Table 4-8: Parameters used for wet kinetic batch grinding tests.

Mill	Inner diameter	mm	155
	Length	mm	218
	Volume	cm^3	4111
Speed	Critical	rpm	117
	Operational (75 % critical)	rpm	88
Balls	Material	alloyed steel balls	
	Diameter	mm	25
	Specific gravity	g/cm^3	7.81
	Average ball weight	g	63.86
	Fractional ball filling		0.22
	Number of balls		67
	Total mass	kg	4.24
Material	Specific gravity	g/cm^3	2.8
	Total powder weight	g	608
	Fractional filling		0.088
	Void filling		1.0

4.3.2 The Standard Bond Test

Bond developed standard laboratory tests for the determination of crushability and grindability indices (Bond 1952) and later modified it (Bond 1961).The indices are the measure of material's resistance to breakage and are applicable in his empirical energy-size-reduction Eqn. (1), to estimate the energy requirement in comminution.

The standard Bond's test is a batch type dry test where the mill is operated in a locked cycle. The charge is ground for a number of mill revolutions, sieved on the desired screen to remove undersized material and then replacing the undersized material with new feed. The procedure is repeated until a constant mass ratio of 2.5 for oversize and undersize is achieved for three consecutive cycles (i.e. equilibrium condition). Mosher and co-worker (Mosher and Tague 2001) found that the minimum number of cycles for the Bond test is seven, no matter how fast the steady state conditions are achieved.

In this study, the standard Bond test protocols were adopted and the complete description of the test may be found elsewhere (Bond and Maxson, 1943; Magdalinović, 1989; Man, 2002). The closing screen used for the investigation is 90 μm. The test gives the standard work index (W_i), which is calculated from the formula (Bond 1952):

$$W_i = \frac{44.5}{P_1^{0.23} \cdot G_{bp}^{0.82} \cdot \left(\frac{10}{\sqrt{x_{P,80}}} - \frac{10}{\sqrt{x_{F,80}}} \right)} \tag{87}$$

Where $x_{F,80}$ and $x_{P,80}$ are 80%-passing size (μm) of feed and product, respectively, P_1 is the test sieve size used (μm), and G_{bp} is the net grams of sieve undersize material produced per mill revolution. Since Bond had used short tons to determine the work index, Eqn. (87) has to be multiplied by a factor of 1.1 in order to convert to metric tonnes. The work index of the material for the present work was calculated as an average of three tests conducted for each bulk sample.

Table 4-9: The standard Bond mill operating parameters used for the tests.

Mill	Inner diameter	mm	305
	Length	mm	305
	Volume	cm³	22273
Mill speed	Critical speed	rpm	79.94
	Operational speed	rpm	70.00 (ψ = 85%)
Balls	Material		alloy steel balls
	Diameter	mm	19, 25, 38
	Specific gravity	g/cm³	7.81
	Number of balls		43 balls Ø 38 mm
			109 balls Ø 25 mm
			143 balls Ø 19 mm
	Total mass	kg	20.55 kg
Material	Gold ore		
	Specific gravity	g/cm³	2.8
	Total material filling	ml	700.00

4.4 Characterization

4.4.1 Mineral Liberation Analysis

In order to characterize the liberation characteristics of the BGM ore blends, an automated mineral liberation analysis (MLA) technique was employed. Therefore samples have been prepared in a screen ball mill with 1 mm screen (see Figure 4-1). The ground product was sieved into five fractions, -1 +0.5 mm, -0.5 +0.25 mm, -0.25 +0.125 mm, -0.125 +0.063 mm and -0.063 mm which were given to automated mineralogical characterization. A broad sample from the mill discharge (i.e. 0-1 mm) was also included in the MLA analysis.

The measurements were performed at the Department of Mineralogy, TU Bergakademie Freiberg, using FEI MLA 600F system (Fandrich et al., 2007; Gu, 2003; Sandmann, 2015; Sandmann et al., 2014; Sandmann and Gutzmer, 2013). Feed samples to the system were prepared as polished grain mounts using epoxy resin (Leißner et al., 2016; Sandmann, 2015; Sandmann and Gutzmer, 2013). Three sample split were prepared from each fraction measured by MLA. The mounts were carbon-coated prior to measurements to obtain an electrically conducting surface. The XBSE measurement mode was employed, and with the electron beam and electron current density being set at 25 kV and 10.0 nA, respectively. For each polished surface between 5000 to more than 300,000 particle sections (Table 4-10) were analyzed.

Table 4-10: Number of particles analysed by MLA for the three bulk samples.

Sample	Size classes (µm)				
	0-63	63-125	125-250	250-500	500-1000
S-1	330,779	48,884	18,026	11,518	6,264
S-2	373,306	63,350	19,629	11,724	5,163
S-3	330,867	52,079	20,161	11,635	8,391

Upon bombardment of an electron beam in a SEM, a mineral phase will backscatter electrons at an intensity defined by its average atomic number as well as release X-rays characteristic of elements that are present. The measurement of Backscattered Electron (BSE) intensities allows the segmentation of mineral phases within a single particle, while X-rays analysis of those phases allows the identification of each mineral phase. The analysis of mineral liberation data was performed by using MLA Dataview

software (Fandrich et al., 2007). For the mineral grains, between 18,000 to more than 300,000 mineral grain counts were analyzed for each fraction (Table 4-11).

Table 4-11: The number of grain counts analysed by MLA for the three samples.

Sample	Size classes (µm)				
	0-63	63-125	125-250	250-500	500-1000
S-1	341,901	67,256	34,931	27,227	19,618
S-2	386,232	81,693	35,120	32,487	18,659
S-3	342,204	69,013	39,996	30,817	21,055

A common problem with quantitative automated SEM-based image analysis is the fact that it is based on evaluation of 2D sections and hence may be subjected to stereological error (Vizcarra, Wightman et al. 2010). This can be minimized when a high number of particles or grains is analysed (Blaskovich 2013, Sandmann 2015).

4.4.2 X-ray Diffractometry (XRD)

X-ray diffractometry (XRD), traditionally called *X-ray powder diffractometry*, is the most widely used technique in materials characterization (Leng 2008). XRD measurements were conducted using PANalytical-Empyrean automatic X-ray diffractometer equipped with a continuous scanning device in order to determine the mineralogical phases in the feed material. For all samples, XRD patterns were collected between 2θ angles of 5–80° (at Co Kα radiation of 35 kV, 35 mA) with a step size of 0.0131° and a step time of 200 seconds per step. The phase identification was made by reference patterns in an evaluation program supplied by the manufacturer of the equipment.

4.5 Modelling and Simulation with MODSIM (3.6.24)

MODSIM is a steady-state simulator that is used to calculate detailed mass balance for any ore dressing plant. The software is based on a modular structure that allows for new models to be added for simulation of various unit operations. MODSIM simulation output include total flow rates of water and solids, particle size distribution of the solid phase, distribution of particle composition and average assay of the solid phase (King 2001, King 2012). MODSIM unit models selected for the simulation of BGM grinding circuit are summarized below. In this work an academic version 3.6.24 MODSIM software was used.

4.5.1 SAG Mill Modelling

One of the models used for SAG mill in MODSIM is SAGP (Semi-Autogenous Grinding with Pebble Ports). The model supports the BGM SAG mill design and was therefore selected for this work. In this model, a SAG mill with grate classification is modeled using full population balance including particle attrition and wear (Austin, Barahona et al. 1987, Austin, Menacho et al. 1987, King 2001). Three distinct breakage mechanisms are modeled, namely surface attrition, impact breakage and self-breakage. The breakage functions for the attrition and self-breakage processes are determined using data from the standard JKMRC attrition and dual-pendulum tests (Goldman and Barbery 1988). Impact fracture is modeled using the standard Austin breakage and selection function, of which their parameters were established from lab-scale tests (see chap. 4.3). The rate of self-breakage is modeled using the variation of particle fracture energy and the consequent breakage probability with size. In this model, the specific parameter for maximum breakage (μ) is scaled-up automatically in MODSIM. The breakage rate parameter (a), was prior scale-up based on concepts provided in chapter 3.4.3.

The mill is assumed to be perfectly mixed with post classification at the discharge grate. The load in the mill is calculated from the mill dimensions and the average residence time is calculated as the ratio of the load to the throughput. Water can be added directly to the mill feed at a pre-specified rate or the simulator will calculate the water addition rate that is required to achieve a specified solid content in the mill discharge (King 2001). The lab-scale selection function data fitted well to the Austin model (Eqn.(38)) as shown in Figure 4-5 and were therefore suitable for scale-up to the industrial BGM operation.

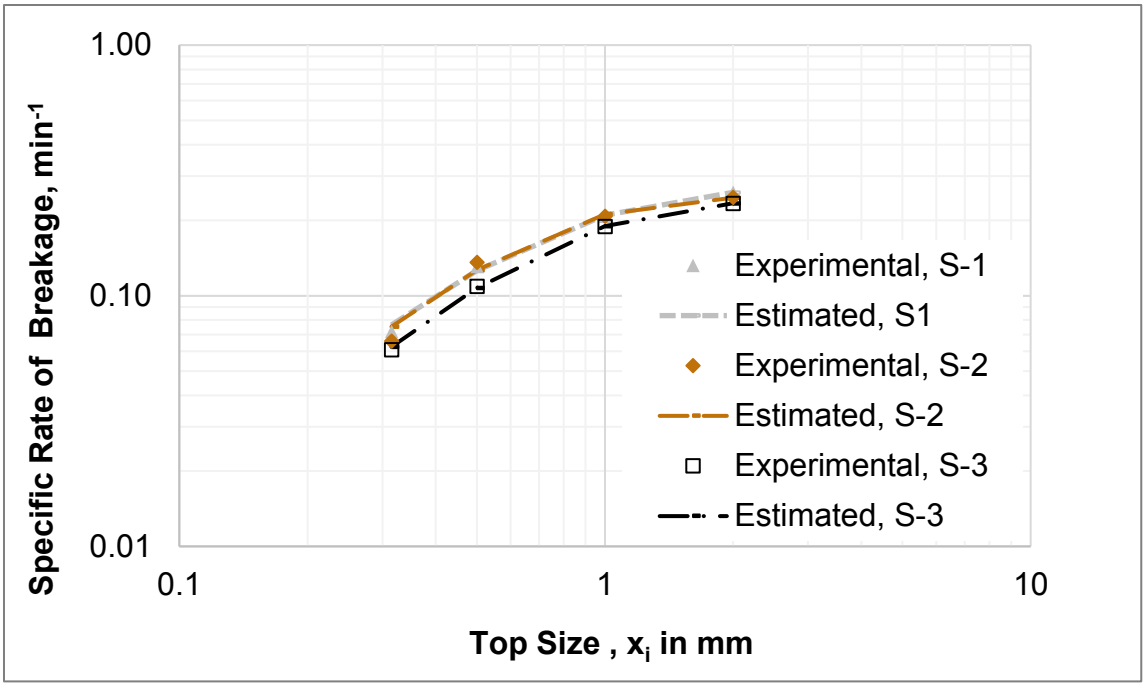

Figure 4-5: Lab-scale selection function fitted with Austin model for the three BGM ore blends.

The impact and abrasion breakage parameters were determined based on concepts described in section 3.4.4.2. Further, for the fracture energy parameters, the parameters established by Orway Mineral Consultants (2012) for the BGM ore were used. The work index and parameters of abrasion and impact breakage mechanisms for the BGM ore are presented in Table 4-12. As an example (S-1), the overall input parameters used for BGM SAG mill simulation can be found in Appendix C.

Table 4-12: Work index, abrasion and impact breakage mechanisms parameters for the BGM ore.

Ore /Sample	W_i (kWh/t)	$A \times b$ (see Eqn.(63))	t_a (see Eqn.(64))
S-1	17.20	56.80	0.43
S-2	18.67	51.70	0.39
S-3	18.47	52.40	0.40

4.5.2 Ball Mill Modelling

The model ”MILL” in MODSIM was selected for the ball mill simulation. In this model, the mill is assumed to be a single perfectly mixed region (King 2001). The selection function is the standard Austin function Eqn. (43) including the maximum that defines the decrease of the breakage rate as size gets large. The breakage function is not necessarily normalized and is also of the standard Austin form Eqn.(38) . The mean residence time of the solids must be given. The model does not need any details of the mill geometry. Water can be added directly to the mill feed at a pre-specified rate or

the simulator will calculate the water addition rate that is required to achieve a specified solid content in the mill discharge. In this case, the specific parameter for maximum breakage (μ) is prior scaled-up before application into MODSIM, while the breakage rate parameter (a), is scaled-up automatically in MODSIM. The lab-scale and industrial mill selection function parameters are shown in Table 4-13 and Table 4-14, respectively.

Table 4-13: Estimated lab-scale model parameters for the selection function.

Material	a	α	μ	λ
S-1	0.53	1.50	0.77	1.65
S-2	0.50	1.50	0.84	1.80
S-3	0.41	1.50	0.93	1.78

It has to be recognized that, only the specific parameter for maximum breakage (μ) and the breakage rate parameter (a) are affected by the mill geometry and hence require scale-up to the industrial mill size.

Table 4-14: Scaled-up model parameters for the selection function.

Material	a	α	μ	λ
S-1	11.06	1.50	3.12	1.65
S-2	10.38	1.50	3.41	1.80
S-3	8.45	1.50	3.75	1.78

The breakage function parameters do not need any scale-up if the material is normalisable (i.e. if the parameter (ϕ_j) is constant for all breaking sizes) (Chimwani, Mulenga et al. 2014). For the BGM ore samples, the parameter (ϕ_j) was constant and hence the breakage function parameters (Table 4-15) were not scaled-up.

Table 4-15: Estimated model parameters for the breakage function.

Material	γ	β	ϕ
S-1	0.82	2.50	1.00
S-2	0.83	2.50	1.00
S-3	0.72	2.50	1.00

The model parameters for the selection function, Eqn. (43), and breakage function, Eqn.(38), shown in Table 4-13 and Table 4-15, respectively were estimated by non-

linear regression using SOLVER function in Microsoft EXCEL. The method searches for the best combination of the fitting parameters of a model by minimization of residual error between experimental and predicted values (Katubilwa and Moys, 2009).

Typical values of breakage function model parameters are γ = 0.5-1.5, β =2.5-5, and ϕ =0-1 (Austin et al., 1984). For selection function, α is reported to have values from 0.5 to 1.5. Hence the parameters in Table 4-13 and Table 4-15 were considered within recommendation and used for simulation studies for the BGM operation.

In Appendix C, extracts from the SOLVER function for S-1 are presented and serve as demonstration of other samples. In the same Appendix, the overall model parameters employed in MODSIM for the BGM ball mill simulation based on S-1 can be referred.

4.5.3 Hydrocyclone Modelling

A suitable hydrocyclone model for the simulation exercise was obtained by fitting of the hydrocyclone cut sizes obtained from survey to several models reported in section 3.4.5 by the aid of the SOLVER tool in Excel. Table 4-16, summarizes the results. It can be seen that Nageswararao model gave closer values to that from the survey.

Table 4-16: Comparison of the cut size from different hydrocyclone models and with survey.

Model	x_T (µm)		
	Survey 1	Survey 2	Survey 3
Survey	220.84	251.45	203.75
Plitt (Eqn. (71))	246.22	298.50	306.40
Lynch and Rao (Eqn. (72)	280.0	280.0	320.0
Schubert (Eqn. (73))	363.80	418.60	315.60
Nageswararao (Eqn. (75))	221	251	204

Therefore this model could confidently describe the behavior of the BGM hydrocyclones and was chosen for this work. All other models predicted higher values than those from the survey. This could possibly be explained by the assumptions used in development of such models as well as their limitations. The Nageswararao (NAGE) model is incorporated in MODSIM and can be selected by the user to simulate hydrocyclone units. The calibration coefficients obtained for the model are shown in Table 4-17. After model calibration, the overall NAGE model inputs for the BGM hydrocyclone simulation can be referred in Appendix C.

Table 4-17: NAGE'S model calibration coefficients for BGM hydrocyclone (S-1).

KD_O	9.1 *10^-5
KQ_O	1.9 *10^3
K_{W1}	2.1*10^3

4.5.4 Data definition in MODSIM

Once the flowsheet has been constructed, MODSIM takes the user through a sequence of menus that will define the data set required by the flowsheet and the included models (Appendix C) for details. The material specific key input information is the so called *"System data"*. The system data describe the characteristics of the ore that is processed in the flowsheet and also the characteristics and quantities of the feed streams. The characteristics of the ore remain fixed throughout the flowsheet.

The system data form is used to set up the system data and to identify streams that feed ore to the plant or that have experimental data which is to be compared to the simulator output. As an example, the system data used for BGM grinding circuit simulation are presented in Figure 4-6.

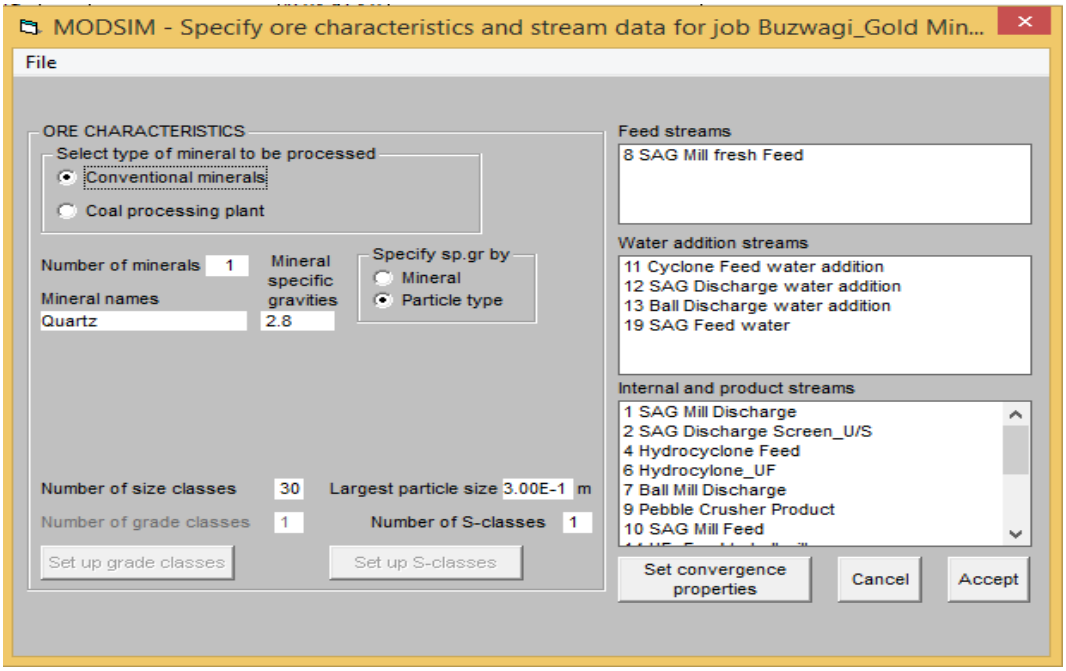

Figure 4-6: MODSIM form showing properties of the ore and streams with input data (bulk sample S-1).

In order to predict the performance of an existing operation (reference case or benchmark), the measured feed stream feed rate and particle size distribution are assumed correct. As an example, the BGM grinding circuit feed stream data which were used as input to MODSIM are shown in Figure 4-7.

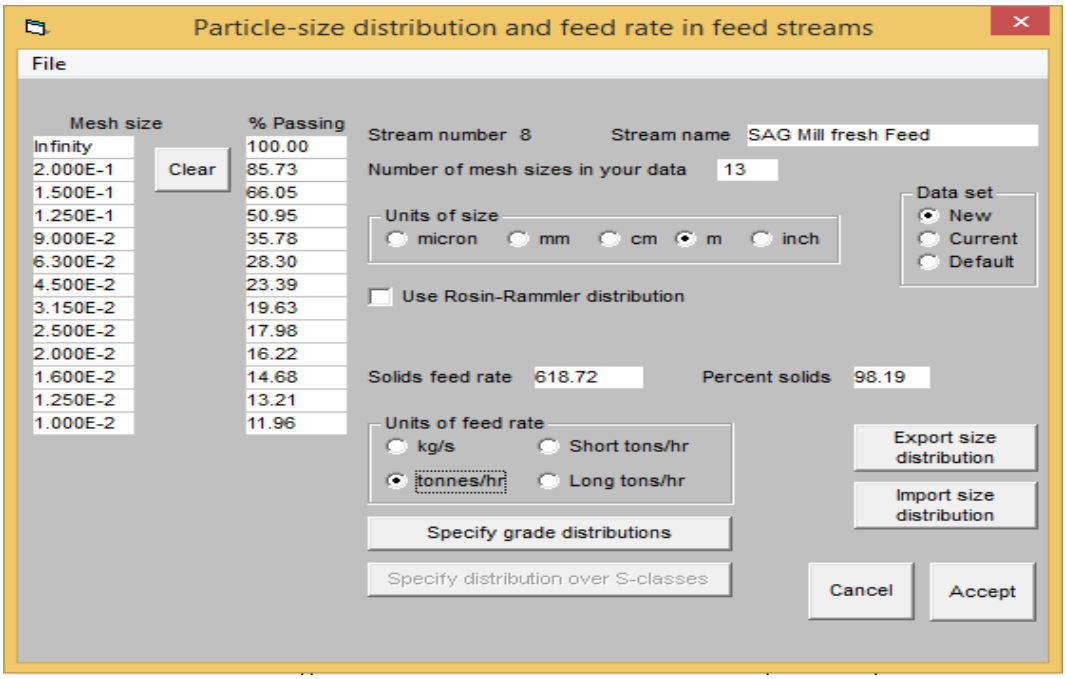

Figure 4-7: Particle size distribution and feed rate of the feed (bulk sample S-1).

5 Results and Discussions

5.1 BGM Grinding Circuit Assessment Based on Survey

5.1.1 Grindability Studies

The work index for the Buzwagi ore deposit was estimated in the plant design stage with a range from 14.5 to 16.5 kWh/t. The currently treated blends (Table 4-1 and chap. 4.3.1) range from 17.20 to 18.67 kWh/t (Table 5-1). These higher work indices indicate a change in hardness of the ore during the last 7 years or wrong assumptions regarding the development of the ore deposit itself. Abbey and co-workers (Abbey et al., 2015) investigated the impact of mining depth on the ore work index and found that the competence of the ore and work indices increase with increasing mining depth.

Overall, higher work indices have a negative impact on the energy costs of milling. Also as the mining progresses, new parts of the deposit may be discovered, which may have different characteristics from the original plant design. This situation requires a periodical re-assessment of the grindability and work indices of the different ore types encountered which was not done by BMG since plant commissioning.

Table 5-1: Comparison of the design and the current work indices for the BGM ore.

Survey	Measured (kWh/t)	Design (kWh/t)
S-1	17.20 ± 0.15	14.50 – 16.5
S-2	18.67± 0.05	
S-3	18.47± 0.2	

5.1.2 Mass Balance

Table 5-2 shows a summary of the mass balance for key streams in the circuit. In all surveys, the throughput was higher up to 22 % than the design capacity (543-566 t/h). Additionally, the designed circulating load of 250-350 % is slightly lower than the average value found during the three surveys (375 %). This implies that the circuit was overloaded. Moreover, the SAG mill dilution ratio was higher for survey 1 (0.54) compared to survey 2 (0.45) and survey 3 (0.37).The pulp density should be as high as possible so that the grinding media is coated with a layer of ore. If the pulp is too dilute, a metal to metal contact increases giving increased steel consumption and reduced grinding efficiency (Schlanz 1987).

Table 5-2: Operational and mass balanced streams around BGM milling circuit (tonnage rates in dry basis).

Stream/Unit name	Survey			Target/Design
	1	2	3	
SAG Mill				
Throughput (t/h)[1]	618.72	674.11	573.35	543-566
Power draw (kW)[1]	5387	6147	6198	6000
Recycle pebbles (t/h)[1]	61.43	70.44	81.39	190
Discharge screen undersize (t/h)	619.13	674.10	573.32	
Discharge screen Oversize (t/h)	61.00	70.00	81.40	
Dilution ratio	0.54	0.45	0.37	
Discharge volume-% solids[1]	44	48	45	52
Ball Mill				
Discharge (t/h)	1109.91	939.83	487.42	
Discharge volume-% solids[1]	48	42	38	48
Power draw (kW)[1]	5294	5399	5230	6,000
%< 125 µm	7.40	9.23	4.65	80
Hydrocyclone				
Feed (t/h) [1]	1729.04	1613.93	1060.74	1462
Feed volume-% solids[1]	42	44	41	33
Underflow (t/h)	1387.48	1249.57	840.08	
Underflow volume-% solids[1]	57	57	56	48-56
Overflow (t/h)	341.82	363.90	220.66	
Overflow volume-% solids[1]	20	24	21	13-16
Circulating load, *C*L (%)	400.00	344.00	381.00	250-350

The fraction <125 µm (target size, see also chap.2.1) in the ball mill product is considered as an indicator for the efficiency of the grinding stage. The results show that this fraction was only between 5 to 9 %. This poor performance might be caused by the high circulating load of the ball mill circuit, which reduces the residence time of the material in the mill and hence leads to a coarser product.

[1] Measured

5.1.3 SAG Mill Circuit

5.1.3.1 Pebble Crusher Performance

The particle size distribution of the pebble crusher streams (Figure 5-1) can be linked to the fact that pebbles recycle rate for survey 1 (i.e. 61 t/h) was lower than that for survey 2 (i.e. 70 t/h) and survey 3 (i.e. 68 t/h). This can be explained by the fact that the feed for survey 2 and survey 3 were harder ore types than for survey 1 (see Table 5-1). When the feed becomes harder, the rate of breakage in the SAG mill decreases, leading to higher proportion of critical size product (pebbles) , the consequence of which is increased recycle load as reflected in the result (Pourghahramani 2012).

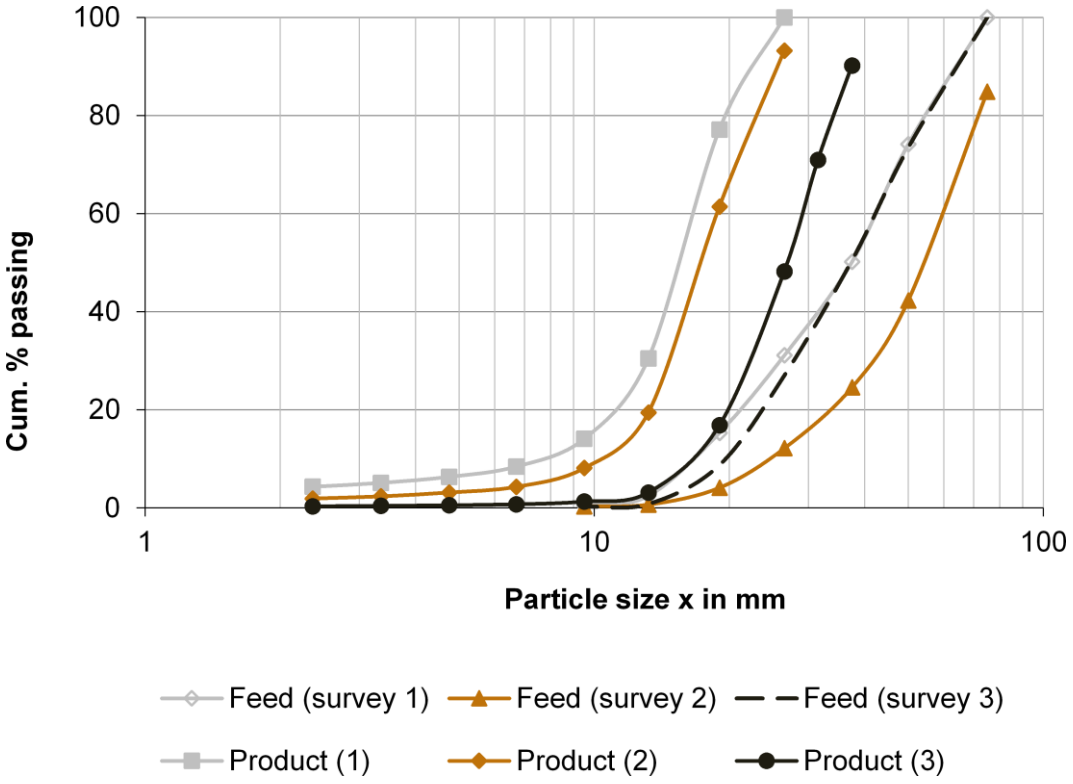

Figure 5-1: Pebble crusher streams particle size distribution.

As it was expected, the product size ($x_{P,80}$) correlates with the operating gap of the crusher (Table 5-3). However, it has to be noted that the crusher feed rate for all three surveys was significantly lower than the design capacity of 190 t/h, implying that this equipment presents a reserve capacity.

Further, it can be observed that the feed and product size distributions for S-3 are quite close to each other. This indicates low reduction ratio of the pebble crusher, which could be due to the large operating gap (closed side setting, see Table 5-3).

Table 5-3: Pebble crusher performance indicators.

Parameter	Survey 1	Survey 2	Survey 3	Design
CSS (mm)	12	13	20	14/10
Feed (t/h)	61.01	70.45	68.53	190
$x_{F,80}$ (mm)	56	72	56	
$x_{P,80}$ (mm)	20	23	34	

5.1.3.2 SAG Mill Performance

The SAG mill feed size (Figure 5-2) for survey 1 (185 mm) was significantly higher compared to survey 2 (102 mm) and survey 3 (122 mm). The reason for this might be due to unmonitored gap of the primary crusher or feeder proportions from the stockpile. Since the design feed size for the SAG mill was 120 mm, this higher feed size will have contributed to the poor grinding performance in survey 1.

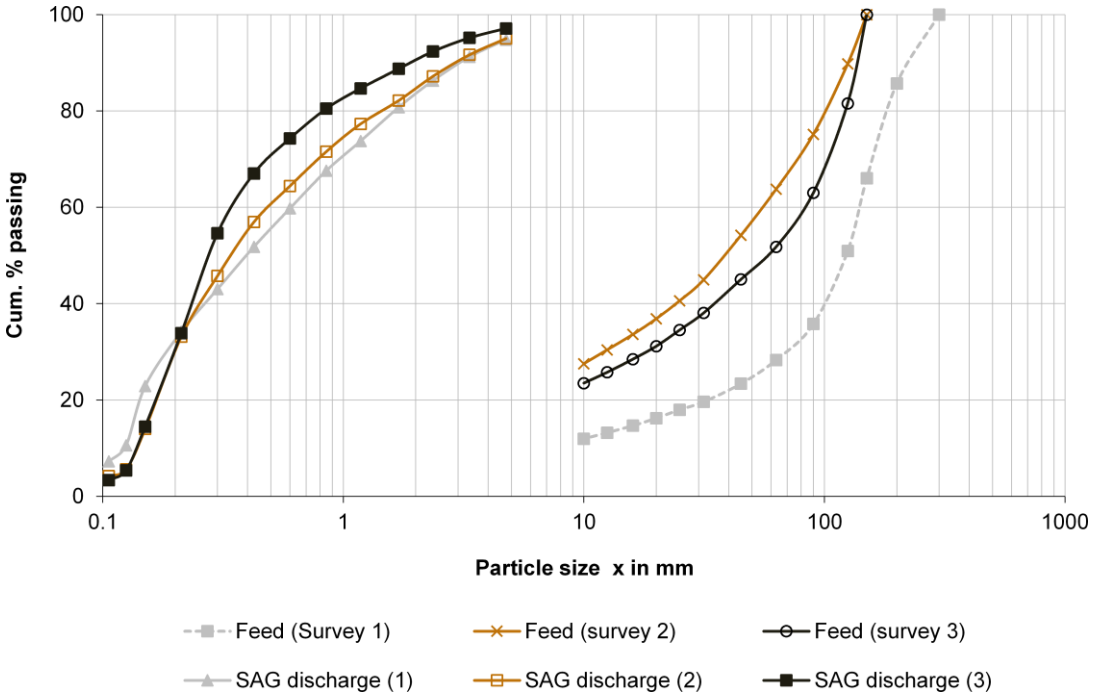

Figure 5-2: **SAG mill feed and product particle size distribution for survey 1, 2 and 3.**

Soft ore is mainly ground by impact breakage while hard ore is subjected to abrasion and attrition events where the media impact could not sufficiently break harder particles (Pourghahramani 2012). Therefore hard ore grinding in the SAG mill results in finer products compared to the soft ore.

This can be reflected in this study, whereby, the harder the feed (see Table 5-1), the finer the SAG mill product (Table 5-4). This had also an influence on the overall circuit product size (i.e. ball mill product). It can further be observed that, SAG mill products size was influenced by the specific energy .The higher the energy input employed, the finer becomes the final product size and vice versa as could be expected. Moreover, the reduction ratios achieved by the SAG mill were within recommendation.

Table 5-4: SAG mill performance indicators.

Parameter	Survey 1	Survey 2	Survey 3	Design
SAG mill feed rate (t/h)	618.72	674.11	573.35	543-566
SAG mill feed, $x_{F,80}$ (mm)	185.45	101.6	122	120
SAG discharge $x_{P,80}$ (mm)	1.644	1.468	0.831	
SAG mill reduction ratio (-)	113	69	147	
SAG mill specific energy (kWh/t)	7.92	8.26	9.47	
Ball load, % volume	14.30	14.30	-	15-20
Material load, % volume	20	20	-	30-35

5.1.3.3 SAG Discharge Screen Performance

The partition curve for the SAG discharge screen is shown in Figure 5-3 and Table 5-5 presents the efficiency indicators. The screen was fairly efficient and stable in the investigated range for all surveys with separation efficiency, κ= 0.80 and cut size, x_T, of approximately 13 mm.

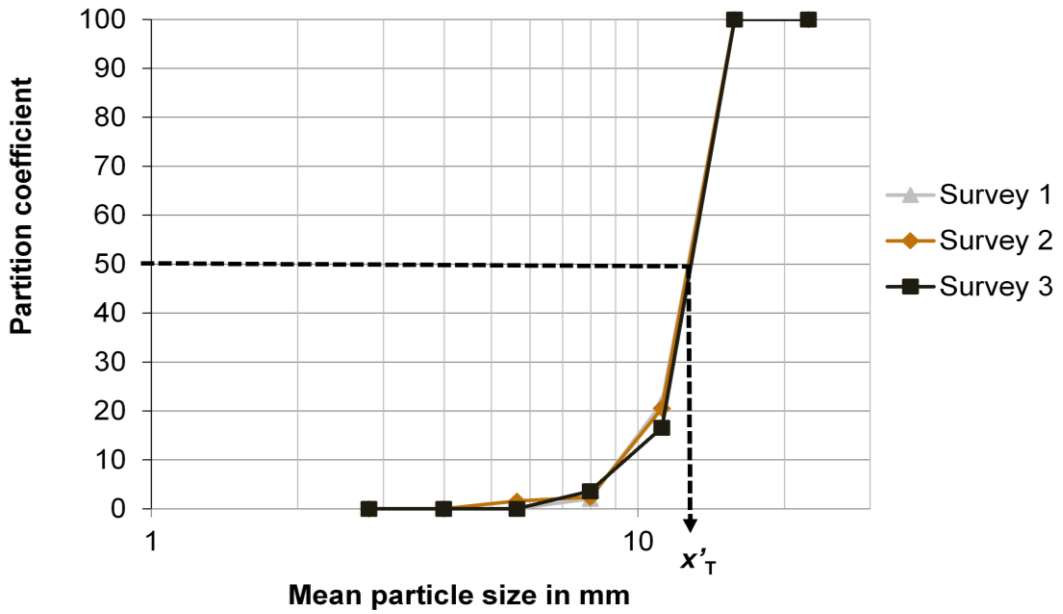

Figure 5-3: SAG Discharge Screen efficiency curves.

Table 5-5: **SAG discharge screen efficiency indicators.**

Parameter	Survey 1	Survey 2	Survey 3
Cut size, x_T (mm)	12.90	12.90	13.10
Sharpness index, κ	0.80	0.80	0.81

The observed fluctuation in SAG mill feed size is a problem that needs to be addressed. Regular monitoring and control of the SAG feed size is important as the change in feed size distribution normally results to corresponding changes in the grinding media size distribution, which has further impact on power and throughput (Napier-Munn, J. et al. 1996, Wills and Napier-Munn 2006). This could be achieved through regular monitoring of the primary crusher performance through analysis of the product size distribution. Since the SAG mill is fed by the ore drawn from the stockpile through three feeders, the SAG mill feed size distribution could also be influenced by the proportion or ratios at which the feeders draw the ore. Hence, closer control of the feeders is also important.

5.1.4 Ball Mill Circuit

5.1.4.1 Ball Mill Performance

The particle size distribution of ball mill streams is presented in Figure 5-4. Little can be seen in terms of differences in the ball mill performance for the three surveys. Based on the product fineness and reduction ratios (Table 5-6), it can be seen that the ball mill operation was inefficient. The poor performance might have been due to higher circulating load (Table 5-2) and coarser SAG mill discharge (Table 5-4) experienced

by the operation. Further, the efficiency of the ball mill is seen to depend on the input energy (Table 5-6) as well as the circuit throughput (Table 5-2).

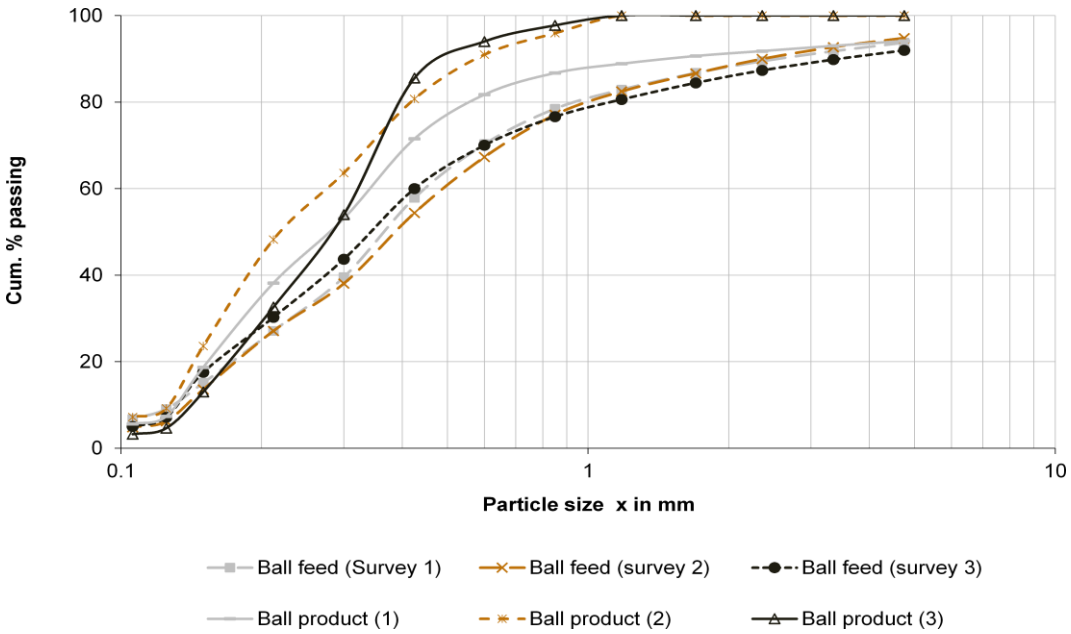

Figure 5-4: **Ball mill feed and product particle size distribution for survey 1, 2 and 3.**

Table 5-6: Ball mill performance indicators.

Parameter	Survey 1	Survey 2	Survey 3	Design
Ball mill feed $x_{F,80}$ (mm)	0. 963	1.028	1.127	
Ball mill discharge $x_{P,80}$ (mm)	0.570	0.419	0.403	0.125
Ball mill reduction ratio (-)	1.70	2.45	2.80	
Ball mill specific energy (kWh/t)	4.77	5.74	10.73	
Ball load, % volume	33	33	-	30-35

5.1.4.2 Hydrocyclone Performance

Figure 5-5 to Figure 5-7 and Table 5-7 present the size distributions and some key performance indicators, respectively, for the BGM hydrocyclones obtained during the three survey. The result shows that the overflow product size ($x_{P,80}$) is much coarser than target (i.e. 125 µm) in all surveys (Table 5-7).

Since the ball mill products were significantly coarser than once designed (Table 5-7), the coarse overflow achieved could also be contributed by the inefficient ball mill. Also the overflow size ($x_{P,80}$) is influenced by hydrocyclone feed rate and feed pulp density (Wills and Napier-Munn 2006).

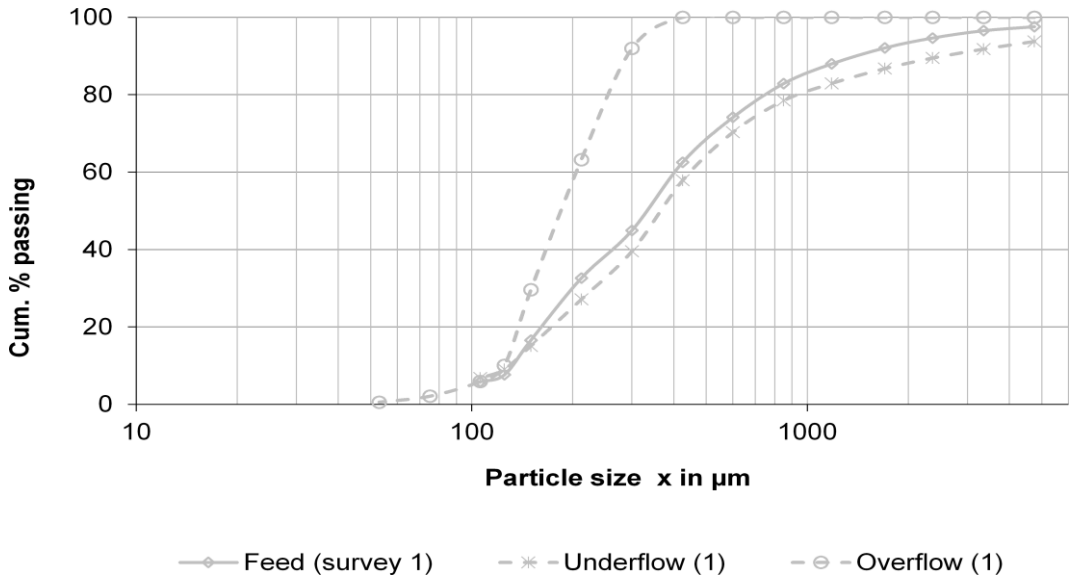

Figure 5-5 : **Hydrocyclone product streams particle size distribution for survey 1.**

The growth of the feed rate increases the centrifugal force effect which causes finer particles being carried to the underflow, and hence decreasing the cut size. Further, the sharpness of separation decreases with increasing pulp density and the separation size rises due to higher resistance to swirling motion within the cyclone which reduces the effective pressure drop (Wills and Napier-Munn 2006). In addition, feed rates for survey 1 and 2 were 10 and 18 % higher than design capacity of 1462 t/h, implying that hydrocyclones were overloaded.

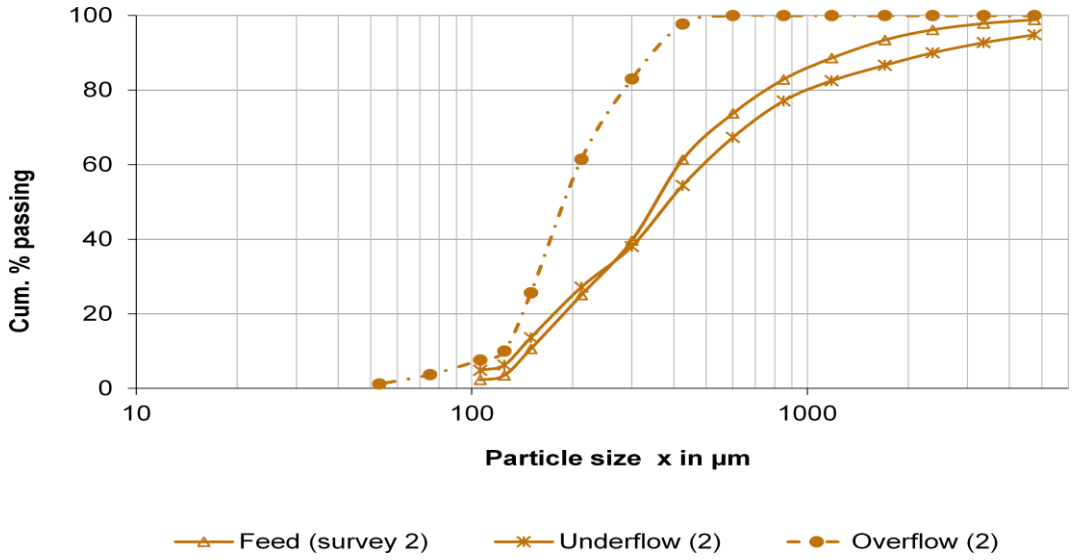

Figure 5-6 : **Hydrocyclone product streams particle size distribution for survey 2.**

Table 5-7: Hydrocyclone performance indicators.

Parameter	Survey 1	Survey 2	Survey 3	Design
Feed rate (t/h)	1729	1614	1061	1462
Operating pressure (kPa)	98	81	92	80-110
Feed volume-% solids	42	44	41	33
Underflow volume-% solids	57	57	56	48-56
Overflow volume-% solids	20	24	21	13-16
Feed $x_{P,80}$ (µm)	768	771	570	
Underflow $x_{P,80}$ (µm)	963	1028	1127	
Overflow $x_{P,80}$ (µm)	266	288	241	125

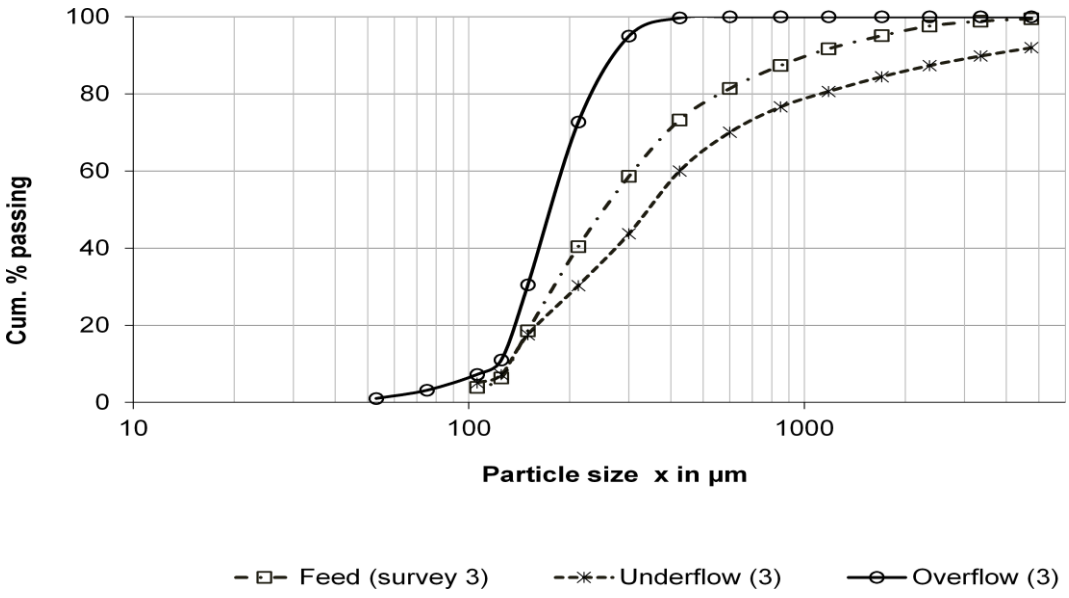

Figure 5-7 : **Hydrocyclone product streams particle size distribution for survey 3.**

The results of hydrocyclone efficiency for the BGM operation are shown in Figure 5-8 and Table 5-8. It can be observed that the by-pass fraction (split) was higher than 50 % and the cut size was higher than 200 µm for all three cases. This may also be related to the higher overflow $x_{P,80}$ obtained; clearly indicating that the current BGM operation is not able to achieve the target overflow size of 125 µm. The cut size and the by-pass fraction are influenced by feed pulp density and feed rate (Table 5-2). This is conforming with previous studies (Wills and Napier-Munn 2006 , Rybinski, Ghersi et al. 2011). In all of the three surveys, the hydrocyclone feed volume-% solids was 17 %

higher than design (33 %v/v) and also higher than recommended values from literature (60 % solids or 35 % v/v) (Wills and Napier-Munn 2006). This is suspected to have contributed to the poor separation efficiency observed.

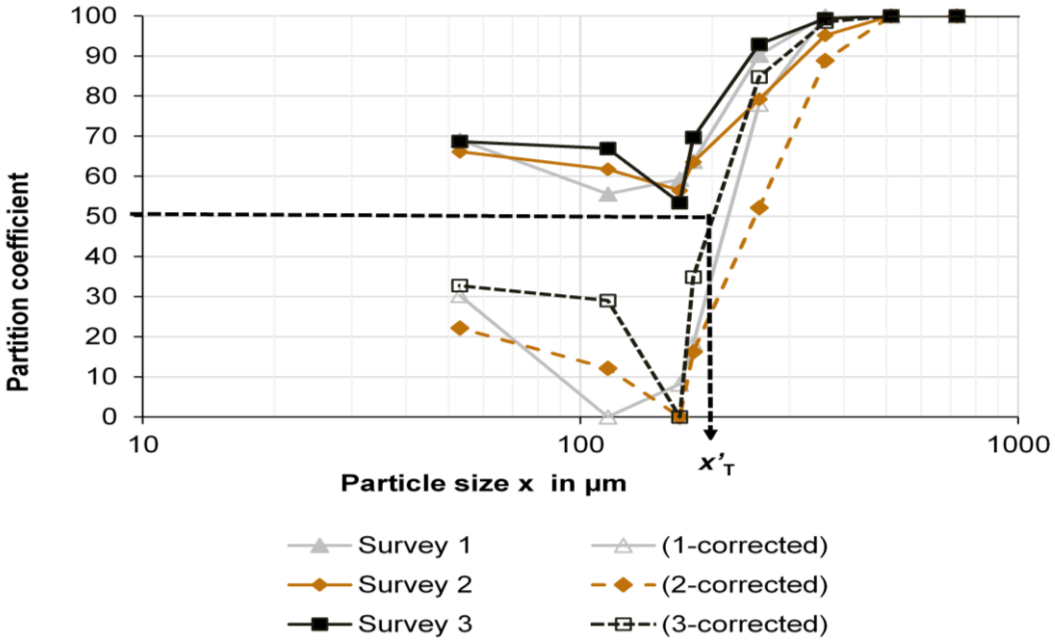

Figure 5-8: Hydrocyclone uncorrected and corrected efficiency curves for survey 1, 2 and 3.

Nevertheless, the separation efficiency, κ *was* fairly good for all surveys if the splitting effect was taken into account (see also chap.3.4.5). The imperfection, *I*, can be used to categorize hydrocyclones (Murthy and Basavaraj 2012). Consequently the hydrocyclones at BGM could be categorized (see Table 5-8, Table 5-9) between very good (i.e. $0.2 < I < 0.3$) and excellent (i.e. $I < 0.2$).

This indicates that the current design is in principle fairly efficient for coarser overflow product and not for the current BGM target (i.e. $x_{P,80}$= 125 µm).

Table 5-8: Hydrocyclone efficiency indicators.

Parameter	Survey 1	Survey 2	Survey3	Design
By-pass fraction (%)	55.60	56.00	53.42	
Cut size, x_T (µm)	220.84	251.45	203.75	
Imperfection, *I*	0.14	0.24	0.16	
Sharpness Index, κ	0.75	0.62	0.74	
Overflow $x_{P,80}$ (µm)	266	288	241	125

Therefore the inefficiencies shown by the higher values of cut size could probably be an indication of the unsuitability of the current design parameters (i.e. D_c, D_i, D_a or D_o)

for the target overflow of 125 µm. The influence of these design parameters on hydrocyclone cut size is clearly explained in literature (Schubert 1985, Wills and Napier-Munn 2006).

Table 5-9: Hydrocyclone efficiency category based on imperfection, *I* (Murthy and Basavaraj 2012).

Imperfection, *I*- values	Separator category
< 0.2	Excellent separator
0.2 < *I*< 0.3	Very good separator
0.3 < *I*< 0.4	Medium separator
0.4 < *I*< 0.6	Poor separator
I >0.6	Bad separator

In practice, the selection of cut size is based on the designed size analysis of the overflow (Metso 2010). For example, for BGM, the target overflow size amounts to $x_{P,80}$ = 125 µm, then the recommended cut size for efficient operation is 132.50 µm (obtained by multiplying target overflow size by the corresponding factor) in Table 5-10.

Table 5-10: Factors for conversion of % passing in the overflow to X_T (Metso 2010).

% passing in the overflow	99	95	90	80	70	60	50
Factor	0.49	0.65	0.79	1.06	1.36	1.77	2.34

Figure 5-9 shows the correlation between the hydrocyclone cut sizes calculated from various models with cut size values obtained from the survey. It can be seen that the BGM hydrocyclones operation could be well explained by Nageswararao and to an extent with Schubert models. Hence, the two models were considered as candidates for further studies (simulation and optimization) of the BGM grinding circuit.

The Schubert model allows for a quick inspection on the relationship between cut size, x_T and the hydrocyclone key design parameters (i.e. D_a and D_o), allowing for suggestion on their suitability for a given operation. Based on this, the influence of apex and vortex finder diameters on the hydrocyclone cut size were evaluated by Schubert model as presented in Figure 5-10. From the figure, it can clearly be seen that, the recommended cut size for the BGM operation (i.e. 132.5 µm) could not be achieved by the current hydrocyclone design (i.e. D_a = 150 mm, D_o = 280 mm).

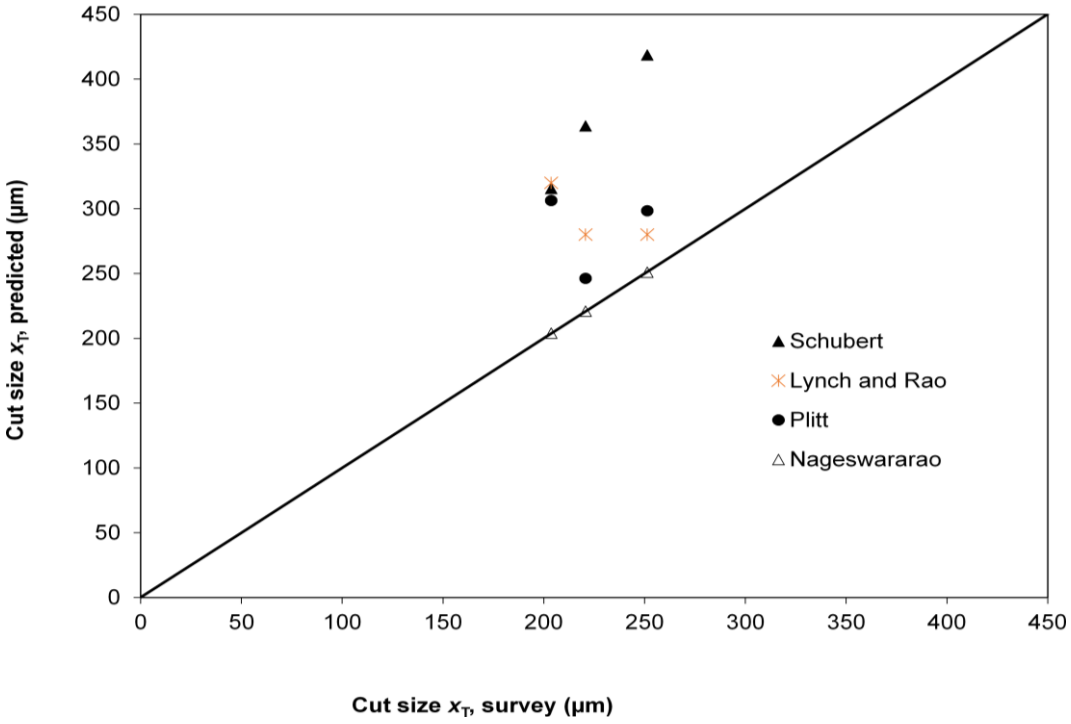

Figure 5-9: Correlation between model calculated and measured (survey) cut size, X_T.

In order to achieve the recommended cut size and possibly the target overflow $x_{P,80}$ of 125 µm, Schubert model indicates a need for adjustments of current vortex finder (D_o) and apex (D_a) to between 140-170 mm and 155-190 mm, respectively.

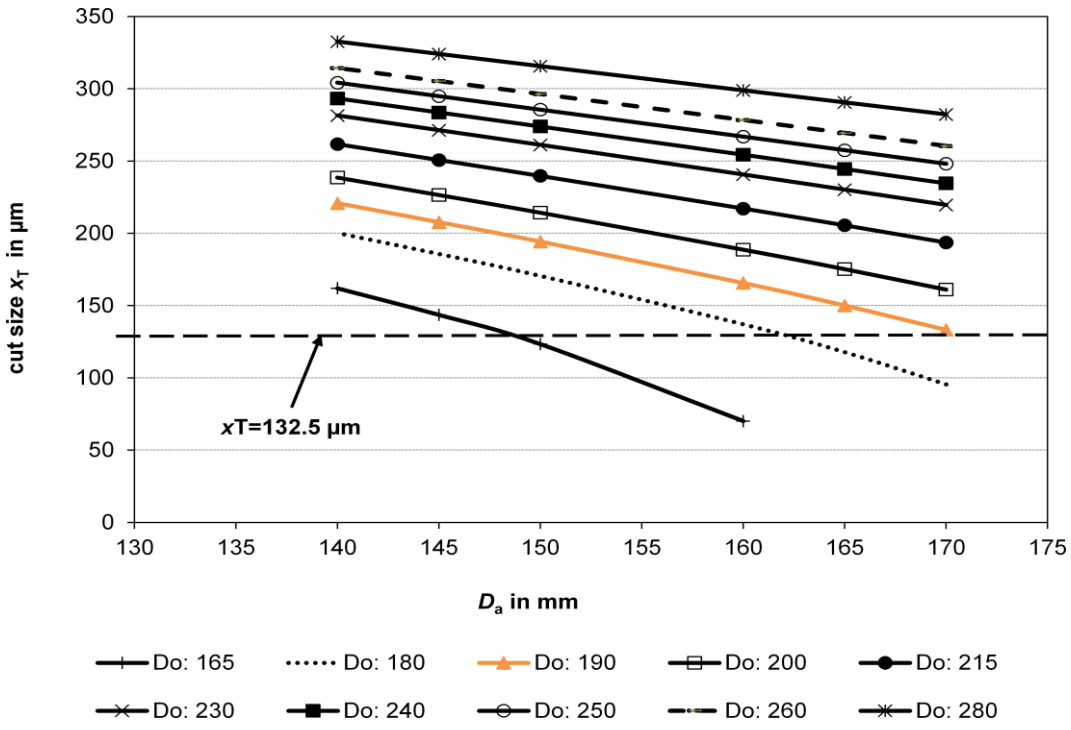

Figure 5-10: Influence of apex, D_a and vortex finder, D_o diameters on cut size, x_T(µm).

5.1.5 BGM Grinding Circuit Efficiency

Table 5-11 and Table 5-12 summarize the energy efficiency characteristic for the BGM operation. From Table 5-11, the operating work index (see chap. 3.3.4) is more than twice the laboratory work index for each of the three surveys. This implies that, the circuit consumes more energy than the laboratory Bond test estimate and hence does not conform to the Bond standards in terms of energy efficiency (C. A. Rowland and Mclavor 2008, Alamouti, Rezai et al. 2011). This can further be revealed by very low Bond efficiency factors (i.e. measure of the relative efficiency of the circuit compared to the prescribed Bond standard energy) of less than 65 %. Therefore, the operation is inefficient and could be optimized through decreased throughput.

Table 5-11: **Energy consumption and operating work index for the current BGM operation**.

	Survey			Design
Parameter	1	2	3	
Throughput (t/h)	618.72	674.11	573.35	543-566
Circuit power (kW)	10,681	11,546	11,428	12,000
Input Energy (kWh/t)	17.26	17.13	19.93	
Operating W_i, (kWh/t)	35.62	30.78	34.91	
W_i (kWh/t)	17.2	18.70	18.50	14.5 -16.5
Bond efficiency, E (%)	48.30	60.70	52.90	

Table 5-12: Input energy and throughput required for the current operation to achieve $x_{P,80}$ of 125 µm .

Survey	$x_{F,80}$ in mm	$x_{P,80}$ in µm	Throughput in t/h (compared to actual throughput)	Input energy in kWh/t
1	185	125	344 (-44.40 %)	31.03
2	102		435 (-35.50 %)	26.56
3	122		378 (-34.10 %)	30.22

The energy efficiency data (Table 5-12) reveal two options for the current BGM operation to achieve the target product size of 125 µm. A significant decrease in throughput by up to 44 % or an increase in input energy by up to 80 % (e.g. survey 1) are required in order to achieve such an improvement. The increase in input energy might be caused by the change in ore hardness as indicated in section 5.1.1. An

increase in input energy requirement is not possible with the existing equipment, as this is equivalent to approximately 19 MW as opposed to the existing equipment capacity of 12 MW.

5.1.6 Mineral distribution within the circuit

The cumulative distribution of minerals in the circuit was measured during the survey and is presented in Figure 5-11 and Figure 5-12 for gold and Figure 5-13 and Figure 5-14 for copper in grinding mills discharge and hydrocyclone streams, respectively. For the case of gold mineral from grinding mills discharge (Figure 5-11), it is seen that, in an average, more than 60 % in mass is found in the less than 300 µm fraction. This gives an indication that better concentration of the mineral could possibly be achieved if ground finer than 300 µm. This information is also indicative of the mesh of grind or liberation size of gold for the BGM ore.

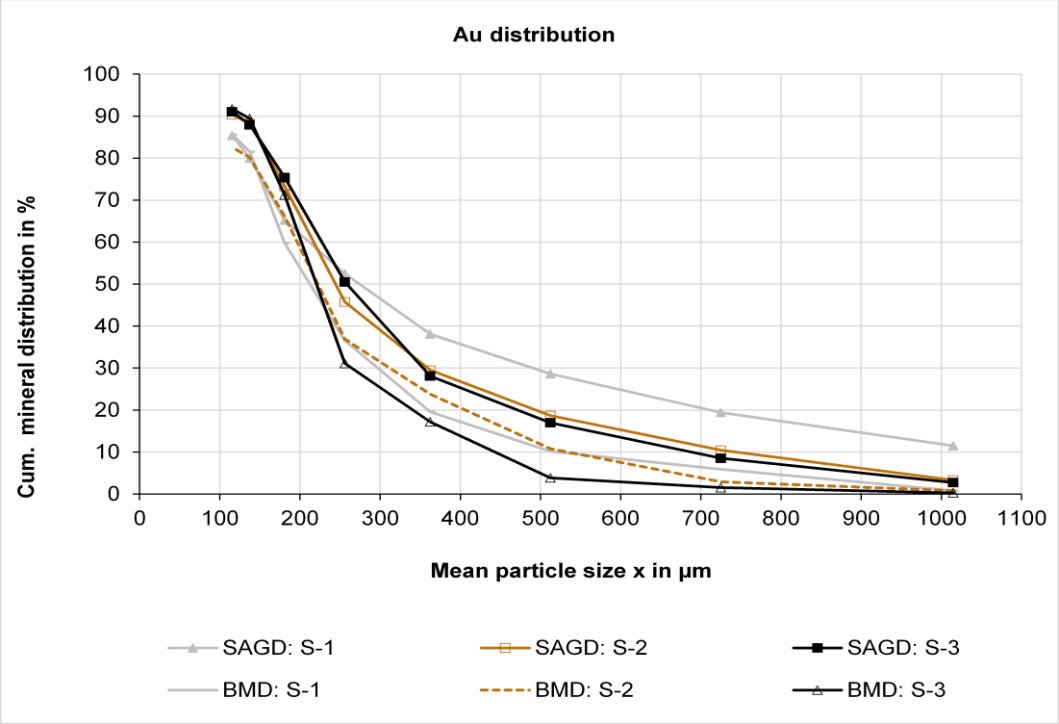

Figure 5-11: Distribution of gold in grinding mill discharge streams. The symbols stands for; SAGD: SAG mill discharge, BMD: Ball mill discharge.

Further, the maximum cumulative gold distribution that could be achieved in mills discharge streams (Figure 5-11) was only around 82-92 % by mass. This can be explained by the fact that size distribution in these streams are coarse (0.6-1.6 mm).

In the hydrocyclone streams (Figure 5-12), better cumulative gold distribution (> 90 % by mass) could be achieved at approx. < 100 µm. This may be explained by the fineness of products from hydrocyclone streams.

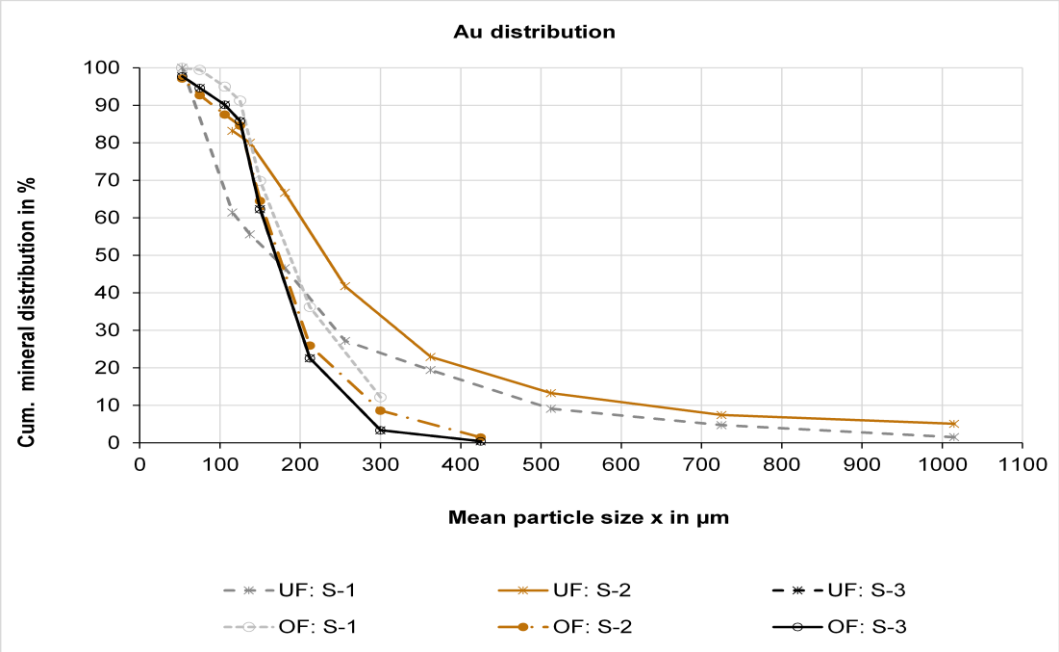

Figure 5-12: Distribution of gold in the hydrocyclone product streams. The symbols stands for; UF: Underflow and OF: Overflow.

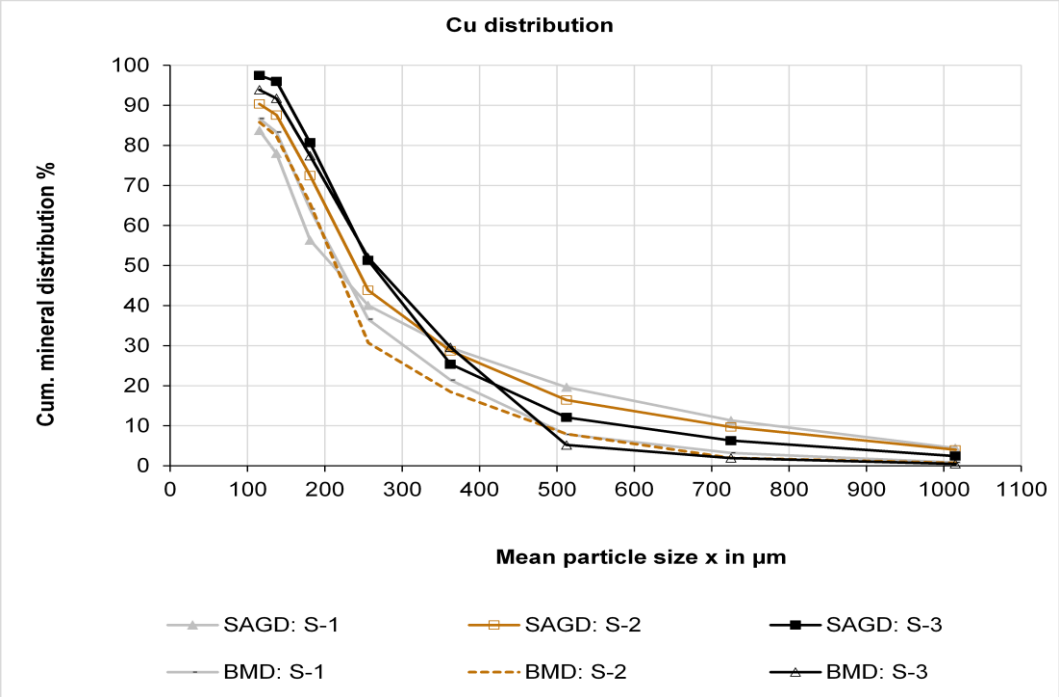

Figure 5-13: Distribution of copper in grinding mill discharge streams. The symbols stands for; SAGD: SAG mill discharge, BMD: Ball mill discharge.

The trend is the same for the copper mineral distribution (Figure 5-13, Figure 5-14). In overall, the finer the particle size the higher the cumulative mineral distribution.

Therefore, the cumulative mineral distribution result for both gold and copper give highlights of to what extent grinding is required (mesh of grind) for better concentration of the valuable minerals for a given process (i.e. < 200 µm in this case).

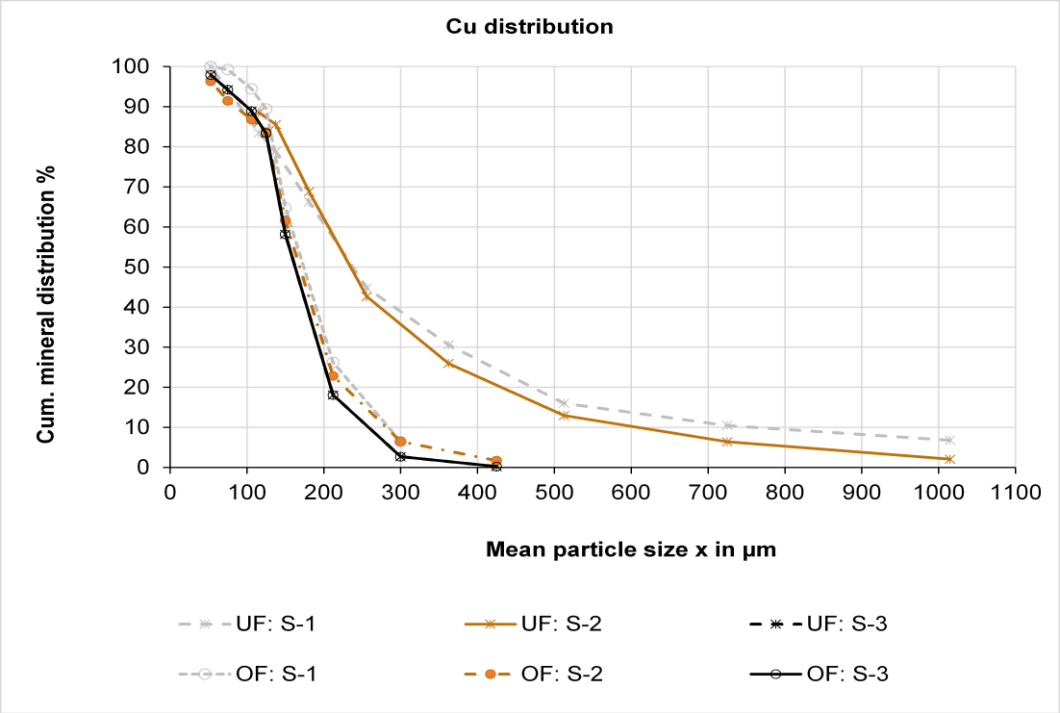

Figure 5-14: Distribution of copper in the hydrocyclone product streams. The symbols stands for; UF: Underflow and OF: Overflow.

Although the mineral liberation results showed that the gold hosting minerals (pyrite-pyrrhotite) could be liberated even at coarser than 300 µm (refer chap. 5.2), yet the efficiency of flotation and cyanidation processes at BGM will require fine grinding of the material for better exposure of gold and copper to flotation and leaching reagents.

The accuracy of measurements of these elements by an Atomic Absorption Spectrometry (AAS) was evaluated by the standard error (refer Appendix E).

5.1.7 First Conclusion and Recommendation on Circuit Survey

5.1.7.1 Observation and conclusions

The following observation could be deduced from survey sampling campaign conducted to evaluate the performance of BGM grinding circuit:

Material

- The Bond work index for the current ore ranges between 17.20 - 18.70 kWh/t which is significantly higher compared to 14.50 - 16.50 kWh/t which was

estimated during plant design. Harder ore means more energy requirement for an efficient operation, the consequence of which are increased costs.

SAG mill grinding circuit

- The SAG mill grinding was influenced by dilution, ore hardness and feed size.
- The SAG feed size ($x_{F,80}$) for the three surveys had an influence on final product size of the SAG circuit. The coarser the feed was the coarser the product became. A higher reduction ratio of the primary crusher might lead to a better grinding performance in the SAG mill circuit.
- The pebbles recycle rate increases with the hardness of the feed.
- The pebble crusher product size was influenced by the operating gap as expected.
- The SAG mill discharge screen is operating at a cut size of 13 mm and at a high and constant separation efficiency of 0.80.
- The circuit operation revealed inefficiency in terms of energy utilization with very low Bond efficiency factors. This implies that the target product size (125 μm) could be achieved by decreasing the throughput of the SAG mill. This could lead to lower circulating load and also higher possible capacity of the recycle crusher and hence improving the fineness of the circuit product.

Ball mill grinding circuit

- The ball mill grinding efficiency is poor. The product fraction < 125 μm is only 5-9 % of the mill discharge.
- The circulating load is higher than designed which will contribute to the poor grinding efficiency of the ball mill circuit due to reduced residence time of the material in the mill and as a consequence of overloading the mill.
- The hydrocyclone overflow product sizes ($x_{P,80}$) have all been significantly higher than the target value of 125 μm. Since this size is influenced by hydrocyclone feed v%-solids, feed rate, and feed size a better classification could be obtained when hydrocyclone feed volume% solids, feed rate, and feed size are decreased.
- Hydrocyclone by-pass fraction was higher than 50 % for all surveys
- Hydrocyclone feed volume% solids were 17 % higher than design as well as recommended values and also the cut size was higher than 200 μm.

- Hydrocyclone efficiency ranged between 0.62 -0.75 which could be categorized as *very good or excellent separator*. This reveals that the current hydrocyclone design could be efficient for overflow product size $x_{P,80}$ > 125µm. Based on cut size values from survey and those calculated using different models, the current BGM hydrocyclones could not achieve the recommended cut size of 132.5 µm (see chap. 5.1.4.2) and target overflow $x_{P,80}$ (i.e. 125 µm).

5.1.7.2 Recommendations

- For the grinding of a harder ore is recommended to lower the throughput or increase the energy input. Also periodical tests of ore hardness development during ongoing mining operations have to be considered. Through this, better blends will be developed as well as appropriate tonnages predicted for the existing ore types, so as to be efficiently treated by the available plant design.
- The hydrocyclone feed has a high percent solids ranging from 66.5 to 68.40 % and had also high percent solids ranging from 41 to 47 % in the overflow. If the hydrocyclone feed is diluted and the overflow allowed to reach a lower density, close to 30 %, the classification efficiency will improve, giving a sharper cut.
- Hydrocyclone cut size of 132.5 µm is recommended for efficient BGM operation and can be achieved by changing vortex finder and apex diameters.
- The feed size fluctuations noted during the survey are significant and in order to improve the SAG mill efficiency, regular monitoring of the feed size is necessary as any change in the feed size distribution would make necessary changes in the grinding media size distribution, which has further impact on power and throughput.
- The change of ore work index from an average of 16 kWh/t during design to current average value of 18 kWh/t is significant. A need for control of feed size as well as blending ratios is necessary for the operation to achieve optimum throughput and final product size.
- An optimization study by computer simulation is further recommended. Through simulation of multi-effects, a deeper understanding of the efficiency problems for the BGM grinding will be facilitated and also may provide possible solutions.

5.2 Liberation Characteristics of BGM Ore

The efficiency of any milling process is evaluated based on both, size reduction and the degree of mineral liberation. In regard to this and in order to add more information to the survey results, ore characterization in terms of mineral liberation was also implemented and this section provides an overview of the liberation characteristics of the three ore blends processed at BGM.

5.2.1 Modal Mineralogy

Table 5-13 gives the modal mineralogy of the three ore samples as determined with an MLA (see chap. 4.4.1). Based on mineralogical reports from the mine pyrite-pyrrhotite is the predominant valuable mineral in the material. Also the pyrite-pyrrhotite phase is considered as the major gold-bearing mineral and is the main phase covered in this section. The gangue phases comprise mainly of quartz, feldspar, muscovite, and biotite-chlorite. Epidote and fluorite are the minor mineral phases.

Table 5-13: Modal mineralogy of the BGM ore material (wt. %).

Mineral	**S-1**	**S-2**	**S-3**
Biotite-Chlorite	7.57	7.31	8.44
Epidote	1.63	3.53	1.60
Fluorite	1.27	1.87	0.72
Feldspars	22.32	19.25	27.20
Muscovite	17.82	15.70	14.91
Pyrite-pyrrhotite	6.54	5.58	3.26
Quartz	39.88	42.45	41.55
Other	2.97	4.31	2.31
Total	100	100	100

The grade variation of epidote and feldspars in the three samples is noticeable. S-2 has the highest epidote grade (1.87 wt. %) compared to S-1 (1.27 wt. %) and S-3 (0.82 wt. %). This might probably indicate that quartz phase is the host for epidote mineral. For the case of feldspars, grade variation trend cannot be deduced, whereby S-2 has the lowest value (19.25 wt. %) compared to S-1 (22.32 wt. %) ad S-3 (27.20 wt. %).

5.2.2 Particle and Mineral Grain Size Distributions

As an example, Figure 5-15 shows the mineral grain size distribution of the major mineral phases for survey 1 blend as determined by an MLA. It can be seen that, pyrite-pyrrhotite has the coarsest grain size distribution followed by quartz and feldspars. Further, it can be seen that, the grain size distributions of quartz and feldspars closely follow the size distributions of the host particles. This implies that such minerals were better-liberated than others. Therefore the results indicate that the milling energy is more used in the grinding of the gangue phases (quartz and feldspars) to finer sizes and has minimal impact on milling of the valuable pyrite-pyrrhotite mineral phase. The mineral grain size distribution trend displayed for survey 1 blend resembles with that for other samples (refer to Appendix B for other samples).

Further, Figure 5-15 indicates that pyrite-pyrrotite mineral grain size is coarser than the size of the host particles. This is an unusual phenomena and might possibly be due to errors during MLA measurements, where particle image segmentation and agglomeration (i.e. fine particles) might have occurred (Gu 2003).

In this investigation, it must be recognised that all measurements for particle size and mineral grain size presented in this section are based on the Equivalent Circle Diameter (ECD). The liberation distribution is based on mineral free surface since the efficiency of most of the mineral beneficiation processes such as leaching or flotation require at least a surface of the valuable mineral to be exposed (Wang et al., 2012; Wills and Finch, 2016). In this study liberation is based on the cumulative mass percentage of the mineral in the >95 % liberation class which is more applicable (Wang, Shi et al. 2012).

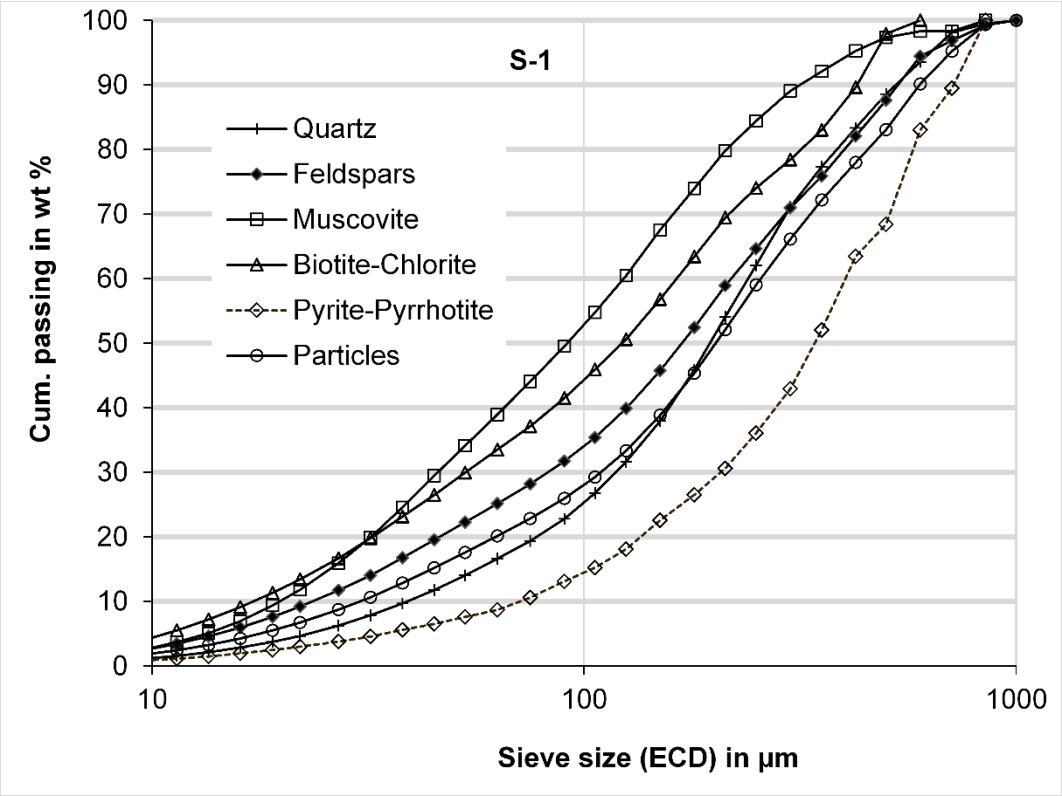

Figure 5-15: Particle and mineral grain size distributions for the blend of survey 1.

5.2.3 Mineral Liberation

The liberation of pyrite-pyrrhotite based on size fractions is shown in Figure 5-16 for the five fractions measured for each sample. The trend is uniform for the three samples whereby the degree of liberation decreases with increase in particle size. Except for the fractions 0-63 µm and 500-1000 µm, in all other fractions the degree of liberation for S-1 and S-3 are closely to each other and is higher than that of S-2. Furthermore, the degree of liberation for S-2 in the fraction 500-1000 µm is the lowest. This is likely due to artefacts of poor particle statistics caused by the low grade of pyrite-pyrrhotite in the ore and the fine mineral grains (see Table 5-14). However, except for the fraction 500-1000 µm the degree of pyrite-pyrrhotite liberation for all size fractions in all samples is higher than 75 %. This indicates that pyrite-pyrrhotite can be liberated at relatively very coarse sizes for the material investigated. Table 5-14 and Table 5-15 provide supplementary information on particle statistics for more illustration. Table 5-15 can be compared with relative number of particle count per size class (Appendix B3).

Table 5-14 : Pyrite-pyrrhotite particle counts for the fractions measured.

Sample	Size class (µm)				
	0-63	63-125	125-250	250-500	500-1000
S-1	5874	1054	551	245	727
S-2	7107	1377	408	767	138
S-3	4914	736	348	309	127

The errors indicated in Figure 5-16 refer to the standard error based on average liberation from MLA measurement of three sample splits for each fraction. The error values increase slightly with particle size due to the decreasing number of particles or grains in the sample splits of these size classes but in overall are acceptable. In addition, the epoxy stirring and cutting techniques may result to inhomogeneous distribution of mineral grains in the epoxy (refer to chap. 4.4.1), which can also contribute to differences in measured values.

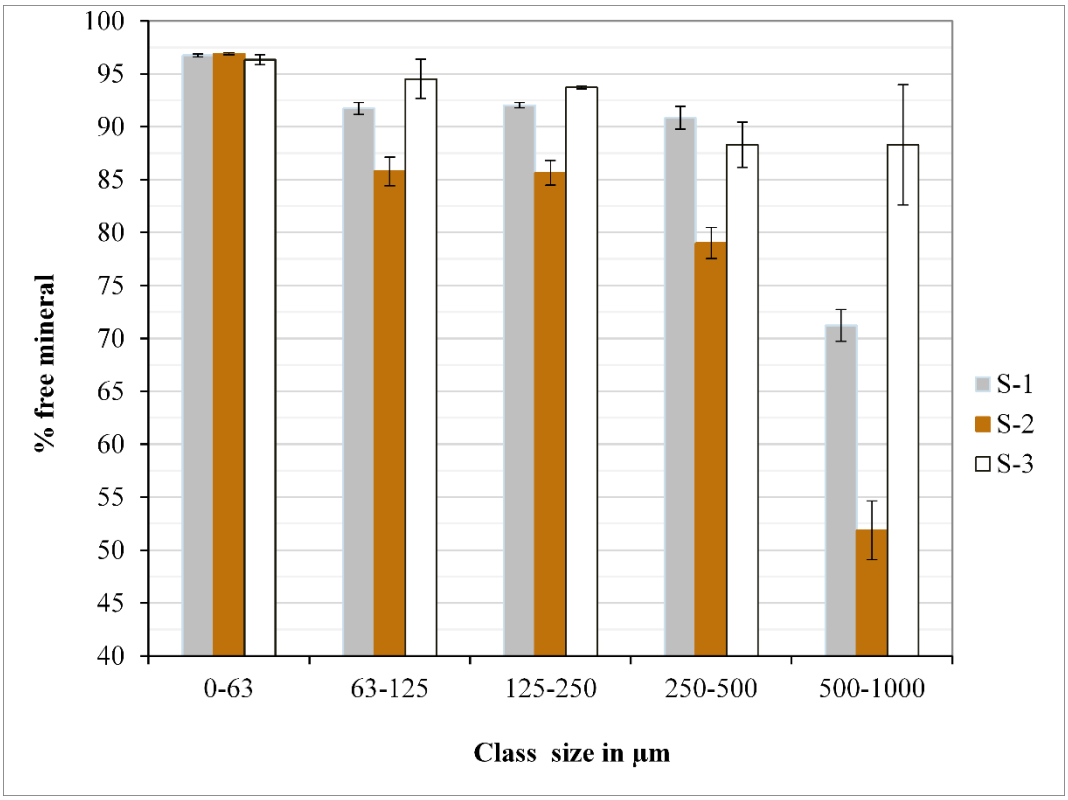

Figure 5-16: Liberation of pyrite-pyrrhotite based on the sieved fractions (average of three sample).

Table 5-15: Pyrite-pyrrhotite particle counts based on liberation classes for S-2 .

Class size (µm)	Pyrite-pyrrhotite free surface of particle (%)					
	0- 20	20- 40	40-60	60-80	80-100	100
0-63	93	19	29	20	15	6929
63-125	33	9	7	7	28	1288
125-250	24	2	5	3	14	350
250-500	30	7	6	4	37	648
500-1000	9	2	0	1	0	121

Figure 5-17 shows the relationship between pyrite-pyrrhotite cumulative liberation and class mean particle size. It is seen that all samples have the degree of liberation >80 %. From this result, it can be concluded that pyrite-pyrrhotite can be economically liberated at very coarse size of approximately 200-400 µm, where the cumulative liberation is already higher than 85 % for all samples. If milling could have been followed by a gravity concentration alone, grinding costs could be saved as the material does not require milling too fine for liberation of valuable phase to be achieved.

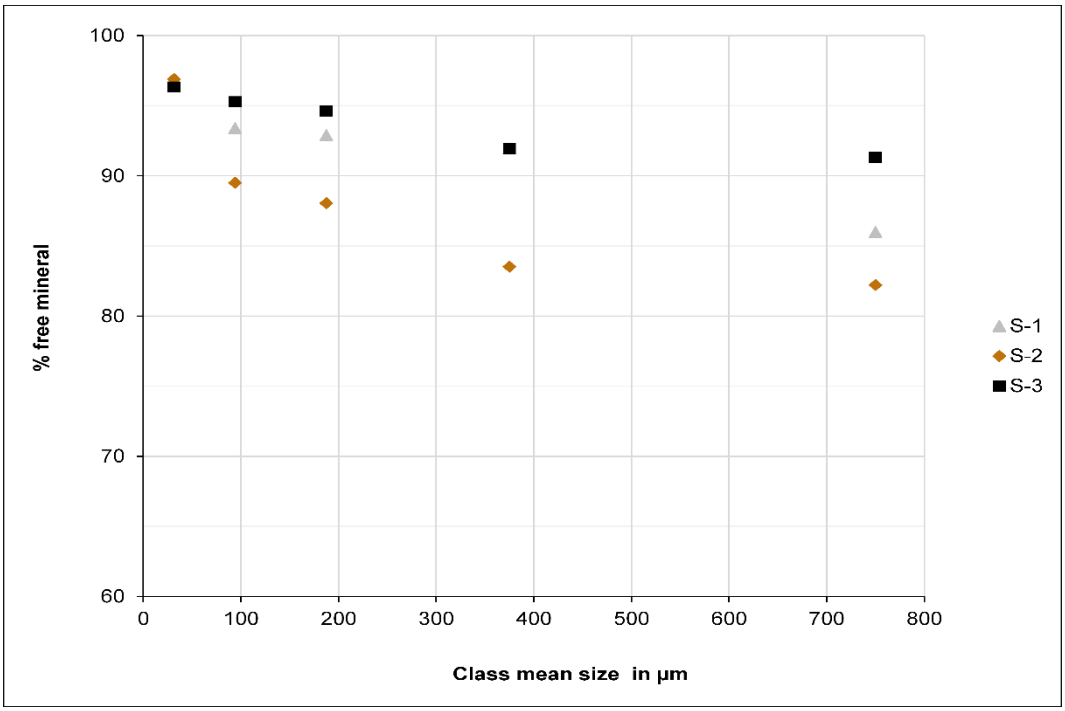

Figure 5-17 : Cumulative pyrite-pyrrhotite liberation vs. class mean particle size.

Figure 5-18 presents the enrichment characteristics of pyrite-pyrrhotite with particle size. This parameter was calculated as the ratio of the grade or content of pyrite-pyrrhotite in a given size fraction (m_{xi}) to that in the feed sample ($m_{x,F}$) (Eqn. (88)) and illustrates that much of the mineral is enriched in the size range 250-500 µm.

$$E_R = \left(\frac{m_{Xi}}{m_{x,F}} \right) \quad (88)$$

Sample S-2 has the highest enrichment in this size range followed by sample S-3 and sample S-1. Surprisingly, sample S-1, shows enrichment even at coarsest size fraction.

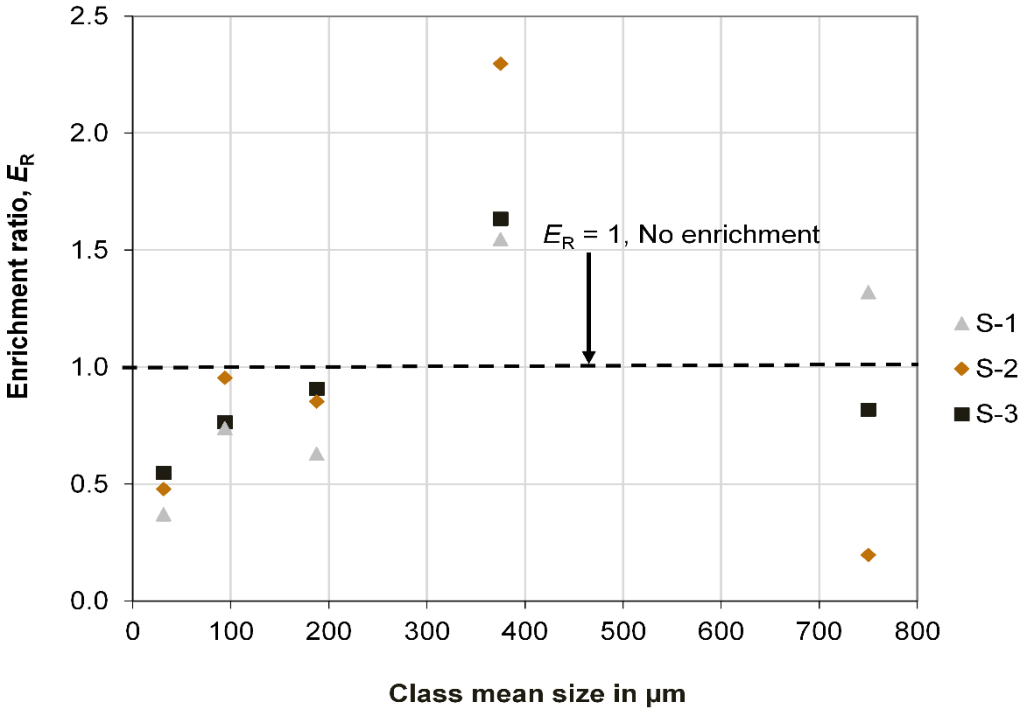

Figure 5-18: Pyrite-pyrrhotite enrichment with particle size.

Figure 5-19 (a) presents the relationship between pyrite-pyrrhotite cumulative liberation with its geometric mean grain size. It can be seen that S-3 has coarser mineral grain size compared to S-1 and S-2. Pyrite-pyrrhotite liberation increases with decrease in mineral grain size for all samples. What can also be speculated from this result is that it seems less milling is required in order to liberate pyrite-pyrrhotite from sample S-3 (i.e. coarsest mineral grain) as compared to S-1 and S-2. This might be one of the reasons for higher pyrite-pyrrhotite liberation also displayed in Figure 5-16 and Figure 5-17.

The ratios between geometric mean sizes of the feed (i.e. feed to screen mill) to that of the sieved fractions (i.e. reduction ratio) was calculated for the three samples and related to cumulative pyrite-pyrrhotite liberation as shown in Figure 5-19 (b). The result indicate that S-3 had the highest reduction ratio than S-1 and S-2 implying that S-3 sieved fractions were finer than S-1 and S-3 fractions. Further, pyrite-pyrrhotite liberation increases with increase in reduction ratio, with S-3 giving higher liberation

than S-1 and S-2 and this is due to better material fineness in S-3 than other samples. Therefore it can be concluded that the better pyrite-pyrrhotite liberation achieved for S-3 fractions is also influenced by their fineness.

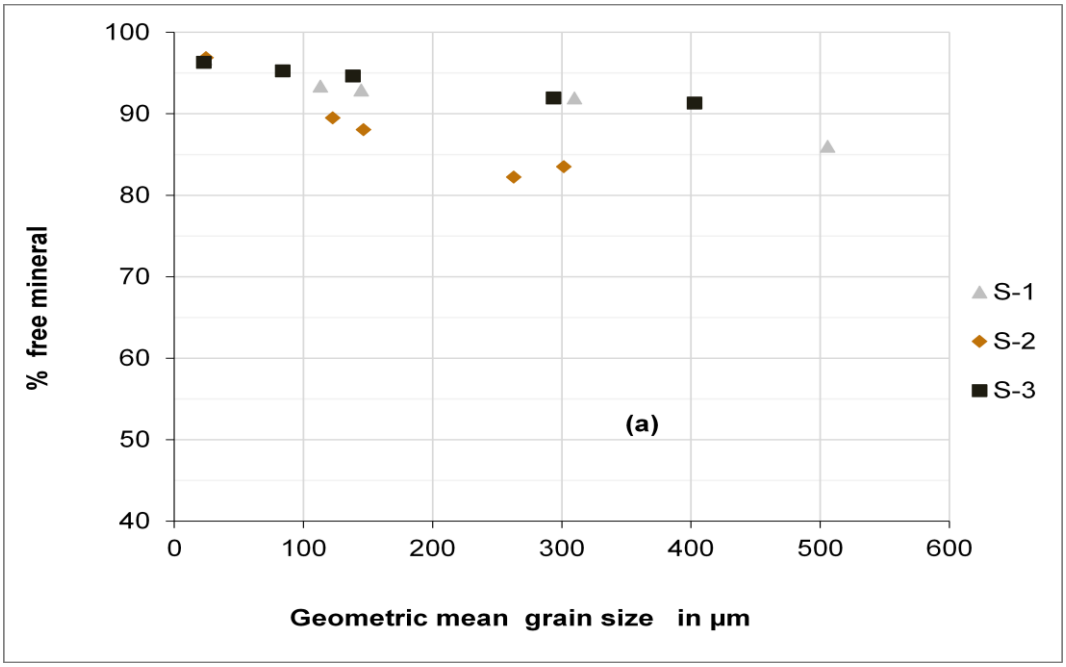

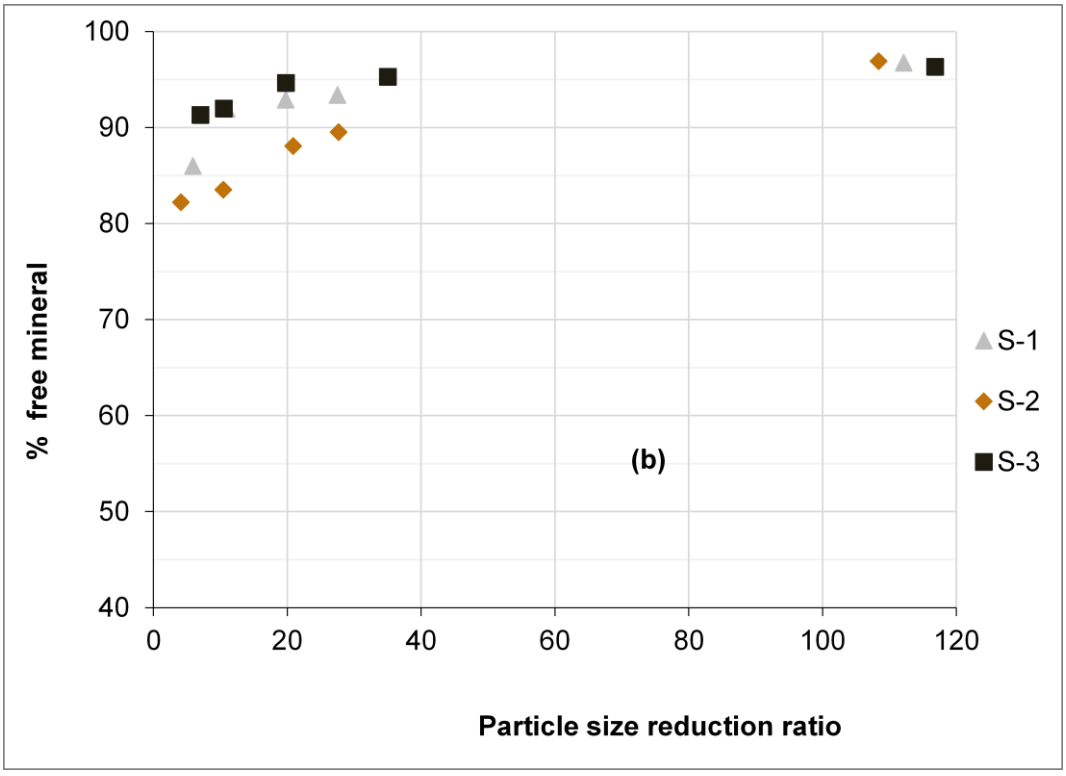

Figure 5-19 : Pyrite-pyrrhotite cumulative liberation as a function of geometric mean grain size; (a), and also as a function of the size reduction ratio; (b), for the three samples.

5.2.4 Mineral Locking

The proportion into which the valuable mineral phase, pyrite-pyrrhotite is locked with other minerals is presented in Figure 5-20 to Figure 5-22. In the previous section 5.2.3 it was revealed that pyrite-pyrrhotite fractional liberation was >80 % for all samples. Therefore the locked mineral phase refers to the < 20% pyrite-pyrrhotite which was indicated as not entirely liberated in section 5.2.3.

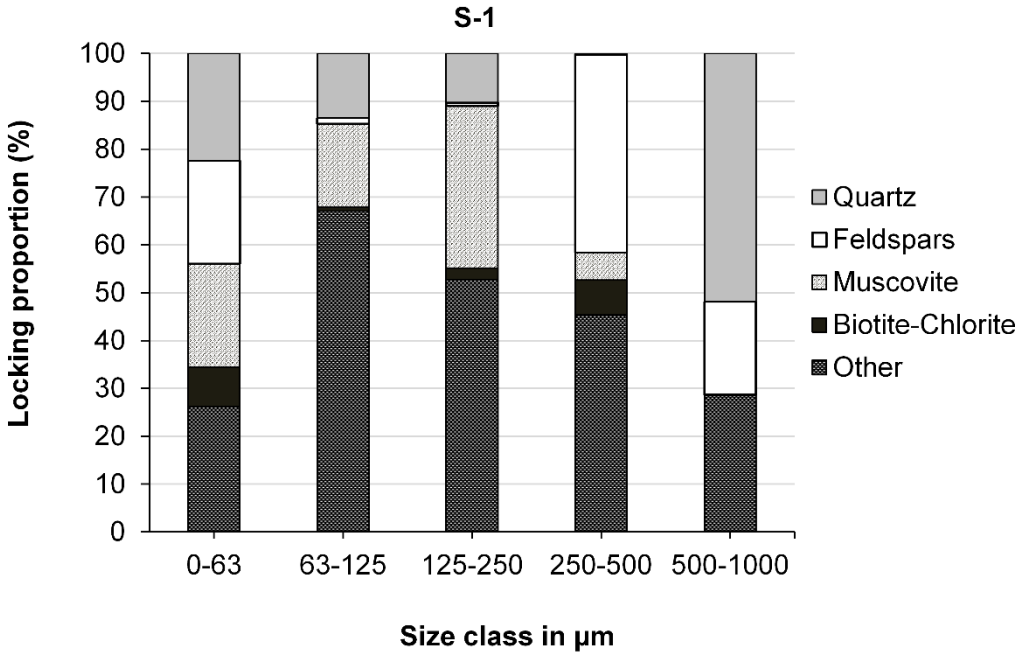

Figure 5-20: Pyrite-pyrrhotite locking as a function particle size, S- 1.

From Figure 5-20 to Figure 5-22, it is seen that there is no consistent trend defining the extent to which pyrite-pyrrhotite is locked with other minerals with respect to the particle size. For most of the fractions in all samples, pyrite-pyrrhotite is locked into the phases ”other”, followed by quartz and muscovite. The extent into which pyrite-pyrrhotite is locked into the phase ”other” is almost constant in all fractions for S-2, as opposed to the fluctuations observed for S-1 and S-3. Moreover, pyrite-pyrrhotite locking into quartz and muscovite varies significantly between fractions in all samples. Note that the mineral group ”other” comprises of phases Epidote, Fluorite, silicates, oxides and other minor sulphides. Therefore it can be assumed the group ”other” is where pyrite-pyrrhotite was mainly locked to for the investigated orebody.

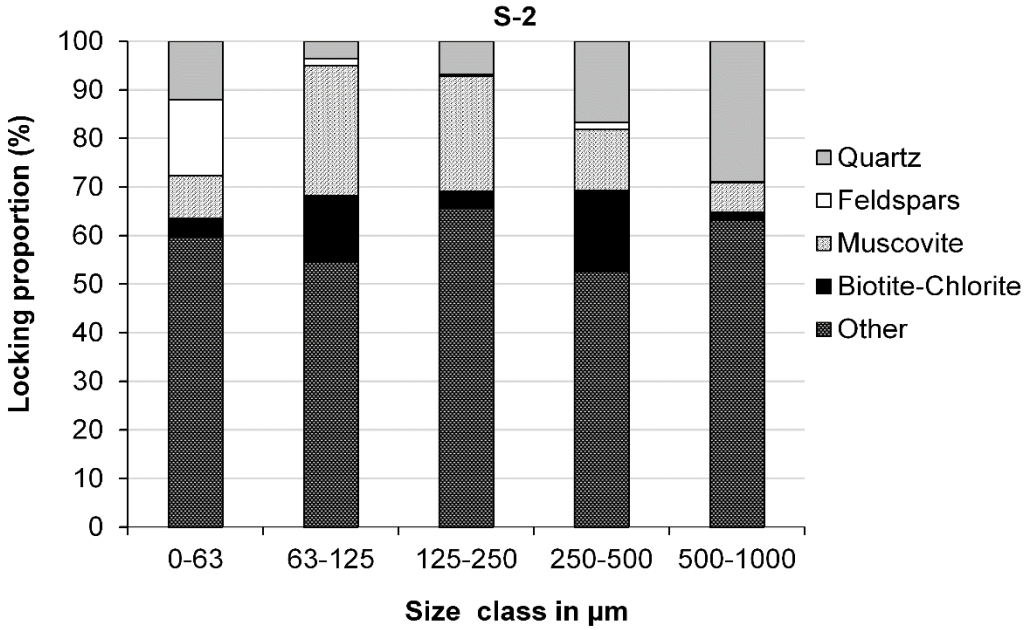

Figure 5-21: Pyrite-pyrrhotite locking as a function particle size, S-2.

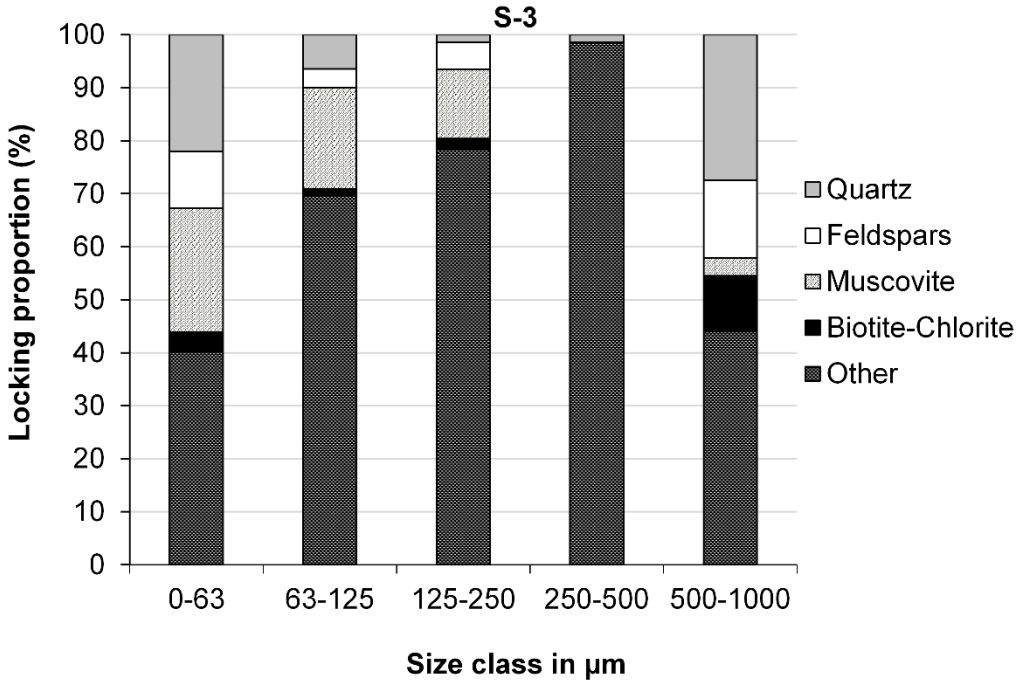

Figure 5-22: Pyrite-pyrrhotite locking as a function of particle size, S-3

5.2.5 Correlations

In order to evaluate the relationship between work index, W_i and quartz content in the ore material, the quartz content values in Table 5-13 and the work index values in

Table **5-1** have been plotted in Figure 5-23. The work index seems to satisfy a linear relationship with quartz content of the ores with the correlation coefficient of 0.95 and the relationship can be expressed as follows:

$$W_i = 0.60 \cdot Quartz(wt.\%) - 6.49 \quad (89)$$

The relationship could be explained by the fact that quartz is the hardest mineral compared to others in the material (hardness value of 7 based on Mohs hardness scale) (Frost 1981). Therefore, the work index for the BGM ore may be predicted based on known quartz content of the material. It can be indicated that the work index of the material will increase with increase in quartz content and vice versa. The model can be useful and replace the tedious Bond tests for quick and rough estimations of the work index for the BGM ore. Thus can be used as a control tool for monitoring the hardness variation for the SAG mill feed.

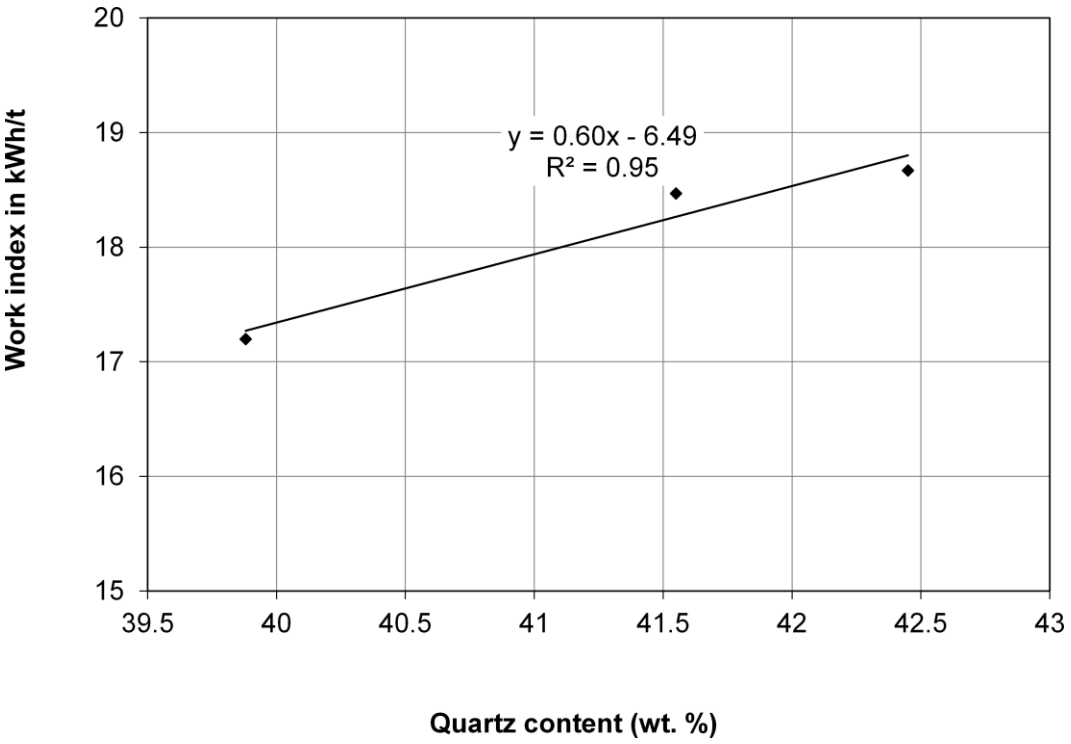

Figure 5-23: Dependence of Work index on Quartz content in the ore material

5.2.6 Conclusions and Recommendations

The mineral liberation studies of the three gold ore blends from Buzwagi Gold Mine reveal the following:

- Pyrite-pyrrhotite is the major valuable mineral phase in the material with an abundance of 6.54, 5.58 and 3.2 % for S-1, S-2 and S-3 respectively. Additionally, quartz, feldspar, muscovite and biotite-chlorite are the main gangue phases in the material.
- The mineral grain size distribution of quartz and feldspars closely follows the particle size distribution of the host particles. Therefore, those minerals phases show a good liberation from the others.
- Pyrite-pyrrhotite mineral grain size distribution is coarser compared to most gangue minerals present. This indicates that most of the milling energy is applied in grinding of the gangue phases (e.g. Quartz and Feldspars).
- Pyrite-pyrrhotite liberation based on fractions was higher than 75 % in all samples for fractions < 500 µm.
- Pyrite-pyrrhotite is liberated at relatively coarse size (i.e. approx. 200-400 µm), with > 85 % cumulative liberation for each sample.
- Higher pyrite-pyrrhotite enrichment was displayed in the size range 250-500 µm with S-2 having the highest enrichment followed by S-3 and S-1.
- Pyrite-pyrrhotite mineral in S-3 was coarser than that in the other two samples.
- Based on reduction ratios, S-3 fractions were finer than S-1 and S-2 fractions.
- The lower pyrite-pyrrhotite liberation levels achieved in S-2 could be contributed to material hardness (i.e. work index for S-2 > work index for S1 and S-3)
- A strong correlation between ore work index and quartz content is obtained. This is recommended for prediction of work index for the BGM material.

Based on BGM plant design, the primary grinding circuit incorporates a gravity unit which concentrates portion of gold contained in the sulphides (e.g. pyrite-pyrrhotite). The final gold recovery from the gravity concentrate is accomplished by intensive cyanidation using the Acacia reactor. After fine grinding, gold and copper are

recovered through flotation. Gold is also recovered from cyanidation of the flotation tailings. The cyanidation plant treating the flotation tailings was introduced later after discovering that the gold recovery could not be entirely achieved by the flotation process. The reason for the inefficient flotation process was suspected to be due to ore mineralogical variations experienced.

Based on the mineral liberation results of the three blends, the sulphide phase (pyrite-pyrrhotite) is liberated at very coarse size (200-400 µm). This implies that, there will be no problem with the efficiency of gravity circuit for the BGM operation. However, the efficiency of flotation and cyanidation processes will still require somehow finer feed.

5.3 Simulation Studies

Based on operating conditions as well as the analysis of survey data; it was concluded that the BGM grinding circuit had some problems such as:

- Inefficient ball mill performance
- Inefficient hydrocyclone classification
- Large operating gap for the recycle crusher
- Fluctuating SAG mill feed size
- High solids content in the cyclone feed and
- High circulating load in the ball mill circuit

Optimization studies by computer simulation using mathematical models for mills and classifiers were conducted in order to find a suitable solution for this bunch of problems. Hence, several parameters were investigated using MODSIM simulation package (see chap. 4.5) and will be mainly reported in this section.

5.3.1 Mass Balance and Modelling

The survey data were mass balanced to confirm their quality and also to determine any stream flow rates that could not be measured. For the BGM plant settings, only flow rates for the SAG mill and hydrocyclone feed streams could be measured. Flow rates for all other streams were obtained through mass balance. Table 5-16 gives a summary of key stream tonnages and $x_{P,80}$ values for the three surveys. The quality of data as indicated by mass balancing is somehow low from all surveys. Nevertheless is assumed to be within tolerance (see Figure 5-25) and hence could be used to describe the existing operation through modelling and simulation.

Table 5-16: Comparison of measured and mass balanced values around BGM milling circuit.

Stream/Unit	Survey 1	2	3
SAG Mill			
Feed (t/h)	618.72	674.11	573.35
Discharge screen undersize (t/h)	619.13	674.10	573.32
$x_{P,80}$-measured in µm	1644	1468	831
$x_{P,80}$-calculated, µm (see Appendix-E)	1600	1551	925
Ball Mill			
Discharge (t/h)	1109.91	939.83	487.42
$x_{P,80}$-measured in µm	570	419	403
$x_{P,80}$-calculated in µm	572	596	421
Hydrocyclone			
Feed (t/h)	1729.04	1613.93	1060.74
$x_{F,80}$-measured, µm	768	771	570
$x_{F,80}$-calculated, µm	760	775	570
Underflow (t/h)	1387.48	1249.57	840.08
Underflow $x_{P,80}$-measured	963	1028	1127
Underflow $x_{P,80}$-calculated	958	945	1081
Overflow (t/h)	341.82	363.90	220.66
Overflow $x_{P,80}$-measured, µm	266	288	241
Overflow $x_{P,80}$-calculated, µm	278	300	215

Further, considering the fact that the liberation characteristics of the three ore blends were almost the same (refer chap. 5.2) and also in (Arinanda 2016, Wikedzi, Arinanda et al. 2018), we decided to use only one sample (survey1) for modelling and simulation of the BGM operation. Also, by comparison, survey 1 data have fewer points where big differences exist between measured and mass balanced values.

MODSIM models for SAG mill, screen, ball mill and hydrocyclone were calibrated based on the survey data (survey 1 in this case), mass balance results, plant operating data, ore characterization tests as well as the design data. The accuracy of the models was controlled by calculating the size distributions of each stream by using only the

measured size distribution of the survey 1 feed. The measured size distributions and MODSIM predicted values for key streams around the circuit are compared (Figure 5-24). There the majority of streams are reflected accurate. Only the hydrocyclone overflow shows a significant difference between the predicted and measured size distributions. Also below 0.2 mm, the predicted SAG mill discharge size distributions are on the lower side compared to the measured ones. Both problems can be explained by model limitations and also the quality of data. Nevertheless it has to be kept in mind that the simulation might predict an intermediate product of the SAG mill with higher fines content as well as a final product which is finer than in reality. In overall, a good predictive capability of the models is demonstrated.

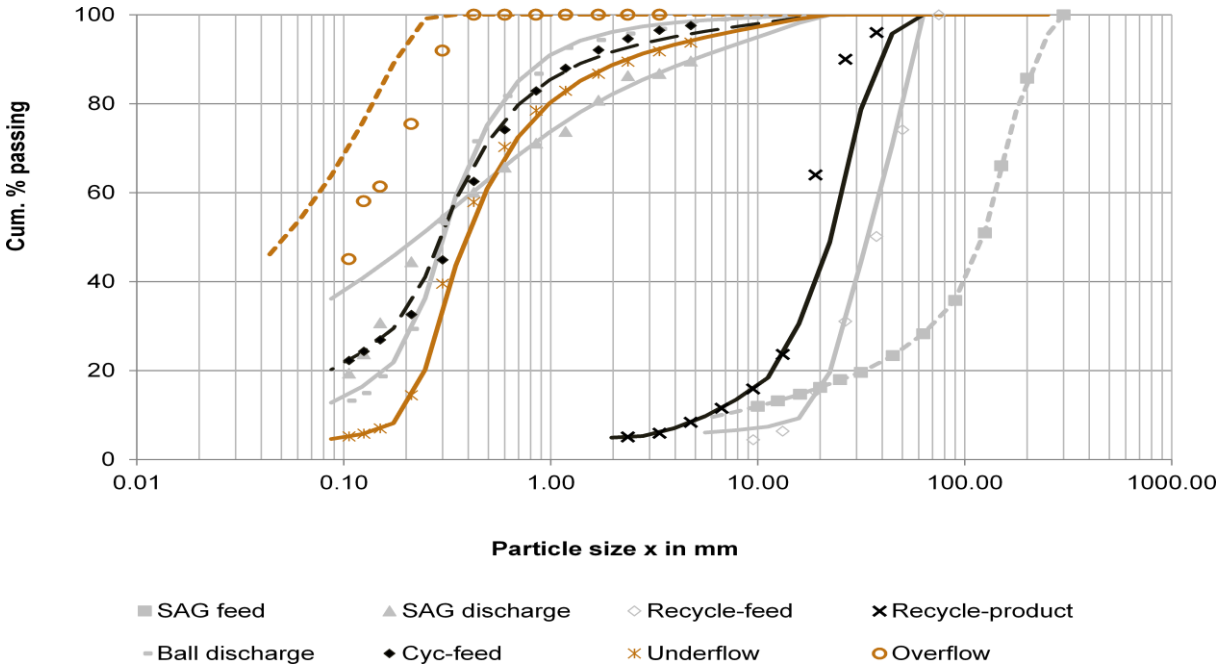

Figure 5-24: Measured and MODSIM predicted size distributions around BGM grinding circuit (survey 1). Points and solid lines represent survey and predicted values, respectively.

The experimental particle size distributions from survey (experimental) are compared to MODSIM predicted values (Figure 5-25). As can be seen from this figure, most of the results are within the error boundaries of ± 20% error, which is tolerable. f

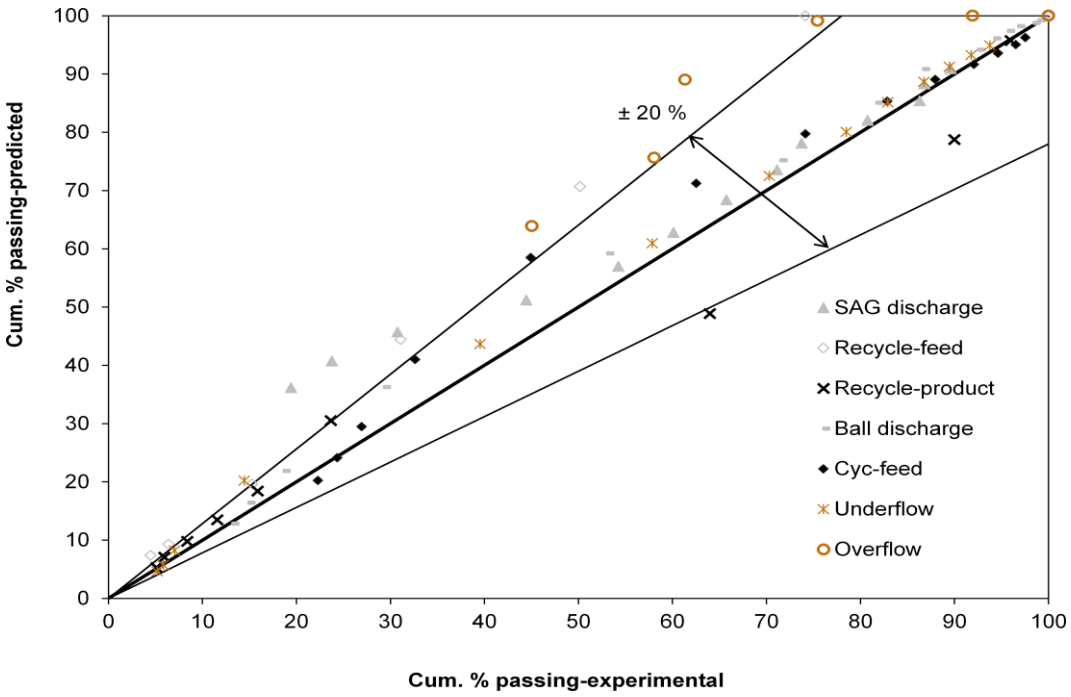

Figure 5-25: Comparison between MODSIM predicted and experimental particle size distributions.

The models were then used to simulate different options in order to improve the grinding efficiency and reduce the final product size for the BGM operation. Table 5-17 gives detailed results for the simulation of BGM operation based on survey 1.

Table 5-17: Survey and MODSIM predicted stream values around BGM grinding circuit.

Stream		Solids (t/h)	$x_{P,80}$ (mm)	%-Solids	Water (m^3/h)
SAG mill discharge	Survey	618.72	1.644	68.50	348.70
	Sim.	619.20	1.640	58.70	362
Recycle scats	Survey	61.40	20	97	2.10
	Sim.	58.60	25	96.30	2.20
Ball mill discharge	Survey	1110	0.57	72.10	133
	Sim.	1300	0.58	80	134.04
Hydrocyclone feed	Survey	1729	0.77	66.70	864
	Sim.	1942	0.71	70	840

Underflow	Survey	1387.50	0.96	79	368.83
	Sim.	1431	0.98	82.5	138
Overflow	Survey	342	0.27	41	494.53
	Sim.	512	0.14	42	701

5.3.2 Optimization studies

Several simulations were conducted in order to evaluate if a finer product could be achieved with the current design and at the same throughput as obtained during survey 1, 619 t/h. Because of the complexity of the circuit being investigated, a stepwise simulation approach was applied. For each proceeding stage, the optimized parameters obtained from previous steps were used as base case/benchmark inputs for optimization of the individual next piece of equipment or circuit. A summary of the simulation results is presented as follows:

5.3.2.1 Optimization of the Existing SAG mill Circuit

Based on survey data, the performance of the SAG mill circuit could be improved by adjustment of SAG discharge screen aperture or the gap of the pebble crusher. However, after several trials, the pebble crusher gap didn't show any significant contribution. The SAG discharge screen showed influence and will be presented.

Influence of SAG discharge screen

From BGM grinding circuit survey results (chap.5.1), it was realized that the pebble crusher presented a reserve capacity. Therefore by decreasing the SAG discharge screen aperture it was expected that the pebble crusher capacity could be utilized with an advantage of improving the SAG mill circuit performance which would have an overall influence on the product fineness of circuit. A trial between 6 mm to 10 mm screen aperture was examined and a 10 mm aperture was found feasible and was simulated. The result for some key performance indicators is presented in Table 5-18. Further, the implications of the changes on the SAG discharge screen aperture on the ball mill circuit performance is summarized in Table 5-19.

Table 5-18: Influence of SAG discharge screen on SAG mill performance.

Parameter	Survey	Survey sim.	Optimized sim.
Recycle (t/h)	61.40	58.60	102.5
SAG discharge screen undersize $x_{,P,80}$ (µm)	1644	1640	1240

Hence, by reducing the screen aperture from 12 mm to 10 mm, the SAG mill screen oversize (i.e. pebble crusher feed) increased from 61.40 t/h to 102.5 t/h. A significant change also is the fineness of SAG mill discharge screen undersize from 1640 mm to 1240 mm. It was expected that the reduced SAG mill product size could have positive influence on the ball mill performance. However, this was minimal as can be reflected in Table 5-19.

Table 5-19: Influence of optimized SAG discharge screen on ball mill circuit performance.

Parameter	Survey	Survey sim.	Optimized -SAG sc.
Overflow-$x_{P,80}$ (µm)	266	140	134
BM-$x_{P,80}$ (µm)	570	579	548
Mill power (kW), Bond	1828	2374	2104
x_T (µm)	221	178	178
Overflow solids (%)	41	42	42.3
*C*L (%)	400	300	270

The simulated particle size distributions for the SAG mill circuit streams for the base case (Bc) as well as optimum conditions (Op) can be seen in Figure 5-26. The other circuit streams characteristics under optimized SAG mill circuit can be referred in Appendix D.

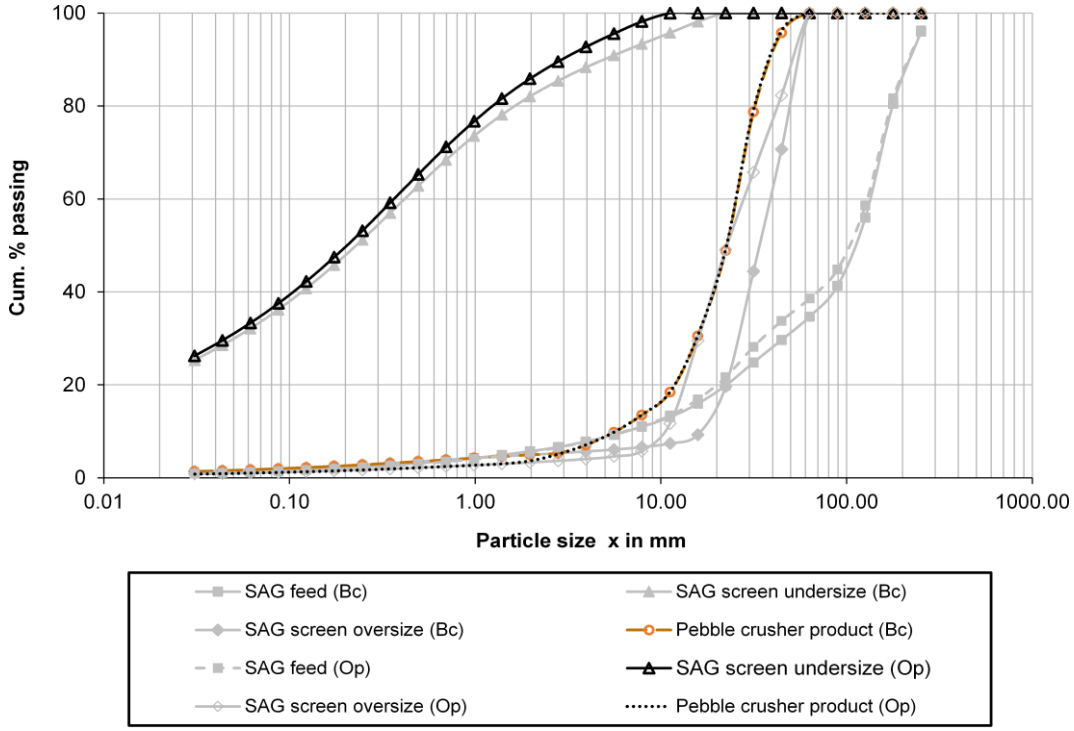

Figure 5-26: Simulated particle size distributions for the SAG mill circuit under base case (Bc) and optimum (Op) SAG screen aperture. Base case refers to survey simulation.

5.3.2.2 Optimization of the Existing Ball Mil Circuit

Three parameters were found feasible in an effort to search for efficient operating conditions of the ball mill through simulation. These are cyclone feed solids content, vortex finder and apex diameters. They were simulated sequentially as listed and the results are summarized in following sections.

Influence of cyclone feed % solids

The effect of cyclone feed solids content was simulated in the range 60-68 in order to search for or establish an optimum value. The optimized parameters from the SAG mill circuit were used as base case inputs. All other parameters were kept at survey simulation settings. The effect of cyclone feed solids content on the circulating load and ball mill discharge fineness is shown in Figure 5-27. It is seen that as the cyclone feed solids content increases due to low dilution, the circulating load decreases due to an increase in cut size. On the other hand, the ball mill discharge becomes finer with decrease in cyclone feed solids content. It can be noted that this parameter influences classification and milling processes in the opposite way. Therefore, a compromise on the efficiency of these processes is necessary for better selection of an optimum cyclone feed solids content.

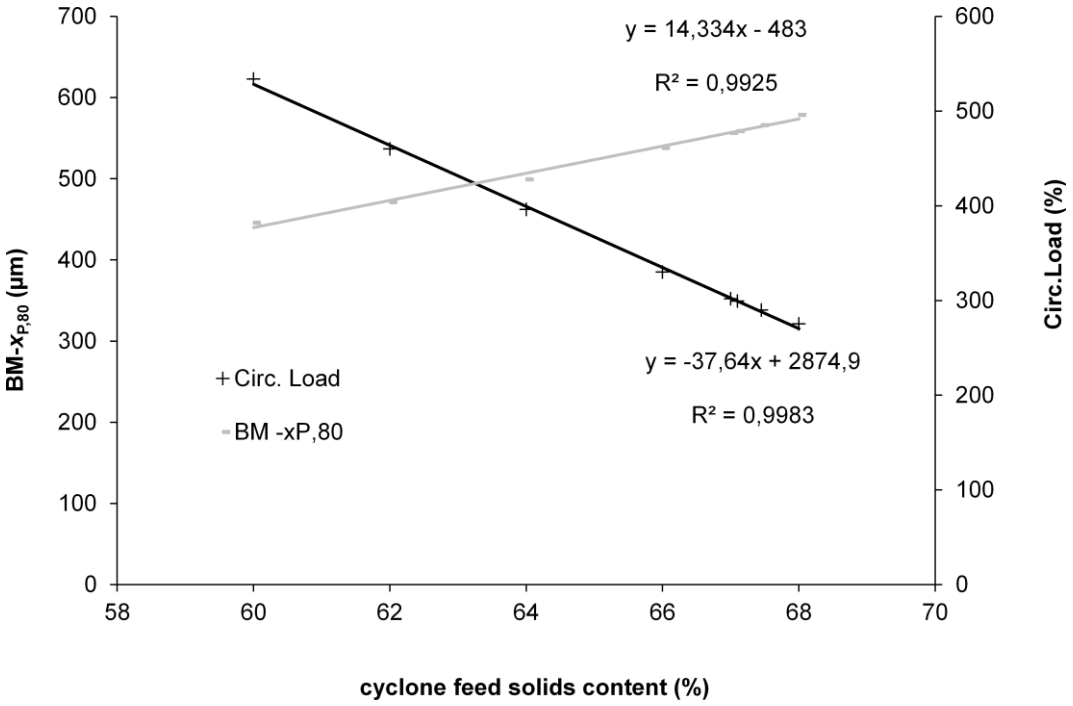

Figure 5-27: Effect of cyclone feed solids content on circulating load and ball mill discharge fineness.

Further, it can be seen that under the range of cyclone feed solids content simulated, the circulating load was quite high. This is not desirable and thus an optimum value of the circulating load has to be constrained by other factors such as cut size and overflow solids content.

The effect of cyclone feed % solids on the cut size and the overflow fineness is given in Figure 5-28. The cut size increases with increase in cyclone feed solids content due to higher resistance to swirling motion within the cyclone which reduces the effective pressure drop (Wills and Napier-Munn 2006).

The change in cut size is significant and is at an average of approximately 10 µm per 1 % increase in cyclone feed % solids. The overflow product became coarser as the cyclone feed density increases. This reflects the effect of increased separation size. All simulations show that a strict control of the feed density is required in order to keep the overflow fineness at a defined and constant level.

Referring to Figure 5-27, it can be noted that under the range investigated, the ball mill product size ($x_{P,80}$) is coarse (380-500 µm). Also, from Figure 5-28, the hydrocyclone cut size ranged between 70-149 µm, implying that such a coarse ball mill product could not be well classified.

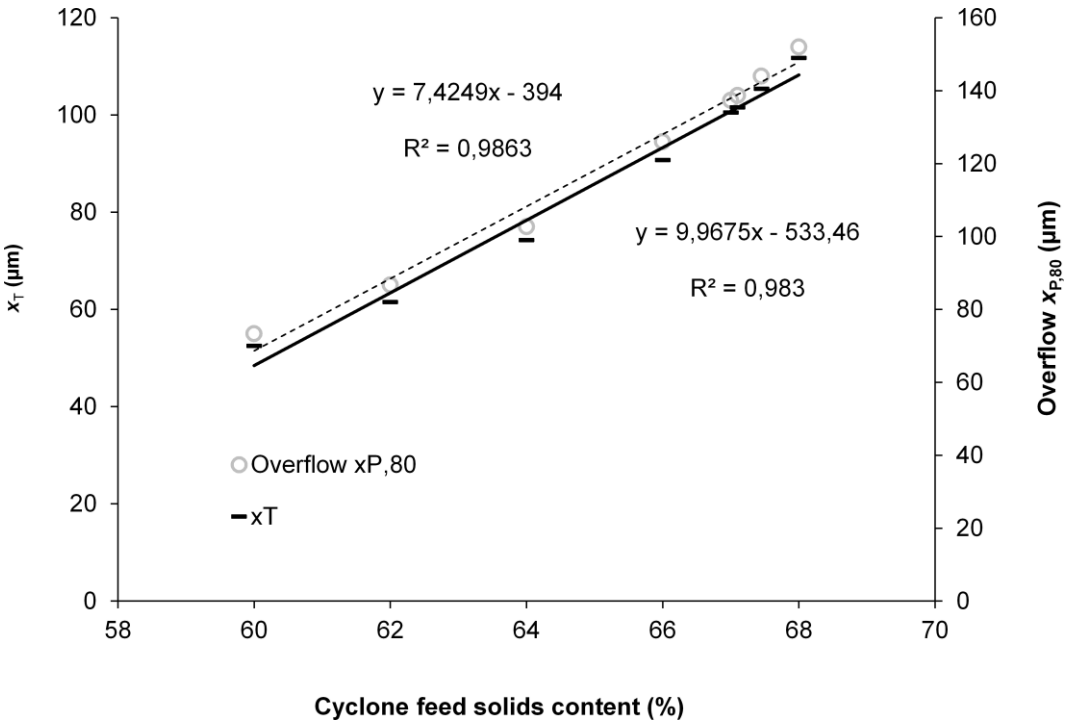

Figure 5-28: Effect of cyclone feed solids content on the cut size and overflow fineness.

It has already been established that the BGM hydrocyclones could reach a lower cut size with different nozzle diameters (refer Figure 5-10). This is an important constraint in deciding for an optimum cyclone feed % solids. Based on this, the cyclone feed density of 67.1 % solids was considered the best (x_T = 135.4 µm). Although this is only 0.4 % higher than the survey value of 66.7 %, it is significant due to its sensitivity on cut size. If this is implemented could result to an improvement of ball mill discharge fineness from 548 µm (base case simulation) or 570 µm (survey) to 460 µm. However, this could also lead to a reduced circulating load of 349 % (Table 5-20), which is approximately 50% lower than survey and base case simulation values (Table 5-19). Another significant improvement to note is the overflow product size, which could be improved from 134 µm (base case) to 104 µm. What could also be noted from both figures is the strong correlation between parameters observed. These correlations were useful for the selection of optimum operating conditions. Figure 5-29 presents simulated particle size distributions of the ball mill circuit based on optimized cyclone feed solids content. The overall performance characteristics of the circuit under optimized cyclone feed solids content can be seen in Appendix D.

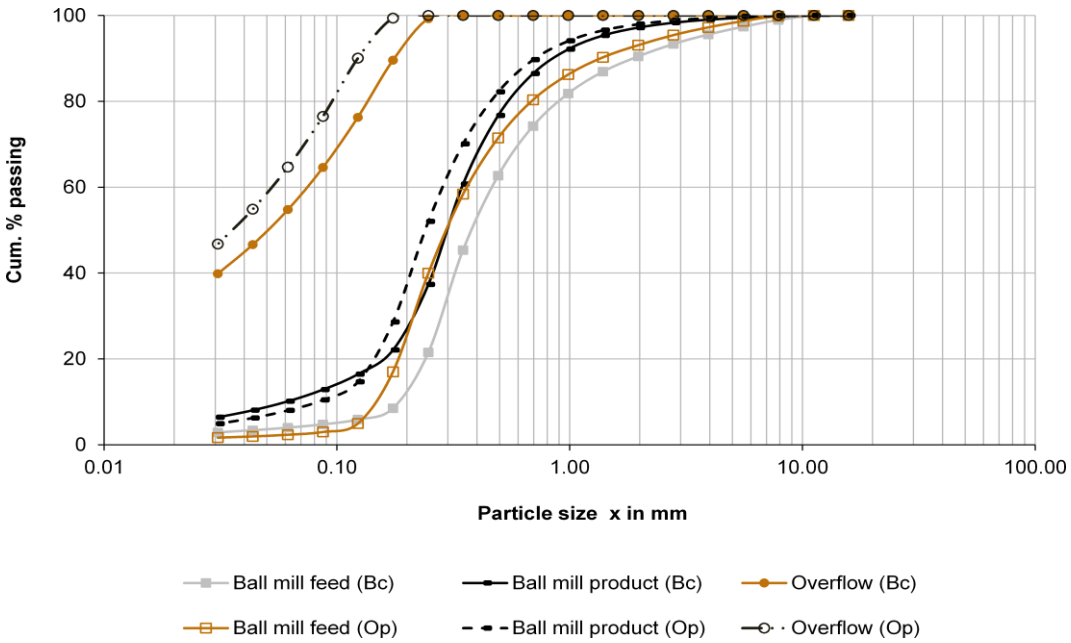

Figure 5-29: Simulated particle size distributions for the ball mill circuit under base case (Bc) and optimum (Op) cyclone feed solids. Base case refers to simulation under optimum SAG screen aperture.

The cyclone feed solids content values obtained during survey were considered slightly higher than recommended, hence presumption for lower values. The slight increase indicated by the simulation might be due to overloaded hydrocyclones (operated at approx. 17 % higher than capacity) or errors during survey.

Table 5-20: Influence of cyclone feed solids content on Ball mill performance.

Parameter	Survey	Base case sim.	Optimized sim.
Overflow-$x_{P,80}$ (µm)	266	134	104
BM-$x_{P,80}$ (µm)	570	548	460
Mill power (kW), Bond	1828	2104	2260
x_T (µm)	221	178	135.4
Overflow solids (%)	41	42.3	34.3
CL (%)	400	270	349

Importantly, it has to be clearly noted that the base case simulation in Table 5-20 refers to the optimum conditions of the SAG discharge screen which were used as benchmark during optimizations of cyclone feed solids content. This has to be distinguished with the survey simulation as can be referred in Table 5-19.

Influence of Vortex Finder Diameter

As it was observed in chapter 5.1, the hydrocyclone diameters for the BGM operation indicated some insufficiency. Therefore various dimensions were simulated in order to search for an optimum one.

The effect of vortex finder diameter on the circuit performance was investigated and altered in the range 165-267 mm. The interval was established based on BGM hydrocyclones manufacturers' available specifications (i.e. Krebs Engineering). The optimum parameters established from previous section were used as base case inputs (SAG screen aperture and cyclone feed solids content). The effect of vortex finder on ball mill discharge fineness and circulating load can be observed in Figure 5-30. Also, the simulated particle size distributions for the ball mill key streams are shown in Figure 5-31.The ball mill discharge product gets finer ($x_{P,80}$) with increasing in vortex finder diameter since this raises the cut size, the impact of which is reduced circulating load as coarser particles will also be carried to the overflow stream. The reduced circulating load results to increased milling residence time and hence increased product fineness. It can further be seen that the improvement in ball mill discharge fineness is a consequence of decreased circulating load with increase in vortex finder diameter.

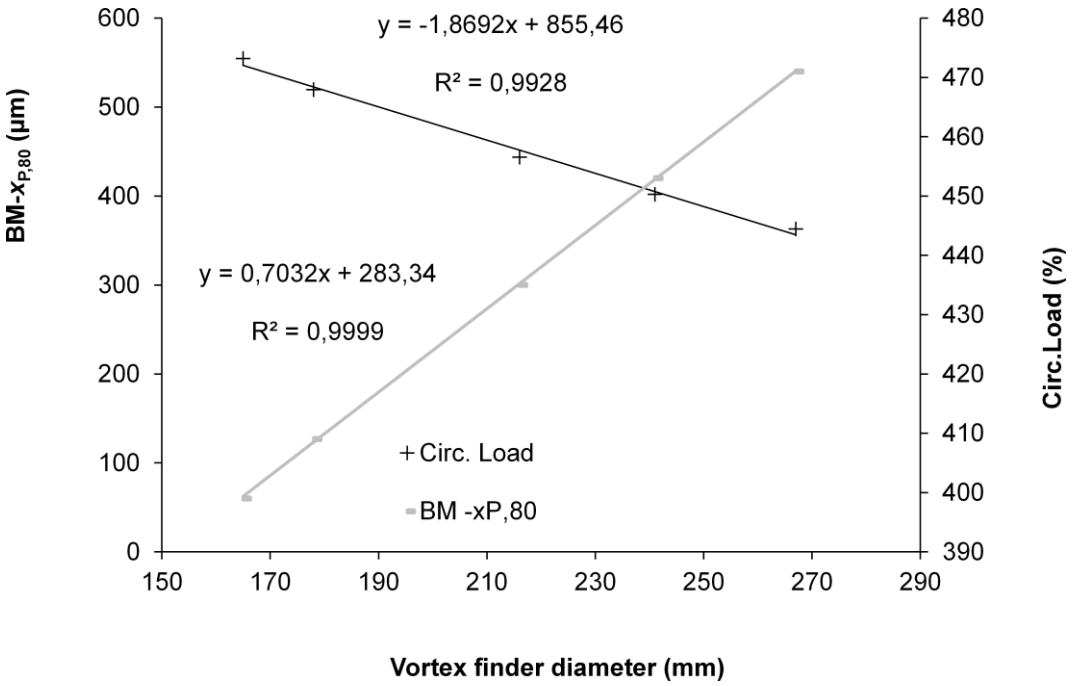

Figure 5-30: Effect of vortex finder diameter on circulating load and ball mill product fineness.

The dependence of cut size and overflow fineness on the variation of vortex finder is presented in Figure 5-32. It can be seen that, the cut size increases with increase in

vortex finder. The overflow product fineness increases with decrease in vortex finder diameter, however, the change is minimal

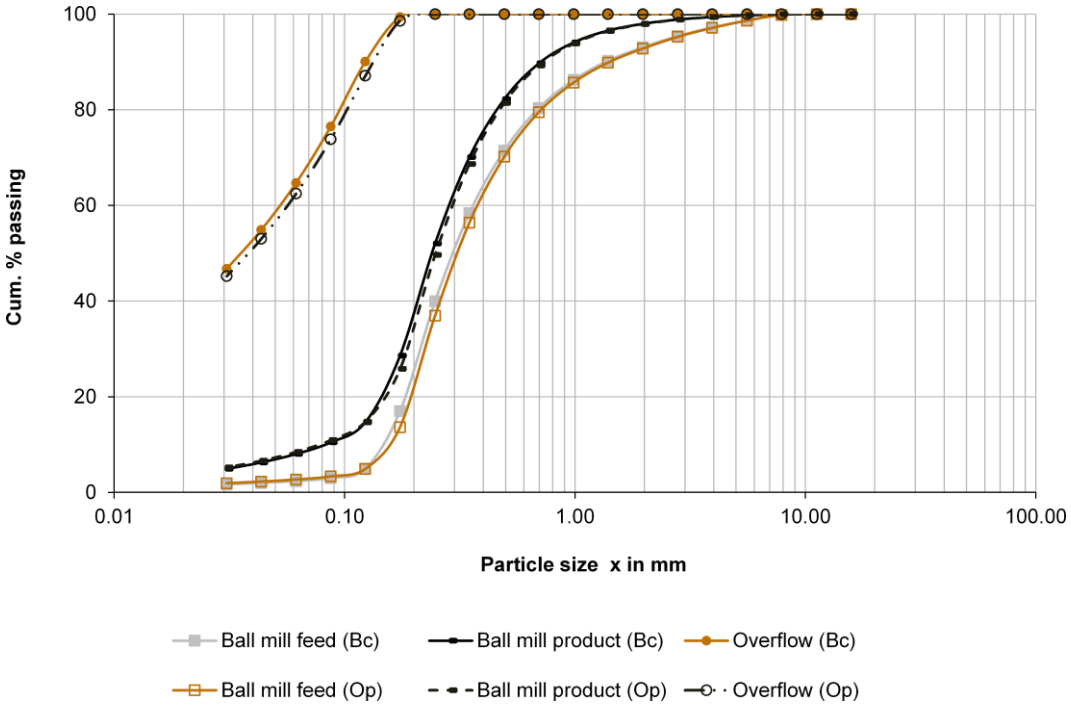

Figure 5-31: Simulated particle size distributions for the ball mill circuit under base case (Bc) and optimum (Op) vortex finder diameter. Base case refers to simulation at optimum cyclone feed solids.

It was found that the performance of 270.30 mm vortex finder was better than others. The ball mill product was the finest (i.e. 475 µm) slightly higher compared to 460 µm (base case). This could also lead to a slight increase in circulating load from 349 % (base case) to 358 %. The settings could also give a cut size of 132.1 µm (close to recommended value).

Table 5-21: Summary of key parameters after simulation of the influence of vortex finder.

Parameter	Survey	Base case sim.	Optimized sim.
Overflow-$x_{P,80}$ (µm)	266	104	110
BM-$x_{P,80}$ (µm)	570	460	475
Mill power (kW), Bond	1828	2260	2269
x_T (µm)	221	135.4	132.1
Overflow solids (%)	41	34.3	33
CL (%)	400	349	358

Other benefits were an improvement in the overflow product size from 104 µm (base case) to 110 µm (close to design value).The comparison of key performance indicators

is shown in Table 5-21. Refer to Appendix D for other ball circuit characteristics under optimized vortex finder.

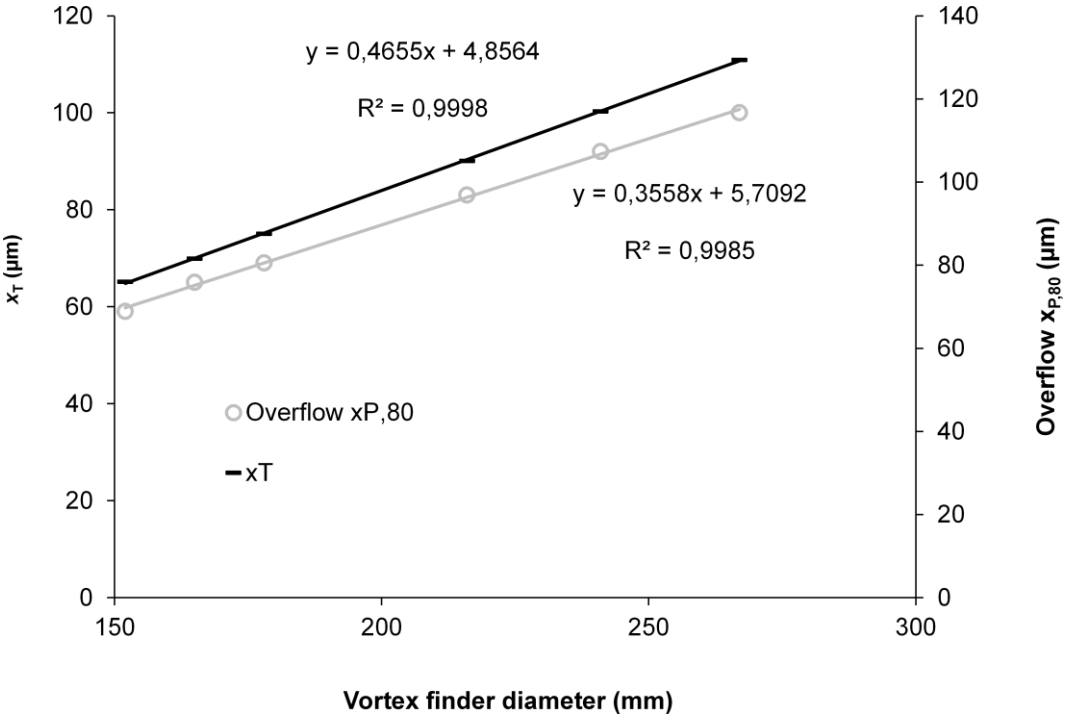

Figure 5-32: Effect of vortex finder diameter on cyclone cut size and overflow fineness.

Influence of the Apex Diameter

The effect of apex diameter on the circuit performance was simulated in the range 152-197 mm. The interval was based on manufacturers' available specifications as for the vortex. Also the optimum parameters from previous sections were base case inputs here. All other conditions were kept constant to the base case simulation. The effect of apex diameter on the ball mill discharge fineness and circulating load is shown in Figure 5-33. Further details for this section can also be seen in Figure 5-34 and Appendix D.

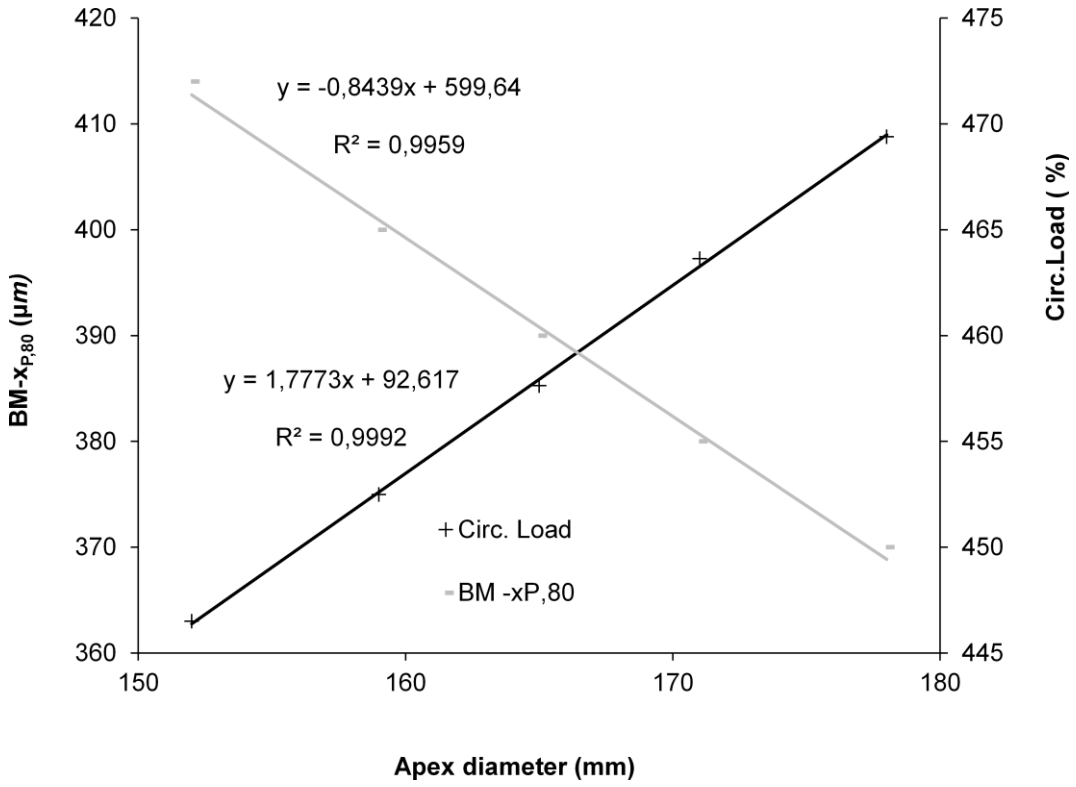

Figure 5-33: Effect of apex diameter on circulating load and ball mill discharge fineness.

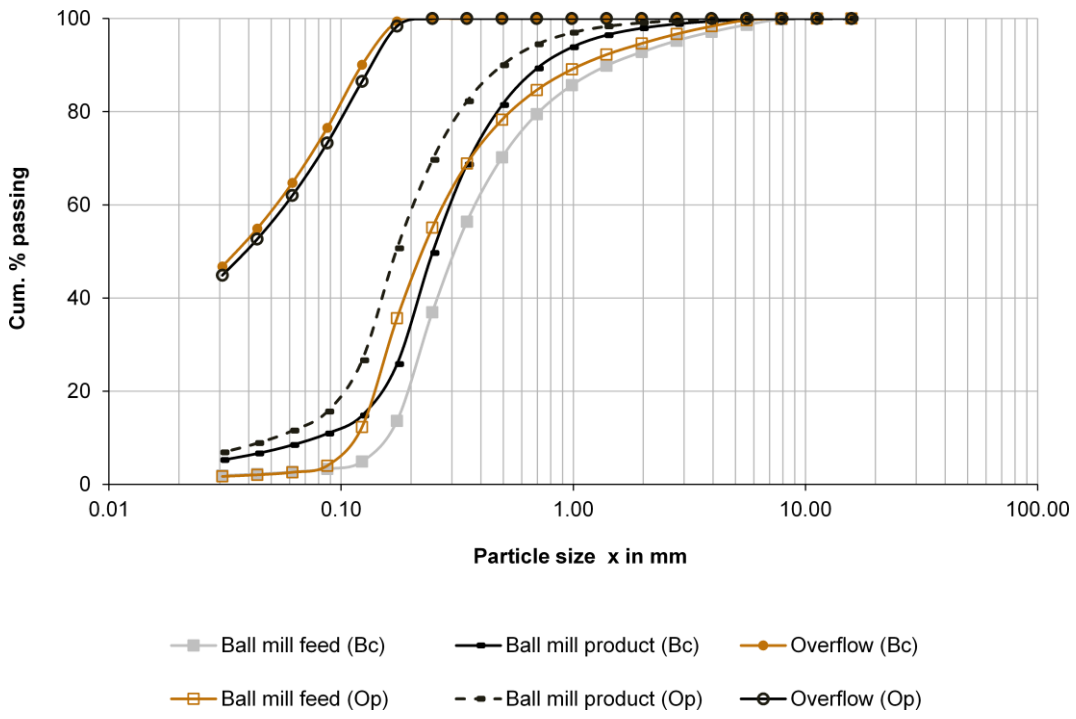

Figure 5-34: Simulated particle size distributions for the ball mill circuit under base case (Bc) and optimum apex diameter (Op). Base case refers to simulation under optimum vortex finder diameter.

The ball mill product size ($x_{P,80}$) gets coarser with increasing apex diameter. Also the circulating load increases. The effect of apex diameter is very pronounced due to its sensitivity on hydrocyclone performance and hence proper selection of this unit would be the key for successful operation. Nevertheless more factors need to be considered in order to decide for an optimum apex diameter. These are cut size, overflow fineness as well as overflow solids content.

The dependency of cut size and overflow product fineness on the apex diameter is presented in Figure 5-35. The cut size decreases with increase in the apex diameter. Further, a minimal change in overflow fineness is experienced with variation in apex diameter. Hence, based on cut size and circulating load constraints, an apex diameter of 145.6 mm was considered the best. Therefore if the change of apex diameter from 150 mm (survey) to 145.6 mm is adopted, the final ball mill product size could be reduced from the base case simulation of 475 µm to 327 µm with a corresponding slight decrease in circulating load from 358 % to 350 %. In addition this could lead to a minor change in overflow product size from 110 µm (base case) to 105 µm.The simulation of this section concludes the loop for the overall grinding circuit and therefore, the result (Table 5-22) is the cumulative effects of the possible parameter modification for the existing design. Further, the result indicates what could possibly be achievable by the present design based on simulation.

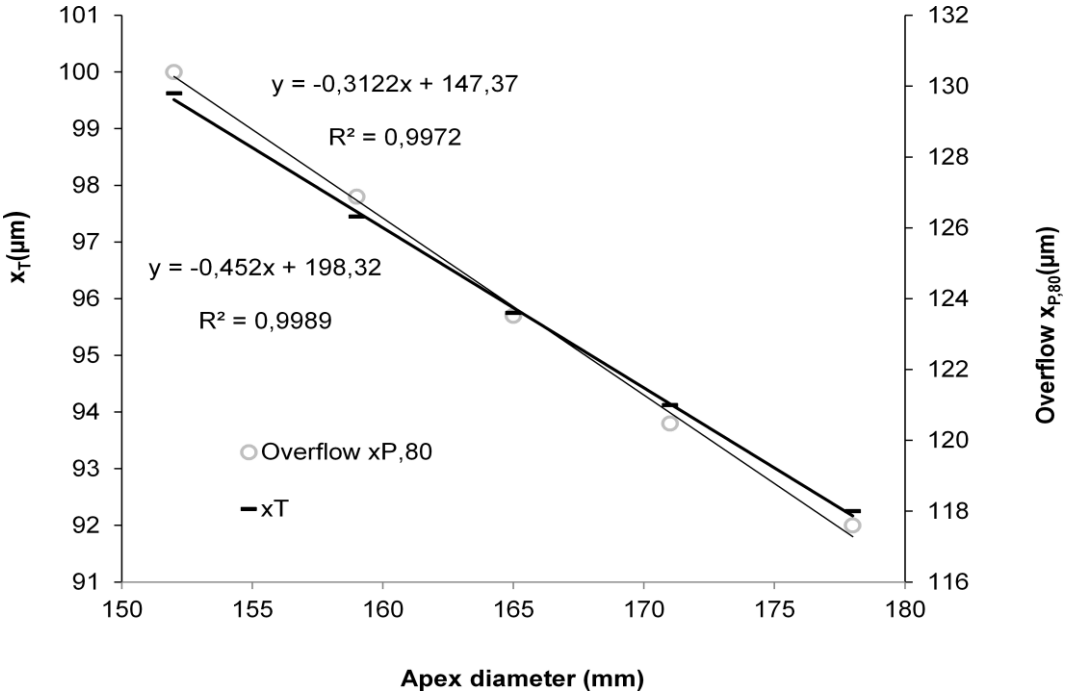

Figure 5-35: Effect of apex diameter on cyclone cut size and overflow product fineness.

Table 5-22: Overall circuit simulation after optimization of the apex diameter.

Parameter	Survey	Base case sim.	Optimized sim.
Overflow-$x_{P,80}$ (µm)	266	110	105
BM-$x_{P,80}$ (µm)	570	475	327
Mill power (kW), Bond	1828	2269	2956
x_T (µm)	221	132.1	133.1
Overflow solids (%)	41	33	32
*C*L (%)	400	358	350
Reycle (t/h)	61.40	102.5	102.5
SAG discharge screen undersize $x_{P,80}$ (µm)	1644	1240	1240

5.3.2.3 Modification of Existing Flowsheet

The simulation of several options presented above showed that the target final product size of $x_{P,80}$=125 µm (ball mill product) could not be achieved with the current design. Thus an evaluation for the possible flowsheet modification alternatives was performed. The flowsheet changes tested range from minor to major. The minor changes could be implemented instantly, while the major ones may be considered as long term solution.

Partial Splitting of Cyclone Underflow Back to SAG Mill

The analysis of BGM operation through survey data indicated that the ball mill performance is the main concern. Hence by partial splitting of the underflow and sending back to the SAG mill and also under the reduced SAG discharge screen aperture from 12 mm to 10 mm, the SAG mill circuit would increase its capacity which is accompanied by utilization of more power. The fineness of the SAG mill discharge could be improved and hence finer feed to the ball mill could result. This could also lead to decreased ball mill load and hence increased residence time in the ball mill, the consequence of which is improved product fineness. Simulations were evaluated using optimum conditions from section 5.3.2.1 and 5.3.2.2 as benchmark and optimally found to be feasible to return up to 10% of the cyclone underflow back to the SAG mill. From the results (Table 5-23) and Figure 5-36, despite the improved SAG mill discharge fineness, little improvement could be realized on the ball mill product (i.e. 326 µm vs.

436 µm). Further, a significant increase in circulating load from 350 % to 496 % was a setback. The overflow product fineness also became too fine (i.e. 92 µm vs. 105 µm) as well as the cut size (i.e. 100 µm vs. 133.1 µm). The poor ball mill performance could be due to poor cyclone classification (i.e. too low cut size) which resulted to higher circulating load and hence reducing the residence time in the mill.

Table 5-23: Effect of partially splitting cyclone underflow back to SAG mill.

Parameter	Base case sim.	Optimized sim.
Overflow-$x_{P,80}$ (µm)	105	92
BM-$x_{P,80}$ (µm)	327	436
Mill power (kW), Bond	2956	2215
x_T (µm)	133.1	100
Overflow solids (%)	32	28.5
CL (%)	350	496
Recycle (t/h)	102.5	118
SAG discharge screen undersize $x_{,P,80}$ (µm)	1240	1140

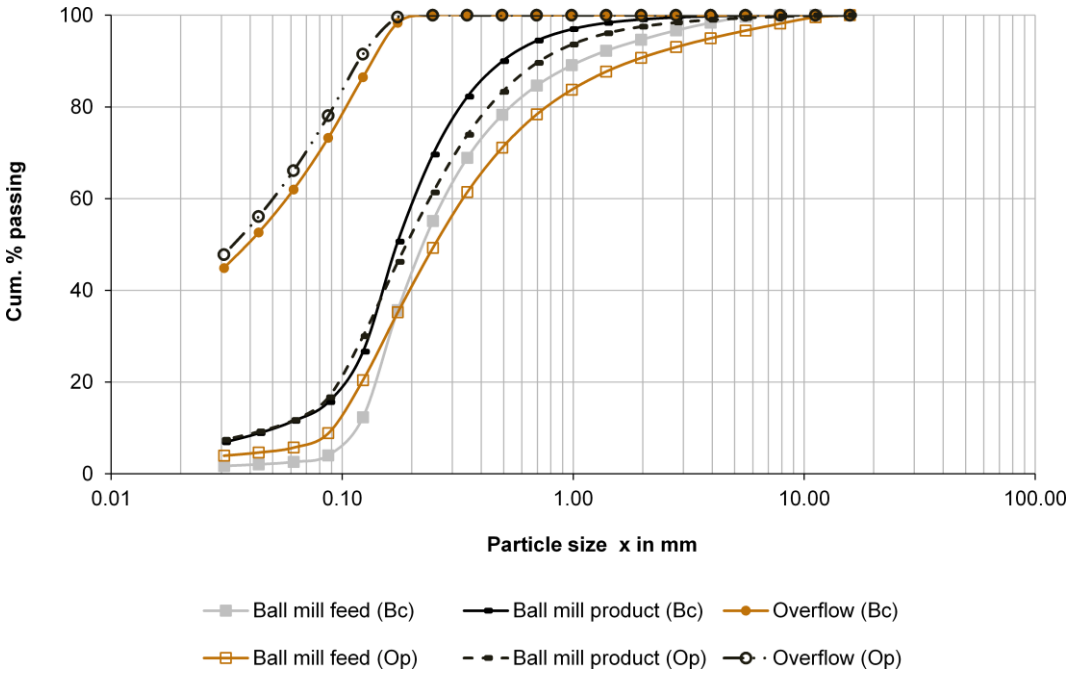

Figure 5-36: Simulated particle size distributions for the ball mill circuit under base case as well as optimized split of the underflow material back to the SAG mill circuit. Base case refers to simulation under optimum apex diameter.

Introduction of a Second Classification Stage

A second cyclone classification stage was introduced and simulated with cyclones of the same dimension as in survey as well as with some modifications (e.g. diameter, apex and vortex finder; refer to Appendix D8 for all parameters used) plus optimized values. The series arrangement of the cyclones was opted as could give improved efficiency due to the cumulative efficiency for the two stages. The optimized SAG mill data in section 5.3.2.1 and 5.3.2.2 were used as base case inputs in this case. The result is summarized in Table 5-24 and reveals no significant circuit improvement in terms of ball mill product. The only better recommendations are the improvements in overflow product fineness, overflow solids content as well as the reasonably low level of circulating load achieved.

The simulated flowsheet containing the two classification stages in the secondary milling section is presented Figure 5-37. This can be clearly distinguished with the current BGM grinding circuit flowsheet (refer Figure 2-1 or Appendix A). Figure 5-38 gives the simulated particle size distributions under optimum conditions for the proposed circuit. In addition other performance characteristics for this case can be referred to Appendix D.

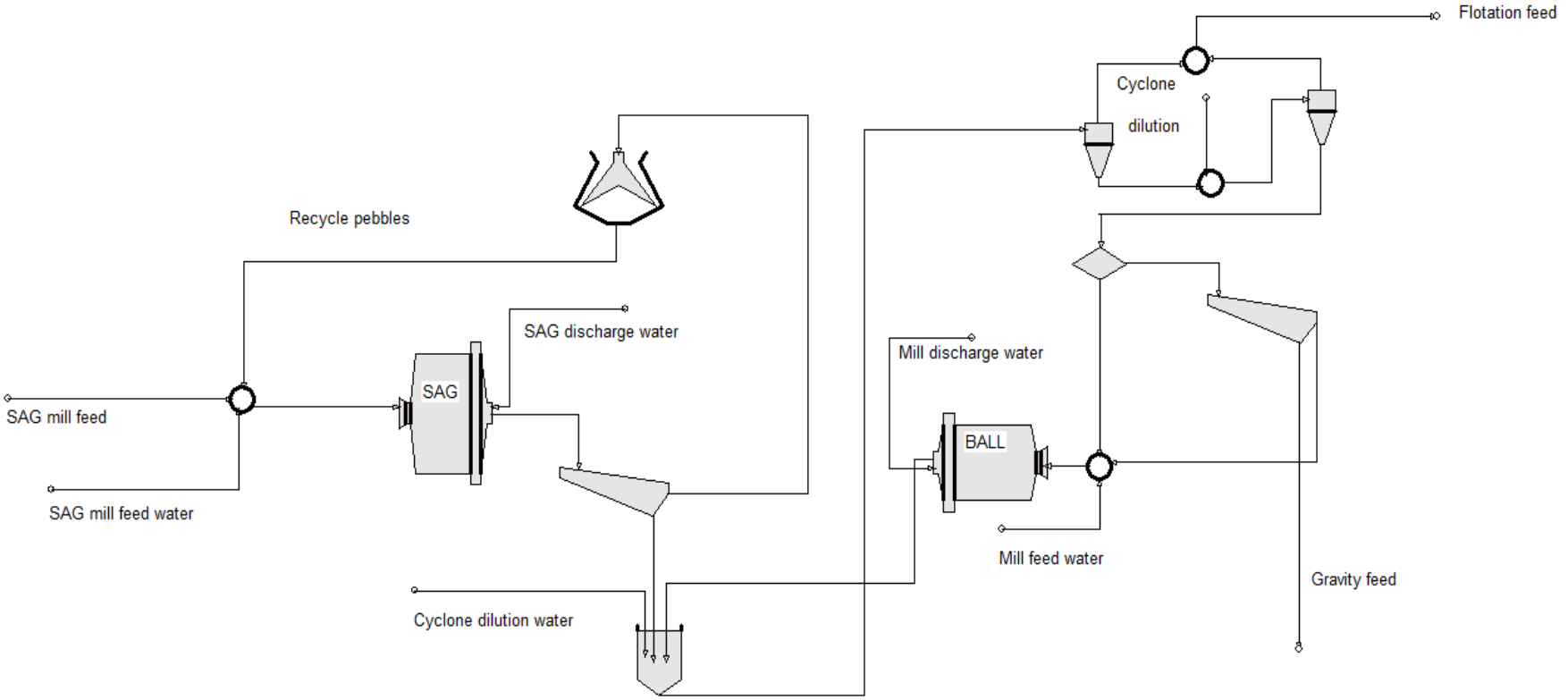

Figure 5-37: Two stage classification BGM grinding circuit flowsheet as modeled by MODSIM.

Table 5-24: Performance figures after addition of second classification stage.

Parameter	Base case sim.	Optimized sim.
Overflow-$x_{P,80}$ (µm)	134	100
BM-$x_{P,80}$ (µm)	548	463
Mill power (kW), Bond	2014	2363
x_T (µm)	178	103
Overflow solids (%)	42.3	29.50
CL (%)	270	400

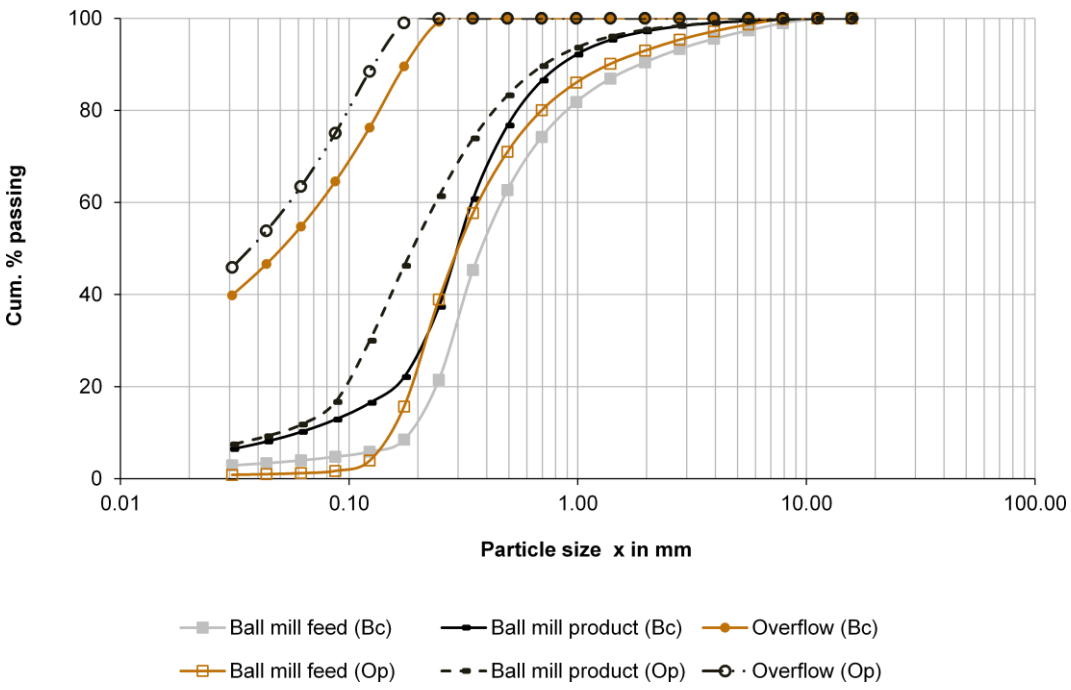

Figure 5-38: Simulated particle size distribution of the key streams for the proposed ball mill circuit with two classification stages under base case (Bc) and optimum conditions. Base case refers to survey simulation.

Introduction of a Second Ball Mill

Using Eqns. (17), (22) and (34) as well as based on the ball mill feed rate of 1300 t/h (survey 1 simulation), a suitable mill could be suggested. A ball mill with a diameter and effective grinding length of 6.40 m and 9.91 m was obtained. However, since the obtained mill size difference with the current one is tolerable and also for simplification in determination of the breakage parameters, a mill of the same size as the current one (6.1 m by 9.05 m) was used. Two options of the new circuit were simulated and optimized; parallel and series configurations.

Since the main objective was still to improve the product fineness, at first, simulations were evaluated by keeping the throughput constant. Later and upon achieving convincing improvements, simulations at varied throughputs were also tested in order to see if there are chances for throughput increase. Table 5-25 gives a summary of the key performance indicators for the two circuit configurations. The result indicates that in both configurations, significant improvements could be achieved; especially in terms of product fineness for ball mill and overflow streams. The series configuration gives better results and is recommended. In this arrangement, the ball mill product could be improved from 579 μm (survey simulation) to 233 μm, with corresponding cut size and circulating load of 172 μm and 493 %, respectively. Simulations conducted at higher throughputs (618 t/h to1000 t/h) indicated that both circuit configurations could facilitate increased throughput in the range of 13 to 26 %. The main bottleneck for the parallel circuit is the higher circulating load achieved. The two circuit configurations evaluated are presented in Figure 5-39 and Figure 5-40. Their respective products size distributions under optimum conditions are presented in Figure 5-41and Figure 5-42. For more details, Appendix D can be referred.

Table 5-25: Overall circuit performance after addition of a second ball mill.

Parameter	Survey sim.	Parallel config.	Series config.
SAG discharge $x_{P,80}$ (µm)	1640	1240.00	1240.00
Overflow $x_{P,80}$ (µm)	140	72.00	167.00
BM-$x_{P,80}$ (µm)	579	373.00	233.00
BM-Power (kW), Bond	2100	2944.64	5383.60
x_T (µm)	178	69.15	172.00
Overflow solids (%)	42.2	19.60	27.90
Circulating Load, *C*L (%)	288	1037.99	493.10
Attainable circuit throughput	618	700.00	780.00

Although this is a capital intensive undertaking, the series circuit is recommended as can give more circuit improvements. In the long run, it should be possible to lower the circulating load by manipulation of the operating conditions.

From previous studies (Luis-Bahena 2001), series circuit configurations have also been reported to be superior to other. In addition, it has been commented that series configurations have the following advantages (Luis-Bahena 2001):

- It is possible to increase the grinding throughput without affecting the particle size in the final product.
- The second mill can be operated with small ball size, which increases the fineness of the overall grinding circuit.
- The second mill can be operated while the other is shut down for maintenance.

One of the feasible options in an effort to optimize the BGM operation was the reduction of ball mill ball size. It is unfortunate that this could not be implemented as the ball mill model ”MILL” in MODSIM that fitted well the BGM data does not give that opportunity. This was found to be a feasible factor due to currently used ball size being considered somehow large (80 mm). The starting ball sizes obtained and recommendable for the current BGM operation based on Eqn. (16) are 27 mm, 29 mm and 30 mm for the three ore blends processed, respectively.

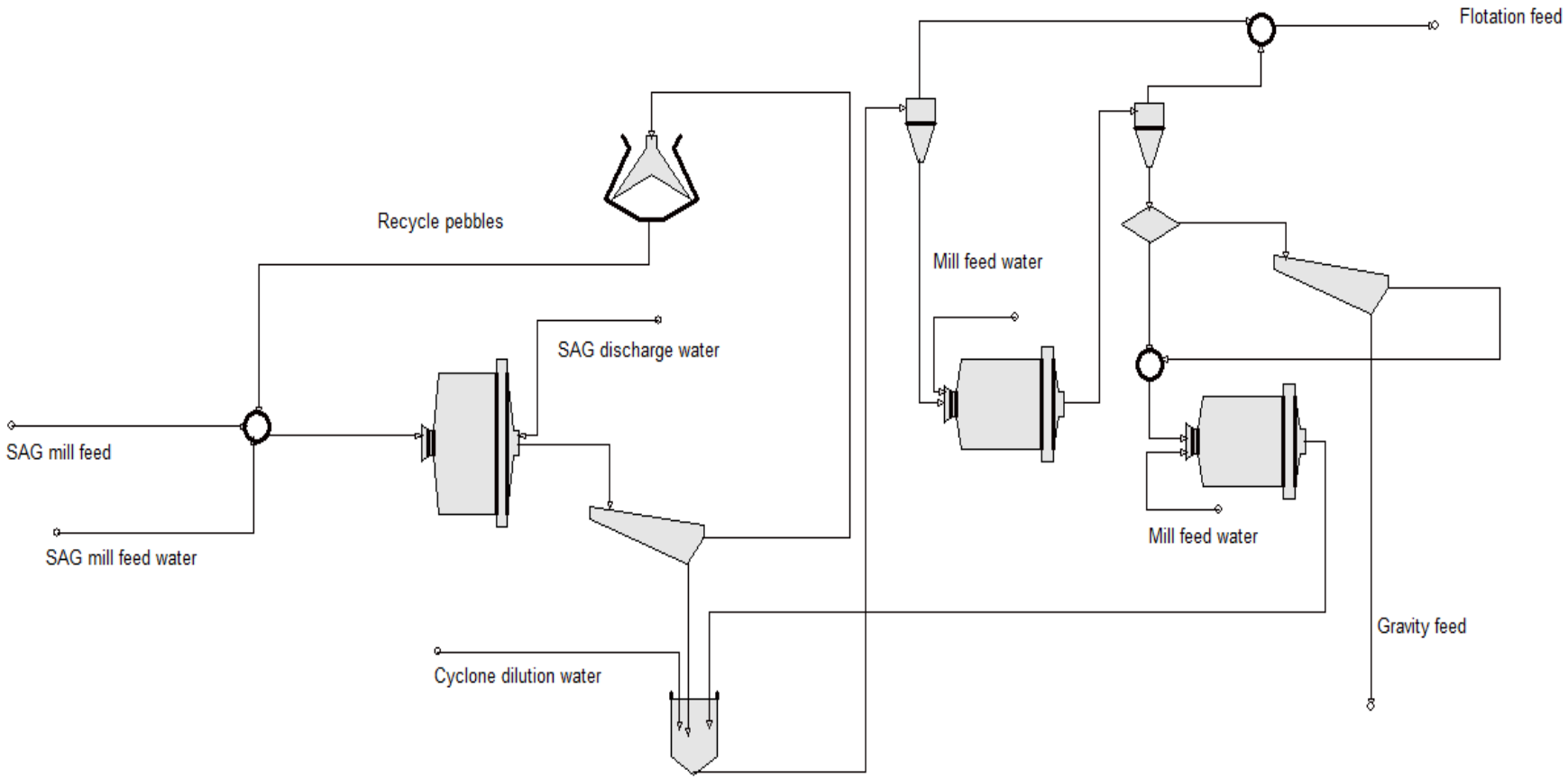

Figure 5-39: BGM grinding circuit flowsheet with ball mills in series configuration as modelled by MODSIM.

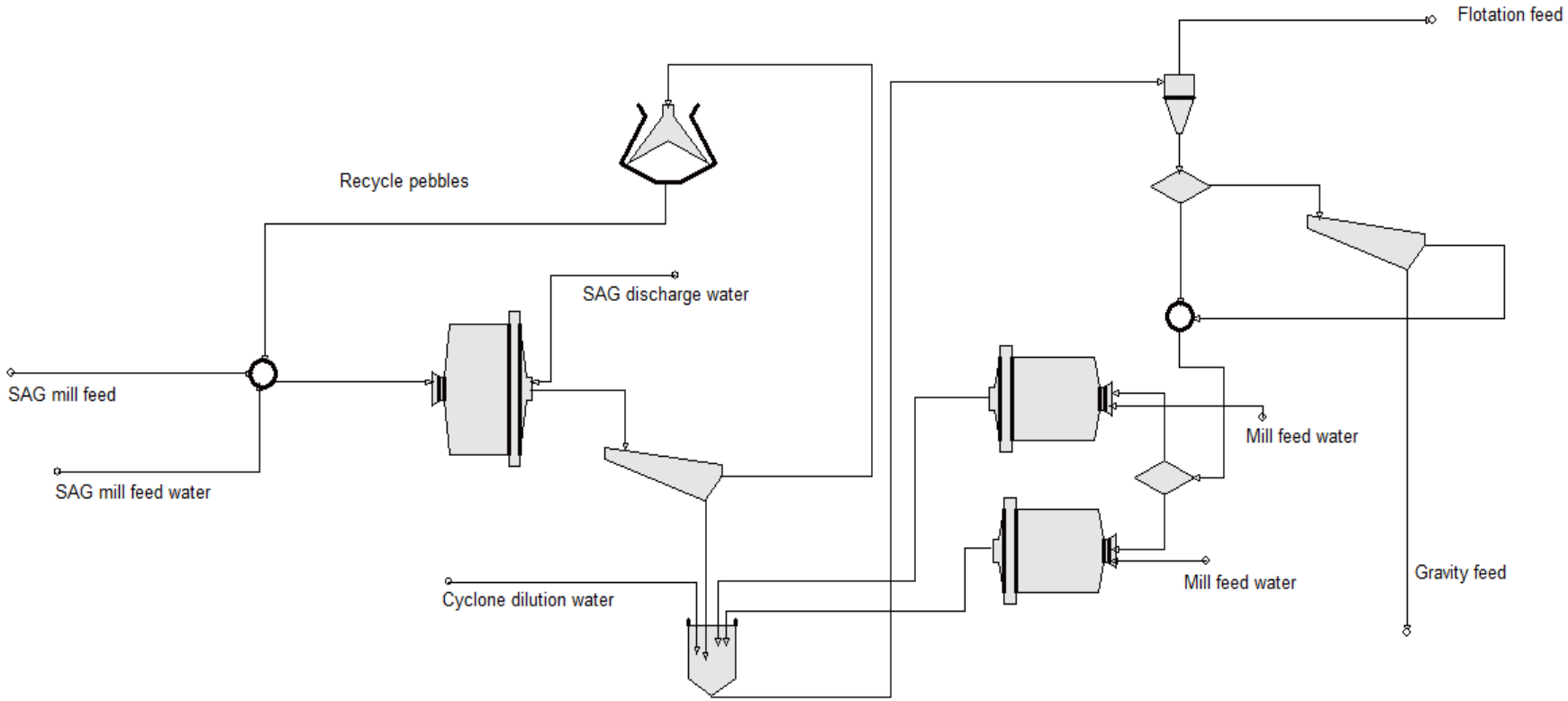

Figure 5-40: BGM grinding circuit flowsheet with parallel configuration of ball mills as modelled by MODSIM.

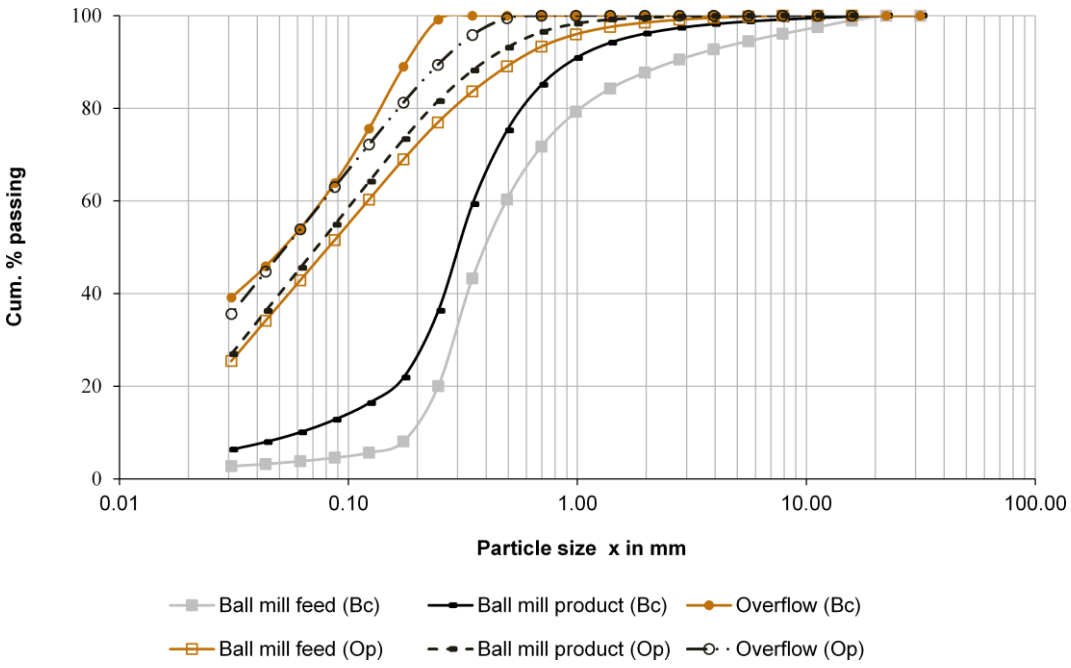

Figure 5-41: Simulated size distributions under survey (Bc) and optimum conditions (Op) for the proposed circuit with two ball mills in series configuration.

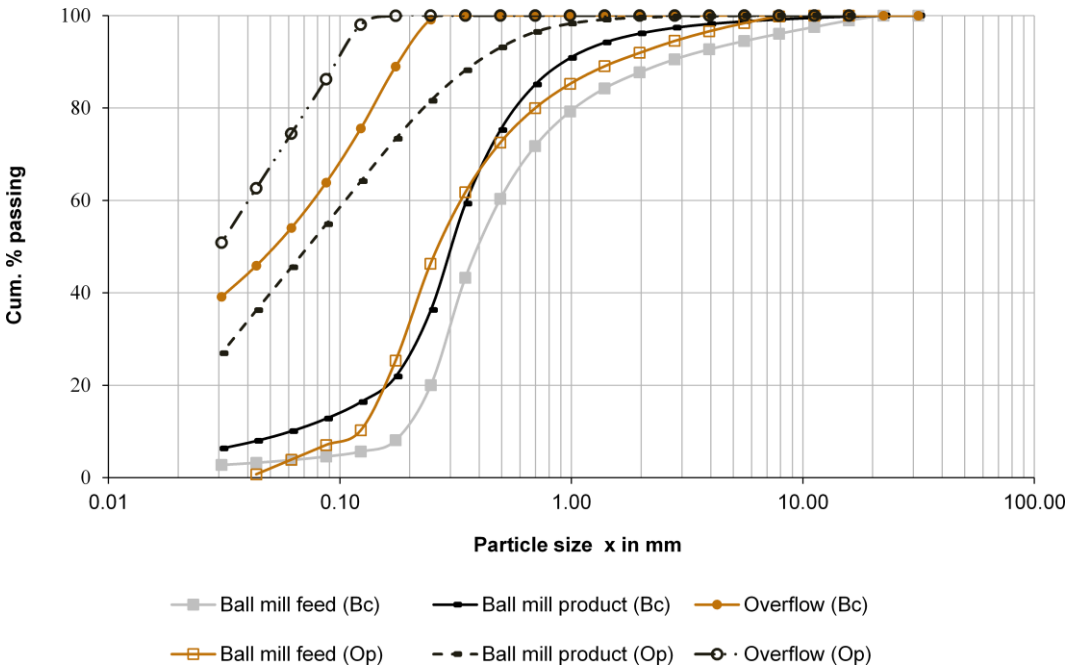

Figure 5-42: Simulated size distributions under survey (Bc) and optimum conditions (Op) for the proposed circuit with two ball mills in parallel configuration.

In MODSIM, the particle size distribution was defined by the Austin's standard breakage function, Eqn. (38) and for the cut size, the Nageswararao model, Eqn. (71) was used. It has been observed that several correlations were experienced, for example, between the cyclone parameters: cut size, x_T , apex (D_a), vortex (D_o) with say

circulating load (*C*L) and ball mill and overflow products ($x_{P,\ 80}$). This could possibly be explained as follows; for the case of breakage function, Eqn. (38), considering the values of φ_j =1 and γ = 0.82 (survey 1 simulated) (Table 4-15), this function reduces to an exponential form. However, since the value of γ is also closer to 1, the function approaches to linear. Therefore, the correlations obtained are assumed to have been brought by the linear behaviour displayed. Further, it can be seen that for the Nageswarao model, Eqn. (71) the cut size expression under variations of apex or vortex finder, is also simply a linear relation as all other parameters are constant.

5.3.3 Conclusions and Recommendations

5.3.3.1 SAG Mill Circuit

- A change of SAG discharge screen aperture from 12 mm to 10 mm was found feasible and could lead to an improvement of SAG discharge $x_{P,80}$ from 1640 mm to 1240 mm.
- As a consequence of the changed SAG screen aperture, an overflow and ball mill product ($x_{P,80}$) of 134 µm and 548 µm could be achieved, respectively.

5.3.3.2 Ball Mill Circuit

Effect of cyclone feed % solids content

- A cyclone feed solids content of 67.1 % was found suitable. This could result to an overflow and ball discharge $x_{P,80}$ of 104 µm and 460 µm, respectively.
- Also hydrocyclone cut size of 135.4 µm and circulating load of 349 % were achieved.

Effect of vortex finder diameter

- A vortex finder diameter change from 280 mm (current) to 270.30 mm was found feasible.
- An overflow and ball mil product size ($x_{P,80}$) of 110 µm and 475 µm, respectively were achieved.
- Also, a circulating load of 358 % and cut size of 132 µm could be achieved.

Effect of apex finder diameter

- An apex diameter of 145.6 mm was found suitable. This resulted to the ball mill circuit and hydrocyclone overflow product size ($x_{P,80}$) of 327 and µm105 µm, respectively.
- A circulating load of 350% and cut size of 133 µm could be achieved.

5.3.3.3 Modification of the Flowsheet

Effect of splitting the cyclone underflow back to SAG mill

- Up to 10% of the cyclone underflow could be returned to the SAG mill. This improved the circuit product fineness to 436 µm. However, increased the circulating load to 496 % and lowered cut size and overflow $x_{P,80}$ to 92 and 100, respectively.

Effect of introducing a second classification stage

- An apex and vortex finder of 165 mm and 178 mm, respectively were found appropriate for both cyclone clusters.
- An overflow and ball mill products fineness of 122 µm and 517 µm could be obtained, respectively.

Effect of introducing a second ball mill

- A series configuration of the mills was found efficient.
- A possible improvement of the ball mil product fineness to 233 µm could be achieved.
- Both configurations (series and parallel) indicate a possible increase of the circuit throughput by up to 26 %.

5.3.3.4 Recommendations

- Based on mineral liberation studies of the BGM ore (chap. 5.2), it was found that the valuable phase is liberated at relatively coarse size (200-400 µm). Therefore, even the optimum ball mill product fineness of 327 µm achieved under simulation of the cumulative effects (i.e. based on existing equipment), if implemented could bring significant contribution to the BGM process efficiency.

- Despite the fact that most of the optimization options couldn't give the circuit product fineness as closer as possible to the target (i.e. $x_{P,80}$ = 125 µm), the obtained overflow product fineness was more improved than the survey for most options simulated (i.e. $x_{P,80}$: < 140 µm vs. > 400 µm) . Therefore any of these options could be implementable and bring improved performance for the BGM operation as finer overflow product is crucial for efficient downstream processes (i.e. flotation and leaching for the BGM case).
- The option to add a second ball mill gave the best product fineness from the simulation ($x_{P,80}$ =233 µm), however, since this option is more capital intensive, may be considered under long term solution. Apart from giving a finer product, also this option has an advantage of increased circuit throughput from current 600 t/h up to 800 t/h, without compromising the efficiency. Hence under long term and especially when the mine aims for increased production, this option might offer the best results.

6 Overall Conclusions and Recommendations

The focus of this work was to evaluate and thereafter optimize the performance of a grinding circuit treating low grade sulphide copper-gold ore. The main objective was to improve the product fineness (from $x_{P,80}$ >400 µm to 125 µm) in order to enhance downstream processes. This was achieved firstly through literature review to understand issues of interest such as; operation and control practices, performance assessment and quality control measures, equipment advancement, and optimization techniques. Then, evaluations of the base case performance as well as optimization studies were achieved through survey campaigns, experimental lab work and simulations. The overall conclusions and recommendations are as highlighted in the following paragraphs.

6.1 Findings

The work index of the Buzwagi gold ore deposit estimated during plant design was between 14.5 to 16.5 kWh/t. The values obtained during the survey range between 17.20 - 18.70 kWh/t.This indicates a change in the hardness of the ore during the last 7 years. Harder ores require more energy input for efficient operation, the consequence of which is increased cost. Thus, a periodic review is required to assess the variation in hardness as mining progresses. This will help in establishing better blends and also predicting an appropriate tonnage for existing ore types, so as to be efficiently treated by the available plant design.

The mineral liberation studies indicated that the valuable phase (pyrite-pyrrhotite) can be liberated at relatively coarse particle sizes (200-400 µm). This implies that the efficiency of the gravity circuit could not be affected by the inefficiency of the current BGM operation, as the gold contained in pyrite-pyrrhotite is easily concentrated at such coarser sizes. However, a finer product is required for downstream processes (i.e. flotation and leaching). Connected to this, the work indices of the ore blends showed a strong linear relationship with their respective quartz mineral content. The established correlation is recommended for prediction of work indices for the Buzwagi ore. Further, the model could be useful and replace the tedious Bond test for quick and rough estimations of work indices for the examined ore and thus could be used as a control and monitoring tool for hardness variations for the SAG mill feed.

The comminution efficiency is determined using the Bond efficiency factor. Bond efficiency factors less than 100 % imply an inefficient operation, meaning that the energy is wasted by the grinding process. Bond efficiency factors of 48-61 % were obtained for the BGM grinding operation, implying that the BGM operation was inefficient and could probably achieve targets through reduced throughput.

The SAG mill feed particle size distribution between the three surveys showed significant fluctuations ($x_{F,80}$: 102-185 mm). Since SAG mills use ore as part of the grinding media, regular monitoring and control of the ore feed size distribution is recommended as the change in feed size distribution normally results to corresponding changes in the grinding media size distribution, which has further impact on power and throughput. This could be fixed through closer monitoring of the primary crusher performance and also control of the ratios of SAG mill feeders which draws the ore from the stockpile.

The assessment of survey data indicated that the inefficiency of the ball mill was contributed by inefficient hydrocyclones. Apart from running at approximately 17 % above the design, hydrocyclones were also characterized by higher feed pulp densities (66.5-68.4 %). In overall, this led to an overload of the ball mill due to increased circulating load. Classification efficiency could be improved by dilution of the feed in order to lower the pulp density, which could also improve the overflow density (i.e. closer to 30 %) and hence giving a sharper cut. Both, survey measurements and models estimation, showed that current BGM hydrocyclones could not achieve the recommended cut size (i.e. 132.5 µm) and target overflow $x_{P,80}$ (i.e. 125 µm). This gave an indication for a possible modification requirement of current hydrocycolne dimensions (e.g. D_a, D_o).

Based on simulation and optimization of the existing BGM grinding circuit, an improvement of product fineness up to 327 µm could be achieved. This represents 43 % increase in product fineness compared to the survey (570 µm) and base case simulation (579 µm). The result was achieved by modification of the current operating conditions such as reduction of SAG mill discharge screen aperture, reduction of vortex finder and apex diameters as well as adjustment of the cyclone feed solids content. The improvement was a consequence of improved SAG discharge mill product fineness from 1.644 mm to 1.240 mm as well as improved hydrocyclone performance with the cut size, x_T reduction from 0.266 mm to 0.105 mm. The changes in vortex

finder and apex diameters indicated is in agreement with what was reflected from the hydrocyclone models. Based on economics, the implementation of this option can be recommended as a short term solution.

Simulations based on flowsheet modification showed that two ball mills in series can improve the product fineness by up to 59 % from the current performance. Another key advantage in this option is the possible increase in throughput by up to 26 % without compromising on the product quality. However, this option is recommended as a solution under long term plans as it is more capital intensive. Further, the decision to implement this option may also be supported by the cost-benefit analysis.

6.2 Future Work

For the BGM ore, gold is hosted in pyrite-pyrrhotite mineralogical phase. Based on MLA results, the phase indicated a significant degree of liberation at coarser sizes. However, this information was found to be useful only for the gravity circuit, where the heavy mineral (pyrite-pyrrhotite) is easily concentrated at such particle sizes. For the benefits of downstream operations (flotation and leaching), understanding the grain size of the minerals to be recovered (e.g. gold) could add more knowledge especially on their liberation size, giving guidance on the extent of grinding required. Due to limitations of an automated mineralogy measurement technique that was applied in this study, the mineralogical information for gold (e.g. grain size, grade, etc.) could not be obtained. Hence, further studies may be conducted to achieve this through application of advanced techniques such as QEMSCAN Trace Mineral Search (TMS).

The obtained simulation results are subject to a certain degree of errors due to sampling and also limitations of models used. Hence, validation of the simulation results is an important and recommended next step. This will be achieved by implementing the suggested changes or modifications on the existing grinding circuit and then conducting new survey campaigns, from which the degree of correlation between the simulated and new survey results will confirm the validity of the suggested solutions.

It is known that the efficiency of any comminution process need to be measured not only based on size reduction, but also the degree of mineral liberation achieved. Hence, further simulation studies may be conducted by employing both, size reduction as well as liberation models. Through this, improved simulations could be achieved

that takes into account optimization of both, size reduction as well as mineral liberation. Simulation software packages such as MODSIM has integrated mineral liberation models and could be employed for extension of this study.

References

(2012). Comminution circuit option study, Orway Mineral Consultants.

Acar, C. (2013). Investigation of Particle Breakage Parameters in Locked-cycle Ball Milling, Middle East Technical University. **Ph.D. Thesis.**

Alamouti, M. A. B., et al. (2011). "Grinding Circuit at Mouteh Gold Mine " Amirkabir/MISC **43**(2): 6.

Allen, P., et al. (1988). Use of Simulation to Investigate the Performance of Autogeneous Milling Circuits. Third Mill Operators' Conference. Cobar, NSW, The AusIMM Cobar Branch**:** 107-112.

Arinanda, M. A. (2016). Review of grindability and liberation behavior for Buzwagi Gold Mine ore Institut für Mechanische Verfahrenstechnik und Aufbereitungstechnik, TU Bergakademie Freiberg. **Msc Thesis**.

Austin, L. G. (1972). "A review introduction to the description of grinding as a rate process." Powder Technology **5**: 1-7.

Austin, L. G. (1990). "A mill power equation for SAG mills." Minerals and Metallurgical Processing: 57–62.

Austin, L. G., et al. (1987). "Investigations of autogenous and semi-autogenous grinding in tumbling mills." Powder Technology **51**(3): 283-294.

Austin, L. G. and K. Brame (1983). "A comparison of the Bond method for sizing wet tumbling ball mills with a size—mass balance simulation model." Powder Technology **34**(2): 261-274.

Austin, L. G., et al. (2007). "Simulation of wet ball milling of iron ore at Carajas, Brazil." International Journal of Mineral Processing **84**(1): 157-171.

Austin, L. G. and R. C. Klimpel (1985). "A note on the prediction of specific rates of breakage for an equilibrium ball charge." Powder Technology **43**(2): 199-201.

Austin, L. G., et al. (1984). Process Engineering of Size Reduction: Ball milling. New York, SME-AIME.

Austin, L. G. and P. T. Luckie (1972). "Methods for determination of breakage distribution parameters." Powder Technology **5**(4): 215-222.

Austin, L. G., et al. (1987). A general model for semi-autogenous and autogenous milling. APCOM 87. Proceedings of the Twentieth International Symposium on the Application of Computers and Mathematics in the Mineral Industries, Johannesburg, SAIMM.

Ballantyne, G. R., et al. (2012). Proportion of Energy Attributable to Comminution. 11th Mill Operators' Conference. Hobart, Tasmania**:** 24-29.

Barkhuysen, N. J. (2009). Implementing strategies to improve mill capacity and efficiency through classification by particle size only, with case studies. Base Metals Conference. Kasane, Botswana, SAIMM**:** 101-114.

Barkhuysen, N. J. (2010). Implementing strategies to improve mill capacity and efficiency, with platinum references and case studies. The 4th International Platinum Conference, *Platinum in transition 'Boom or Bust*. Sun City, Rustenburg, South Africa SAIMM**:** 85-90.

Baum, W. (2014). "Ore characterization, process mineralogy and lab automation a roadmap for future mining." Minerals Engineering **60**(Supplement C): 69-73.

Baum, W., et al. (2004). Process mineralogy—a new generation for ore characterisation and plant optimisation. SME Annual Meeting. Denver, Colorado, SME.

Bérubé, M. A. and J. C. Marchand (1984). "Evolution of the mineral liberation characteristics of an iron ore undergoing grinding." International Journal of Mineral Processing **13**(3): 223-237.

Blaskovich, R. J. (2013). Characterizing waste rock using automated quantitative electron microscopy. Mining Engineering. Vancouver, The university of British Columbia. **Msc. Thesis**.

Bond, F. C. (1952). "The Third Theory of Comminution." Transaction AIME (Mining) **193**: 484-494.

Bond, F. C. (1958). "Grinding Ball Size Selection " Mining Engineering **10**(592): 592-595.

Bond, F. C. (1961). "Crushing and grinding calculations, Part I-II." British Chemical Engineering **6**: 378-385, 543-548.

Boucaut, S. (2017). "Energy in Mining." Retrieved 28th November 2017, from https://ceecthefuture.org/why-smart-companies-are-focusing-on-comminution/.

Brochot, S., et al. (2006). Modeling and Simulation of Comminution Circuits with USIM PAC. Advances in Comminution, Littleton, Colorado, USA, SME.

Brosh, T., et al. (2014). "DEM–CFD simulation of particle comminution in jet-mill." Powder Technology **257**(Supplement C): 104-112.

C. A. Rowland, J. and R. E. Mclavor (2008). The Standard for Comminution Efficiency. SME Annual Meeting. Salt Lake City, UT, SME**:** 2.

Celik, I. B., et al. (2007). "The influence of grinding technique on the liberation of clinker minerals and cement properties." Cement and Concrete Research **37**(9): 1334-1340.

Chimwani, N., et al. (2014). "Scale-up of batch grinding data for simulation of industrial milling of platinum group minerals ore." Minerals Engineering **63**: 100-109.

Cleary, P. (2001). "Modelling comminution devices using DEM." International Journal for Numerical and Analytical Methods in Geomechanics **25**(1): 83-105.

Cropp, A. and W. Goodall (2017). The influence of rock texture on mineral processing. ABN : 51 118 344 602, MinAssist Pty Ltd.

Curry, J. A., et al. (2014). "Mine operating costs and the potential impacts of energy and grinding." Minerals Engineering **56**(Supplement C): 70-80.

Danha, G. (2013). Identifying Opportunities for Increasing the Milling Efficiency of a Bushveld Igneous Complex (BIC) Upper Group (UG) 2 Ore, University of Witwatersrand. **Ph.D. Thesis.**

Denız, V. (2011). "Computer Simulation of Product Size Distribution of a Laboratory Ball Mill." Particulate Science and Technology **29**(6): 541-553.

Drozdiak, J. A. (2011). A Pilot-Scale Examination of a Novel High Pressure Grinding Roll / Stirred Mill Comminution Circuit for Hard-Rock Mining Applications, University of British Columbia. **Msc. Thesis.**

Dundar, H., et al. (2011). "Simulation assisted capacity improvement of cement grinding circuit: Case study cement plant." Minerals Engineering **24**(3): 205-210.

Ergün, L., et al. (2005). Optimization of Çayeli (Çbi) Grinding Circuit By Modelling and Simulation. The 19th International Mining Congress and Fair of Turkey, JMCET 2005. Izmer, Turkey**:** 309-320.

Evans, C. L., et al. (2011). "Application of process mineralogy as a tool in sustainable processing." Minerals Engineering **24**(12): 1242-1248.

Fandrich, R., et al. (2007). "Modern SEM-based mineral liberation analysis." International Journal of Mineral Processing **84**(1–4): 310-320.

Francioli, D. M. (2015). Effect of Operational Variables on Ball Milling, Universidade Federal do Rio de Jeneiro. **BSc. Thesis.**

Frost, M. J. (1981). Mohs scale of hardness. Mineralogy. Boston, MA, Springer US**:** 283-284.

Fuerstenau, D. W., et al. (2011). "Simulation of the grinding of coarse/fine (heterogeneous) systems in a ball mill." International Journal of Mineral Processing **99**(1–4): 32-38.

Fuerstenau, M. C. and K. N. Han (2003). Principles of Mineral Processing. Colorado SME.

Gay, S. L. (2004). "A liberation model for comminution based on probability theory." Minerals Engineering **17**(4): 525-534.

Goldman, M. and G. Barbery (1988). "Wear and chipping of coarse particles in autogenous grinding: Experimental investigation and modelling." Minerals Engineering **1**(1): 67-76.

Gottlieb, P., et al. (2000). "Using quantitative electron microscopy for process mineralogy applications." JOM **52**(4): 24-25.

Gu, Y. (2003). "Automated Scanning Electron Microscope Based Mineral Liberation Analysis-an Introduction to JKMRC/FEI Mineral Liberation Analyser." Minerals & Materials Characterization & Engineering **2**(1): 33-41.

Gupta, A. and D. S. Yan (2006). Introduction to Mineral Processing Design and Operation. Perth.

Gupta, C. K. (2003). Chemical Metallurgy: Principles and Practice. Weinheim, WILEY-VCH.

Herbst, J. A., et al. (1988). "Optimal control of comminution operations." International Journal of Mineral Processing **22**(1): 275-296.

Hoal, K. O., et al. (2009). "Research in quantitative mineralogy: Examples from diverse applications." Minerals Engineering **22**(4): 402-408.

Hsih, C. S. and S. B. Wen (1994). "An extension of Gaudin's liberation model for quantitatively representing the effect of detachment in liberation." International Journal of Mineral Processing **42**(1): 15-35.

Jeswiet, J. and A. Szekeres (2016). "Energy Consumption in Mining Comminution." Procedia CIRP **48**(Supplement C): 140-145.

Katubilwa, F. M. and M. H. Moys (2009). "Effect of ball size distribution on milling rate." Minerals Engineering **22**(15): 1283-1288.

Kelly, E. G. and D. J. Spottiswood (1990). "The breakage function; What is it really?" Minerals Engineering **3**(5): 405-414.

Khumalo, N. (2007). The Application of the Attainable region analysis in Comminution University of the Witwatersrand **Ph.D. Thesis**.

King, R. P. (2001). Modeling and Simulation of Mineral Processing Systems. Oxford.

King, R. P. (2012). Modelling and Simulation of Mineral Processing Systems. Englewood, Colorado, USA, SME.

Kingman, S. W., et al. (2004). "Recent developments in microwave-assisted comminution." International Journal of Mineral Processing **74**(1–4): 71-83.

Klichowicz, M., et al. (2014). Self-similarity and energy-size relationship of coarse particles comminuted in single particle mode. In XXVII International Mineral Processing Congress (IMPC), Santiago, Chile.

Leng, Y. (2008). Materials Characterization: Introduction to Microscopic and Spectroscopic Methods. 2 Clementi Loop, # 02-01, Singapore 129809, John Wiley & Sons (Asia) Pte Ltd.

Lippek, E., et al. (1988). Mathematisches Sichtermodell für die Simulation von Mahlanlagen. Freiberger Forschungshefte, Freiberg Veb Deutscher Verlag Für Grundstoffindustrie.

Lotter, N. O. (2011). "Modern Process Mineralogy: An integrated multi-disciplined approach to flowsheeting." Minerals Engineering **24**(12): 1229-1237.

Luis-Bahena, J. (2001). Modelling and Simulation of the Grinding Circuit at 'ELPILON' Mine. JKMRC Conference. Brisbane**:** 181-196.

Maria, A. (1997). Introduction to Modeling and Simulation. Winter Simulation Conference

Binghamton, NY 13902-6000, U.S.A.

Masuda, H., et al. (2007). Powder Technology: Handling and Operations, Process Instrumentation, and Working Hazards. Boca Raton Taylor and Francis.

Metso (2010). Basics in Minerals Processing

Michaelis, H. V. (2017). "Real and potential metallurgical benefits of HPGR in hard rock ore processing ". Retrieved 19th Dec., 2017.

Mineral Technologies International, I. (2009). MODSIM -User Manual.

Minkov, L., et al. (2014). "Computer simulations of the Fish-Hook effect in hydrocyclone separation." Minerals Engineering **62**(Supplement C): 19-24.

Mishra, B. K. (2003). "A review of computer simulation of tumbling mills by the discrete element method: Part II—Practical applications." International Journal of Mineral Processing **71**(1): 95-112.

Morari, M. (1983). "Design of resilient processing plants—III." Chemical Engineering Science **38**(11): 1881-1891.

Morrell, S. (1996). "Power draw of wet tumbling mills and its relationship to charge dynamics - Part 2: An empirical approach to modelling of mill power." Trans. Instn Mining Metall. **105**((Sect. C: Mineral Processing Extr Metall.)): C54–C62.

Morrell, S. (2004). "Predicting the specific energy of autogenous and semi-autogenous mills from small diameter drill core samples." Minerals Engineering **17**(3): 447-451.

Mosher, J. B. and C. B. Tague (2001). "Conduct and precision of bond grindability testing." Minerals Engineering **14**(10): 1187-1197.

Mular, A. L., et al. (2002). Mineral Processing Plant Design, Practice, and Control, SME.

Mulenga, F. K. (2017). "Sensitivity analysis of Austin's scale-up model for tumbling ball mills — Part 1. Effects of batch grinding parameters." Powder Technology **311**: 398-407.

Murthy, N. and K. Basavaraj (2012). Assessing the performance of a floatex density separator for the recovery of iron from low-grade australian iron ore fines – a case study XXVI International mineral processing congress (IMPC) New Delhi 10.

Mütze, T. (2012). Self-similarity in particle bed comminution. In XXVI International Mineral Processing Congress (IMPC), New Delhi, India.

Nageswararao, K., et al. (2004). "Two empirical hydrocyclone models revisited." Minerals Engineering **17**(5): 671-687.

Napier-Munn, T. J. and A. J. Lynch (1992). "The modelling and computer simulation of mineral treatment processes — current status and future trends." Minerals Engineering **5**(2): 143-167.

Napier-Munn, T. J., et al. (1996). Mineral Comminution Circuits: Their Operation and Optimisation. Queensland, JKMRC.

Neesse, T., et al. (2004). "Separation of finest particles in hydrocyclones." Minerals Engineering **17**(5): 689-696.

Nikkhah, K. and C. Anderson (2001). The role of software in design and operation of metallurgical plants: A case study. SME Annual Meeting. Denver, Colorado.

NRC (1981). Comminution and Energy Consumption. Washington D.C., National Material Adivisory Board, Commission on Sociotechnical Systems, National Research Council (U.S.).

Ozcan, O. and H. Benzer (2013). "Comparison of different breakage mechanisms in terms of product particle size distribution and mineral liberation." Minerals Engineering **49**(Supplement C): 103-108.

Petruck, W. (2000). Applied Mineralogy in the Mining Industry. Amsterdam, The Netherlands, ELSEVIER SCIENCE B.V.

Pokrajcic, Z. and E. Lewis-Gray (2010). Advanced comminution circuit design – essential for industry. Minerals processing 38-42.

Pourghahramani, P. (2012). "Effects of ore characteristics on product shape properties and breakage mechanisms in industrial SAG mills " Minerals Engineering **32**: 8.

Powell, M. S. and R. D. Morrison (2007). "The future of comminution modelling." International Journal of Mineral Processing **84**(1): 228-239.

Rao, D. V. S. (2011). Mineral Beneficiation: A Concise Basic Course. Boca Raton, Taylor & Francis.

Rosario, P. P. (2010). Comminution Circuit Design and Simulation for the Development of a Novel High Pressure Grinding Roll Circuit, University of British Columbia. **Ph.D. Thesis.**

Rowland, C. A. (2006). Bond's Method for Selection of Ball Mills. Advances in comminution

Littleton, Colorado, USA, SME.

Rumpf, H. (1965). "Die Einzelkornzerkleinerung als Grundlage einer technischen Zerkleinerungswissenschaft." Chemie Ingenieur Technik **37**(3): 187-202.

Rybinski, E., et al. (2011). Optimisation and continuous improvement of Antamina comminution circuit SAG. Winnipeg

Sandmann, D. (2015). Method Development in Automated Mineralogy. der Fakultät für Geowissenschaften, Geotechnik und Bergbau, der Technischen Universität Bergakademie Freiberg. **Ph.D Thesis**.

Saramak, D., et al. (2010). "Aspects of comminution flowsheets design in processing of mineral raw materials." Gospodarka Surowcami Mineralnymi **26**(4): 59-69.

Sba'rbaro, D. and R. d. Villar (2010). Advanced Control and Supervision of Mineral Processing Plants. London, Springer

Schlanz, J. W. (1987). Grinding: An Overview of Operation and Design. Mill Operators Symposium. Spruce Pine, NC.

Schönert, K. (1996). "The influence of particle bed configurations and confinements on particle breakage." International Journal of Mineral Processing **44**: 1-16.

Schubert, H. (1985). "A hydrocyclone separation model in consideration of the turbulent multi-phase flow." Particulate Science and Technology **3**(1-2): 1-13.

Schubert, H. (2003). "Zu den Ursachen 'anomaler' Verläufe der Trennkurve bei der Feinstkornklassierung in Hydrozyklonen – insbesondere zum so genannten Fish-Hook-Effekt*)." Aufbereitungs Technik **44**(2): 5-17.

Schubert, H. (2010). "Which demands should and can meet a separation model for hydrocyclone classification?" International Journal of Mineral Processing **96**(1): 14-26.

Schubert, H. and K. Mühle (1991). "The role of turbulence in unit operations of particle technology." Advanced Powder Technology **2**(4): 295-306.

Schubert, H. H. (2003). Handbuch der Mechanischen Verfahrenstechnik. Weinheim, Wiley-VCH Verlag.

Shoji, K., et al. (1982). "Further studies of ball and powder filling effects in ball milling." Powder Technology **31**(1): 121-126.

Smith, H. (2005). "Process simulation and modelling." Developments in Mineral Processing **15**: 109-121.

Smythe, D. M., et al. (2013). "Rare Earth Element deportment studies utilising QEMSCAN technology." Minerals Engineering **52**: 52-61.

Somani, A., et al. (2017). "Pre-treatment of rocks prior to comminution – A critical review of present practices." International Journal of Mining Science and Technology **27**(2): 339-348.

Sönmez, B. and H. Demirel (1996). Determination of breakage parameters in laboratory scale ball mill and scale-up of ball milling: changing scopes in mineral processing. Proc. 6th International Symposium. Kusadasi, Turkey**:** 617–620.

Tavares, L. M. (2017). "A Review of Advanced Ball Mill Modelling." KONA Powder and Particle Journal **34**: 106-124.

Tromans, D. (2008). "Mineral comminution: Energy efficiency considerations." Minerals Engineering **21**(8): 613-620.

Veasey, T. J. and B. A. Wills (1991). "Review of methods of improving mineral liberation." Minerals Engineering **4**(7): 747-752.

Vedat, D. (2011). "Influence of interstitial filling on breakage kinetics of gypsum in ball mill." Advanced Powder Technology **22**(4): 512-517.

Vizcarra, T. G., et al. (2010). "The effect of breakage mechanism on the mineral liberation properties of sulphide ores." Minerals Engineering **23**(5): 374-382.

Wang, E., et al. (2012). "Mineral liberation by high voltage pulses and conventional comminution with same specific energy levels." Minerals Engineering **27–28**: 28-36.

Weerasekara, N. S., et al. (2013). "The contribution of DEM to the science of comminution." Powder Technology **248**(Supplement C): 3-24.

Wikedzi, A., et al. (2018). "Breakage and liberation characteristics of low grade sulphide gold ore blends " Minerals Engineering **115**(C): 33-40.

Wills, B. A. and K. Atkinson (1993). "Some observations on the fracture and liberation of mineral assemblies." Minerals Engineering **6**(7): 697-706.

Wills, B. A. and J. A. Finch (2016). Wills' Mineral Processing Technology: An Introduction to the Practical Aspects of Ore Treatment and Mineral Recovery. Oxford, Elsevier.

Wills, B. A. and T. Napier-Munn (2006). Wills' Mineral Processing Technology: An Introduction to the Practical Aspects of Ore Treatment and Mineral Recovery. Oxford, Butterworth-Heinemann.

Zhu, G. F., et al. (2012). Computer simulations of the Fish-Hook effect in hydrocyclone separation. 18th Australasian Fluid Mechanics Conference. Launceston, Australia**:** 1-4.

Appendices

Appendix A: BGM Grinding Circuit Survey Data

A1: Buzwagi Gold Mine Process Plant flowsheet

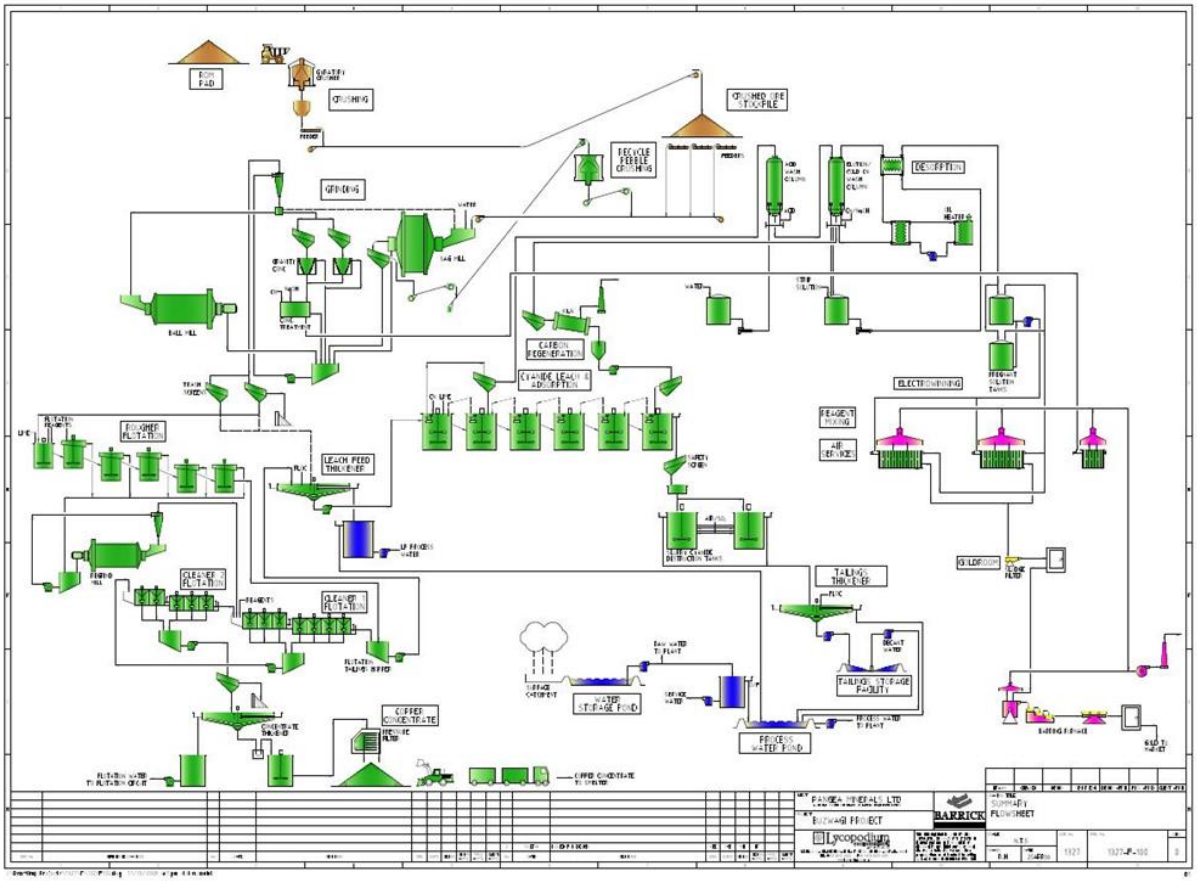

A2: Implemented Survey Plan at BGM Grinding Circuit

S/N.	Sample description	Sampling point	Tools	Frequency
1	SAG mill feed	SAG feed conveyor	20 L buckets Shovel Stopwatch	1 x (Belt cut)
2	Pebble crusher feed	Diverter chute		6 x (20 min. intervall)
3	Pebble crusher product	Discharge chute		
4	SAG discharge screen	Screen launder	10 L buckets Cutter Stopwatch	8 x (15 min. intervall)
5	Hydrocyclone feed	Feed hopper		
6	Ball mill discharge	Discharge launder		

7	Hydrocyclone O/F	Trash screen feed box		
8	Hydrocyclone U/F	U/F stream-Alternating		

A3: Summary of design criteria for BGM grinding circuit

Design parameter	SAG Mill	Pebble Crusher	Ball Mill	Hydro-cyclone
Feed rate in t/h	460-543	190		1462
Feed $x_{F,80}$ in mm	120			
Power in kW	6000	315	6000	
Ball charge in % volume	15-20		30-35	
Total charge in % volume	30-35			
Critical speed in %	75		75	
Ball size in mm	65/90/120/150		80/65/50	
CSS in mm		10-14		
Final product $x_{P,80}$ in µm			125	
Bond Ball Mill Work Index in kWh/t			11.6-14.8	
Bond Rod Mill Work Index in kWh/t			15.3-16.5	
Pressure in kPa				80-110
Circulating load in %				250-350
Overflow product $x_{P,80}$ in µm				100-125

A4: BGM grinding circuit operating parameters during the survey

Stream/Unit name	Survey 1	Survey 2	Survey 3
SAG Mill			
Feed size, $x_{F,80}$ in mm	185.45	101.60	122.0
Power draw in kW	5387.0	6146.84	6198.25
Specific power in kWh/t	7.92	8.26	9.47
Feed rate in t/h	630.13	686.54	583.029
Feed moisture in %	1.80	1.81	1.66
Feed water addition in m^3/h	348.69	318.24	232.52
Discharge water addition in m^3/h	0.42	0.40	0.48
Discharge solids content in %	68.53	72.41	69.80
Ball charge in % volume	14.3	14.3	-
Recycle crusher			
Power draw in kW	70.46	74.50	54.24
Feed rate in t/h	62.90	72.63	83.76
Closed side setting (CSS) in mm	12.0	13.0	20.0
Ball Mill			
Power draw in kW	5294.10	5398.93	5229.66
Specific power in kWh/t	4.77	5.74	10.73
Overall specific power in kWh/t	12.69	14.0	20.20
Discharge solilds content in %	72.12	67.20	63.38
Discharge water addition in m^3/h	0.64	0.70	36.83
Ball charge in % volume	33	33	-
Product size, $x_{P,80}$ in µm	570	419	403
Hydrocyclone			
Pressure in kPa	97.90	80.80	92.13
Flow rate in m^3/h	1481.54	1321.68	913.04
Underflow solids content in %	79.0	79.0	77.70
Overflow solids content in %	40.90	46.84	42.90
Feed density in %	66.70	68.41	66.50
≠ of cyclones in operation	4	4	4

Appendix B: Mineral Liberation Data for BGM Ore Blends

B1: Particle and mineral grain size distributions for S-2.

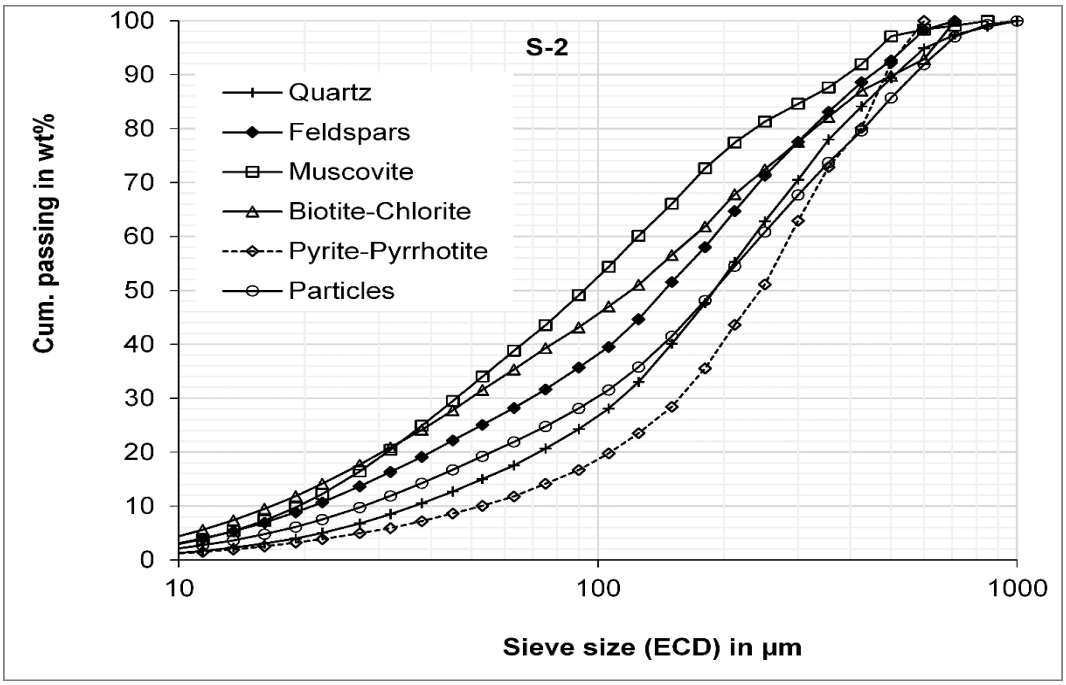

B2: Particle and mineral grain size distributions for S-3.

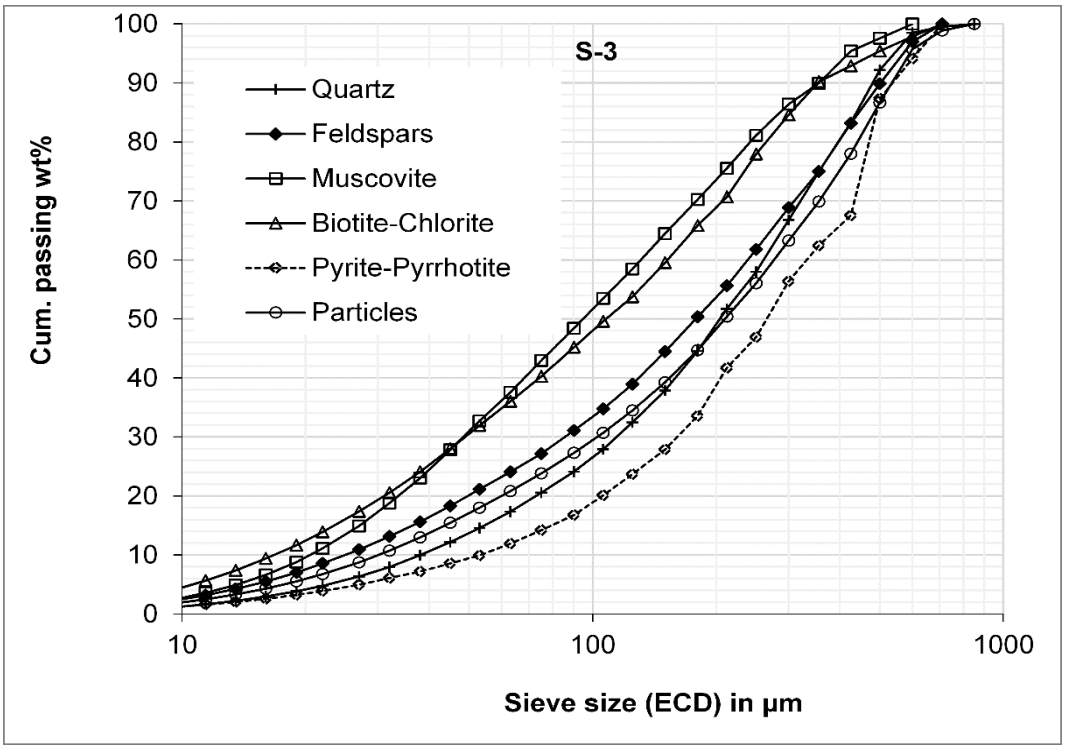

B3: Pyrite-pyrrhotite particle counts relative number per size class for S-2 .

Class size (µm)	Pyrite-pyrrhotite free surface of particle (%)					
	0- 20	20- 40	40-60	60-80	80-100	100
0-63	0.49	0.49	0.62	0.57	0.16	0.74
63-125	0.17	0.23	0.15	0.20	0.30	0.14
125-250	0.13	0.05	0.11	0.09	0.15	0.04
250-500	0.16	0.18	0.13	0.11	0.39	0.07
500-1000	0.05	0.05	0.00	0.03	0.00	0.01

Appendix C: MODSIM Input Data Definition

C1: Specification of parameters for the SAG mill model SAGP

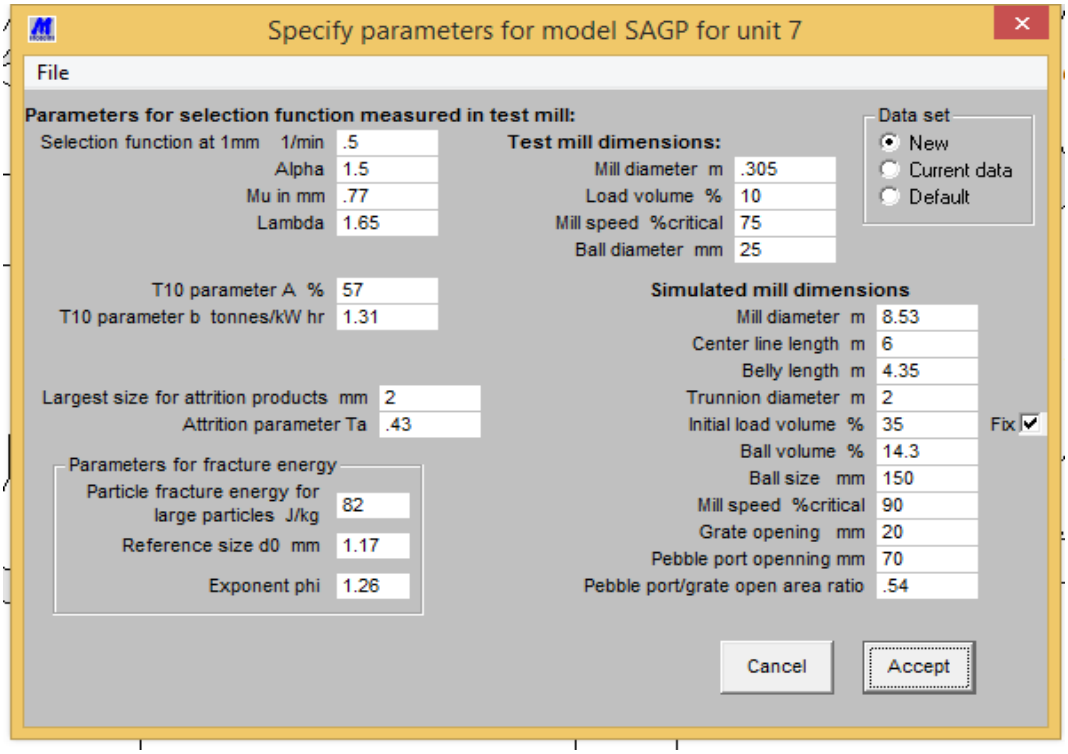

C2: Specification of parameters for the ball mill model MILL

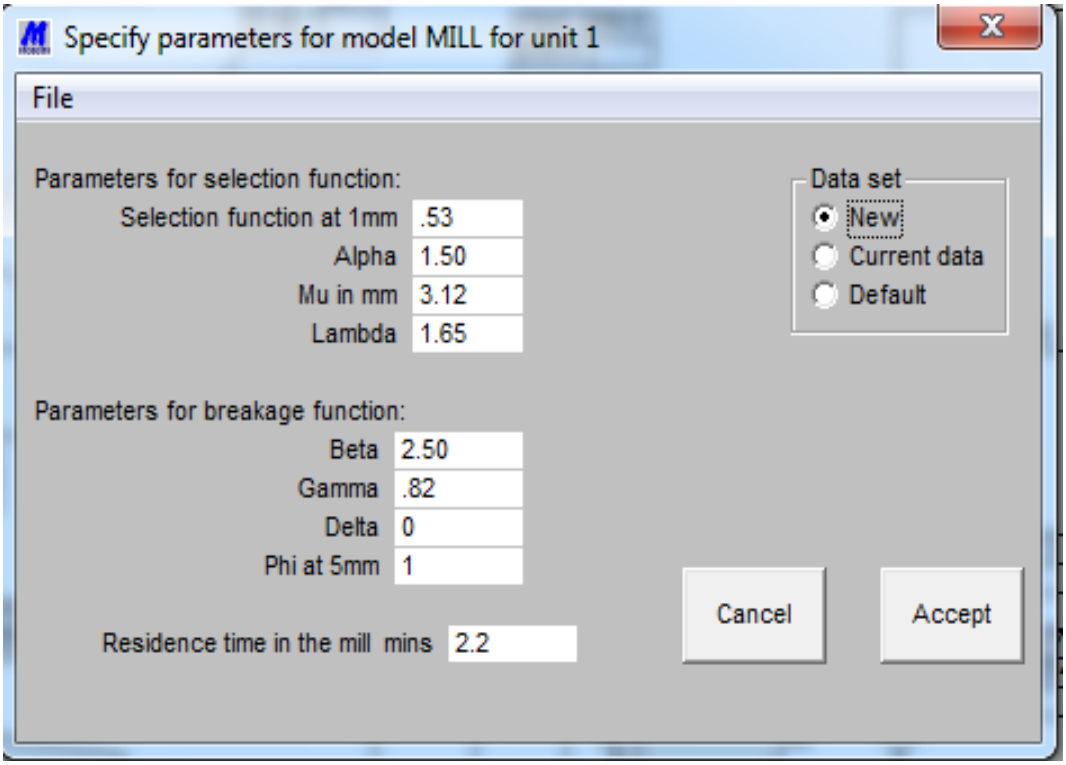

C3: Specification of parameters for the Hydrocyclone model NAGE

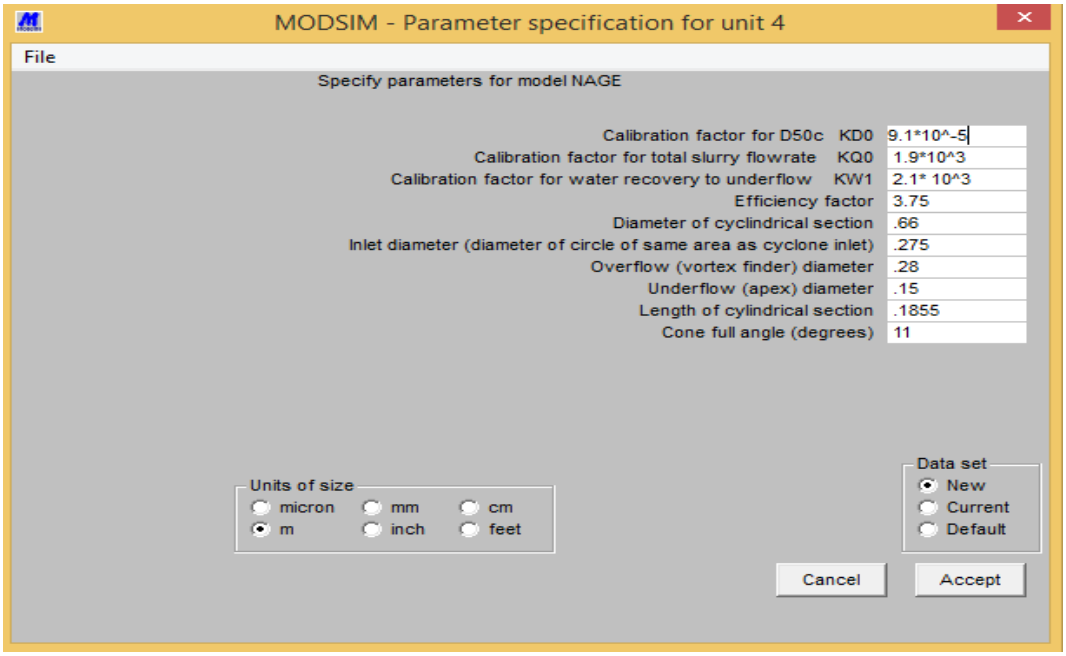

C4: Selection function model parameters obtained by non-linear regression with SOLVER function for S-1

Top size in mm	$S_{i-\exp}$	S_{i-pd} (Eqn. 43))	$\left(S_{i-\exp}-S_{i-pd}\right)^2$	Fitting parameters	
0.315	0.0720	0.0765	1.98839E-05	*a*	0.53
0.5	0.1310	0.1262	2.31501E-05	α	1.50
1	0.2080	0.2098	3.26932E-06	μ	0.77
2	0.2590	0.2586	1.9158E-07	λ	1.65
		$\text{Residue} = \sum\left(S_{i-\exp}-S_{i-pd}\right)^2$	4.64948E-05		
		R^2	0.998		

Note: S_i-exp and S_i-pd stands for the experimental and model predicted selection function values for different size fractions.

C5: Breakage function model parameters obtained by non-linear regression (fraction -2+1 mm, S-1)

Passing size in mm	$B_{i,j-\exp}$	$B_{i,j-pd}$ (Eqn.(38))	$\left(B_{i,j-\exp}-B_{i,j-pd}\right)^2$	Fitting parameters	
2	1.0000	1.0000	0	γ	0.67
1	0.2081	0.2078	4.91354E-08	β	2.50
0.5	0.0665	0.0674	8.65012E-07	ϕ	1.0
0.2	0.0278	0.0267	1.10525E-06		
0.09	0.0185	0.0144	1.67081E-05		
0.063	0.0061	0.0111	2.51141E-05		
		$\text{Residue} = \sum\left(B_{i,j-\exp}-B_{i,j-pd}\right)^2$	4.38415E-05		
		R^2	0.999		

Note: The overall breakage function model parameters were obtained as average values from all mono-size fractions used (i.e. +2+1 mm, -1+0.5 mm, -0.5+0.315 mm and -0.315 + 0.2 mm).

Appendix D: Simulation and Optimization Data

D1: Simulated circuit stream properties at optimum SAG discharge screen aperture (i.e. 10 mm)

Stream Name	Solid flow (t/h)	Water flow (m^3/h)	% solids
SAG feed	618.00	11.40	98.20
SAG feed water	0.00	349.00	0.00
SAG discharge	721.00	438.00	62.20
SAG discharge water	0.00	75.40	0.00
SAG screen undersize	618.12	435.60	58.75
SAG screen oversize	102.50	2.20	97.87
Cyclone feed	1924.92	840.00	69.62
Cyclone feed water	0.00	150.00	0.00
Overflow	515.52	701.64	42.40
Underflow	1410.00	138.30	91.10
BM feed	1305.00	253.40	83.70
BM feed water	0.00	133.42	0.00
BM discharge	1305.00	254.02	83.70
BM discharge water	0.00	0.64	0.00
Pebble crusher product	102.50	2.20	97.87
Gravity feed	281.92	27.66	91.10

D2: Simulated circuit stream properties at optimum cyclone feed solids content (i.e. 67.1 %)

Stream Name	Solid flow (t/h)	Water flow (m^3/h)	% solids
SAG feed	618.00	11.40	98.20
SAG feed water	0.00	349.00	0.00
SAG discharge	721.00	438.00	62.20
SAG discharge water	0.00	75.40	0.00
SAG screen undersize	618.12	435.60	58.75
SAG screen oversize	102.50	2.20	97.87
Cyclone feed	2138.04	1048.32	67.10
Cyclone feed water	0.00	360.00	0.00
Overflow	476.64	912.60	34.31
Underflow	1661.76	135.65	92.45
BM feed	1517.04	251.82	85.76

BM feed water	0.00	133.42	0.00
BM discharge	1519.92	252.43	85.76
BM discharge water	0.00	0.64	0.00
Pebble crusher product	102.50	2.20	97.87
Gravity feed	332.32	27.13	92.45

D3: Simulated circuit stream properties at optimum vortex finder diameter (i.e. 270.3 mm)

Stream Name	Solid flow (t/h)	Water flow (m^3/h)	% solids
SAG feed	618.00	11.40	98.20
SAG feed water	0.00	349.00	0.00
SAG discharge	721.00	438.00	62.20
SAG discharge water	0.00	75.40	0.00
SAG screen undersize	618.12	435.60	58.75
SAG screen oversize	102.50	2.20	97.87
Cyclone feed	2157.48	1057.68	67.10
Cyclone feed water	0.00	367.92	0.00
Overflow	468.72	919.80	33.76
Underflow	1688.76	137.84	92.45
BM feed	1539.40	253.62	85.85
BM feed water	0.00	133.42	0.00
BM discharge	1539.40	254.27	85.82
BM discharge water	0.00	0.64	0.00
Pebble crusher product	102.50	2.20	97.87
Gravity feed	337.75	27.57	92.45

D4: Simulated circuit stream properties at optimum apex diameter (i.e. 145.62 mm)

Stream Name	Solid flow (t/h)	Water flow (m^3/h)	% solids
SAG feed	618.00	11.40	98.20
SAG feed water	0.00	349.00	0.00
SAG discharge	721.00	438.00	62.20
SAG discharge water	0.00	75.40	0.00
SAG screen undersize	618.12	435.60	58.75

SAG screen oversize	102.50	2.20	97.87
Cyclone feed	2140.20	1049.40	67.10
Cyclone feed water	0.00	366.84	0.00
Overflow	472.32	920.88	33.90
Underflow	1667.88	128.45	92.85
BM feed	1522.10	246.10	86.10
BM feed water	0.00	133.42	0.00
BM discharge	1521.72	246.71	86.05
BM discharge water	0.00	0.64	0.00
Pebble crusher product	102.50	2.20	97.87
Gravity feed	333.58	25.70	92.85

D5: Optimum parameters of the grinding circuit based on simulation of the existing plant

Parameter	Survey	Survey sim.	Optimum
SAG screen aperture in mm	12.00	12.00	10.00
Cyclone feed solids content in %	66.70	70.00	67.10
Cyclone diameter, D_c in mm	660.00	660.00	660.00
Inlet diameter, D_i in mm	275.00	275.00	275.00
Vortex finder, D_o in mm	280.00	280.00	270.30
Apex diameter, D_a in mm	150.00	150.00	145.62
BM feed solids content in %	72.10	80.00	74.00

D6: Simulated circuit stream properties after 10 % of underflow is split back to SAG mill

Stream Name	Solid flow (t/h)	Water flow (m^3/h)	% solids
SAG feed	618.00	11.40	98.20
SAG feed water	0.00	349.00	0.00
SAG discharge	960.12	477.72	66.78
SAG discharge water	0.00	75.40	0.00
SAG screen undersize	830.88	475.20	63.62
SAG screen oversize	129.42	2.40	98.20
Cyclone feed	1803.60	929.16	66.00
Cyclone feed water	0.00	111.42	0.00
Overflow	288.10	665.64	30.21

Underflow	1515.60	263.30	85.20
Underflow split to SAG	227.34	39.40	85.20
BM feed	1006.92	353.74	74.00
BM feed water	0.00	179.93	0.00
BM discharge	972.72	342.40	73.96
BM discharge water	0.00	0.64	0.00
Pebble crusher product	129.42	2.39	98.20
Gravity feed	303.10	52.67	85.20

D7: Simulated circuit stream properties for the optimized two stage classification circuit

Stream Name	Solid flow (t/h)	Water flow (m^3/h)	% solids
SAG feed	618.00	11.40	98.20
SAG feed water	0.00	349.00	0.00
SAG discharge	721.00	438.00	62.20
SAG discharge water	0.00	75.40	0.00
SAG screen undersize	618.12	435.60	58.75
SAG screen oversize	102.50	2.20	97.87
Cyclone feed (1)	2194.92	1032.84	68.00
Cyclone feed water (1)	0.00	42.44	0.00
Overall overflow	460.80	1206.40	27.64
Underflow (1)	1852.60	152.64	92.40
Cyclone feed water (2)	0.00	400.68	0.00
Underflow (2)	1733.80	227.23	88.41
BM feed	1576.80	554.04	74.00
BM feed water	0.00	362.20	0.00
BM discharge	1576.80	554.76	73.97
BM discharge water	0.00	0.64	0.00
Pebble crusher product	102.50	2.20	97.87
Gravity feed	346.79	45.43	88.42

D8: Optimum parameters for the grinding circuit with two classification stage

Parameter	Survey	Opt. class. 1	Opt. class. 2
SAG screen aperture in mm	12.00	10.00	10.00
Cyclone feed solids content in %	66.70	68.00	76.50
Cyclone diameter, D_c in mm	660.00	450.00	280.00
Inlet diameter, D_i in mm	275.00	275.00	275.00
Vortex finder, D_o in mm	280.00	270.30	165.00
Apex diameter, D_a in mm	150.00	145.62	145.62
BM feed solids content in %	72.10	74.00	74.00

D9: Simulated circuit stream properties for the optimized circuit with two ball mills in parallel

Stream Name	Solid flow (t/h)	Water flow (m^3/h)	% solids
SAG feed	618.00	11.40	98.20
SAG feed water	0.00	349.00	0.00
SAG discharge	721.00	438.00	62.20
SAG discharge water	0.00	75.40	0.00
SAG screen undersize	618.12	435.60	58.75
SAG screen oversize	102.50	2.20	97.87
Cyclone feed	2116.80	1243.44	63.00
Cyclone feed water	0.00	430.92	0.00
Overflow	374.40	1110.60	25.21
Underflow	1742.40	132.73	92.92
Gravity feed	435.60	33.19	92.92
BM 1 feed	749.52	54.83	93.18
BM 1feed water	0.00	133.42	0.00
BM 2 feed	749.52	54.83	93.18
BM 2 feed water	0.00	133.42	0.00
BM 1 discharge	749.52	188.24	79.93
Pebble crusher product	102.50	2.20	97.87
BM 2 discharge	749.52	188.24	79.93

D10: Optimum parameters of the grinding circuit with two ball mils in parallel

Parameter	Survey	Optimum
SAG screen aperture in mm	12.00	10.00
Cyclone feed solids content in %	66.70	63
Cyclone diameter, D_c in mm	660.00	660.00
Inlet pipe diameter, D_i in mm	275.00	275.00
Vortex finder diameter, D_o in mm	280.00	178.00
Apex diameter, D_a in mm	150.00	165.00
BM feed solids content in %	72.10	74.00

D11: Simulated circuit stream properties for the optimized circuit with two ball mills in series

Stream Name	Solid flow (t/h)	Water flow (m^3/h)	% solids
SAG feed	618.00	11.40	98.20
SAG feed water	0.00	349.00	0.00
SAG discharge	721.00	438.00	62.20
SAG discharge water	0.00	75.40	0.00
SAG screen undersize	618.12	435.60	58.75
SAG screen oversize	102.50	2.20	97.87
Cyclone feed (1)	2295.36	1377.00	62.50
Cyclone feed water (1)	0.00	505.08	0.00
Overall overflow	444.96	1144.80	27.99
Overflow (1)	39.85	1052.28	3.65
Overflow (2)	405.00	92.41	81.42
Underflow (1)	2255.40	324.76	87.41
Underflow (2)	1850.40	365.76	83.50
BM 2 feed	1677.24	302.98	84.70
BM 2 feed water	0.00	133.42	0.00
BM 2 discharge	1677.24	302.98	84.70
Pebble crusher product	102.50	2.20	97.87
Gravity feed	370.08	73.15	83.50

D12: Optimum parameters of the grinding circuit with two ball mils in series

Parameter	Survey	Optm. stage 1	Optm. stage 2
SAG screen aperture in mm	12.00	10.00	10.00
Cyclone feed solids content in %	66.70	62.50	87.70
Cyclone diameter, D_c in mm	660.00	660.00	660.00
Inlet diameter, D_i in mm	275.00	275.00	275.00
Vortex finder, D_o in mm	280.00	197.00	197.00
Apex diameter, D_a in mm	150.00	165.00	165.00
BM feed solids content in %	72.10	83.10	79.40

Appendix E: Miscellaneous information

E1: An example of separation curves with fish-hook behaviour obtained in a 25 mm-hydrocyclone with nine different quartzite materials (Gehart as cited in (Schubert 2010))

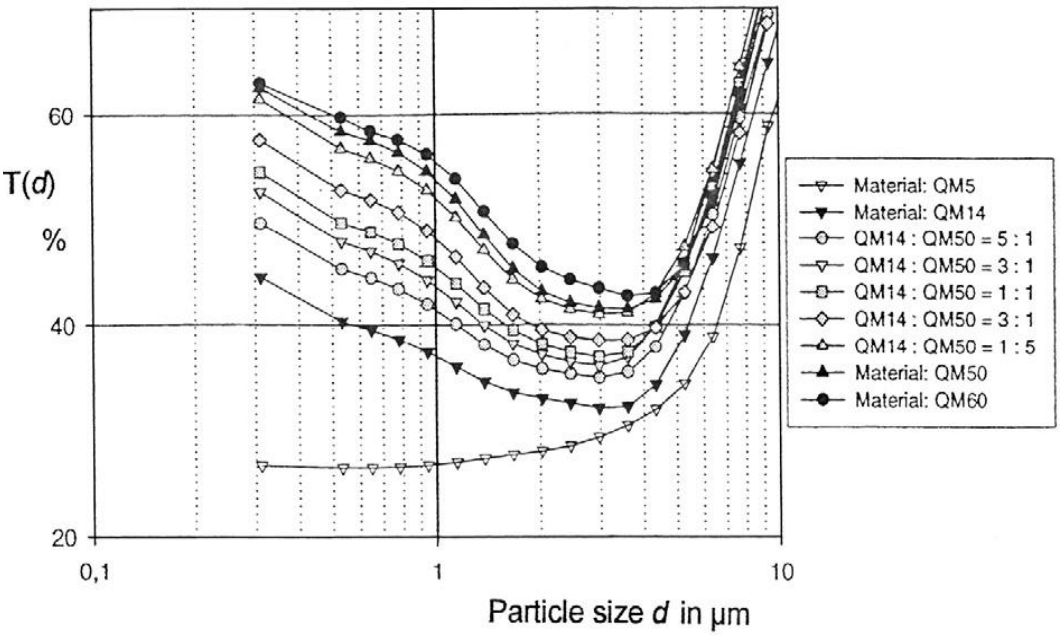

E2: Example of size balance formulae used to calculate size distributions for some key streams based on the survey data, mainly based on the two product formula (Wills and Napier-Munn 2006).

Formulae	Definition of terms
$C_f = m_u.C_u + (1-m_u).C_o$	C_f =hydrocyclone feed size distribution, m_u and m_o are fractions of feed to underflow and overflow respectively
$\dot{m}_F.P_{i,F} = \dot{m}_1.P_{i,1} + \dot{m}_2.P_{i,2}$	$\dot{m}_F, \dot{m}_1 \; and \; \dot{m}_2$ =solids mass flow rates in corresponding streams. $P_{i,F}$, $P_{i,1}$ and $P_{i,2}$=weight fractions in the feed, product 1 and product 2 for a given size fraction i

E3: Standard error of measurement for gold and copper AAS measurements.

$$\sigma_S = \sqrt{\frac{\sum (n_i - \mu_1)^2}{n-1}} \qquad \text{and} \qquad SE = \frac{\sigma_S}{n}$$

δ_s=standard deviation of measurement

n_i= the ith measurement replicate

μ_1=mean of measurement replicates

SE=standard error

n= number of measurement replicates